The University Of Sheffield.

Department Of Mechanical Engineering

Novel Materials and Architectures for the Gas Diffusion Layer of Polymer Electrolyte Membrane Fuel Cells.

By:

Florence Cecilia Lee

A thesis submitted in partial fulfilment of the requirements for the degree of Doctor of Engineering

University of Sheffield

Faculty of Engineering

Department of Mechanical Engineering

Energy 2050

November 2023

Acknowledgements

Firstly, I wish to express my thanks to the Engineering and Sciences Research Council, The International Flame Research Foundation, and the Centre for Doctoral Training in Carbon Capture, Storage & Cleaner Fossil Energy for supporting my professional and academic development, and for the funding that I received. The Doctor of Engineering programme gave me space to explore the wider avenues of sustainable energy research that I would otherwise be unable to explore. This multi-disciplinary approach allowed me to acquire new skills, moreover, it provided perspective and solidified the relevance of my research in times of doubt.

I would like to extend my gratitude to Professor Pourkashanian for allowing me to use his labs and resources, and for accepting me in the Energy 2050 research group. Thank you to Professor Derek Ingham whose kindness knows no bounds, your words of encouragement and the hours checking my work were appreciated by me. To, Dr Kevin Hughes, thank you for your help in the lab especially your support through the pandemic which enabled me to carry out my experimental work when there were so many barriers in the way. Thank you, Professor Lin Ma, for your help during the weekly group meetings and your support with my lab documentation. A special thanks is for Dr Mohammed Ismail to whom I struggle to express my gratitude. Your continuous support went above and beyond that of a supervisor; I not only learned so much from you in terms of scientific knowledge but also from your strength of character, your patience, and the treatment of your students.

I would like to express my gratitude to my supervisors for the opportunity to carry out research projects at Kyushu University, thanks to the bilateral grant between Energy 2050 and i2cner. Many thanks to Professor Stephen Lyth and his research team at Kyushu University who gave me a home away from home in Itoshima. The hours that Professor Lyth spent reading through my work and thinking of witty remarks will not be forgotten. I extend my thanks to Dr Albert Mufundirwa who trained me on many experimental procedures and who remains a dear friend of mine.

Finally, I would like to thank my family and friends who have provided me with the love and support needed during this time. Thank you to my friends and colleagues in the Energy 2050 office who created

a hospitable working environment and made me feel comfortable. Although, the pre-pandemic days of “Cakey Tuesdays” and “Napoli Fridays” are behind us, I look on those times with fondness. Thank you to my parents, Judith Bell and Richard Lee, and my sister Jessica Lee, as well as my partner, Damian Li. A special thank you goes to my daughter Rosalyn Li for whom I wish to create a better world. You make me a better person and are my motivation to persevere through the challenges that I encounter.

Abstract

Rapid population expansion and increased global development have led to a significant surge in energy demand. It is critical that the energy needs of this growing population are met in a sustainable way to provide energy security for future generations and to promote harmonisation between the built and natural environment. Global climate change caused by anthropogenic carbon dioxide emissions and greenhouse gases is the single biggest threat facing humanity today. Energy efficient designs and the increased use of renewable energy sources and hydrogen energy systems are a realistic means for the mitigation of CO_2 emissions.

Polymer Electrolyte Membrane fuel cells are a key component in the hydrogen economy, and they offer significant potential as prospective replacement for fossil fuel-based technologies. PEM fuel cells, as they are known, benefit from high power density, efficiency and most importantly versatility. Although their commercialisation is in the developmental phase, the technology has a broad spectrum of use, being implemented in fuel cell vehicles (Honda Clarity, Toyota Mirai, Japan), residential combined heat and power (Enefarm, Japan), and portable electronics (Intelligent Energy, UK). There are, however, limitations affecting the wide scale deployment of PEM fuel cell technology. The gas diffusion layer and the microporous layer are essential components for maintaining the balance of liquid water in the fuel cell, and the removal of excess liquid water from the cathode porous media continues to pose problems for the PEM fuel cell operating in humid conditions and at high current densities. The microporous layer is a layer applied to the catalyst interface of the gas diffusion layer of the PEM fuels, thus it plays an integral role in the efficient operation of the cell. It is responsible for ensuring the effective transfer of heat, electrons, and mass, as well as preserving the balance of liquid water to simultaneously maintain membrane hydration and remove excess liquid water. In this thesis, we present three chapters on novel materials and architectures for the microporous layer of the Polymer Electrolyte Membrane Fuel Cell.

Conventional microporous layers are produced from carbon black and a hydrophobic binder. Microporous layers were produced with inclusions of graphene in order to alter the microstructure and

consequently, the ability to reduce liquid water flooding. The inclusion of graphene nanoplates in the microporous layer resulted in changes to the microstructure and the physical properties of layer. The graphene nanoplates imparted desirable characteristics onto the layer, notably increasing the hydrophobicity of the layer and its electron conductivity. These improved characteristics resulted in significant performance enhancements in high humidity operation (50% relative humidity and greater) for microporous layers containing ≤ 50 wt.% of graphene.

Graphene foam was considered a novel MPL material, in order to do so graphene foams were synthesised from the pyrolysis of sodium ethoxide in different atmospheres, 100% N_2 and 95% N_2 and 5% H_2 to produce N-GF and NH-GF foams respectively. XPS was used to quantify the carbon content and SEM revealed the open pores structure of the foams. These graphene foams then formed the basis of novel microporous layers which were characterised alongside microporous layers produced from conventional carbon black and graphene nanoplates. The N-GF exhibited better ex-situ characteristics, such as higher electron mobility, and produced greater power density in the single cell measurements.

Alternative architectures were considered from the construction of bi-layer porosity-graded microporous layers. Whereby microporous layers were produced by applying two separate layers of MPL ink formed of carbon black and graphene nanoplates. Each layer exhibits its individual physical and microstructural properties, where the carbon black layer is microporous, the graphene nanoplates were characterised by large mesopores. These layers were characterised ex-situ in terms of their microstructural, physical, and electrochemical properties, and in single cell measurements where higher power densities and limiting current densities were achieved with the bi-layer microporous layers.

Academic Publications

1. The work in **Chapter 2** of the thesis appeared in part in the publication as the following:
   F. C. Lee, M.S. Ismail, D.B. Ingham, K.J. Hughes, L. Ma, S.M. Lyth and M. Pourkashanian. "Alternative architectures and materials for PEMFC gas diffusion layers: A review and outlook," Renewable and Sustainable Energy Reviews, vol. 166, p. 112640, 01/09/ 2022, doi: https://doi.org/10.1016/j.rser.2022.112640.
2. The work in **Chapter 4** of the thesis appeared in publication as the following:
   F. C. Lee, K. Zhang, M.S. Ismail, A. El-Kharouf, F.Aldakheel, D.B. Ingham, K.J. Hughes, L. Ma, and M. Pourkashanian. "Optimisation and Characterisation of Graphene-based Microporous Layers for Polymer Electrolyte Membrane Fuel Cells". International Journal of Hydrogen Energy. 18/05/2023, doi: https://doi.org/10.1016/j.ijhydene.2023.05.003.

Oral and Poster Presentations

1. Participated and presented at three workshops in the series held by The University of Sheffield and Kyushu University in Japan: "Sheffield-Kyushu Workshop Joint on Electrochemical Energy Conversion (SKWEEC), Sheffield, UK".
2. Participated in a knowledge exchange between Energy 2050 Group at The University of Sheffield and Professor Lyth's group at Kyushu University. This resulted in two trips to Kyushu University as a PhD exchange student (March 2019 and January 2020). Whilst in Japan participated in two more workshops held between University of Sheffield and Kyushu University (SKWEEC).
3. Actively participated in Energy Week 2020 held at the i^2cner Institute, Kyushu University Japan.
4. Prepared and presented as poster at the Electrochemical Society Conference on-line. (PRIME, 2020):
   F. C. Lee, M.S. Ismail, D.B. Ingham, K.J. Hughes, L. Ma, S.M. Lyth and M. Pourkashanian. "An Assessment of Novel Graphene Foam and Graphene-Based Microporous Layers for Polymer Electrolyte Fuel Cells: Fabrication and Characterisation," ECS Meeting Abstracts, vol. MA2020-02, issue 33, (2020) pp. 2116-2116, 2020/11// 2020, doi: https://doi.org/10.1149/MA2020-02332116mtgabs.

5. Presented research findings at the World Hydrogen Energy Conference 2022 held in Istanbul, Turkey (WHEC 2022). “Optimisation and Characterisation of Graphene-based Microporous Layers for Polymer Electrolyte Membrane Fuel Cells”
6. Prepared and presented as poster at the Electrochemical Society Conference in Atlanta, USA (ECS Atlanta 2022). The work in **Chapter 5** of the thesis appeared in publication as the following:

   F. C. Lee, M.I. Kudashany, K. Zhang, M.S. Ismail, D.B. Ingham, K.J. Hughes, L. Ma, S.M. Lyth and M. Pourkashanian. “Preparation and Characterisation of Microporous Layers Derived from Graphene Foam”. ECS Meeting Abstracts, vol. MA2022-02, issue 39, (2022) pp: 1394-1394. doi: https://doi.org/10.1149/MA2022-02391394mtgabs

Awards and Prizes

1. EPSRC CCSCFE Winter School 2019. Student Presentation.
2. Mechanical Engineering Student Poster Presentation 2020, University of Sheffield (2nd Place).
3. 1st UK-Japan Symposium on Advanced Materials for Hydrogen and Fuel Cells 2021 (Joint 2nd Place).

Table of Contents

List of Figures

Nomenclature

Roman Symbols	Definition	SI Units
a	Specific Area	m^{-1}
D	Diffusivity	-
D_{eff}	Effective Diffusivity	-
I	Current	A
K	Permeability	m^2
L	Thickness Of Porous Medium	m
M	Molecular Weight	kg/mol
$\dot{m}$	Mass Flow Rate	kg s^{-1}
P	Pressure	Pa
R	Measured Resistance	Ω
T	Temperature	K
t	Time	s
u	Velocity	m s^{-1}
V	Potential	V
W	Power	W

Greek Symbols	Definition	SI Units
ε	Porosity	-
ρ	Density	kg m^3
μ	Dynamic Viscosity	Pa s
ρ	Electrical Resistivity	Ω cm
σ	Electrical Conductivity	S cm^{-1}

List of Abbreviations

Abbreviation	Definition
AFC	Alkaline Fuel Cell
CB	Carbon Black
CL	Catalyst Layer
CNT	Carbon Nanotubes
EIS	Electro Impendence Spectroscopy
FEP	Fluorinated-ethylene-Propylene
GDE	Gas Diffusion Electrode
GDL	Gas Diffusion Layer
GF	Graphene Foam
GNP	Graphene Nanoplates
MIP	Mercury Intrusion Porosimetry
MEA	Membrane Electrode Assembly
MPL	Microporous Layer
PAN	Polyacrylonitrile
PEM FC	Polymer Electrolyte Membrane Fuel Cell
PFPE	Perfluoropolyether
PTFE	Polytetrafluoroethylene
SEM	Scanning Electron Microscopy
XCT	X-Ray Computed Tomography

Chemical Symbols	Definition
CH_4	Methane
CO_2	Carbon Dioxide
H_2	Hydrogen Molecule
H_2O	Water
Ni	Nickel
N_2	Nitrogen Molecule
Pt	Platinum
O_2	Oxygen Molecule
Ti	Titanium

Chapter 1: Introduction

1.1 Introduction to the Hydrogen Economy

Fuel cells hold great potential for the advancement of a decarbonised global energy system. The link between global climate change, carbon dioxide emissions, and fossil fuels is well established, thus there is a need for a non-carbon-based energy vector. Hydrogen has been identified as playing a significant role in this carbon-free future [12-16]. Hydrogen fuel cells do not produce greenhouse gases or harmful gases, the only product being water.

The "hydrogen economy" is a term used to describe a holistic system where hydrogen is used as the energy vector in the way that traditionally hydrocarbon fuels were used. Hydrogen fuel cells as a part of the hydrogen economy will have a large role in the play in replacement of conventional carbon-based systems; ultimately if the vision of a hydrogen economy is successful, hydrogen will be responsible for the provision of electricity, heat, industry, and transport and energy storage. The potential of this has already been acknowledged, however for the hydrogen economy to be realised there needs to be a radical change in infrastructure and a reduction in the cost of hydrogen fuel cells in comparison to combustion sources. Japan is a country at the forefront of the emergence of the hydrogen economy; its plan is a three-phase transition away from fossil fuels to a hydrogen-based society. Currently, it is promoting fuel cell vehicles, hydrogen production, and residential fuel cells, by 2030 it aims to have integrated hydrogen supply chains into the energy system, and by 2040 it aims to establish a carbon-free hydrogen economy [15, 17]. This need for change is driven by the economic pull factors of being a fossil fuel importer as much as the environmental push factors of climate change. Previously for the UK, the hydrogen economy was predominantly seen as a means to reduce greenhouse gas emissions [18]. However, as the conflict between Russia and Ukraine has demonstrated so succinctly, an energy system's reliance on fossil fuel imports means energy security is inextricably associated with political relations and the whims of global leaders. This has not escaped the notice of the general public, where polls conducted by Vattenfall shortly after the Russian invasion (March 2022) revealed that nearly two-thirds of consumers (61%) thought that the use of renewable energy sources is the most effective means to guarantee UK energy security [19]. The UK government and commercial sector have realised that

hydrogen is a necessary energy vector to support the shift towards renewable energy systems with the target of 5 GW of low-carbon hydrogen production by 2030 [16]. More reliably, the commercial sector has invested in hydrogen technology with the creation of hydrogen divisions in engineering firms such as Arup, RWE, and Atkins. This is a strong indication of the growth of the hydrogen economy as hydrogen is becoming commercially viable.

1.2 Polymer Electrolyte Membrane Fuel Cell and its Applications

PEMFCs use the electrochemical reaction between hydrogen and oxygen-producing water to generate a current. As such they generate no greenhouse gases, at least at the point of use, and can be regarded as a carbon-free alternative to conventional combustion. Referring to Table 1.1 [20], the advantages of PEMFC lie in their high power density, relatively low operating temperature (60°C to 80°C), rapid start-up time, and scalability. The strength of the technology has led to PEMFC fuel cells becoming the focus of significant research and commercial interest as an alternative to vehicular internal combustion engines and as a means of grid balancing at periods of peak load and generation [21, 22].

Energy storage is an accepted necessity for renewable energy power generation [23, 24]; the intermittency of wind and solar power requires an energy storage system capable of charging with a variable power supply. PEMFC have been cited as the most suitable option due to their rapid start-up and reaction time. Commercially, fuel cell vehicles using PEMFC technology are available on the market, of which the Asian manufacturers lead with the Toyota Mirai, the Honda FCX Clarity, and the Hyundai ix35. The majority of large automotive manufacturers have developed prototype fuel cell vehicles, some of which have been marked for production, notably the BMW FCV [25]. The hydrogen vehicle market for public transport has been more successful than private vehicles, with the adoption of hydrogen buses by some city councils (Aberdeen, Birmingham, Dundee, Liverpool, and London), indeed Transport for London strives to be the "world leader in hydrogen and fuel cell activity" [26].

Due to the scalability of the PEMFC technology, the diversity of its application extends further than battery technology; from portable chargers for mobile devices produced by Upp and Intelligent Energy UK to residential stationary CHP plant at ENE FARM, Japan [27]. Commercial development of

polymer electrolyte membrane fuel cells has recently spread to the broader engineering sector, a notable example is the announcement by Johnson Matthey of the construction of a UK-based facility for manufacturing of PEM fuel cell components [28]. These developments will accelerate the growth of the technology by increasing its availability, improving knowledge in the sector, and reducing capital and operating costs.

Types of Fuel Cells

Table 1-1: A Comparison of Fuel Cell Technologies [20].

Fuel Cell	Polymer Electrolyte Membrane	Alkaline	Solid Oxide	Molten Carbonate	Phosphoric Acid	Direct Methanol
Catalyst	Platinum	Platinum	Ceramic	Nickel	Platinum	Platinum
Common Electrolyte	Solid organic polymer poly-perfluorosulfonic	Potassium Hydroxide (KOH)	Yttria-Stabilized Zirconia (YSZ)	Eutectic molten alkaline carbonate (Li-K)	Concentrated phosphoric acid soaked in a matrix	Polymer membrane
Operating Temperature	30-100°C	60-250°C	650–1000°C	600–800°C	150°–200°C	60-130°C
Fuel	Hydrogen	Hydrogen Ammonia	Natural gas Methanol Ethanol Biogas	Natural gas Methanol Ethanol Biogas Coal gas	Hydrogen	Methanol
Electrical Efficiency	53–58%	60%	35–43%	45–47%	40%	20-25%
System Output	<1 kW-250 kW	10-100 kW	<1-3 MW	<1-3 MW	100-400 kW	<1.5 kW
Advantages	• Quick start-up time • Low temperature • Solid electrolytic reduces corrosion and electrolyte problems. • High energy density	• Faster ORR kinetics in alkaline electrolyte • Variety of catalysts	• High efficiency • Fuel flexibility	• High efficiency • Fuel flexibility • Variety of catalysts • Suitable for CHP	• High efficiency • Suitable for CHP • Fuel flexible	• Low temperature • No need for fuel reformer

1.3 Polymer Electrolyte Membrane Fuel Cell

1.3.1 Working Principles

The polymer electrolyte fuel cell uses a polymer electrolyte membrane, sandwiched between a cathode and anode, to conduct protons for ion exchange. PEMFC are fed with hydrogen fuel and an oxidant, typically oxygen; their operation relies on two simultaneous electrochemical reactions:

$$H_2 \rightarrow 2H^+ + 2e^- \tag{1.1}$$

The anode side oxidation reaction, where hydrogen is ionised at the anode catalyst layer to become two hydrogen ions (protons) and two electrons.

$$\tfrac{1}{2}O_2 + 2H^+ + 2e^- \rightarrow H_2O \tag{1.2}$$

The oxygen reduction reaction that occurs at the cathode catalyst layer combines oxygen, hydrogen, and electrons to form water.

$$\frac{1}{2}O_2 + H_2 \rightarrow H_2O + \text{Heat} \tag{1.3}$$

Equation 1.3 is the overall reaction of the fuel cell which is a combination of the anode and cathode side reactions. This reaction sees the production of heat and thus is exothermic.

Referring to Fig. 1.1, humidified hydrogen is fed into the anode-side inlet (on the left hand side), where at the catalyst-gas-membrane interface the H_2 molecules are ionised to form two H^+ ions. The electrons produced by the ionisation of hydrogen enter the external circuit to generate direct current (DC). Oxygen (O_2) enters the cathode-side inlet and diffuses across the porous gas diffusion layer to the catalyst layer. At the cathode catalyst layer the strongly negatively charged oxygen atoms attract the H^+ ions across the proton exchange membrane. At the cathode catalyst layer the oxygen atoms combine with the H^+ ions and two electrons from the outside circuit to form a water (H_2O) molecule.

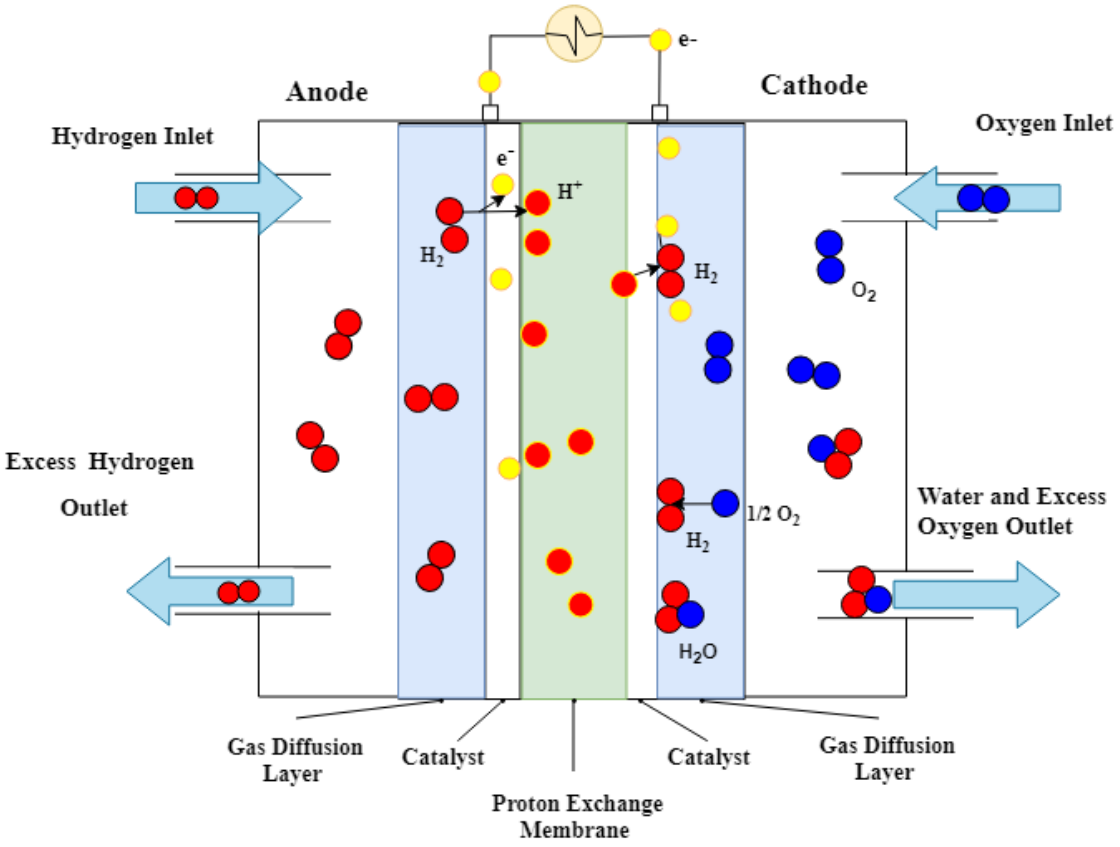

Figure 1-1: The principles of operation of PEMFC

1.3.2 Polymer Electrolyte Membrane Fuel Cell Components

Flow-field plates: The flow-field plates provide the main structural support to the stack, aside from this they conduct electrons produced by the anode catalyst reaction to the outer circuit. They are also responsible for the uniform distribution of gases to the gas diffusion and catalyst layers as flow-field plates must house the flow-field channels. There are 3 main channel configurations for the flow field plates: serpentine, parallel and interdigitated channels.

Anode gas flow-field channel: The anode gas flow-field channel is housed in the flow-field plate, the anode side reactant gases, hydrogen, and water vapour enter the fuel cell here. Its purpose is to ensure that: reactant gases are uniformly distributed to the gas diffusion and catalyst layers; pressure drop is minimised; and liquid water can be removed.

Anode porous gas diffusion layer: The gas diffusion layer facilitates the diffusion of reactant gases from the electrode to the anode catalyst layer and conducts electrons from the catalyst layer to the current collector.

Anode porous catalyst layer: Hydrogen molecules are oxidised here to form hydrogen ions and electrons.

Proton exchange membrane: Hydrogen ions, protons, diffuse across the membrane electrolyte to the cathode catalyst layer to react with the negatively charged oxygen. Hydration of the membrane is necessary to ensure good conductivity of protons (H^+) and prevents electrons moving across the membrane. Dissolved molecules of water are typically transported from the cathode to the anode by back diffusion and from the anode to cathode by electro-osmotic drag.

Cathode porous gas diffusion layer: Reactant gases travel from the cathode gas channel through the porous gas diffusion layer to the catalyst layer.

Cathode porous catalyst layer: The oxygen reduction reaction takes place here, where water is produced from hydrogen, oxygen, and electrons from the outer circuit.

Cathode gas channel: The oxidant gases enter the fuel cell here. The cathode gas channel must also ensure that gases are distributed evenly, and the pressure drop is minimised.

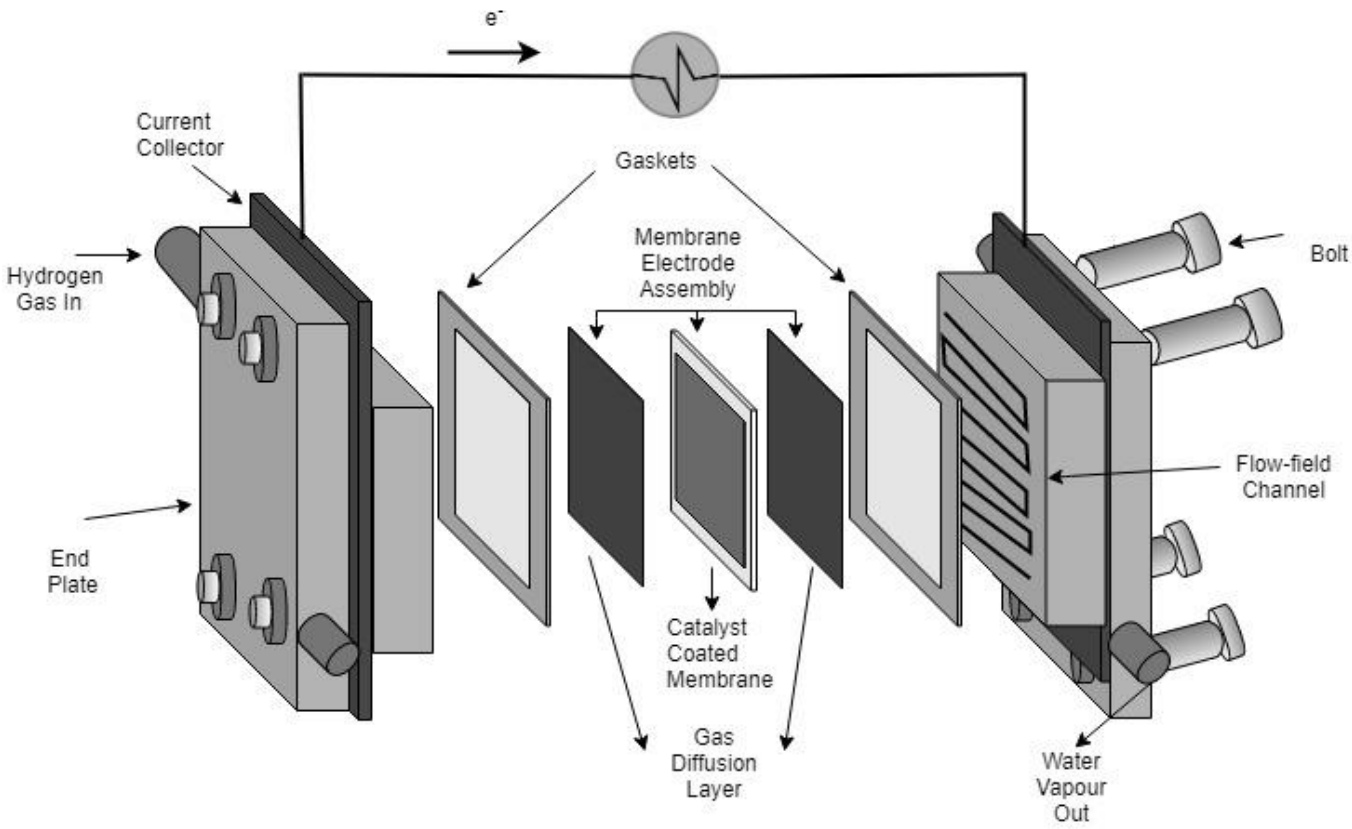

Figure 1-2: A diagram of the layers and components of the polymer electrolyte membrane fuel cell.

1.3.3 Thermodynamics and Polarisation Curve

1.3.3.1 Thermodynamics

Referring back to equation 1.3, the reaction between hydrogen and oxygen is exothermic. The heat produced can be calculated using the equation:

$$\Delta H = (h_{f_{H_20}}) - (h_{f_{H_2}}) - \frac{1}{2}(h_{f_{O_2}}) \quad (1.4)$$

where h_f is the heat of formation of a chemical species.

The higher heating value of hydrogen is 286 kJ, using the heat of formation of liquid water can be calculated at 286 kJ mol-^{1}. This is a spontaneous reaction where a form of energy (heat) is released, to move to a thermodynamically stable state. The Gibbs free energy (G) is useable work that can be performed outside of temperature or pressure change. The Gibbs free energy equation can be used to describe the energy content and evaluate the spontaneity of the reaction when the energy content changes; a negative change in Gibbs free energy ($-\Delta G^0$) denotes a spontaneous reaction [29]. In hydrogen fuel cells, the portion of hydrogen enthalpy that can be converted into electricity is the Gibbs free energy. It can be defined in terms of relationship to entropy and enthalpy during the reaction at standard state:

$$\Delta G^0 = \Delta H^0 - T\Delta S^0 \quad (1.5)$$

where ΔG^0 is the change in the Gibbs free energy, ΔH^0 is the change in enthalpy and ΔS^0 is the change in entropy of the substance and T is the temperature. As such Gibbs free energy varies in accordance with temperature.

In fuel cells it is the change in the Gibbs free energy of formation ΔG_f that releases energy; it is the difference between the Gibbs free energy of the reactants $\Delta G_{f,R}$ and the Gibbs free energy of the products $\Delta G_{f,P}$ and this is given by:

$$\Delta G_f = \Delta G_{f,P} - \Delta G_{f,R} \quad (1.6)$$

In hydrogen fuelled PEMFC, the change in molar Gibbs free energy of formation is given by equation 1.8, the subtraction of the free energy of hydrogen and oxygen from the free energy of water.

$$\Delta\bar{g}_f = \left(\overline{g_f}\right)_{H_2O} - \left(\overline{g_f}\right)_{H_2} - \frac{1}{2}\left(\overline{g_f}\right)_{O_2} \quad (1.7)$$

The standard reversible cell voltage (ΔE^0) is based on the chemical potential of hydrogen in the oxidation reaction and oxygen in the reduction reaction. The reversible potential is related to Gibbs free energy by the following and thus the entropy and enthalpy. It is given by the following equation:

$$\Delta E^0 = \frac{-\Delta G^0}{n_e F} = -\left(\frac{\Delta H}{nF} - \frac{T\Delta S}{nF}\right) = \frac{237.34\ \text{J mol}^{-1}}{2 \cdot 96.485\ \text{As mol}^{-1}} = 1.229\ \text{V} \quad (1.8)$$

where ΔE^0 the reversible cell is potential for each electrode, $\Delta G^0$is the change in Gibbs free energy at standard conditions, F is Faraday number and n is the number of transferred electrons. Thus, the theoretical potential of a hydrogen/ oxygen fuel cell at 25°C is 1.229 volts.

Anode: $H^2 \rightarrow H^+ + 2e^-$ $E_a^0 = 0V$ (1.9)

Cathode: $2H^+ + \frac{1}{2}O_2 + 2e^- \rightarrow H_2O$ $E_c^0 = 1.229V$ (1.10)

Overall: $H_2 + \frac{1}{2}O_2\,H_2 \rightarrow H_2O + electricity$ $E_{cell}^0 = 1.229V$ (1.11)

The reversible cell potential of H_2 reduction is 0 as there is no change in the Gibbs free energy. The standard cell potential of the O_2 reduction reaction based on the higher heating value (HHV), is 1.229V. In accordance with equation (1.11) the overall reversible cell potential of a PEMFC hydrogen fuel cell is 1.229 V [30, 31]. When there are no energy losses in the fuel cell then all of the Gibbs free energy is converted to electrical energy. This voltage is known as the theoretical reversible cell potential. The Open Circuit Voltage (OCV) is defined as the cell voltage at equilibrium where no current is being generated and this should theoretically be the same as the theoretical reversible cell potential. In reality the OCV is very different from the theoretical reversible cell potential, usually less than 1V [1]; this is due to a number of factors which are hydrogen cross-over and mixed potentials.

1.3.4 Theoretical Efficiency

Theoretical efficiency is defined as the ratio of useful energy output and energy input. For PEM, the energy output is electrical energy, and the energy input is the enthalpy of the formation of water. Taking the higher heating value (HHV) of hydrogen, if all of the Gibbs free energy from the fuel can be converted into electrical energy then the theoretical efficiency of a hydrogen fuel cell is:

$$\eta = \frac{\Delta G}{\Delta H} = \frac{237.34}{286.02} = 83\% \tag{1.12}$$

where, ΔG is the change in Gibbs energy and ΔH is the enthalpy of hydrogen.

Frequently the lower heating value (LHV) of hydrogen is used to ease comparison with the internal combustion engine, in which case the theoretical conversion efficiency becomes:

$$\eta = \frac{\Delta G}{\Delta H} = \frac{228.59}{241.98} = 94.5\% \tag{1.13}$$

1.3.5 Non-standard Conditions: Nernst Equation

The Nernst equation is used to calculate the change in the Gibbs free energy (ΔG) in non-standard operating conditions, as follows:

$$\Delta G = \Delta G_0 + RT\, ln\left(\frac{P_{H_2 0}}{P_{H_2}\ P_{O_2}^{0.5}}\right) \tag{1.14}$$

where, R is the universal gas constant, T is the temperature and P is the partial pressures of the product and reactants.

From substituting in equation 1.11, the cell potential can be expressed as a term of partial pressure of the product and reactants. For the PEM fuel cell, the Nernst equation becomes:

$$E_e = E_0 + \frac{RT}{n_e F} ln\left(\frac{P_{H_2} P_{O_2}^{0.5}}{P_{H_2 0}}\right) \tag{1.15}$$

When liquid water is produced $P_{H_2 0} = 1$. It is clear that higher partial pressures of the reactants give higher cell potentials.

where E_0 is the theoretical voltage, n_e is the number of electrons and F is the Faraday number.

1.3.6 Polarisation Curve and Irreversible Losses

These performance and voltage losses of a fuel cell are characterised by its polarisation curve, which is a plot of cell potential vs current density. The voltage losses in a fuel cell can be categorised as the following:

- Activation Losses
- Fuel Crossover
- Ohmic Losses
- Mass Transport Losses

Fig. 1.3 is an example of a typical polarisation curve from a PEMFC. As can be seen, the polarisation curve can be split into 3 clear regions: the low current density region is dominated by activation losses; the middle current density region is characterised by the effect of ohmic losses; and at high current densities voltage drops are associated with mass transport losses. An approximation of the PEMFC polarization curve can be derived from the following equation [1]:

$$E_{cell} = E_{r,T,P} - \eta_{act} - \eta_{ohm} - \eta_{conc} \tag{1.16}$$

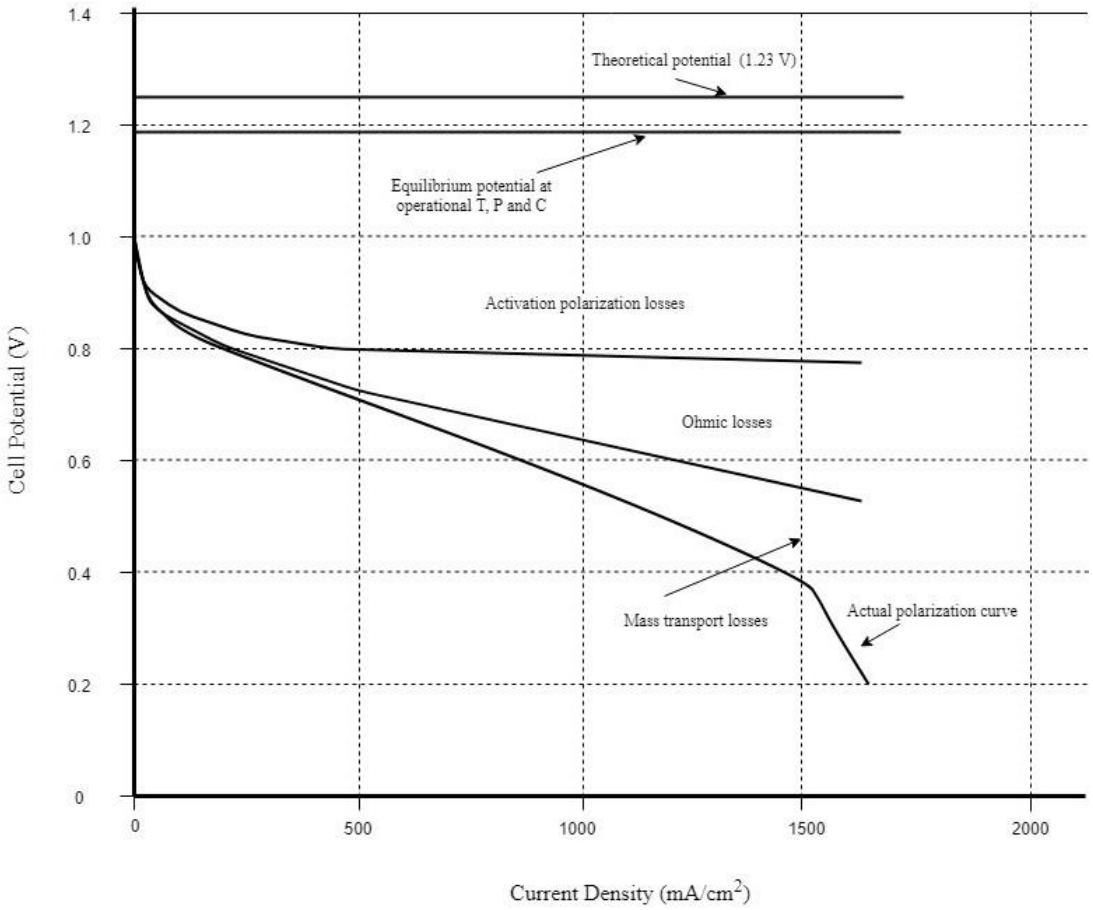

Figure 1-3: Typical polarisation curve showing potential loss in PEMFC (adapted from [1]).

1.3.6.1 Activation Losses

In order to start the electrochemical reaction some voltage difference from equilibrium is required. This is known as the activation polarisation; it is dependent on the electrode reaction kinetics. Losses occur at both electrodes; however, as the oxygen reduction reaction kinetics are much slower than hydrogen oxidation these losses are greater at the cathode than the anode. The higher the exchange current density, then the lower the activation polarisation losses.

The first term in the Butler-Volmer equation dominates at high negative over potentials, cathodic activation losses can thus be expressed as a function of current density as follows:

$$\eta_{act,c} = \frac{RT}{\alpha_c F} \ln\left(\frac{i}{i_{0,c}}\right) \tag{1.17}$$

where, α_c is the transfer coefficient for the cathode, i is the current density at the electrode and $i_{0,c}$ is the exchange current density.

The activation losses at the anode electrode are typically very small and they are therefore assumed to be negligible.

$$\eta_{act} = \eta_{act,c} + \eta_{act,a} = \frac{RT}{\alpha_c F} \ln\left(\frac{i}{i_{0,c}}\right) + 0 = \frac{RT}{\alpha_c F} \ln\left(\frac{i}{i_{0,c}}\right) \tag{1.18}$$

1.3.6.2 Fuel Crossover

Fuel crossover losses are caused by un-oxidised hydrogen fuel crossing the membrane and reacting with oxygen at the cathode catalyst layer. This causes a drop in cathode-side efficiency as well as creating the unwanted product of hydrogen peroxide. Hydrogen peroxide causes degradation of the catalyst and the membrane reducing the efficiency and lifetime of the fuel cell.

1.3.6.3 Ohmic Losses

Ohmic losses in potential in PEMFC are caused by two factors: resistance from the cell components and resistance in the electrolyte. Resistance from the cell components is due to the materials resisting the flow of electrons; this is normally considered to be negligible. Resistance from the electrolyte is a result of resistance ionic flow through the membrane; caused by chemical and membrane structure.

Ohmic loss from the electrolyte is a product of current density (i) and the specific area of resistance in the membrane(R_m).

$$\eta_{ohm} = \eta_{mem} = iR_m \tag{1.19}$$

Typical resistance losses are between 0.1 and 0.2 Ω [32].

1.3.6.4 Mass Transport Losses

Mass transport losses (also known as concentration losses) are caused by the decrease in partial pressure of the reactant gases with current increase. As the current increases the reactant gases are consumed and their partial pressures decreases at the electrodes; this causes a potential loss at the electrode [33]. The surface concentration of reactants will eventually reach zero; where the consumption rate of the reactants exceeds their diffusion rate, resulting in what is typically termed as limiting current density. The latter is the following equation to calculate the concentration losses:

$$\eta_{conc} = \frac{RT}{nF} \ln\left(\frac{i_L}{i_L - i}\right) \tag{1.20}$$

where, i is the current density and i_L is the limiting current density.

1.4 Thesis Overview

The aim of this thesis is to enhance the performance of current polymer electrolyte membrane fuel cells by material and architectural modifications of the microporous layer (MPL). Novel microporous layer materials i.e., graphene and graphene foam will be investigated alongside conventional carbon black in order to reduce current limitations to PEMFC performance, notably mass transport losses from liquid water saturation. Relevant literature pertaining to recent research developments on the microporous layer, along with an overview of experimental characterisation methods for the gas diffusion media is outlined in Chapter 2. Chapter 3 details the experimental methodology for the fabrication and the characterisation of the MPL-coated gas diffusion layers. In Chapter 4, commercially produced graphene is introduced as an MPL material; this chapter explores the optimisation of graphene concentration in the microporous layer by ex-situ characterisation and polarisation curves in different operating conditions. Chapter 5 outlines an investigation executed in collaboration with Kyushu University, in which graphene foam is fabricated and microporous layers are then produced from the graphene foam. These novel graphene foam microporous layers undergo ex-situ characterisation and polarisation curves to assess their potential to enhance MEA performance in comparison to carbon black and commercially produced graphene. The architecture and microstructure of the microporous layer is manipulated in Chapter 6 building on the findings revealed in Chapter 4; graphene is used in conjunction with carbon black to produce microporous layers with a pore size gradient with the aim of removing excess liquid water. The viability of this design is examined from ex-situ characterisation and polarisation curves in various humidity conditions. Finally, Chapter 7 summarises the findings of this research, their impact on the development of the microporous layer design, and Chapter 8 suggests the future work that should be undertaken on the MPL to further enhance the fuel cell performance.

Chapter 2: Literature Review

2.1 Characterisation of Porous Media

To understand the behaviour of the porous media in PEMFC, it must be quantified in certain characteristics. These are divided into two types: the morphological properties, which relate to the physical structure of the media, and the transport properties of the material. It should be noted that the morphological properties have been shown to highly influence the transport properties. In addition, more recently imaging has played a greater role in the characterisation of the porous media of PEMFC as it has enabled the visualisation of the internal structures and the surface morphology of the porous media. This has furthered a greater understanding of the impact of the physical structure on the characteristics of the material, such as electrical and thermal conductivity, mass transfer ability and water removal. One of the focal points of this research is to use micro-scale imaging of the gas diffusion and catalyst material, as such a section on micro and nano-scale imaging has been presented.

2.1.1 Morphological Properties of Porous Media

Anisotropy

Anisotropy is defined as the property of a substance to exhibit different values for a physical property when measured along different directions. The GDL ideally consists of cylindrical fibres and due to the orientation of the carbon fibres, the GDL has an anisotropic structure. This means that the GDL exhibits strong anisotropic properties, that is, permeability, mass diffusivity, thermal conductivity, and electrical conductivity.

Previously researchers have assumed an isotropic structure for the GDL, and this has led to over-estimation in cell performance. One such isotropic model of a GDL exhibited a current density of approximately 10% greater and an operating cell voltage of 0.3 V higher than the anisotropic model [34]. More recently research has been on the effect of anisotropic properties on the transport characteristics of GDLs [11, 35-38]. The three-dimensional, two-phase fuel cell models developed by Wu et al. [39] and Yang et al. [40] were highly influential as they considered the anisotropic structure of the GDL in their analysis of thermal and water transport. Their models have been adopted by Li et

al. [34] who compared the predicted oxygen mass fraction, temperature, liquid water saturation, water content, and local current density from isotropic and anisotropic models. Their results showed that the current density and the overall cell performance are exaggerated in the isotropic case. Recently X-ray imaging techniques have provided strong insights into the antistrophic structure of the GDL as it enables the visualisation of the fibrous structure of the porous media [41-43].

Porosity

The porosity of a material is a measure of the void space of the material. The GDL is a highly porous structure, and typically commercial GDLs have a porosity between 40-90% [44]. The dual-layer GDL consists of a highly porous carbon substrate (for structural support, electron transfer and mass transport) and a thin microporous layer (MPL) which is in contact with the catalyst layer. The bulk porosity ($\varepsilon(x)$) of the GDL can be determined from the ratio of the void space volume over the total volume, solid volume, and void volume.

$$\varepsilon(x) = \frac{\text{Void Volume}}{\text{Solid volume} + \text{Void Volume}} \tag{2.1}$$

As discussed previously, the pore sizes of the GDL range from micropores, of a few nanometres in diameter, to macropores which measure several micrometres in diameter. The pores of the GDL are also classed by their accessibility; open pores are accessible from the outside of the material, whereas closed pores are characterised by their inaccessibility from the outside. A common problem in the modelling of gas diffusion layers is the assumption of homogenous porosity profiles which are heterogeneous [45]. This assumption of homogenous porosity has led to an incorrect characterisation of the transportation properties based on an idealised structure[46].

Experimental procedures and imaging techniques have been successfully used to understand the bulk porosity of the GDL. Of the experimental methods, the Brunauer-Emmett-Teller (BET) measurements and the mercury intrusion porosimetry (MIP) have been widely used. MIP is a commonly used technique to measure the bulk porosity of the GDL; a mercury pore analyser is used to measure the

mercury intrusion into the pores of the porous media as a function of the pressure applied. MIP measurements are based on the Washburn equation which relates the pressure of the gas to the pore size; the pressure needed to enable mercury intrusion is related to the pore diameter. MIP has been used successfully to determine the pore size distribution in GDLs [47]. X-ray CT is a non-destructive technique that allows imaging of the internal structure of a material, and the phase segmentation of the images produced has led to the determination of the porosity of the GDL using this technique. Büchi et al. [45] used X-ray CT where they were the first to show the heterogeneous profile of the GDL porosity by the determination of the porosity and pore size distributions in the through-plane direction. Wargo et al. [46] investigated the GDL microstructure using a combination of FIB-SEM and X-ray CT to obtain an estimation of the bulk porosity value of the GDL and MPL, however, their automated segmentation did not define a precise value. A combination of MIP measurements and X-ray CT imaging has been used by several researchers [48, 49]. Malik et al. [48] used a combination of MIP with X-ray computed tomography to visualise the nano-pore structure of the cathode side catalyst layer whereas [49] used the bulk porosity obtained from MIP to find a threshold value for the X-ray CT image reconstruction of a TGP-H-120 GDL.

Pore Size Distribution

As previously addressed in the porosity discussion, the GDL is comprised of pores of differing sizes: macropores, mesopores and micropores. The distribution of these varying pore sizes through the porous media is termed the pore size distribution (PSD). The variation in pore sizes, their distribution and accessibility are essential factors in determining the characteristics and performance of porous media [50], particularly in terms of reactant and water transport. Fig. 2.1 shows the pore size distributions in the carbon paper macroporous substrate (MPS) and two MPLs produced from acetylene black (AB) and Vulcan XC72 (VXC). It is evident that the pores of the MPS are distributed mainly as macropores; whereas within the MPL a sharp peak is present in the microporous region, thus indicating that the vast majority of pores in the MPL are micropores.

.

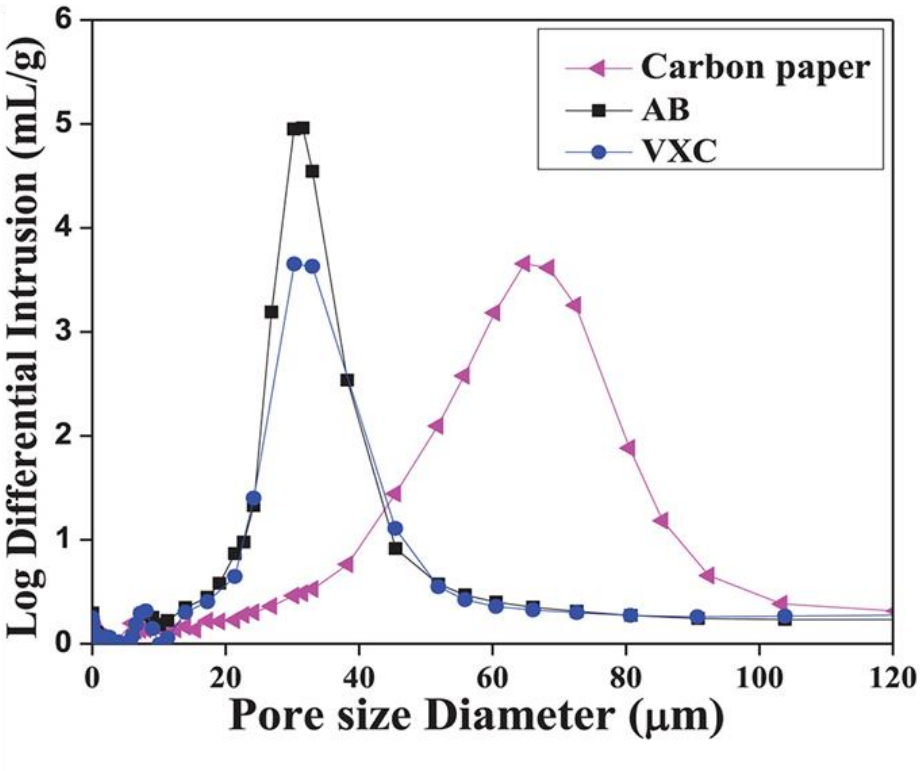

Figure 2-1: Differential pore size distributions of a carbon paper macro-porous substrate (Carbon Paper) and two different MPLs produced from acetylene black (AB) and Vulcan XC 72 (VXC) [3].

Micropores are responsible for the diffusion of gases from the flow-field channels to the catalyst layer whereas macropores are primarily responsible for the transportation of liquid water. As such the pore size distribution measurements can be used to obtain water retention curves, which are plots of capillary pressure against liquid water saturation [51]. In a hydrophobic medium, fluid invades macro-pores first as the surface tension that is needed to be overcome is less than that of the smaller pores. The fluid then progressively fills the meso and micropores. As such, knowledge of the PSD of GDL is extremely important in predicting water transport in the porous media. Experimental methods of measuring PSD in the porous media of GDLs include mercury intrusion porosimetry (MIP) and standard porosimetry (MSP). The most widely used method for measuring pore size distribution of PEMFC GDLs is mercury intrusion porosimetry (MIP) [44, 47, 52]. This technique is frequently used to measure the distribution of accessible pore volume by entry pressure for pores between 1 nm and 1 mm; where a sample is

submerged in mercury and the capillary pressure is increased until the micro-pores of the sample are filled. Based on the Washburn Equation, the capillary pressure used along with the volume can be used to obtain the pore size distribution as follows[53]:

$$\mathrm{P_c} = 2\sigma \cos \theta \mathrm{r} \tag{2.2}$$

where P_c is the capillary pressure (MPa), σ is the mercury interfacial tension (N/mand), θ is the contact angle between the liquid and the pore surface (°), and r is the pore radius (μm).

The use of MIP to measure the PSD of a porous media has limitations, one of which is the "necking effect", in which a void behind a neck is mistaken for a narrow pore [43]. Others have observed that MIP measurements depend on the accessibility of the pores [54] and that the results of MIP are highly subjective to the input parameters used, such as mercury surface tension, which varies with mercury porosity and the value of the assumed contact angle [55]. Standard porosimetry (MSP) differs from MIP as it operates using a wetting fluid, rather than a non-wetting fluid, where the most common wetting liquid is octane. Gostick et al. [51] compared the results obtained from MIP and MSP measurements with the manufacturer's measurements; they found good agreement between their measured data and the manufacturer's. Moreover, Gostick et al. [51] highlighted the potential of MSP for the study of GDL pore distribution in particular as it can be used to differentiate the hydrophilic porosity from the hydrophobic porosity. Thus, MSP holds greater potential for analysing the effect of differing pores on liquid water and gaseous transport.

Zamel et al. [56] observed a reduction in overall porosity with PTFE loading and significant changes in pore size distribution; micropores of the GDL were found to be unaffected by increased PTFE content whereas macropore diameter was greatly reduced by the addition of PTFE. Chen et al. [57] modeled the PSD of GDLs treated with 10, 20, and 30% wt. PTFE. They observed that the greatest reduction in pore volume occurred in pores of ~30 μm in size. Moreover, they found that the greatest uniformity in pore sizes occurred at that at 20% wt. PTFE. Experimental visualisations such as X-ray CT and SEM have been used to great effect to quantify the PSD of the GDL [43, 58-60]. More recently a combination of visualisation techniques and measured values have been used for accurate PSD measurements. A combination of SEM imaging and MIP measurements have been used by various research groups to

quantify the PSD of the GDL substrate in order to investigate how MPL penetration varies with local pore size profiles [61] and the effect of PTFE on pore size and cell performance [62]. The combination of PSD distribution measurements and SEM has allowed for an increased understanding of the importance of surface morphology of the MPL and the GDL on permeability and liquid water transport.

Tortuosity

Tortuosity is defined as the ratio of the actual path mean length (l_a) divided by the thickness (l) of the porous medium in the direction of gas diffusion [63]. The term is commonly used to describe gas diffusion in a porous medium. As such tortuosity can be used to quantify the porous structure inside the PEMFC gas diffusion layers and this plays a large role in their micro-structural analysis. Furthermore, it is linked to the porosity of the material (ε) and the effective gas diffusivity (D^{eff}) by the following relationship:

$$\tau = \frac{\varepsilon \times D}{D^{eff}} \tag{2.3}$$

where τ is the tortuosity, D is the gas free space diffusivity, ε is the porosity and D^{eff} is the effective gas diffusivity [64]. The Bruggeman relation attempts to define the tortuosity as only a function of the porosity alone, as can be seen as follows:

$$\tau = \varepsilon^{-0.5} \quad \text{or} \quad f(\varepsilon) = \varepsilon^{1.5} \tag{2.4}$$

This has been proven as a valid approximation for large materials, however, it has been regarded as inappropriate due to the porous media of the gas diffusion layers of PEMFC as it is based on packed spherical fibres. Instead, the Tomadakis and Sotirchos model was proposed for randomly orientated media is far more applicable to gas diffusion media [65]. The validity of the Tomadakis and Sotirchos model for paper and felt GDL materials has been shown by various numerical [66, 67] and experimental investigations [51].

Fishman and Bazylak [66] used heterogeneous porosity distributions obtained from X-ray CT to calculate the local distributions of tortuosity in PEM GDLs. Espinoza et al. [68] generated a 2D model and used the Lattice Boltzmann method to compute the gas-phase tortuosity in an artificially generated

GDL; their work, although in 2 dimensions, showed good agreement with experimental data reported by Gostick et al. [51]. Usually, the through-plane tortuosity is about a factor of 2 to 3 larger than the in-plane for commercial GDLs with carbonaceous binder [63].

Contact Angle/ Hydrophobicity

It is important that the GDL has a degree of hydrophobicity by which it is able to remove the liquid water produced from the cathode catalyst reaction. This is particularly a problem at higher current densities where greater volumes of liquid water are produced. In order to increase the hydrophobicity of the GDL, it is treated with a hydrophobic, or wet-proofing agent, this is typically PTFE or FEP. GDLs which are untreated with a hydrophobic agent have a much higher risk of flooding than uncoated GDLs [34, 61]. As the hydrophobic treatment has adverse effects on the electrical conductivity and permeability of the GDL, its presence in the GDL should be optimised so that cell performance is neither limited by excess nor inadequate wetting.

The hydrophobicity of a material can be characterised by what is known as the contact angle. The contact angle is the angle (θ) between the solid phase and the interface between the two fluids, as demonstrated in Fig. 2.2. If the two fluids are water and air then the substance is considered hydrophilic if the angle measured is $< 90^{\circ}$, conversely if this angle is $> 90^{\circ}$ it is hydrophobic (Fig. 2.2 (a)). Fig 2.2(b) is on the cusp of hydrophobicity with a contact angle of 96°. Carbon is considered a hydrophilic material as the contact angle for water on a carbon surface is about 80°, whereas PTFE is hydrophobic as the contact angle is measured at approximately 110° on a flat surface [69]. The internal contact angle of GDL materials was reported to vary between 88° and 101° depending on the material. This seems reasonable as a range between the angles of carbon and PTFE [70].

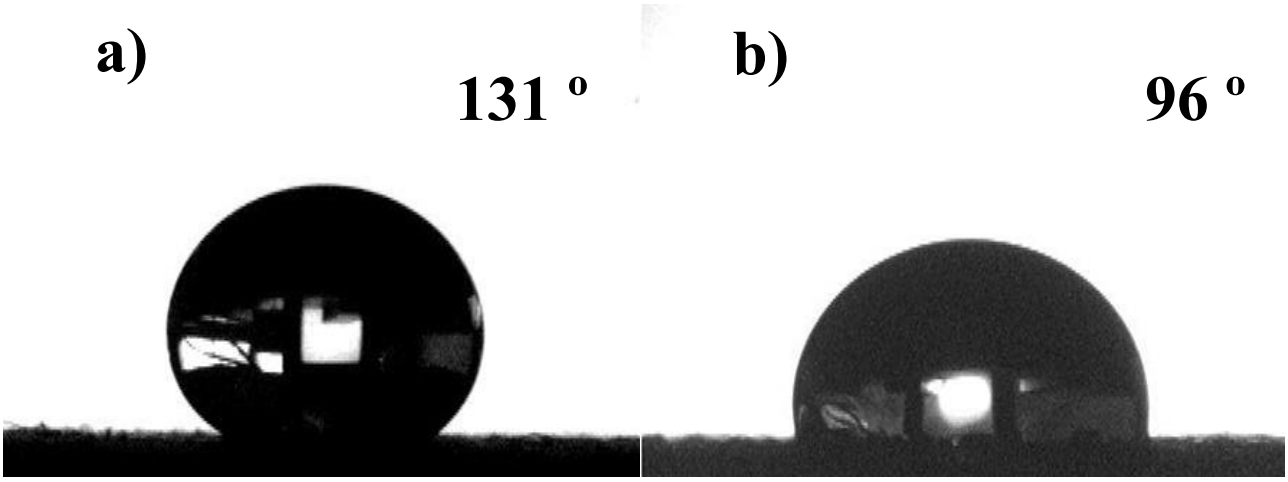

Figure 2-2: Water droplets on the surface of a titanium gas diffusion layer, (b) shows the increased hydrophobicity from treatment with a hydrophilic coating [10].

The hydrophobicity of a GDL is highly important for water transport, especially for materials on the cusp of hydrophobicity, about 90˚ [69]. For very hydrophilic GDLs with contact angles of less than 90˚ capillary wicking is the dominant method of water transport, and for contact angles greater than 100˚ then a compact pattern characterised by a flat invasion front is observed. It is widely acknowledged that super-hydrophobic GDLs (contact angle >150˚) are the most effective for reducing the saturation of the porous media. In doing so this reduces mass transport losses which results in a higher voltage at high current densities and therefore an increased maximum power density. The treatment of the GDL with PTFE is found to generally decrease the porosity and the tortuosity of the GDL [44]; this reduction in porosity is caused by the blocking of the pores, where the tortuosity is effected by the blocking of closed and longer pores. This change in GDL structure has led to the various studies on the detrimental effect of PTFE treatment on the transport properties of the GDL i.e. electrical conductivity, thermal conductivity [4] and permeability [8, 44].

Generally, PTFE adversely affects the permeability and conductivity of the GDL; however, it has emerged that the relationship between PTFE content and transport properties of the GDL is not clear. El-Kharouf et al. [44] conducted ex-situ characterisation tests on a variety of Toray and Sigracet GDLs treated with PTFE. They found that PTFE increased the permeability of some GDLs and decreased it

for others; the increased permeability was attributed to the reduction in tortuosity whereas the reduction in permeability was caused by the loss of porosity and increased GDL thickness.

As PTFE is an insulator, it has a negative effect on the conductivity of the GDL. Alhzami et al. [71] found that in-plane thermal conductivity decreases with PTFE content in the GDL whereas Velayutham et al. [72] used cyclic voltammetry to confirm that the addition of PTFE to the GDL substrate reduces the thermal and electrical conductivity. However, they did not compare the in-plane and through plane conductivities. Ismail et al. [8] found that the in-plane conductivity of the GDL is unaffected by PTFE loading, whereas the PTFE content was a major contributing factor to through-plane conductivity. This is due to the carbonaceous structure of the fibres being unaltered by the PTFE in the in-plane direction.

In order to balance the benefits and limitations of PTFE treatment some research groups have attempted to optimise the PTFE treatment of the GDL. Chen et al. [73] treated commercial carbon fibre GDL substrates with various percentages of PTFE (0, 10, 20, and 30%), they observed that the highest maximum power output generated (1.003 W cm^{-2}) was with the GDL treated with 10% wt. PTFE. Su et al. [74] similarly found that minimal quantities (15% wt.) of PTFE in the GDL exhibited the greatest power density in their single cell tests.

Some research groups have branched out into alternative non-wetting agents in order to address the detrimental effects of PTFE on permeability and conductivity. Of which research conducted by Latorrata et al. [75] is insightful as a comparison of the alternatives to PTFE. The use of ex-situ characterisation tests alongside in-situ power measurements indicated that low transfer resistance and high contact angle are important characteristics when comparing the treated GDLs. However, more work can be done on these materials, particularly an experimental comparison of their application in MPL. The majority of studies on the hydrophobicity still focus on improvements that can be achieved whilst using PTFE as the non-wetting agent.

2.1.2 Transport Properties of Porous Media

Gas Permeability

Permeability is the ability of a porous material to allow fluid through its pores as such permeability of a porous medium is extremely influential in determining the fluid flow rate through the pores. A high GDL permeability is important as it allows for more reactant gases to flow to the catalyst layer, additionally it allows water produced at the catalyst layer to be directed to the fluid flow channels to prevent electrode flooding. Low permeability increases the reactant transport resistances and creates a higher pressure gradient, it increases the necessary power input to maintain the flow rate of the reactant gases. Thus, the gas permeability of the GDL is a critical factor when considering reactant transport, water management and effectively the overall cell performance in PEMFCs.

The coefficient of gas permeability is usually measured experimentally according to Darcy's law by measuring the pressure drop at specific flow rates across the sample [76-78]. Darcy's law is an approximation of the Navier-Stokes equation, which is valid for only laminar flow rates, where the velocity of flow can be assumed to be Stokes flow. At high-velocity, non-Stokes flow occurs and the Forchheimer term is used as it takes into account the inertial effects of the flow. At the low Reynold's number flows in PEMFC and porous media, the inertial effect is minimal and so Darcy's Law can be used.

Darcy's Law states that the flow rate through a porous body is equal to the product of the permeability and the pressure gradient across the porous body, divided by the viscosity of the fluid. It is calculated as follows [51]:

$$v = \frac{k}{\mu}\frac{\Delta P}{\Delta x} \tag{2.4}$$

where, v is the velocity of the fluid passing through the porous media [m s^{-1}], k is the permeability (m^2), Δx is the thickness of the layer (m) and μ is the viscosity of the fluid flowing through the porous medium (Pa s) and ΔP is the pressure difference across the layer (Pa).

From previous experimental data, the gas permeability of the carbon paper/cloth GDL is in the range of $6–70\times10^{-12}$ m^2 [76-78]. Zhao et al. [79] provide a good summary of the reported gas permeability

measurements of GDLs and previous experimental work. Permeability has a well correlated increase with porosity; Gostick et al. [51] measured the in-plane and through-plane permeabilities of carbon GDLs. They were able to show the anisotropy of the in-plane direction from measuring the permeability in different perpendicular directions of the in-plane where they found that that the in-plane permeability differed greatly. Moreover, they reported higher permeability coefficients in the in-plane than the through-plane; this is in agreement with Ihonen et al. [80] who reported that the in-plane permeability was twice as high as the through-plane. Typically, the in-plane permeability is higher than the through-plane permeability based on the preferential orientation of the carbon fibres. Gostick et al. [51] used the Carman–Kozeny equation in order to predict the permeability from the porosity, fibre diameter (d_f) and the Carman–Kozeny constant (K_{CK}), which depends on the type of media used. They defined different values of K_{CK} depending on the alignment and the arrangement of the fibres. Despite the structural differences of the GDLs, the measured permeability was found to have a strong dependence on porosity which was well described by their Carman–Kozeny model and their measured data.

Tomadakis and Sotirchos developed a comprehensive model for the permeability of fibrous media which allows for the prediction of anisotropic permeability through random fibre beds [65]. Their models have been applied to the GDL structure to predict the gas permeability [66]. Holzer et al. [59] found that the non-linear relationship between permeability and porosity are well described using the Tomadakis-Sotirchos model for fibrous media. Whereas Zamel et al. [76] found that Tomadakis and Sotirchos model over predicted the observed measurements. Simulations using the Lattice-Boltzmann models and Computational Fluid Dynamics have also been used effectively to predict the gas permeability, some of which have been less effective as they do not use local porosity profiles, and therefore validity of some models are not accurate**.** A two-phase model, developed by Hossain et al. [81] simulated the effect of anisotropic permeability on PEMFC performance. They found that the permeabilities should be high in both the in-plane and through-plane directions for high cell performance. Moreover, their simulations showed that high in-plane permeability is more critical to cell performance than high through-plane permeability. This is a point of contention as other researchers [66] argue the importance of a high through-plane permeability on cell performance. Rama et al. [36]

used the Lattice Boltzman method to simulate gas transport from 3-dimensional structures obtained from μX-ray CT, and they reported strong agreement between the LB model and measured data. Fishman and Bazylak [66] used X-ray computed tomography visualisations of the GDL micro-structure and Lattice-Boltzmann simulations in order to confirm the validity of applying the Tomadakis and Sotirchos equation to calculate the single phase permeability in random fibrous and porous media, they found a generally good agreement between the measured values and the model. However, the agreement was much better in the in the felt GDL rather than the paper.

The effect of a microporous layer and PTFE loading on the permeability of the GDL has been studied. Ismail et al. [8] measured the through-plane permeability for treated and untreated GDLs, they reported an optimum through-plane permeability at 5 wt.% PTFE. Prassanna et al. [82] investigated the through-plane permeability of GDL samples of 10-40% PTFE, their results indicated that permeability decreases with increasing PTFE loading [82]. A detailed study by Orogbemi et al. [83] experimentally investigated the effect of the MPL on gas permeability of the GDL; they measured gas permeability for GDLs with MPLs of 30 different compositions, finding that gas permeability was the lowest at 20% PTFE loading in the MPL. Gas permeability was shown to decrease with the addition of a microporous layer [83]. Williams et al. [84] measured the nitrogen flow through uncoated and MPL-coated GDL substrates in the through-plane direction. They also observed a substantial decrease in the through-plane permeability with the MPL-coated GDL.

Effective Diffusivity

The slow oxygen reduction reaction in the polymer electrolyte membrane fuel cell is one of the main limitations to its performance [85, 86]; it is influenced by the kinetics of the catalytic reaction and the oxygen concentration at the catalyst. The concentration of oxygen at the reaction site is dictated by the ease of oxygen transport from the gas flow fields to the catalyst later. At high current densities of peak operation, oxygen consumption at the catalyst becomes greater and therefore the oxygen concentration decreases, and when the oxygen is depleted then the current limiting density is reached. Therefore, oxygen transport is fundamental to maintaining and enhancing the power density of PEMFC [87, 88].

As the gas permeability of commercial GDLs is relatively low, diffusion is the dominant mode of oxygen transport in these layers. The effective relative diffusivity is an important material constant as it characterises the resistance of the porous media to the diffusive flow of oxygen. Typically, the diffusivity of the gas-phase flow through a porous medium (D_{eff}) is defined using Fick's law to account for the solid-phase obstacles, porosity, and tortuosity. Solid obstacles reduce the effective area for the flux and increase the length of diffusion pathways; it is usually defined by the following expression:

$$D_{eff} = f(\varepsilon)g(S)D \tag{2.5}$$

where, D_{eff} is the effective bulk gas-phase diffusivity, D is the diffusivity, ε is the porosity and S is the saturation of liquid water, and $f(\varepsilon)$ and $g(S)$ are the relative functions of porosity and liquid saturation [56]. Focusing on the structural and morphological effects of the GDL on the gas diffusivity, the effect of water saturation can be negated. Thus $g(S)$ is set to unity, and water is only regarded in the vapour state [6]. Thus equation 2.5 becomes:

$$D_{eff} = f(\varepsilon)D \tag{2.6}$$

The literature on the gas diffusivity in PEMFC gas diffusion layers is expansive, where multiple experimental and numerical studies have been undertaken. These have provided valuable insights into the understanding of gas diffusivity in GDLs; gas diffusivity has been shown to be anisotropic and dominant in the in-plane direction due to the fibre orientation [60]. Rashapov et al. [89] conducted various measurements on the in-plane diffusivity as a function of compression and PTFE loading, and they found that the diffusivity decreased due to an increase in tortuosity. Through-plane diffusivity has been the focus of experimental studies, as reactant and product diffusion in a fuel cell is directed in this direction [90, 91].

Experimentally the effective diffusivity of the GDLs has been measured as part of the whole fuel cell in operando using X-ray synchrotron imaging [92]. Other groups have used ex-situ electrochemical methods, such as: electrochemical diffusimetry which uses the relationship between Ohm's and Fick's Law, [93, 94] the limiting current density technique [90] and a diffusion bridge [95, 96]. Koresawa and Utaka [97] obtained effective oxygen diffusivity measurements of a GDL using a galvanic cell oxygen

absorber, these were then validated using ANSYS fluent. Numerical models have been used to the solve gas effective diffusivity using pore networks [98] and stochastic models [63, 99]. Ismail et al. [6] found that the use of the Bruggeman relation significantly overestimates the gas diffusivity of the GDL by a factor of 2 or greater.

Recently reconstructed X-ray CT and FIB-SEM images have been used to obtain the GDL geometry from which the gas diffusivity was modelled numerically [60, 100]. X-ray CT was used to reconstruct GDL geometry to calculate the effective oxygen diffusion in the porous media under varying degrees of compression [49]. Froning et al. [101] also investigated the effects of compression on gas transport in the GDL using geometry from X-ray CT although using a Lattice-Boltzmann method. The effective oxygen diffusion obtained was shown to be reduced with increased compression, due to reduced porosity; this is in agreement with Zhou et al. [102], who reported that at higher rates of compression, the porosity of the GDL decreases which leads to an increase of in the gas transport resistance, thus limiting PEMFC efficiency. Therefore, an optimum compression of the GDL needs to be achieved to balance oxygen diffusivity, and electrical and thermal conductivity which are improved with compression. This is addressed at length in a recent paper by Hasanpour et al. [42].

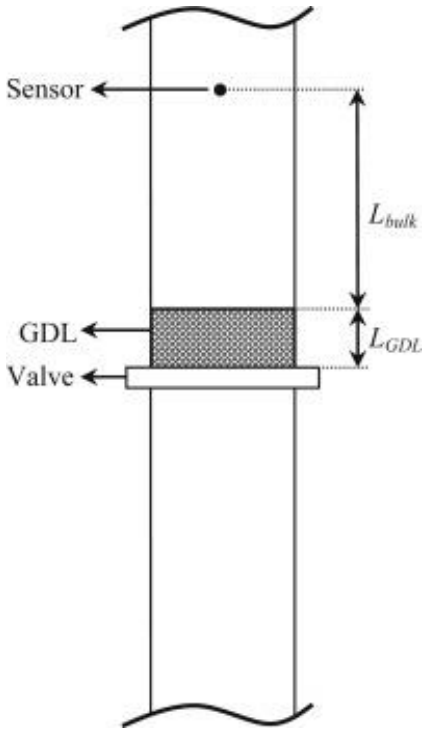

Figure 2-3: Loschmidt diffusion cell for measuring gas diffusivity. Two different gases are placed in the top and bottom chambers with the GDL in the middle. The change in concentration of the gas in the bottom chamber shows the effective diffusivity of the materials [6].

The effect of liquid water saturation on the effective oxygen diffusivity has been a focal point of a number of recent research groups [60, 78, 90, 100, 103]. At low-relative humidity, oxygen transport resistance across the GDL is high and contributes 32-61% the of total oxygen transport resistance in PEMFC. Conversely liquid water accumulation at the cathodic gas diffusion layer has a detrimental effect on effective oxygen diffusivity as it reduces the available pore space for oxygen transport, thus reducing cell performance. Muirhead et al. [60] found that liquid water accumulation and reduction in effective oxygen diffusivity is greater at higher current densities. Power losses at high current densities are widely attributed to reduced reactant transport due to pore saturation by the generated liquid water.

To observe the effect of liquid water saturation on oxygen transport, García-Salaberri et al. [100] calculated the effective diffusivity of a gas layer by performing Lattice Boltzmann simulations on reconstructions from X-ray computed tomography. They compared the gas diffusivity of saturated and dry GDLs, finding that the dry values matched those of previously observed data. Gas transportation resistance was greatly influenced by local saturation distribution, furthermore this was found to be more

influential in the through-plane, where through-plane gas diffusion was extremely limited in materials with high saturation and noticeably reduced with slight saturation.

Hossain et al. [78] used a two-phase CFD model to investigate the best means of modelling the effect of liquid water on effective gas diffusivity. They found that the power law model with an exponential factor of 2 has a good representation of species diffusivity that match the experimental cell voltages.

Thermal Conductivity

The thermal conductivity of a GDL depends on its morphological properties (porosity, tortuosity, wettability); it is an important contributor for fuel cell performance as ineffective thermal management can lead to a reduction in fuel cell lifetime. Isolated regions of heat can cause hot spot formation, localised drying and this can lead to membrane pinhole formation, whereas thermal cycling increases component stress and degrades the fuel cell material [104].

Most of the heat is generated in the MEA and this is due to the inefficient oxygen reduction reaction at the cathode catalyst layer where reaction charges overcoming the over-potential generates heat [105]. The production of waste heat and the correct thermal management is a critical limitation of PEMFC technology as excess heat generated limits the efficiency of PEM fuel cells to around 50% [104]. For PEMFC with no active cooling, heat is conducted away from the MEA by the GDL, hence a good thermal conductivity is an important property of a GDL.

Fourier's law of conduction can be used to calculate the rate of heat transferred by conduction in the GDL. It is proportional to temperature change (dT) and related by the following:

$$Q_x = -kA\,\frac{dT}{dx} \tag{2.7}$$

where, k is the thermal conductivity ($Wm^{-1}k^{-1}$) and A is the finite cross-sectional area. It is generally accepted that thermal conductivity decreases with the increase in the porosity, as heat is conducted through the carbon fibres of the material. This means that the thermal conductivity of a GDL is heavily influenced by fibre orientation and periodicity. Different carbon substrates have different thermal conductivities; carbon paper has no periodicity as the fibres are random whereas carbon cloth is a uniform woven material that has regular spaces where no fibres are present [106]. Sadeghifar [107]

presented a model that uses fibre spacing instead of porosity to calculate the thermal conductivity of gas diffusion layers, their predictions show that porosity-based models either over or underestimate the true thermal conductivity of the porous structure.

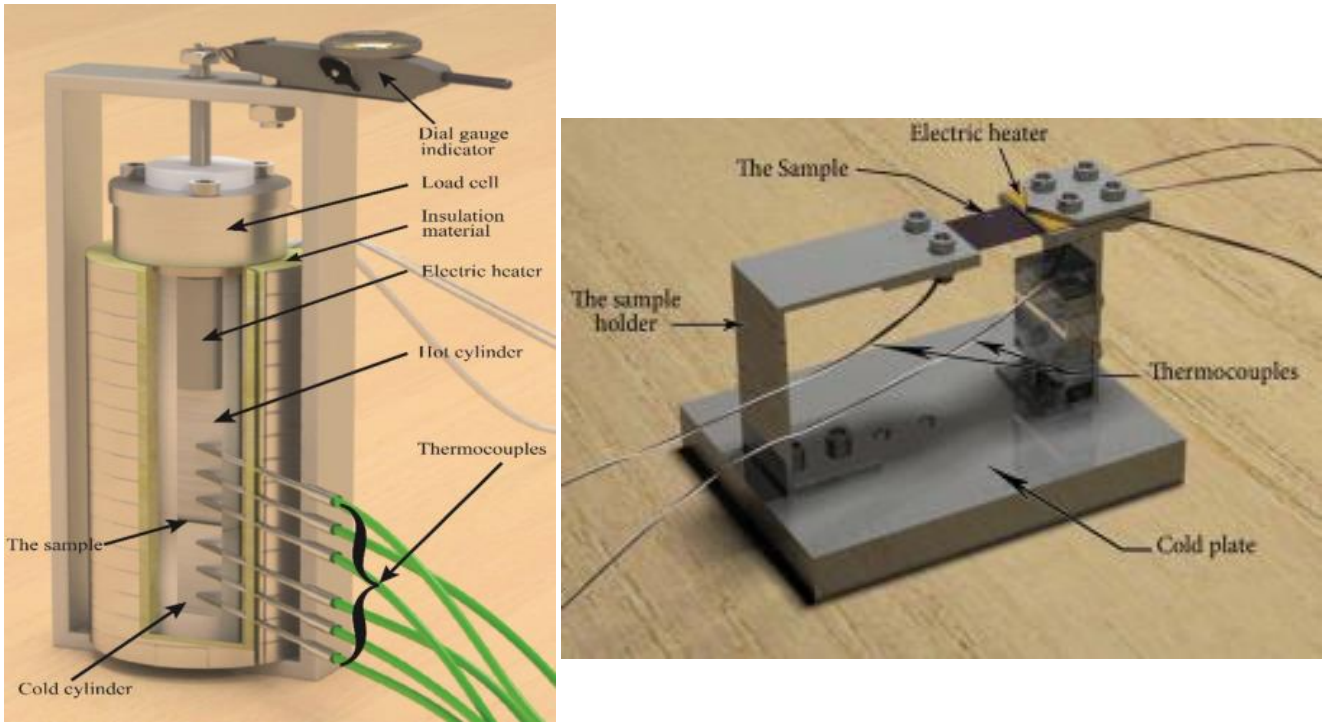

Figure 2-4: The experimental set-ups to measure the through-plane (top) and in-plane (bottom) thermal conductivities of the GDL [4].

Experimentally derived measurements along with numerical models for the thermal conductivity have been reported in the literature. Xu et al. [108] and Burheim et al. [109] found that the thermal conductivity gradually increases with liquid water content. This is attributed to liquid water attaching to the hydrophilic matrix and existing preferentially at the fibre joints which decreases the local thermal resistance, additionally water bridges the thermal contact between the carbon fibres [105].

Similarly the PTFE loading of the GDL is highly influential on its thermal conductivity; as such it has received much research attention in the in-plane [76, 107], and through-plane directions [109, 110]. Burheim et al. [109] investigated the through-plane thermal conductivities and thermal contact resistance of commercial GDLs with different PTFE contents. They found an increased amount of PTFE

in the GDL results in a slight reduction in the through-plane thermal conductivity of the GDL. This agrees with a model created by Yablecki and Bazylak [111] and Fishman and Bazylak [66] who predicted that PTFE leads to a decrease in thermal conductivity in the through-plane. In the through-plane, heat transfer is from fibre to fibre and the PTFE insulates carbon fibres from one another as it has a much lower thermal conductivity than the carbon fibres. Thus, the through-plane thermal conductivity is decreased with PTFE loading. Whereas in the in-plane direction heat is transferred along the fibres, and the addition of PTFE reduces the contact resistance between the fibres and increases conductivity [112].

The effect of compression on the thermal conductivity of GDLs has been researched by several research groups [113, 114]. Karimi et al. [113] experimentally derived the effect of compression onthe through-plane thermal conductivity and thermal contact resistance of a SpectraCarb uncoated GDL. Chowdhury et al. [115] measured the effect of inhomogeneous compression on the thermal conductivity by subjecting Toray carbon paper GDLs to various degrees of compression (0.34 to 1.71 MPa). The thermal conductivity was shown to increase non-linearly with compression as the increase in microscopic contact area between the carbon fibres is increased. Their results show the importance of replicating typical operating conditions where the compression is inhomogeneous, as the homogenous compression resulted in higher thermal conductivities.

The anisotropic nature of the GDL fibres means that early computational models of the thermal conductivity were oversimplified. Recently antistrophic models have been used to more accurately predict the thermal conductivity. Yablecki et al. [111] used a two and three dimensional two-phase Lattice Boltzmann to show that the antistrophic morphology of the GDL results in anisotropic thermal conductivity, where the in-plane thermal conductivity was greater than the through-plane thermal conductivity. This conclusion matches those found by Pfrang et al. [106] who used X-ray CT GDL reconstructions to compare the in-plane and through-plane conductivities of the GDLs. The through-plane had a significantly lower thermal conductivity than the in-plane, due to fibre orientation being more aligned in the in-plane direction.

Electrical Conductivity

The GDL is made up of densely packed carbon fibres that act as a route for lateral electron transport for current collection. The capacity of the GDL to transport electrons is therefore dictated by the carbon fibre structure, and this can be measured from the in-plane, through-plane and contact resistance tests. The transport of electrons depends on the electrical conductivity, thickness, porosity, and heterogeneous anisotropic structure of the GDL; it has been the subject of several research papers.

The Van der Pauw method is commonly used to measure the in-plane conductivity of the GDL by applying four probes to measure the in-plane electrical resistance. Two adjacent probes are used to apply a current whilst the two probes are used to measure the electrical potential [116]. This method measures the electrical resistivity (ρ) of the GDL material which can be calculated by the following equation:

$$\rho = G \cdot \frac{\Delta V}{I} \tag{2.8}$$

where, G is the geometrical factor, ΔV is the potential difference and I is the applied current.

The PTFE content has been shown to have a positive effect on the through-plane conductivity of the GDL. Mathias et al. [32] observed the effect of PTFE loading on the through-plane contact resistance. They found when the GDL was treated with 3.5% PTFE then the electrical conductivity of the GDL increased. Ismail et al. [117] analysed the effect of PTFE loading on the through-plane and in-plane electrical conductivities of the GDL. They found that the in-plane conductivity increases almost constantly with PTFE loading. Moreover, their work went further into the anisotropy of the in-plane by measuring samples in two in-plane directions. The reported measurements were different by a factor of 2 which indicates a high degree of anisotropy of the in-plane direction.

Aydin et al. [118] addressed the challenges associated with measurements of the electrical conductivity of the GDL; they used 3 variations of the Van der Pauw four-point-probe technique to measure the through-plane resistance of Toray TGP-H 120 and SGL 10 BA GDLs. Their results indicated that there is an inherent electrical contact resistance between the electrode and the GDL, thus measurement of the GDL electrical conductivity should be taken on the sample surface using micro-wires. The significance

of determining the electrical resistance of the isolated GDL has been challenged by Zhou et al. [102] who found that when using realistic electrical conductivities the through-plane and in-plane resistances of the GDL have little effect on the current density and the overall cell performance. They developed a three dimensional fuel cell model which incorporated electron transport to determine the effect of the GDL resistivity on current density distribution. Their model showed that the interfacial contact resistance between the GDL and the catalyst layer, and the GDL and the flow-field plates has a more pronounced effect on overall cell performance than that of the GDL itself. Nitta et al. [114] found that non-uniform compression of the GDL promotes an uneven current distribution across the MEA and this affects the contact resistance between the GDL and the flow-field plates.

The addition of an MPL to the GDL at the flow field interface has been shown to reduce the electrical contact resistance between the GDL and flow-field plates as the compressibility of the MPL allows them to occupy the spaces that exist in the field-flow plates, thus establishing good contact between them and the GDL [11]. Ismail et al.'s research also showed that the addition of an MPL layer reduced the above contact resistance due to the conductivity of the carbon particles.

Whilst in operation, the GDL and MEA components need to be under sufficient pressure to reduce the electron contact resistance; however, if the rate of compression is too great then damage can be caused to the MEA. In order to simulate the operating conditions of the PEMFC, various research groups have studied the effect of compression on the electrical conductivity of gas diffusion layers [11, 116, 119-121]. Chang et al. [120] reported that the electrical contact resistance dropped from 1000 $m\Omega\ cm^2$ to 180 $m\Omega\ cm^2$ under an external clamping pressure of 2.5 bars. Mishra et al. [121] measured the contact resistances of various paper and cloth-based GDLs under differing rates of compression. El-kharouf et al. [44] studied the in-plane and the electrical contact resistance of a variety of commercial GDLs under various levels of compression. They found that the relationship between electrical contact resistance and mechanical stress is non-linear; this was also observed by El Oualid et al. [122]. Similar results were found by Hamour et al. [116], who noted that the electrical conductivity ceases to increase with compression at pressures of 8MP and greater. This plateau in electrical conductivity was attributed to the realignment of the carbon fibres under compression.

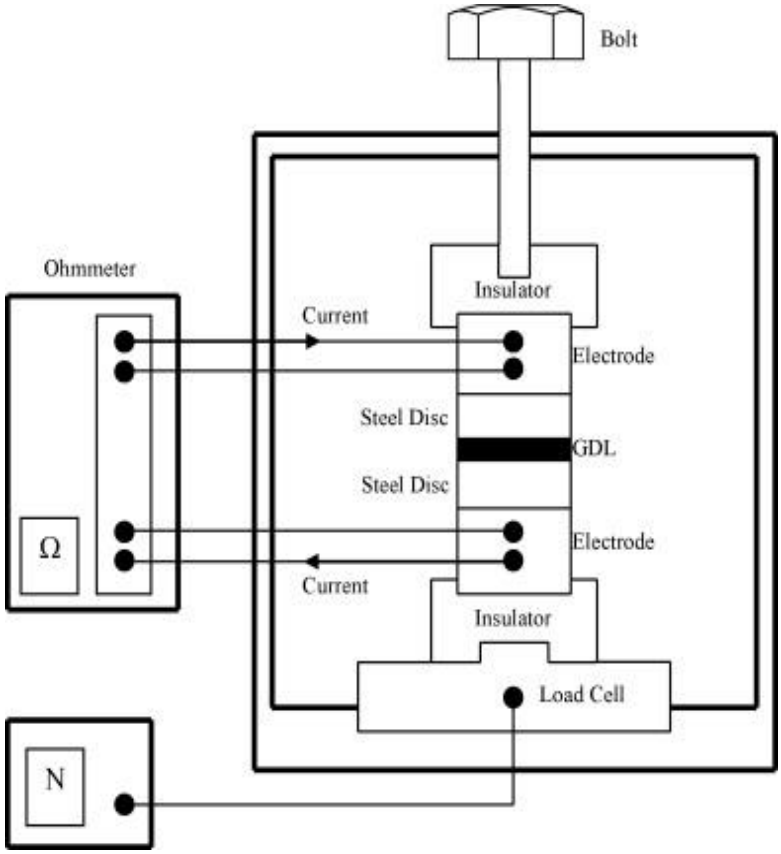

Figure 2-5: The experiment configuration for measurement of the through-plane electrical conductivities of the GDL [11].

Liquid Transport

Recently liquid water management has been one of the major topics of research in PEMFC. Correct water management is a crucial aspect of fuel cell operation as a correct balance of water needs to be maintained in the PEMFC. Liquid water needs to be present in order to minimise the ohmic losses as the polymer membrane needs to be well humidified for ionic transport [123], however excess liquid water leads to saturation of the open pores of the GDL and the catalyst which is detrimental to fuel cell performance. Saturation of the GDL pores with liquid water is known as flooding; a phenomenon that limits reactant transport to the catalyst layer and reducing electrochemical reactant activity by reactant starvation [100]. Flooding of the gas diffusion layers, and the channels has been linked to critical problems in fuel cell operation, such as mass transport over-potential [105]. An increase in liquid water content by a few milligrams per square centimetre in the GDL results has a significantly detrimental effect on cell performance [124].Thus the presence of liquid water has a significant impact on PEMFC

operation [125]. To this end extensive research has been conducted into the mechanisms of liquid water transport in the GDLs of PEMFC and various hypothesis have been made.

The main mechanism for liquid water transport in the GDL is permeation, resulting from an absolute pressure gradient. As the liquid flow in the GDL is largely due the capillary-force dominated percolation, it is driven by capillary pressure gradients [126-128]. The capillary pressure through the GDL is highly dependent on the physical porous structure, mainly the pore size distribution, as well as PTFE treatment of the GDL. The movement of liquid water through the gas diffusion layer has been theorised [67, 129-132]. A branching-type geometry was suggested by Nam and Kaviany [67], in which large streams of water act as the main route for macro-transport of water whereas smaller streams act as corridors transporting micro-droplets to macro-droplets. They theorised that water vapour condenses on the GDL fibre surfaces to produce micro-droplets which intermittently agglomerate to form large droplets followed by water flowing towards the larger pores. A similar branching mechanism for water transport was theorised by Pasaogullari and Wang [130], who hypothesized that liquid water percolated in a tree-like manner following condensation. However, Lister et al. [131] hypotheses that fingering and channelling and highly dynamic eruptive water transport processes dominated liquid water transport at the surface of the GDL and that "dead ends" exist where water transport recedes at the formation of breakthrough channels. Bazylak et al. [132] suggested that water accumulation and transport could be characterised by preferential pathways which evolve over time. Observations made by Manke et al. [133], using synchrotron X-ray radiography, showed that in some areas a capillary tree like process occur. However their imaging also found that other transport mechanisms exist such as those suggested by Lister et al. [131] and Bazylak et al. [132].

To further understand the behaviour of liquid water in PEMFC, the mechanisms for liquid water transport in the GDL have been investigated experimentally and via simulations. Early experiments were based on the GDL behaviour ex-situ. Litster et al. [134] conducted experiments using injected fluorescent dye to observe liquid water transport from the bottom of the GDL to 30 μm below the surface. They reported that water droplets emerging on the GDL surface draw the water into the GDL, and that the structure of the GDL and the gas channel affects the draining of liquid water. Although

these experiments provided significant insight to liquid water transport, they are restricted to the surface of the GDL.

The MPL is a critical component of the PEMFC for the correct management of water. The MPL is a thin hydrophobic layer that sits between the GDL and the catalyst layer; the role it plays at the anode and cathode side GDLs is highly important [104]. The MPL at the cathode side GDL helps to move the liquid water into the hydrophilic pores of the cathode back to the anode, whereas at the anode GDL, the MPL restricts water vapour transport away from the catalyst layer and therefore reduce dry out. There is a large volume of literature focused on the effect of MPL coating on liquid water transport in the GDL where it is widely accepted that uncoated GDLs are subject to high flooding [135, 136]. In-situ visualisations by Deevanhxay et al. [137] confirmed that the presence of an MPL reduced water accumulation at the GDL/ catalyst layer interface, this corresponded to high cell voltages at greater current densities (0.6-1.3A cm^{-2}). Nam et al. [129] found that the addition of an MPL layer at the catalyst and GDL interface reduced the size and saturation of water droplets on the catalyst layer interface. Oberholzer et al. [138] found that the MPL at the GDL/cathodic catalyst layer interface was more influential on the power density than at the anode catalyst interface. This is unsurprising as liquid water is generated at the cathode catalyst layer; they observed that the absence of the cathodic MPL leads to liquid water accumulation in the catalyst pores and at the catalyst layer/ GDL interface which limits the mass transport. However, they observed that for optimum voltage, an MPL should be used at both the anodic and cathodic catalyst/ GDL interfaces.

Turham et al. [139] hypothesised that MPL cracks and the interface morphology between the MPL and the GDL substrate have significant effects on the water distribution. This was confirmed by Fishmann and Bazylak [140] who observed that the cracks and holes in the MPL act as initial points of entry for water into the GDL and this means that liquid water transport is highly localised and subject to the surface morphology of the MPL, whereas uncoated GDLs have a uniform surface liquid water distribution, and this is due to the more uniform porosity profile.

Various types of computational models have been used to attempt to predict the liquid water distribution in the GDL of PEMFC. The continuum two-phase flow method, based on Darcy's Law describes the

flow and mass transport has been applied in a number of models [141, 142]. However, the accuracy of continuum models is limited due to the scarcity in the necessary measured parameters. A number of works are based on the pore-network model, which was originally developed for fluid flow through solids and rocks [143]. Their focus has been on the determination of the macroscopic two-phase properties [144], and seldom is the actual mechanism of water flowing through the GDL clarified. The applicability of such models to the micro-porous media of GDL is questionable [60]. The Lattice Boltzmann method has recently become a popular model predict the two-phase flow in porous media of PEMFC; this is due to its applicability in dealing with complex boundaries and microscopic multi-phase problems. The Lattice Boltzmann method uses the Boltzmann equations to simulate fluid and collision models and has been used effectively for a number of models to predict liquid water and gas interactions in the GDL [145-147].

Direct experimental visualisation of liquid water in the GDL using imaging techniques have greatly furthered understanding of the mechanisms for liquid water transport internally. X-ray computed tomography has been a valuable tool for observation of liquid water transport and behaviour whilst in situ and ex-situ. Early research highlighted the possibility of analysis of in-situ liquid water accumulation measurements using X-ray computed tomography, thus paving the way for potential future work. Cho and Mench [148] used ex-situ X-ray CT to observe the evaporation front of liquid water from a pre-saturated GDL. More recently Zenyuk et al. [43] measured the GDL evaporation rates in-situ and found limitations were from diffusion. Likewise, X-ray CT imaging has been able to confirm and refute previous hypotheses about liquid water behaviour in the GDL.

Research conducted by Roth et al. [149] using in-situ X-ray CT reported that the local liquid water distribution is highly dependent on the microscale substrate structure. This is supported by X-ray CT analysis by Markötter [150] which showed a strong correlation between carbon fibre orientation of the first layers of the GDL and coinciding with the liquid transport paths.

In-situ X-ray CT imaging by Eller et al. [151] visualised liquid water saturation in the GDL for 4 minutes, they reported that liquid water droplets exist in the GDL as disconnected droplets that are not connected the water pathway. However, their findings were limited by the resolution which could not

properly define the moving liquid water, and as such the scans produced were slightly blurred. Limitations exist as it is difficult to observe the dynamic behaviour of liquid water due to the resolution time. High resolution neutron imaging and synchrotron X-ray computed tomography can be used to directly measure liquid water saturation in operating fuel cells. Neutron imaging has been used effectively for in-situ experiments by research groups to: measure liquid water content in the GDL in relation to current density [152] investigate the water accumulation in the cathode GDL under the land and under the channel [153]; and compare cross-flow rates and saturation rates of Sigracet SGL 25BC and 10BC cathodic GDLs [154]. Due to the high cost associated with neutron imaging its use is restricted to a few research groups. Synchrotron X-ray tomography in particular has been effectively used by researchers for in-situ [60, 99, 151] visualisation of water saturation in an operating PEMFC. However, synchrotron X-ray tomography requires extremely specialised fuel cell design and can cause irreparable damage to fuel cell membranes. Other research groups have chosen to use synchrotron X-ray radiography as it can be used to measure liquid water behaviour at spatial resolutions between 2–10 μm [133, 155, 156] and requires minimal fuel cell design alterations and lower beam intensities [92].

The visualisation of liquid water in the GDL also provides insight into the influence of non-uniform porosity profiles on liquid water behaviour in the GDL. The ramifications of which may alter the design and production of GDLs in the future, where potentially GDL design could be tailored for effective water management [60, 85, 132].

2.2 Macroporous Substrate (MPS)

2.2.1 Conventional Carbon Fibre-based MPS

The macroporous substrate is usually the primarily component of a GDL. Carbon fibres sheets are generally used for the MPS, due to their high gas permeability, impressive strength and elasticity under compression, corrosion resistance in acidic environment, and excellent electrical conductivity [52]. They are typically formed from extruded polymer fibres such as polyaniline, which are graphitised at high temperature (i.e., < 2000˚C). The individual carbon fibres formed through this process generally have diameters of 5 to 10 μm, and the orientation of these depends on the manufacturing process [53].

The most common types of carbon fibre sheets used in GDLs are carbon cloth, carbon paper, or carbon felt. Carbon cloth typically comprises interlocking bundles of carbon fibre woven together with a regular structure (Fig. 2.6 (a)). In carbon paper, the fibres are rigid, straight, and randomly oriented (Fig. 2.6 (b)). As such, they are generally less porous compared to carbon cloth [157] and because the fibres are preferentially orientated in-plane, the microstructure is highly anisotropic. This impacts the gas transport properties, the thermal conductivity, and the electrical conductivity [158]. Meanwhile, carbon felt is made-up of spaghetti-like fibres oriented randomly (Fig. 2.6 (c)).

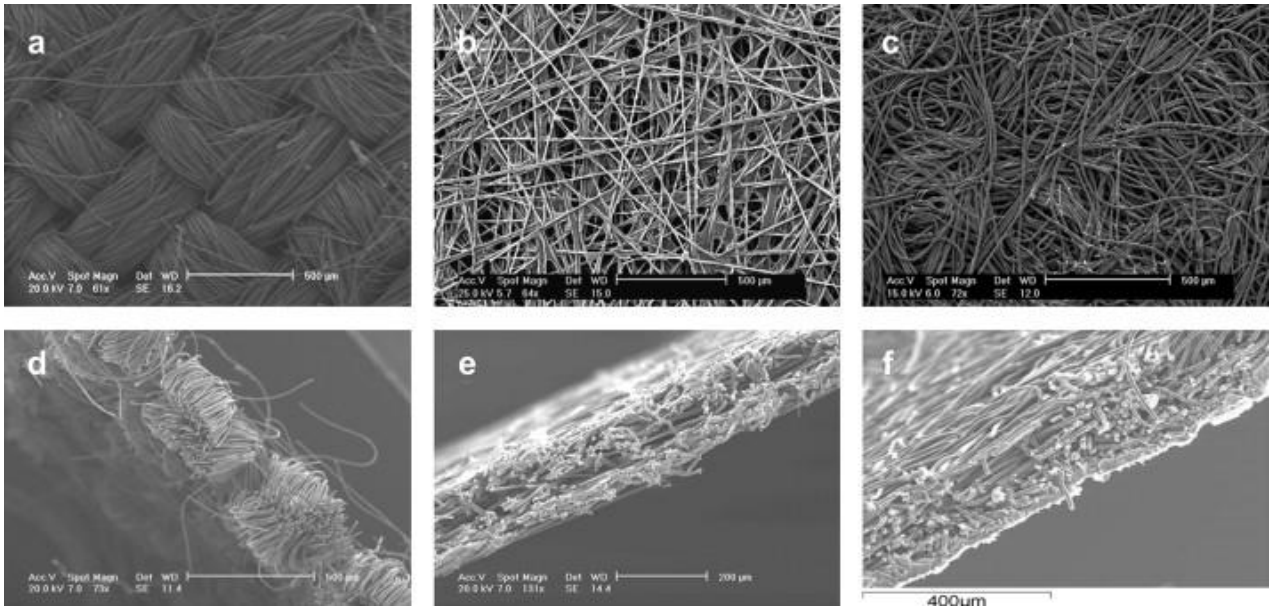

Figure 2-6: SEM images the surfaces (top row) and cross-sections (bottom row) of: (a, d) carbon cloth (Ballard 1071HCB); (b, e) carbon paper (Toray H-060); and (c,f) carbon felt (Freudenberg C2)[12].

Carbon fibre sheet porosity is normally in the range of 70 to 90%, and the density can vary from between 0.2 to 0.75 g cm^{-3} , whilst the substrate thickness can vary between e.g. 100 and 500 μm [44]. The thickness, porous structure and structural anisotropy of the carbon fibres all influence the two-phase transport properties of the resulting GDL (i.e., how the reactant gases and liquid water pass through the layer) [120, 159]. However, there is a trade-off between the gas transport properties and the electronic conductivity in GDLs, since electrons are conducted through the solid, non-porous phase of the carbon fibre sheet. As such, the structure of the substrates should be optimised to ensure adequate mass transport and sufficient electrical conductivity.

The porosity is a key factor in determining the fuel cell performance of a particular GDL. Macropores are defined as pores being over 5 μm in diameter, mesopores are defined as being between 0.07 μm and 5 μm in diameter, and micropores are defined as being less than 0.07 μm (70 nm) in diameter. In electrochemical systems, macropores are generally considered to be hydrophobic, functioning as gas transport pathways. Mesopores are considered to be both hydrophobic and hydrophilic, aiding both gas diffusion and liquid water transport. Finally, micropores are considered to be hydrophobic, helping to condense water vapour to liquid, which can subsequently be transported out of the cell [160]. The MPS is largely a macroporous component of the GDL, with larger pores designed to aid mass transport. Fig. 2.7 shows the representative pore size distribution of three different GDLs, as obtained by mercury intrusion porosimetry (MIP) which highlights the distribution of macropores [161]. A wide range of macropore diameters is observed, with prominent peaks at ~80 nm, ~1 μm, and ~40 to 70 μm. Each GDL has markedly different pore size distribution depending on the structure, as highlighted in Fig. 2.7 (b).

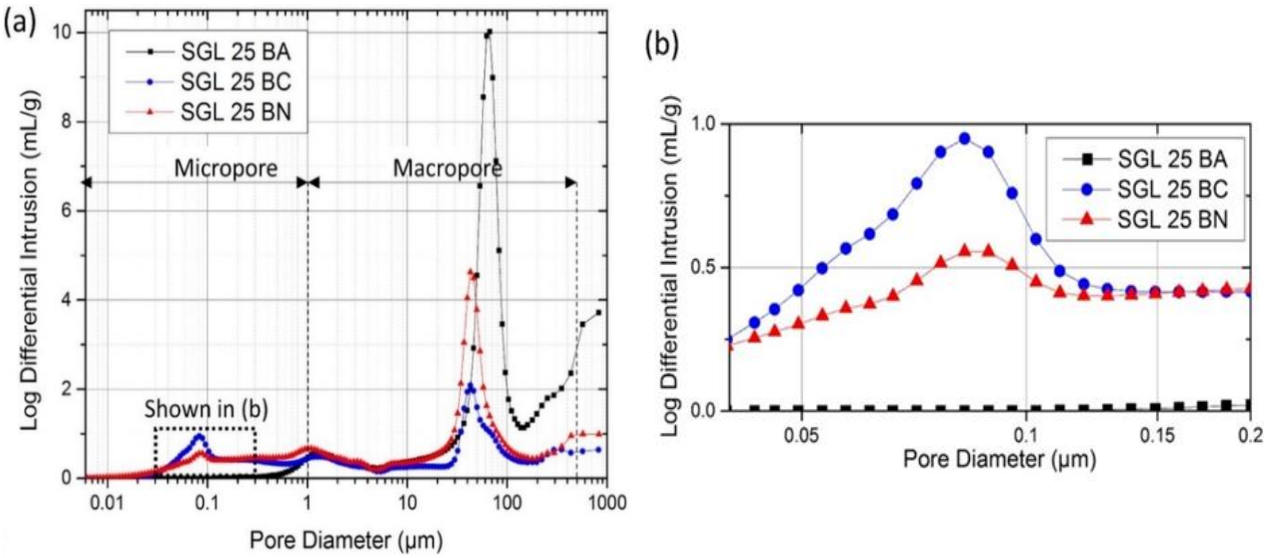

Figure 2-7: (a) Pore size distribution of SGL 25 BA (uncoated carbon paper); SGL 25 BC (MPL-coated carbon paper); and SGL 25 BN (carbon paper coated with an in-house MPL), measured by mercury intrusion porosimetry (MIP). (b) Magnified region highlighted by the dashed area in (a)[16].

Our understanding of the ability of the substrate to transport mass, conduct electrons and transfer heat in conventional GDLs has been improved by extensive characterisation in a large number of studies. This has helped to inform the choice of substrate materials, and how their fabrication and design impacts the final properties of the GDL in a polymer electrolyte fuel cell. Key areas of improvement in GDL design are based around optimising the porosity, changing the surface properties, and improving the electrical conductivity. Recently in-situ imaging is emerging as a promising field to understand the performance of GDLs. For example, Fig. 2.8 shows in-operando images of liquid water at the cathode, obtained via x-ray computed tomography. This type of technique has provided significant insights into the state of liquid water and reactant gases, during operation [162-164], and this will enable further development of optimised pore structures for GDLs.

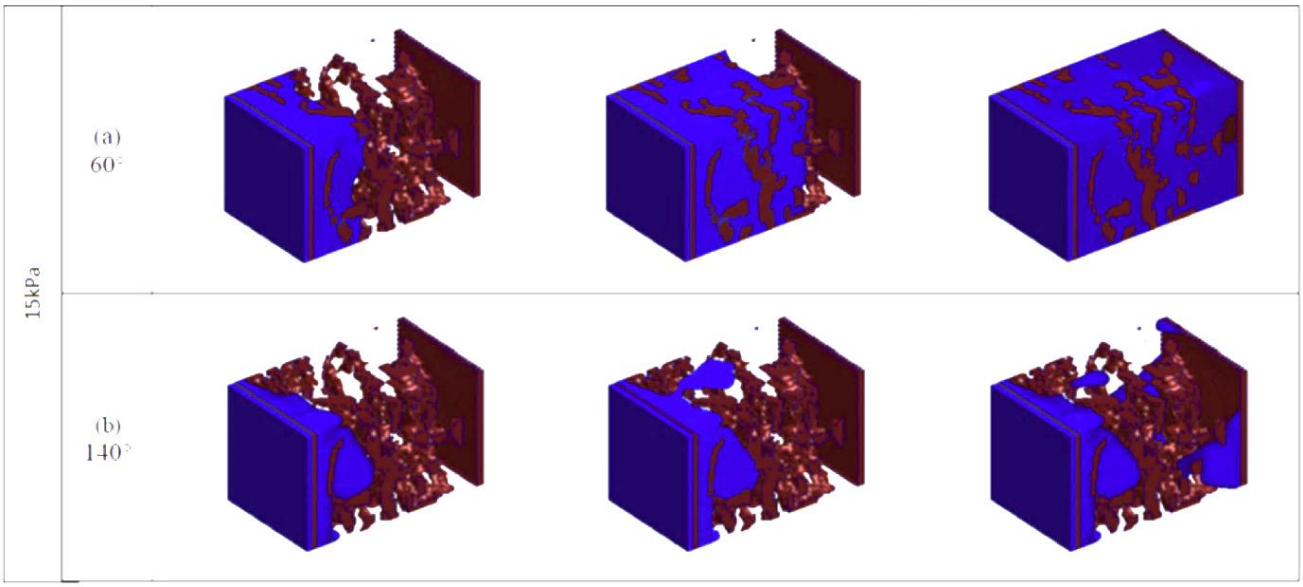

Figure 2-8: Intrusion of liquid water into SGL 24AA, based on 3D reconstructions from X-ray computed tomography, for different water contact angles [195].

2.2.2 Alternative MPS Architechtures

Here, we focus on summarising research into alternative materials for the macroporous substrate (MPS) in GDLs. Various groups have aimed to improve on conventional GDLs by changing the materials used. As well as improving cell performance and durability, other motivations for using alternative materials include reducing the cost of manufacture and improving sustainability.

Electrospun MPS

Electrospinning is a recent manufacturing technique (from 2012) used for the production of continuous fibres of sub-micron to nanometre scale [165]. From adjustment of the parameters during the spinning process, it is possible to control the fibre diameter, pore size, fibre alignment and surface properties of a material. In essence, it is possible to fabricate a macroporous substrate, or e-GDL with an optimised microstructure for mass transport and for the management of liquid water. To this end, electrospinning has been used by several researchers to optimise GDL design in terms of: pore size [92, 166-169], and hydrophobicity [168].

Chevalier et al. [92] conducted a comprehensive study into the optimisation of electrospun MPS, where various parameters were altered including fibre length, fibre diameter, wettability and fibre orientation.

The eGDLs were then characterised in-situ and ex-situ; they reported that the e-GDL with the smallest fibre diameter (0.20 μm compared to 1.13 μm) had a smallest inter-fibre space and therefore smallest pore size, which promoted thus improved liquid water removal and decreased mass transport resistance. This resulted in an increased power density than the thicker fibre e-GDL (501 versus 275 mW cm^2). The wettability and the fibre alignment also had a significant effect on the MEA performance, increasing the maximum power density by 12%.

Ren et al. [168] attempted optimisation of the electrospun GDL for use in self-humidifying PEMFCs by modification of the production parameters, including concentration of the polymer solution and the fibre diameter. They reported that their e-GDL had greater water retention capabilities and therefore was suitable for low humidity conditions by alleviating membrane dehydration. However, electrochemical and polarisation curves were not performed and as such the full conclusion of the capability of the e-GDL in a PEMFC has yet to be confirmed.

Certain challenges need to be overcome to improve e-GDL durability as Balakrishnan et al. [170] reported a notable drop in contact angle (from 136° to 44°) after accelerated stress tests in hydrogen peroxide due to a degradation of the fluorinated monolayers. Polarisation curves indicated that the degraded electrospun GDL suffered higher levels of liquid water accumulation and mass transport losses than the pristine with a significant potential drop voltage following the 0.5 A cm^{-2}. The importance of durability tests, which are often neglected, should not be underestimated as they are as important as the performance tests (e.g., the peak power density or the limiting current density).

Perforated MPS

Attempts to improve the water management capabilities of the GDL have resulted in various modifications to the design of the macroporous substrate, one of which is the perforation of the cathode MPS [150, 171-178]. Different methods have been used to create large holes (relative to the pore size of the substrate) in the cathode MPS substrate with the aim of creating pathways to divert liquid water from the pores of the cathode diffusion media and the catalyst layer to the gas flow channel, thus relieving the porous media of the cathode side from liquid water saturation and enabling mass transport.

Various techniques have been employed to create a pathway for excess water including manual micro-drilling [176], electric discharge machining [176], and laser perforation [150, 171-174, 177, 178]. Laser perforation has been used the most extensively though researchers noted that it (and also electric discharge machining) resulted in the formation hydrophilic holes due to the removal of PTFE material from the surrounding area [150, 174, 176, 178]. When using laser perforation to enhance water management it is essential that perforation diameter is optimised as other it may result in power loss.

Gersteisen et al. [172, 173] extensively researched the effect of MPS perforations on liquid water transport and on MEA performance. In their initial study they produced 80 μm holes by laser perforation in a Toray TGP-H-090 MPS; this was reported to have enhanced PEMFC performance where limiting current density was increased by 22% [172]. Polarisation curves performed identified less mass transport losses with the perforated macroporous substrate indicating reduced accumulation of liquid water with this MPS. Scale-up from a single cell to a PEMFC stack showed the viability of their design for real world applications [173]. This is a crucial but often neglected step by researchers as the GDL designs and modifications are not extended beyond the single cell stage.

The imaging of the MEA through E-SEM [178], in-operando synchrotron X-ray radiography [150, 174], and synchrotron tomography [174] has helped with the validation of this research and provided clarity on the effect of these modifications on the liquid water front. Haussman et al. [174] used synchrotron X-ray radiography and tomography to reveal the preferred water transport pathways in the perforated GDL; the optimal dimeter of the holes (60 μm) was attributed to the different filling behaviour of the pores. Numerical studies performed by Fang et al. [171] and Niu [175] supported the experimental work on the topic and aided in design optimisation. Niu et al. [175] modelled two phase fluid flow using the two-phase volume of fluid (VOF) model in a reconstruction of the perforated GDL where the diameter, depth and the location of the perforations were assessed. Their oxygen diffusion models supported the experimental data in that MPS perforation increases oxygen concentration and reduces oxygen transport resistance in the GDL. Their model, compared to the case with no perforations, predicted an increase of more than 100% in oxygen concentration with 100 μm perforations. However, holes of a smaller diameter (e.g., 25 μm) was found to have negligible effects on the water saturation.

This in agreement with the optimisation experimental data from Manahan et al. [179] who reported a 25% increase in power density with an MPS with 100 μm perforations and almost negligible improvements with much smaller perforations [172, 174]. They [179] also reported that the perforation location far from the GDL centre and at the liquid water break-through point was more effective at reducing liquid water saturation. Experimental work on MPS perforation has fallen out of trend recently; however, the recreation of this study experimentally with water visualisation, i.e., by employing synchrotron X-ray radiography or X-ray computer tomography, would prove beneficial in terms of optimisation of the GDL design.

2.2.3 Alternative MPS Materials

Graphite

Natural graphite has been explored as an additive to the MPS in order to enhance its electrical conductivity, density, and mechanical strength. For example, Kaushal et al. [180] added natural graphite to polyacrylonitrile fibres before carbonization at 1800°C, forming carbon fibres with increased bulk density, and lower in-plane electrical resistivity (from 6.7 vs 5.3 mΩ cm). Additions of graphite were 0.25, 0.5, 0.75, 1.0 and 1.5%, where fuel cell power density increased with graphite concentration, up to 563 mW cm^{-2} at 1.0 wt%. Graphite loading higher than this decreased the power density. Greater improvements could be seen if e.g., the graphitisation temperature was further increased to improve the conductivity, but this would increase the cost of manufacture.

Another innovation by Gurau et al. [181] used flexible graphite sheets produced from expanded graphite flakes. These were perforated to produce a flexible, macroporous graphite based MPS, with high electrical and thermal conductivity, and low contact resistance compared to a conventional carbon fibre GDL. The perforation densities of up to 10,000 holes per 6.5 cm^2 and porosities of between 0.05% to 35% could be varied simply by altering the tooling geometry, thus optimising the porosity and pore size distribution for PEMFC operation. Larger porosity and lower density of perforations were reported to result in the highest power densities. Whilst this is an interesting concept, providing an easy way to

introduce macropores into arbitrary substrates, the results were not compared with conventional GDLs, making it difficult to assess the usefulness of this innovation.

Carbon Nanotubes (CNT)/ Single Wall Carbon Nanotubes (SWCNT)/ Multi Wall Carbon Nanotubes (MWCNT)

Carbon nanotubes are useful materials for use in GDLs due to their large aspect ratio, excellent electrical conductivity (10^6– 10^7 S cm^{-2}), high thermal conductivity, and high strength / stiffness (>100 GPa and 1.2 TPa, respectively) [182-186]. The large aspect ratio of carbon nanotubes means that they can form free-standing membranes (known as buckypaper), without the need for a binder. Many research groups have explored carbon nanotubes as electrode materials in PEMFCs, but this has been largely limited to the electrocatalyst layer and the microporous layers [5, 9, 187]. A smaller amount of research has been conducted into the fabrication of carbon nanotube based MPSs.

For example, Tang et al. [5] produced a porous buckypaper via vacuum filtration of single wall carbon nanotubes (SWCNTs), and applied this as a gas diffusion electrode in PEMFCs, in comparison with conventional carbon cloth (ELAT®). Although innovative in design, the buckypaper resulted in much lower membrane electrode assembly (MEA) performance (despite being much thinner), and the polarisation curve exhibited significant fluctuation. This may be partly due to the much smaller pore size in SWCNTs (i.e., nanometer scale), compared the macroporous structure of conventional gas diffusion electrodes. However, the polarisation curve suggests that the activation region and the ohmic region are responsible for most of the voltage drops. This suggests that the SWCNT layer negatively affects catalyst utilisation, and that the contact resistance may be much higher (e.g., due to the lack of interpenetration between the electrocatalyst layer and the gas diffusion electrode).

Maheshwari et al. [187] also fabricated freestanding gas diffusion electrodes for PEMFCs, in this case from multiwall carbon nanotubes (MWCNTs) with different aspect ratios. As shown in Fig. 2.9, the buckypapers made from longer MWCNTs (referred to as B in Fig. 2.9) with larger diameter had the better PEMFC performance (~60 mW cm^{-2}). This poor performance of smaller MWCNTs (~35 mW cm^{-2}) was attributed to the broader and uneven pore size distribution, and to the higher electrical resistance compared to the larger MWCNTs. Interestingly, a composite gas diffusion electrode

comprising a layer of smaller MWCNTs on top of a layer of larger MWCNTs (referred to as D in Fig.2.9) produced the highest power density (110 mW cm^{-2}). This more closely approximated the pore size distribution of conventional GDLs, with the smaller MWCNTs acting as the MPL, and the larger MWCNTs acting as the MPS.

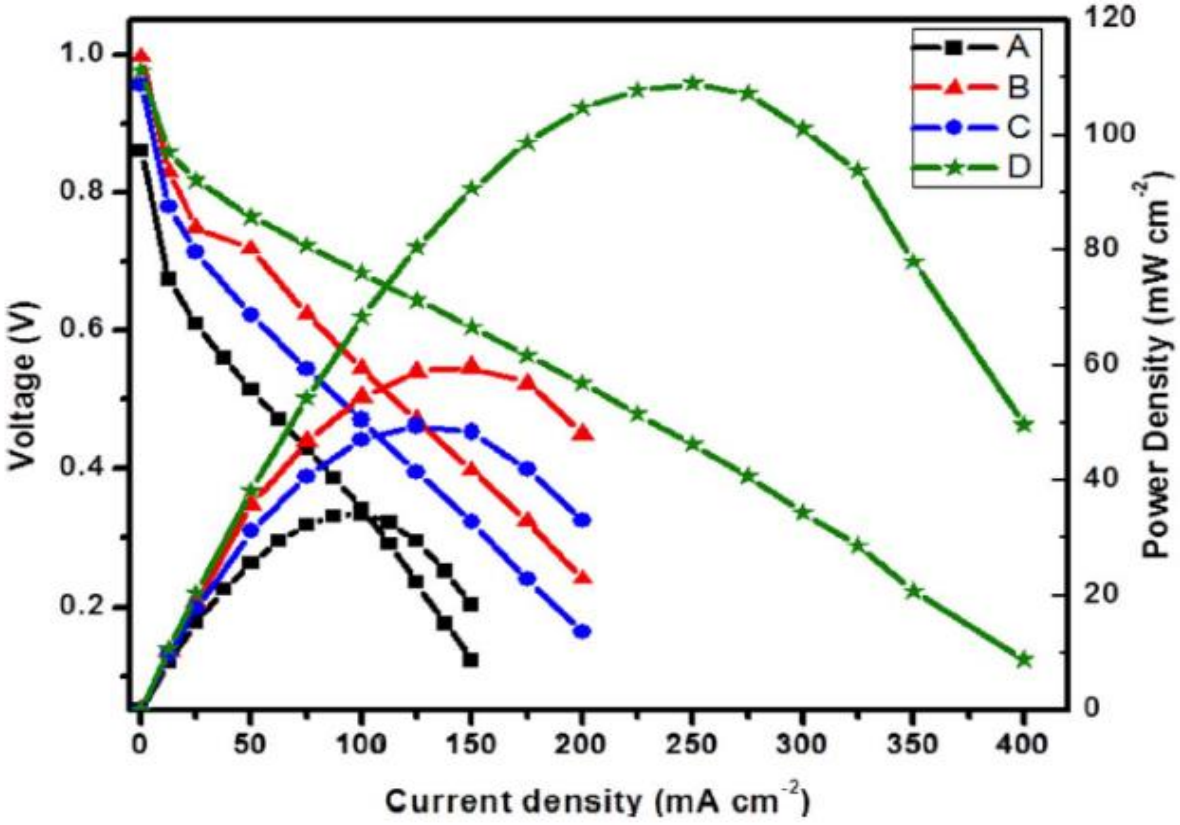

Figure 2-9: Polarization curves of gas diffusion electrodes fabricated from MWCNTs with: (A) 20–30 nm diameter and ~1.5 μm length, (B) 80–120 nm diameter and >500 μm length, (C) MWCNT（A） layered on top of MWCNT (B), and (D) MWCNT（A） layered on top of MWCNT (B). [46].

Meanwhile, Gao et al. [188] produced a sintered carbon paper composite, fabricated from carbon nanotubes, polyacrylonitrile based carbon fibre, and PTFE. In a direct methanol fuel cell (DMFC) the CNT-based MPS exhibited a higher maximum power density (76 mW cm^{-2}) than an MPL-coated conventional Toray 060 GDL (60 mW cm^{-2}) at lower current densities (< 400 mA cm^{-2}) which was attributed to the wider pore size distribution and higher porosity of the composite. Several other groups have performed similar studies. For example, Deng et al. [189] fabricated a MWCNT-based MPS,

which demonstrated a 45% higher maximum power density (23.2 mW cm^{-2}) than an MPL-coated commercial TGP-H-090 (16.2 mW cm^{-2}).

Biomass-based Carbon Fibres

Other research groups have attempted to reduce the cost of the MPS by fabricating them from more sustainable materials, such as cellulose [190, 191], bamboo [192, 193], coconut fibres [194, 195], and other biomass-derived carbons. For example, Destyorini et al. [194] fabricated an MPS using activated carbon powder and carbon fibre derived from coconut coir, mixed with an ethylene vinyl acetate (EVA) as a binder, polyethylene glycol (PEG) as a dispersant, and PTFE as the hydrophobic agent. SEM micrographs of the cross-sections of the GDL substrates are shown in Fig. 2.10 (where (a),(b) and (c) are the carbon powder, carbon fibre and Toray TGP H-120 respectively). The electrical conductivity was much lower (1.53 S cm^{-1}) compared to a Toray TGP-H-120 carbon paper (4.5 S cm^{-1}). However, the porosity, average pore diameter, and water contact angle were comparable. The maximum PEMFC power density achieved was 168 mW cm^{-2}, compared with 208 mW cm^{-2} for the Toray carbon paper. They attributed this to the much lower surface area (~15 vs 214 m^2 g^{-1}), but due to the clear difference in the ohmic region on the polarization curve, it likely to be due to the lower electrical conductivity.

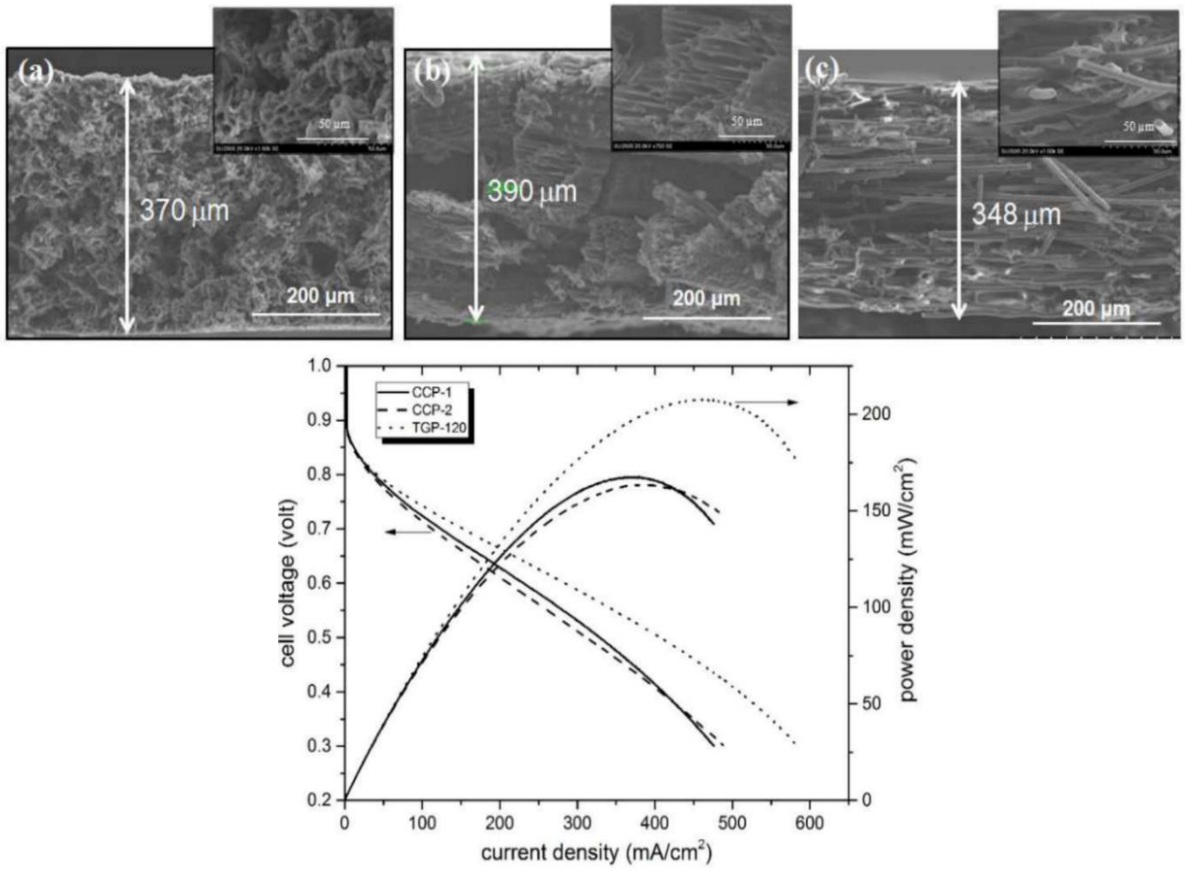

Figure 2-10:SEM cross sectional images of the GDL (a) CCCP1-80% carbon powder (b) CCCP2- 70% wt. coconut fibre and 10% wt. carbon powder and (c) Toray TGP-120. The polarisation curve showing power density, voltage, and current density. [53].

Ghobadi et al. [190] mixed carbon fibre with cellulose as a binder in a wet-laying process to produce an MPS, the cellulose was then removed by phase inversion using an ionic liquid, and the substrate was then sprayed with graphene nanoplates to increase conductivity and hydrophobicity. The carbon fibre content was varied (20, 40, 60 and 80% wt.) as was the volume of ionic liquid used for cellulose removal (20, 50 and 70% v.) SEM micrographs of the composite papers with different volumes of ionic liquid and carbon fibre (Fig. 2.11) show the cellulose content of the surface structure. Fig. 2.11 (b) shows clumps of cellulose covering the carbon fibre network and pore space, whereas it is not visible in Fig. 2.11 (c). The electrical conductivity of the papers increased with carbon fibre weight, where the 80% wt, carbon fibre MPS was comparable to the measured AvCarb MGL190 at (4.5 S m^{-1} and 4.95 S m^{-1}

respectively). This carbon fibre/cellulose-based substrate was able to achieve an impressive 911 mW cm^{-2} at 1200 mA cm^{-2} and 50% relative humidity. However, at 75 and 100% relative humidity, the performance dropped significantly. This was attributed to the hydrophilic nature of the cellulose binder. Wet proofing the cellulose based MPS with a "green" alternative to PTFE was proposed to improve the performance at high relative humidity.

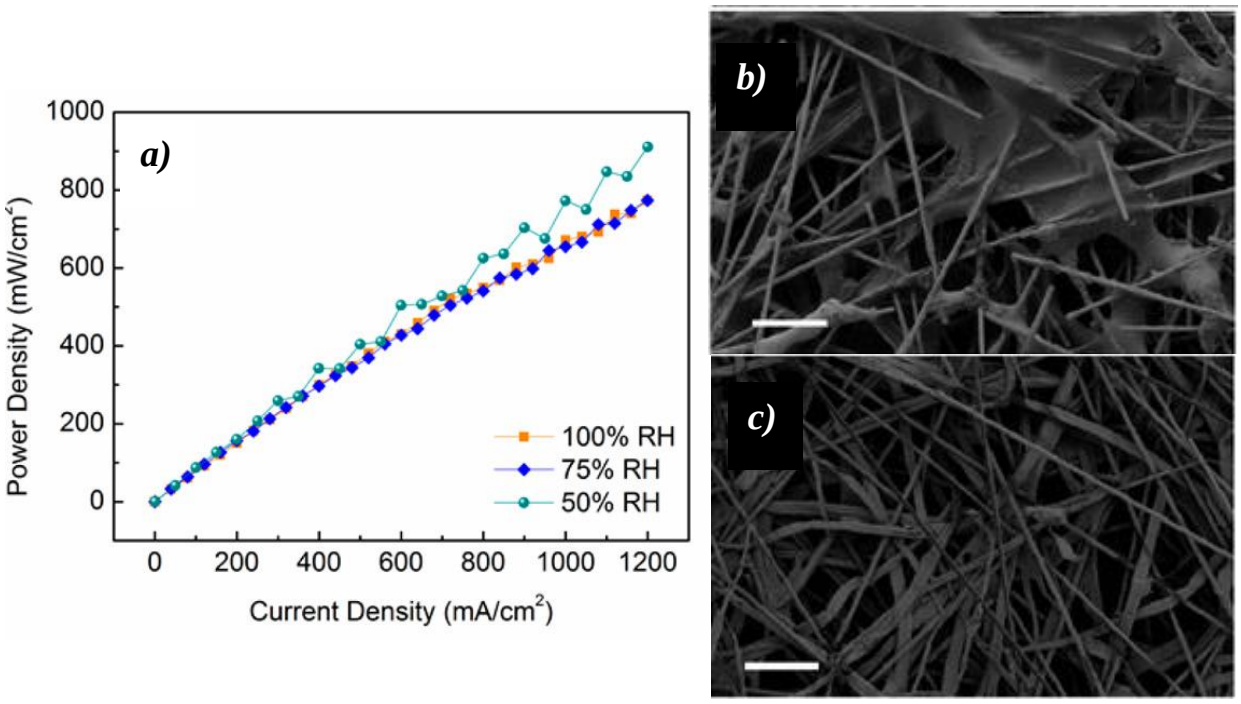

Figure 2-11:) Power density vs. current density for the 80:20 carbon fibre: cellulose MPS. SEM images of the composite papers with different volumes of ionic liquid 50% v. ionic liquid and 80% carbon fibre 70% ionic liquid and 60% carbon fibre. [491.

Similarly, Kaplan et al. [191] also experimented with a cellulose-based MPS, with varying amounts of carbon fibre. These were hot pressed, and no MPL was used. An optimal ratio of 70:30 carbon fibre to cellulose had the lowest resistivity and high strength, as well as pore size distribution similar the conventional AvCarb®MG GDL. In PEMFC polarisation tests conducted at 50ºC the carbon fibre/cellulose based macroporous substrate had a similar performance to the commercially-used AvCarb®MG GDL, featuring relatively low ohmic and mass transport losses in low-voltage region.

However, at 60ºC, the performance with fibre/cellulose based MPS was notably worse than that with AvCarb®MG GDL. The authors did not provide an explanation on why the results were different at different temperatures; however, this could be attributed to the superior thermal conductivity of AvCarb®MG GDL that allows for larger heat dissipation at elevated temperatures and subsequently larger level of membrane hydration compared to fibre/cellulose based macroporous substrate.

Pitch-based Carbon Fibres

Recently Heo et al. [196] fabricated a GDL substrate from a composite of carbon black, pitch-based carbon fibre, and phenolic resin binder. Pitch was used because it is a low-cost waste product. The GDL substrates were carbonised at < 800ºC in order to reduce the energy intensity of the production process, and the effect of the carbonisation temperature on the conductivity and porosity was compared. As expected, carbonisation at a higher temperature increased the conductivity significantly. A porosity of 82.6% and a water contact angle of 117.57° were achieved. However, PEMFC measurements were not conducted.

Aerogels

Sodium-carbon aerogels have been investigated as gas diffusion media [197, 198]. Glora et al.[197] produced a carbon aerogel with a large surface area and meso-porous pore volumes for gas transport; they reported an electronic conductivity of 28 S cm^{-1} in an 80% porous GDL of < 500 μm thick. Wang et al. [198] also researched aerogels; their fabrication method of pyrolysis led to large variation in GDL porosity potentially resulting in large discrepancies in mass transport properties and fuel cell operation. Trefilov et al. [199] fabricated a hybrid graphene-carbon xerogel dual-layer GDL with a gradually decreasing porosity through its profile. Their methodology allowed for a controllable structure, where the centrifugal speed during xerogel formation determined the microstructure, pore size and porosity. As can be seen from the polarisation curves (Fig. 2.12), increasing the centrifugal speed in aerogel fabrication increased the power density of the GDLs (0 G force:0.07 W cm^{-2}, 125 G force: 0.11 W cm^{-2} and 250 G force: 0.14 W cm^{-2}), which was attributed to the lower porosity and increased bulk density

of the aerogel which meant it accumulated liquid water less readily. The addition of graphene layers improved the conductivity and mass transfer of the xerogel.

Although aerogels offer an exciting means of producing the macroporous substrates, the method of fabrication is, compared to the current materials and methods, less attractive for large scale production on fuel cell manufacturing; the current materials and fabrication methods are more cost-effective and/or simpler.

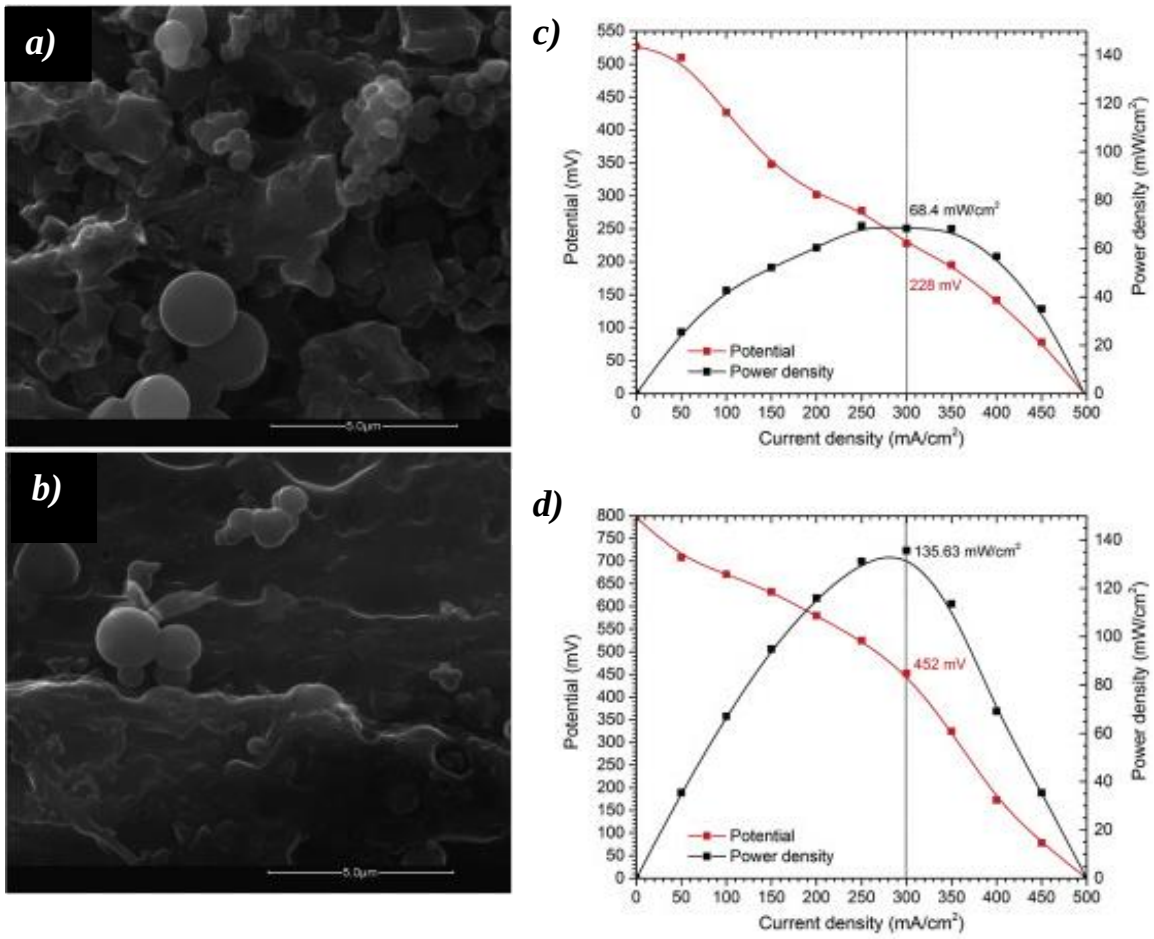

Figure 2-12:(Left) SEM images of composite xerogel (a) 0 G centrifuged (b) 250 G centrifuged. (Right) Polarisation and power density curves for xerogels (c) 0 G centrifuged (d)250 G centrifuged. [58].

Metal Foams

Conventional carbon-based GDLs suffer severe corrosion in PEMFC cathodes due to start-stop potential cycling at high voltage (~1.5 V), limiting the durability. In addition, mechanical degradation of the GDL occurs due to compression within the membrane electrode assembly (MEA). The development of a carbon-free GDL could therefore improve the durability, simplify the manufacturing process, and reduce the cost. One tactic is to produce GDLs from metal-based materials which are mechanically stable, have relatively high thermal and electrical conductivity, and can be machined into a desired structure. Titanium metal has been explored as a gas diffusion electrode by various groups [200-204]. Various attempts to fabricate metal-based carbon-free GDLs are discussed in the following sections.

Foams are defined as a gaseous phase uniformly dispersed inside a solid or liquid phase; where metallic foams have been produced from a wide variety of metals including titanium, aluminium, magnesium, copper, zinc and nickel [205]. Their use encompasses biomedical applications, such as tissue engineering [206]; construction materials, for thermal and sonic insulation; and as an impact absorber in vehicular transportation [207]. Lightweight metallic foams made from titanium and aluminium are the most applicable for use in the PEMFC, being strong, highly porous materials with high corrosion resistance and minimal ion leaching. The most desirable aspect of this material is the tunability of the physical structure produced by alteration of the manufacturing parameters and foaming material used, as such the pore size, structure and distribution can be modified, as seen in Fig. 2.13 (a) and (b) where metallic foams produced from aluminium with a varying number of pores per square inch (6.5 cm^2) were produced. The open pore structure of the foam can be seen in the SEM image (Fig. 2.13 (c)) [208].

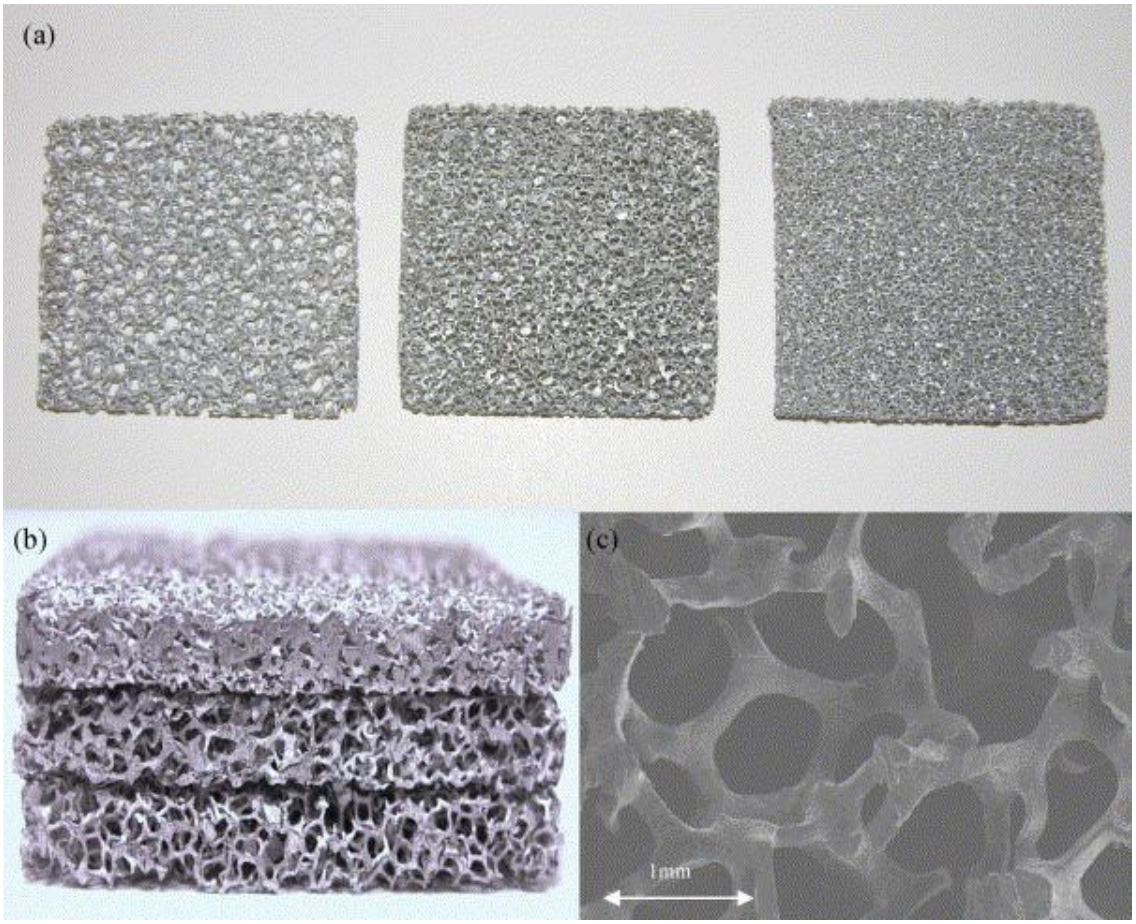

Figure 2-13:Metal foams produced. (a) Foams with 10, 20 and 40 pores per 6.5 cm^2 (per square inch, ppi) (b) a cross sectional view (c) SEM image of 20 ppi metal foam with an open pore structure [67].

Previous works have demonstrated the validity of metal foams in fuel cell engineering as a flow-field plate [209, 210], however the physical properties of metal foams make them highly applicable as the gas diffusion substrate. They possess not only good material characteristics of metals (high electrical and thermal conductivity, weldability and plasticity) but have architectural advantages such as tuneable pore structure and permeability, and high specific surface area [211]. Moreover, some metallic foams (e.g., nickel foams) have adequate corrosion resistance that allows them to be directly used in PEMFCs without the need for applying protective corrosion-resistance coatings to them.

Choi et al. produced a flexible titanium foam GDL with a controlled pore structure from freeze casting [201] which was used as the anodic GDL in a polymer electrolyte fuel cell. The single cell measurements not only exhibited a higher current density than those using the commercial carbon GDLs

for the anode, (462 mA cm^{-2}) and (278 mA cm^{-2}) respectively at 0.7 V, but also incurred minimal loss in weight and thickness in accelerated corrosion tests, unlike the commercial GDLs. Their work signifies the potential application of metal foams for the anodic GDL in PEMFC; further research should undertake using their freeze-casting and alternative methodology to produce similar metallic foams from different metals. Fig. 2.14 shows a comparison of the pore size distribution in the titanium foam anode GDL and SGL 35BC GDL determined by MIP. As their methodology enabled the manipulation of pore size and structure, further research could be undertaken to optimise these two characteristics. However, to gain a fuller understanding of the potential of a material it is important that they are tested as the cathodic GDL where the conditions are more corrosive, and the reaction kinetics are less favourable.

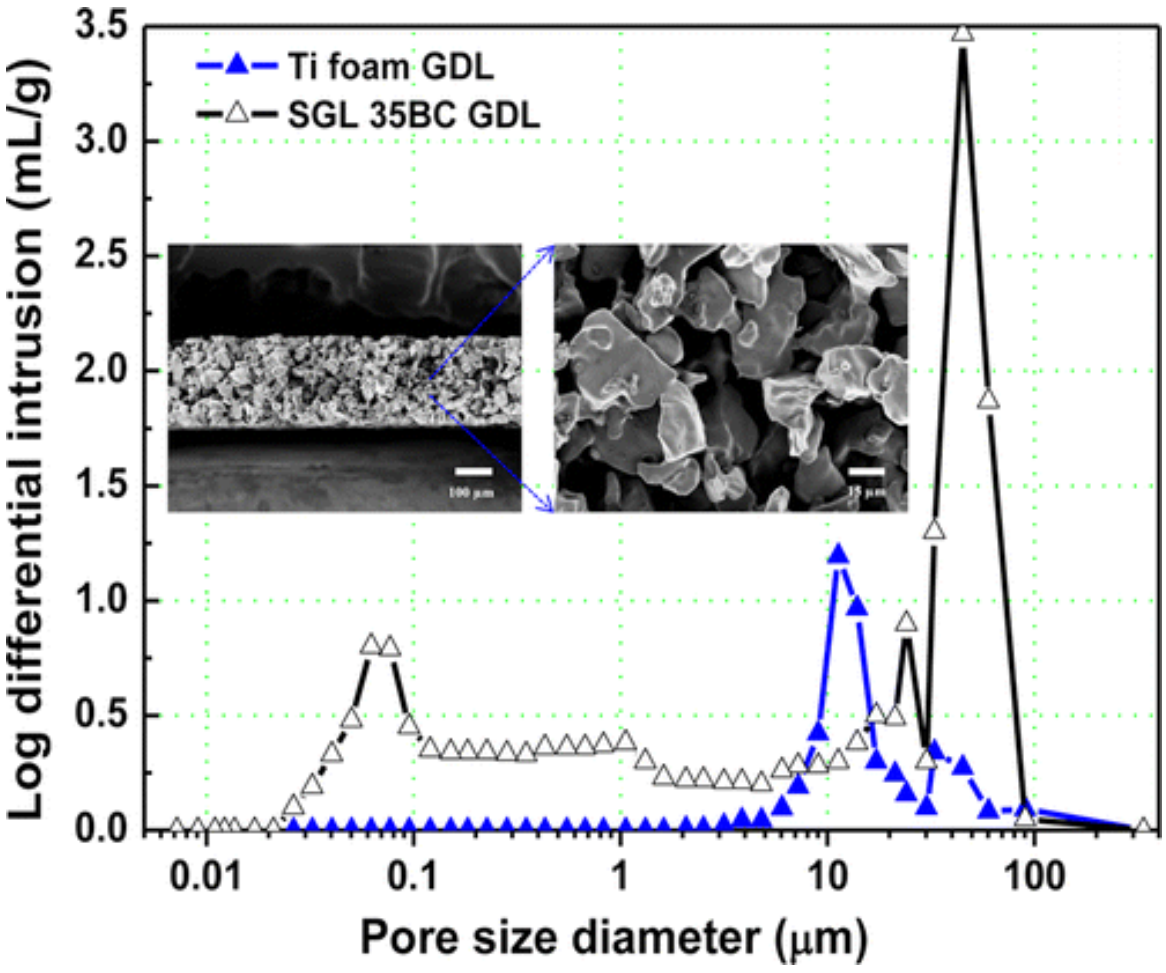

Figure 2-14:Pore size distribution in the Ti foam anode GDL (blue line) and SGL 35BC GDL (black line) determined by MIP. SEM images of a cross-section of the Ti foam anode GDL [60].

Metal-based Machined Substrates

The machining of materials is a proficient method to manufacture substrates into a predetermined form and physical structure. Research groups have used machining to produce GDL substrates of varying architectures, including adjustment of pore diameters, pore location and substrate thickness, to optimise GDL design. The majority of this work has been centred on machined metal GDL substrates, silicon has been used for micro-PEMFC applications [212]. Fushinobu et al. [202] micro-machined thin film titanium GDLs, of 5 μm and 20 μm thick, to produce highly durable components for high performance PEMFC applications and concentration overpotential modelling (Fig. 2.15, (right)). The design parameters of the titanium film were varied on the cathodic GDL, whilst the porosity was kept constant, to see the effect of film thickness, hole diameter and hole patterning on the i-V performance of the MEA. The performance was shown to be extremely varied depending on the film thickness and the hole diameter, where the thinner film and smaller hole-diameter thickness produced greater power density. The placement of the perforations above the rib as well as the channel further improved cell performance, comparable to the carbon paper GDL in the low current density regions (< 350 mA cm^{-2}).

Their work indicates that thin titanium films can be suited for PEMFC gas diffusion media, potentially improving on current carbonaceous materials, however it signifies the importance of well-developed design. Ideally further work would further optimise the design by examination: various hole diameters machined into the same film; smaller hole diameters; thinner films and even more randomised hole distribution models.

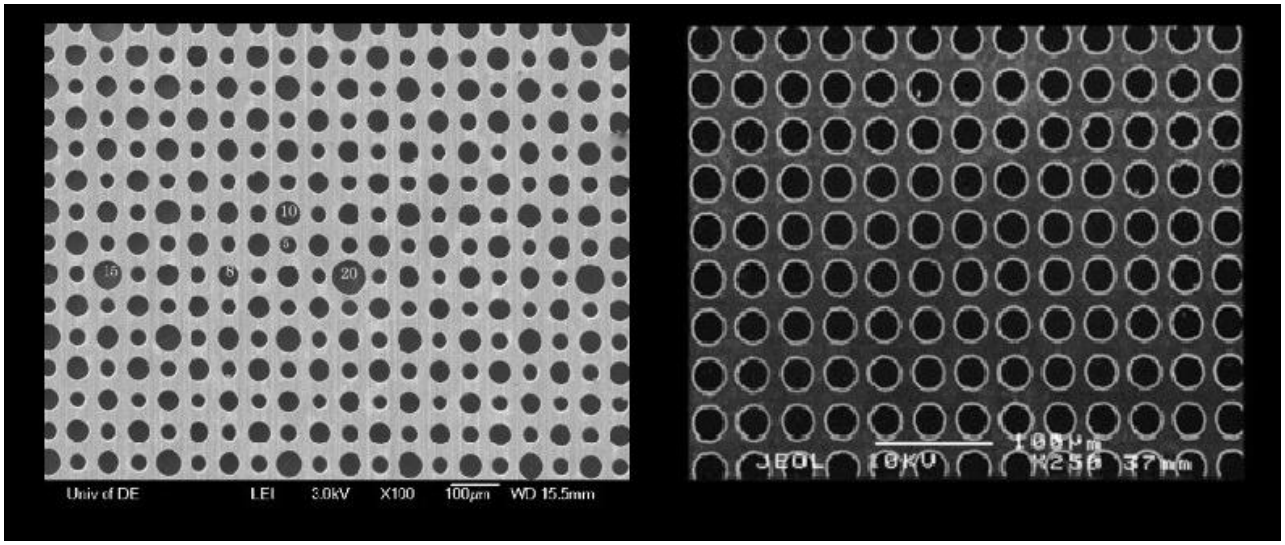

Figure 2-15:SEM images of the machined metal GDLs. (Left)Copper foil GDL with varying machined pore sizes produced by Zhang et al. (Right) Ti GDL top view with 25-μm diameter micro through-holes by Fushinobu et al.72].

Zhang et al. [213] developed a similar porous GDL with improved electrical and thermal conductivity and controlled the porosity using a 12.5 μm thick copper foil with an applied MPL of Vulcan XC-72 (Fig. 2.15, (left)). Their copper foil substrate had various pore sizes and straight pore profile and when coated measured a contact angle of 152°. Although the Cu GDL exhibited a lower maximum power density (0.45 W cm^{-2}) compared to MPL-coated Toray TGP-H-060 (0.59 W cm^{-2}), the achievable controlled permeability, pore shape, porosity, and surface properties of this method allows for tailored design which will lead to improved reactant and product transport. Other research groups have focused on the use of titanium sinters; Liu et al. [214] used titanium sinters as the GDL in a free-breathing PEM fuel cell, nickel meshes, though for the DMFC.

3D Printed Substrates

3D printing is an interesting and novel method to produce micro-structured metal sheets for GDL applications. Jayakumar et al. [215] produced a carbon-free nylon-aluminium substrate using 3D printing technology which was infused with graphene to increase electrical and thermal conductivity; it was then compared to the commercial SGL 39 BC. The fabricated GDL exhibited comparable porosity

(42%), good tensile strength (≥ 4 N cm^{-1}), and an excellent thermal conductivity (0.588–0.512 W mK^{-1}). However, it was characterised by a high through-plane resistance resulting in a lower conductivity than the Sigracet GDL. This is attributed to the graphene particles being poorly embedded into the substrate which limited the conductivity of the substrate. 3D printing of substrates offers significant potential as a means of producing GDL substrates with tailored microstructure. However, 3D printing as a technology is currently in its early development. As the technique becomes more widespread, a greater number of materials and thread size would become more available, and the technique can be then more easily optimised for MPS designs.

2.2.4 Summary of Alternative Materials and Designs of the Macroporous Substrate

The addition of enhancing materials to the GDL such as natural graphite can significantly improve MEA efficiency with very little alteration to the GDL substrate production process. Moreover, the ease of a simplified production process is key to the reduction of manufacturing costs of the GDL and the fuel cell as a whole, thus will make PEMFC more commercially competitive. The idea of cellulose based GDLs and GDLs produced from abundant sustainable biomass material may reduce cost and provide a truly "green" fuel cell. Despite these aspirations, the power density is uncompetitive with the commercial alternatives; therefore, if they are to see any commercialisation as materials, significant research needs to be undertaken to improve the performance before any work can be done to elevate them from the lab-scale.

Non-carbonaceous gas diffusion materials are highly promising, though in their current state they lack the thorough research to elevate them from the research level. Of the materials that have been explored the largest potential seems to lie in metallic foams and aerogels. The desirable characteristics of metals, notably: high electrical conductivity, mechanical strength, wettability, and corrosion resistance, make them applicable as a substrate material. However, it is the control over pore size and structure that will lead to significant jumps in the improvement of the fuel cell efficiency and durability. However, metal foams have yet to be tested as the cathodic GDL which is the true test of GDL potential, due to the potential of water flooding from the ORR.

One area that should not be neglected in the pursuit of novel materials for the macroporous substrate is the effect that compression and fuel cell fabrication via hot pressing of the components on has on these materials and their microstructure. Innovative works have indicated that the temperature of hot pressing [216] and uniformity of the compression [41] is influential in the electrochemical performance of the membrane electrode assembly (MEA) of the fuel cell, and the capability of the GDL for mass and electron transfer.

2.3 The Conventional Microporous Layer

In order to optimise GDL microstructure, an extensive literature review has been undertaken on innovative microporous layer architectures and novel materials. However, it is first necessary to outline the conventional microporous layer, its constituents and design.

The MPL is applied to the GDL where it is positioned between the carbon substrate and the electrocatalyst layer. It is formed of carbon particles dispersed in a polymeric hydrophobic binding agent, its high hydrophobicity provides a high capillary pressure to barrier to promote membrane hydration and to prevent water flooding. Its presence has been shown to significantly improve fuel cell performance and durability; Owejan et al. [103] found a 20-30% increase in performance with MPL-coated GDLs under fully humidified conditions, whereas Zhou et al. [217] observed a large reduction in ohmic losses with MPL-coated GDL. Although initially added to the GDL in order to improve the electrical contact between the GDL and the electrocatalyst layer [39, 156], Chen et al. [73, 218] were also able to show that the MPL improved liquid water management in the MEA. The main improvements are due to the MPLs ability to modify water accumulation and transport through the GDL [72, 142, 217, 219-222]. Thus, reducing flooding of the pores of the macroporous layers and increasing catalyst availability for the ORR. The composition of the MPL is a mixture of carbonaceous particles, usually carbon black, and a hydrophobic wetting agent, typically PTFE. The effect of MPL composition on its transport abilities has been the focus of numerous research papers; in particular the effect of PTFE weighting in the MPL [223-225], the optimisation of carbon mass per cm^2 of the substrate [83, 226, 227], and the type of carbon black [228-230] have been the focal point of research.

Optimisation of the carbon black content in the MPL has been a point of contention for various research groups; initially Jordan et al. [226] found that optimal loading Acetylene Black carbon in the MPL is between about 1.25 and 1.9 mg cm^{-2}, whereas Park et al. [227] suggested that a carbon loading 0.5 mg cm^{-2} was optimal for fuel cell using air as the oxidant. This is due to the thinness of the layer allowing for better air permeation. More recently, Orogbemi et al. [83] found that a carbon loading of 2.0 mg cm^2 is optimal for gas permeability. Typically, carbon weighting in the MPL ranges from 1.0 -2.0 mg cm^2, this has a noticeable effect on MPL thickness and subsequently its mass and water transport capabilities [231].

Fig. 2.16 [232] shows SEM micrographs of the MPL-coated gas diffusion layer, where Fig. 2.16 (a) uses PTFE as the hydrophobic agent and Fig. 2.16 (b) uses PFPE. Both figures show the defined microporous layer on the carbon substrate with visible surface cracking. The anisotropy of the gas diffusion layer is shown by the fibre orientation where Fig. 2.16 (a) shows a fibre in the through-plane, whereas a fibre in the in-plane direction is visible in Fig. 2.16 (b).

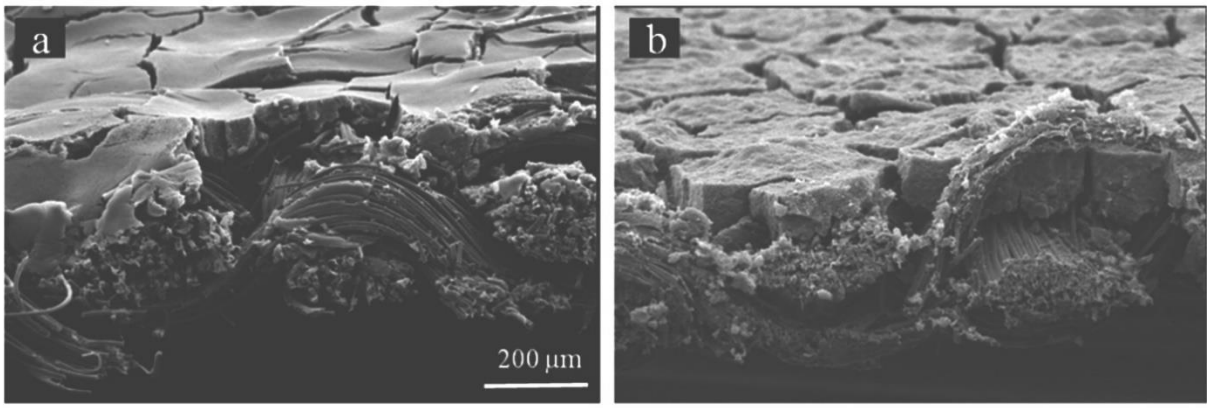

Figure 2-16: An SEM micrograph showing a cross section of the MPL-coated gas diffusion layer [232].

The application of the MPL to the carbon substrate is carried out by various techniques. These include brush coating; the doctor blade technique; spray coating; rod coating; or screen printing [30] although novel methods of application are also under investigation [233]. The viscosity of the MPL slurry dictates the application method by which the MPL is applied to the carbon substrate; more viscous slurries can be applied to the substrate by brush or doctor blade coating whereas thinner slurries tend to be applied by spray coating. The MPL-coated GDL is then heat treated and sintered at e.g. 350 °C in order to melt the PTFE and thus sufficiently bond the MPL to the carbon substrate and homogeneously bind the PTFE and carbon black particles [228, 234] The MPL has been shown to penetrate into the GDL under the compression of the fuel cell to create hybrid layer of substrate and MPL [158].

Conventional MPLs have been shown to increase power density when used in PEMFC MEAs. However, there are several drawbacks to their design. Thus, material and design improvements have been explored with in-situ and ex-situ tests to increase PEMFC efficiency. As previously mentioned in Section 2.1.2, although PTFE provides hydrophobicity to the GDL, its presence in the MPL has been shown to compromise its capability for reactant transport and electron transfer [8, 44, 61]. Moreover, MPL slurries prepared using PTFE have been remarked on for having several issues; the insolubility of PTFE means that the production of a homogenous CB/PTFE slurry is difficult as the PTFE is only dispersed in the solution. Other issues exist with PTFE based MPL slurries, notably: high viscosity; low phase stability due to viscosity changes over time; cracking on the GDL surface during drying; and difficulty in the coating process [52]. As such, new materials and architectures are required.

Another branch of research is focused on the improvement of the carbonaceous element of the MPL, essentially the substitution of carbon black with alternative materials. The motivation behind this research is largely to improve the physical properties of the MPL and thus PEMFC efficiency, whilst other groups have cited the secondary motivation of sustainability. Carbon black is produced from the partial thermal degradation of oil or natural gas as such its production is based on the fossil fuel industry. The following section details attempted design and material improvements that have been made to the MPL by first addressing the carbonaceous element and then the wetting agent.

2.4 Alternative Designs for Microporous Layers

There has been a significant volume of work undertaken into the optimisation of carbon black in the MPL; these studies largely focus on the microstructural properties of the material, such as pore size distribution [3, 47, 48, 147, 235, 236], and improvements in MPL design such as carbon weighting [83, 227, 237] and type of carbon black [228-230].

As the MPL is a critical component for the transport of reactant gases and liquid water to and away from the catalyst layer, the porosity, and the pore size distribution of the MPL are determining factors in its ability to carry out this task successfully. Attempts have been made to control the pore structure of the MPL by using carbon black of different porosity profiles. Wang et al. [230] produced a composite MPL from carbon blacks with dissimilar physical characteristics in order to create a bi-purpose pore structure, for the optimal transportation of liquid water and reactant gases. Their results showed that the use of a two carbon blacks with differing porosity and pore size distribution produced MPLs with a more even PSD than superior carbon black, thus making them more suitable for both the transport of liquid water and reactant gases; this was shown in the higher power density of the polarisation curves. More importantly, this technique allowed for the fabrication of an MPL with a graduated porosity and thus a gradient for fluid flow.

Tang et al. [238] also fabricated a triple-layer MPL with graduated pore sizes; they were able to achieve this by the use of a pore forming agent (NH_4Cl) in their screen printing production process. They created a porosity gradient where pore diameter was increased from the substrate to the catalyst layer interface with the aim of increasing the capillary pressure forcing liquid water away from the catalyst. Their microstructural design appeared to be effective with high power density at high current densities (>700 mA cm^2), where liquid water saturation becomes the limiting factor. Their methodology highlights how the pore size can easily be controlled and varied by the addition of pore forming agents. Moreover, their findings support those of Wang et al. [230] that performance of the graduated MPL is greater than the homogenous MPL especially at high current densities where liquid water saturation is a problem.

2.5 Alternative Materials to Carbon Blacks

In order to improve the MEA efficiency, several research groups have explored other carbonaceous materials, notably carbon nano-tubes [161, 239-241], graphene [242-245] and carbon-fibres [246]. The aim of using these materials has largely been to enhance two-phase flow in the MPL through improved pore size distribution, and to increase MPL conductivity enhancing the bulk conductivity and reducing contact resistance.

Carbon Nanotubes

Carbon nanotubes (CNT) have shown potential as an exciting new MPL material due to their high electrical conductivity and high durability in oxidative environments. A large range of investigations has shown the potential of CNT as a carbonaceous MPL material [161, 234, 239-241, 247-249]. The majority of these studies have focused on CNT / carbon black composites, though early work by Kannan et al. [248, 250] replaced Vulcan XR-72 carbon black with graphitized CNT. Their ex-situ experiments indicated that the graphitized CNT exhibits more desirable characteristics for use in the MPL; having a contact angle of 150^{o} and more homogenous surface morphology; the polarisation data from MEA testing produced greater power density especially in the high current density region. The addition of carbon fibres added to the mechanical stability of the layer.

Work by Gharibi et al. [249] showed that the addition of multi walled carbon nanotubes (MWCNT) to the carbon black based MPL increased gas permeability, pore volume and conductivity in the MPL, consistent with results and observations by Stampino et al. [251] and Lin et al. [241]. Lin et al. [241] created an MPL using CNT in addition to acetylene black; their results indicated that carbon nanotubes exhibited relatively greater electrical conductivity and permeability. From the polarisation curves, they found an optimum carbon loading of 1.5 mg cm^{2} and an optimum mixing ratio of acetylene black to CNT at 1:4 (mass: mass). Investigations into CNT MPLs show that they are characterised by superior electronic conductivity and permeability. Schweiss et al. [240] applied an in-house MWCNT MPL to a Sigracet SGL 25BN GDL which was compared to the commercially dual-layer Sigracet SGL 25 BC. They observed that gas permeability was nearly 8 times greater in the MWCNT MPL GDL than the

commercially available and ohmic resistance was reduced by 9%. Interestingly the resulting MPL had hydrophilic properties and was able to successfully remove liquid water from the catalyst.

Lee et al. [161] produced an MPL from the addition of 21% wt. CNT into the carbon black and PTFE dispersion; this was compared to the commercially available uncoated and coated GDLs SGL 25BA and 25BC respectively. The PSD of the CNT MPL was found to be better distributed than the commercial CB MPL; this may be due to the favourable aspect ratio of CNT which prevents agglomeration of the CB particles in the MPL. Ex-situ characterisation of the in-house CNT coated GDL showed a much lower mass transport resistance than the commercially coated GDL SGL 25BC; this favourable PSD and reduced mass transport resistance increase the fuel cell power density when tested in-situ. Their work is highly informative as they were able to visualise the distribution of liquid water in the MEA in-operando. Interestingly, although the liquid water saturation was shown to be greater in the CNT-MPL rather than the commercial MPL, the in-situ performance of the CNT MPL was greater even at high RH. At high current densities (>250 mA cm^{-2}), the CNT MPL improved power density by 94.1%. This was attributed to the much thinner MPL in the CNT MPL and the higher effective porosity and larger pores. Thus their research highlights the importance of pore size in the MPL, this supports the theory proposed by Kong et al. [47] that an increased amount of small macro pores in the MPL increases PEMFC performance. As although this allows permeation of liquid water, it also does not confine reactant gas pathways and thus eases their transportation.

Similar findings were reported by Tanuma et al. [252] who conducted a thorough comparison of composite MPLs by preparing hydrophilic MPLs from carbons with different physical and micro-structural properties: carbon black, MWCNT, CNT and vapour grown and melt spun carbon fibre. They investigated the pore size distribution and mean pore diameter prior to in-situ polarisation measurements, finding that the vapour grown carbon fibres had the largest median pore diameter and carbon black and melt-spun carbon fibres have the lowest. Carbon black and melt-spun carbon fibres also yielded the lowest output power whereas the vapour grown carbon fibres produced the highest. Thus, observing that the larger pore volume, the smaller the mass transport losses as it is more effective at simultaneously removing liquid water and providing a pathway for reactant gas transport.

Grown Carbon Fibres and Carbon Nanotubes

Innovative work has been undertaken by replacing the MPL with grown nano-carbon fibres on a carbon paper GDL [246]. The aim of which is to increase the contact between the GDL and the catalyst layer, thus improve the diffusion characteristics, reduce charge transfer losses, and increase catalyst utilisation. Sandström et al. [246] reported a significant reduction charge transfer resistance of 38% whilst using the in-situ grown CNT as the MPL. Tang et al. [239] used the same methodology grow CNT on Toray TGPH 090, as a hybrid microporous/catalyst layer. Fig. 2.17 shows the (a) pristine carbon fibre and (b-f) the grown CNT under different conditions. However, the durability of the carbon nano-fibre layer was untested. The change in the morphology of the carbonaceous layer to spindle fibres from a carbon powder likely has a reduced durability due to the fragility of the fibres.

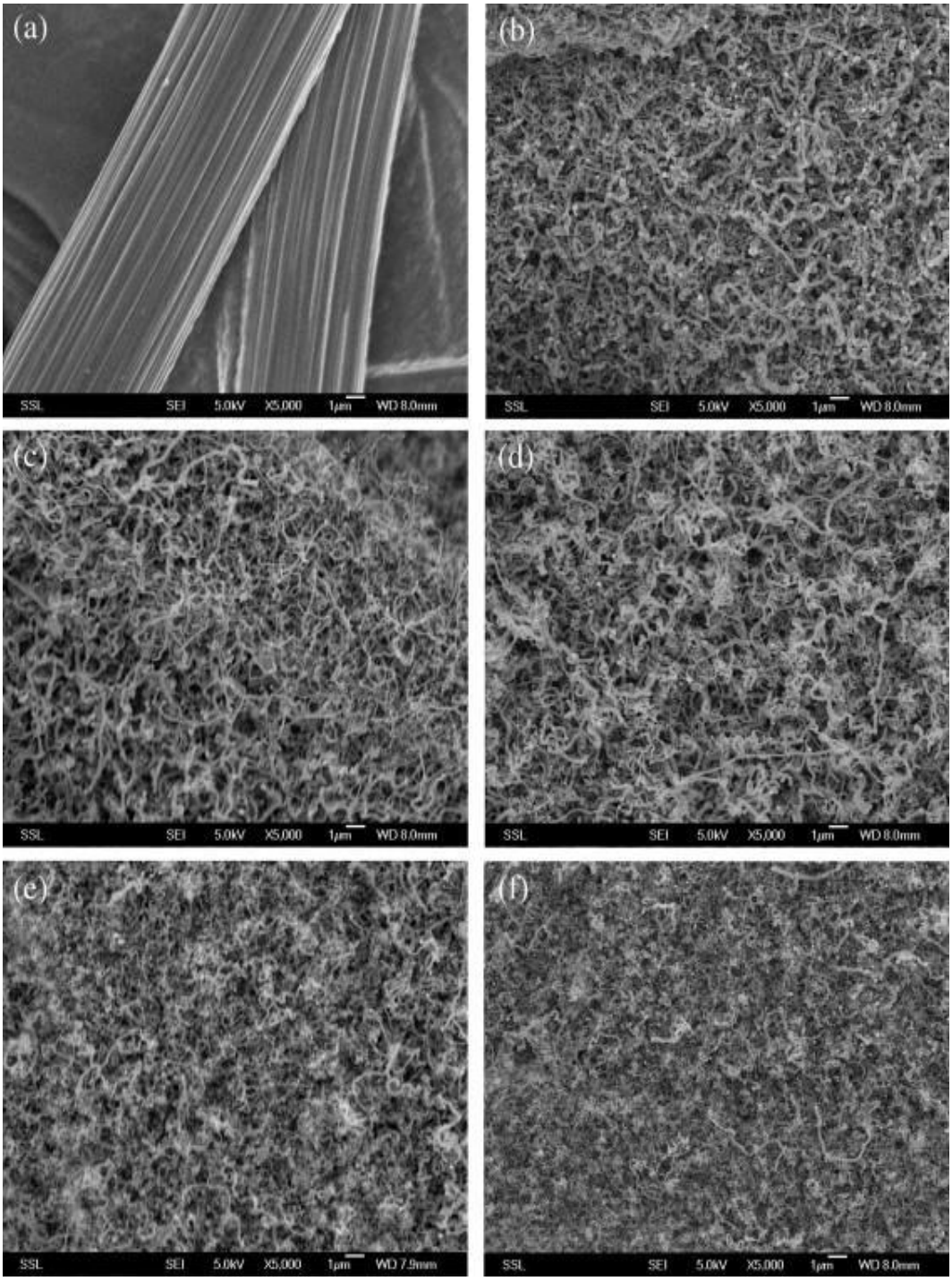

Figure 2-17: SEM images of (a) pristine carbon paper, and CNTs grown under C_2H_4 flow rate of (b) 5 cm^3 min^{-1}, (c) 10 cm^3 min^{-1}, (d) 15 cm^3 min^{-1}, (e) 20 cm3 min^{-1} and (f) 20 cm^3 min^{-1})[5].

Graphene

A recent trend has seen graphene being explored in a couple of studies as an alternative to carbon black for use in the MPL. Graphene is a monolayer of carbon atoms in a two-dimensional matrix, and as such it has good mechanical stiffness and elasticity [147]. More importantly, the compact ordered morphology mean that graphene has an extremely high single particle electrical conductivity (~108 S m^{-2}) and thermal conductivity (1500 – 2500 W m K^{-1}) due to lower in-plane and through-plane resistance [148]. Graphene has also been shown to have enhanced water management characteristics regardless of operating conditions [149].

Leeuwner et al. [244] fabricated a free-standing MPL for the cathodic GDL from commercial compressed graphene foam. The in-plane electrical conductivity of the graphene MPL was high due to the conductive pathways within the graphene foam and the compressibility of the foam enabled good contact between the GDL and the catalyst layer, reducing charge transfer losses. However, the lack of treatment with hydrophobic agent was a limiting factor to its wettability which showed large variance in the measured contact angles (87° ± 16.5); this was also attributed the inhomogeneity of the graphene foam surface when compressed. From the polarisation curves the graphene MPL performs very well in the mid-current densities (~700 mA cm^{-2}), at 500 mA cm^2 the graphene MPL produced 362 mW cm^{-2} compared to 334 mW cm^{-2} produced by the commercial MPL. However, at the higher current densities (>1500 mA cm^{-2}) the commercial MPL. This performance in higher current densities could be improved by increasing the hydrophobicity and thus decreasing liquid water saturation.

Najafabadi et al. [253] produced electrochemically exfoliated graphene for use as an MPL material; however the graphene sheet-like structure prevented water removal from the three-phase boundary, and hence led to performance drop under high-humidity operation due to flooding. This was addressed with mixing the graphene plate structures with carbon black spherical particles. Though successful, this was undertaken on small scale fuel cells with electrodes of 5 cm^2. Leeuwner et al. [244] further investigated exfoliated graphene by using the methodology of Najafabad et al. [253]. They investigated the physical and transport properties of graphene based MPLs, where graphene oxide, graphite and exfoliated graphene were sprayed onto Toray H-060 with 20% wt. PTFE. The graphene based MPLs were shown

to have a smaller contact and in-plane resistance than carbon black MPL; however, their lower hydrophobicity lead to mass transport losses at high RH due to water retention at the catalyst. A composite MPL formed from graphene and carbon black exhibited higher power density at high RH and enhanced durability from galvanostatic testing; their work shows the potential of composite MPL materials for the multifaceted role of the MPL.

Ozden et al. [242] fabricated a graphene based MPL which was compared to a Vulcan XR72 MPL. They conducted ex-situ microstructural analysis as well as in-situ power measurements and ex-situ electrochemical and physical characterisation tests. The graphene based MPL exhibited a higher in-plane conductivity than the Vulcan CB MPL and the peak power density of the graphene based MPL was shown to be higher than the Vulcan based MPLs at a range of relative humidity of 40-100%. This was attributed to the morphology of the MPL which aids liquid water management and reactant transport. Ozden et al. [242] research is based on graphene flakes, much of the success of their MPL was attributed to the physical structure in the stacking of these flakes in the MPL. Overall, research into graphene based MPLs remains extremely limited.

Carbon-free MPLs

Carbon-free, metal MPL materials have also been explored due to their high electron conductivity and corrosion resistance. The work in this field is as yet extremely limited, though research has been conducted in metal powders [152, 41, 153, 154, 155] and steel plates [150]. Leeuwner et al. [150] investigated a series of free-standing MPLs fabricated from different materials, one of which was a perforated stainless-steel sheet. Although the in-plane resistance was extremely low, the interfacial contact resistance with the catalyst layer was a factor of 3 larger than the commercial MPL. This can be attributed to the steel plate having the lowest surface roughness which transposes as less contact between the smooth steel and the catalyst interface. The polarisation curve showed that the perforated steel sheet produced a power density lower than the uncoated GDL substrate; this could be due to the contact resistance though it is also likely that the perforated sheet does not possess the multi-porous three-dimensional network typical of the MPL and essential for reactant transport. This lack of an interconnected pore network that may have limited mass transport between the GDL and the catalyst.

Titanium has also attracted research interest as an MPL material. Fang et al. [156] deposited titanium as a thin film by magnetron spluttering. Titanium based powders also seem to offer potential as an MPL material where: iridium-titanium nitride (Ir-TiN) [41], iridium oxide and Titanium particles IrO_2/T [152] and Titanium (Ti) [153, 154, 155] have been explored. Hwang et al. [155] found that the titanium powder MPL increased meso-pore size and MPL wettability, improving liquid water management and reactant transport at high RH 100%; however, at lower RH (66%), where water is more present in the vapour phase, it proved less effective. Metal powders are promising in terms of their desirable transport characteristics and pore structure. Moreover, advances in 3D metal powder printing, as demonstrated by Jayakumar [88] for the substrate, will allow control over pore size and structure. However, limitations exist in the cost of materials, production costs and arguably dimensions of the MEA on upscale.

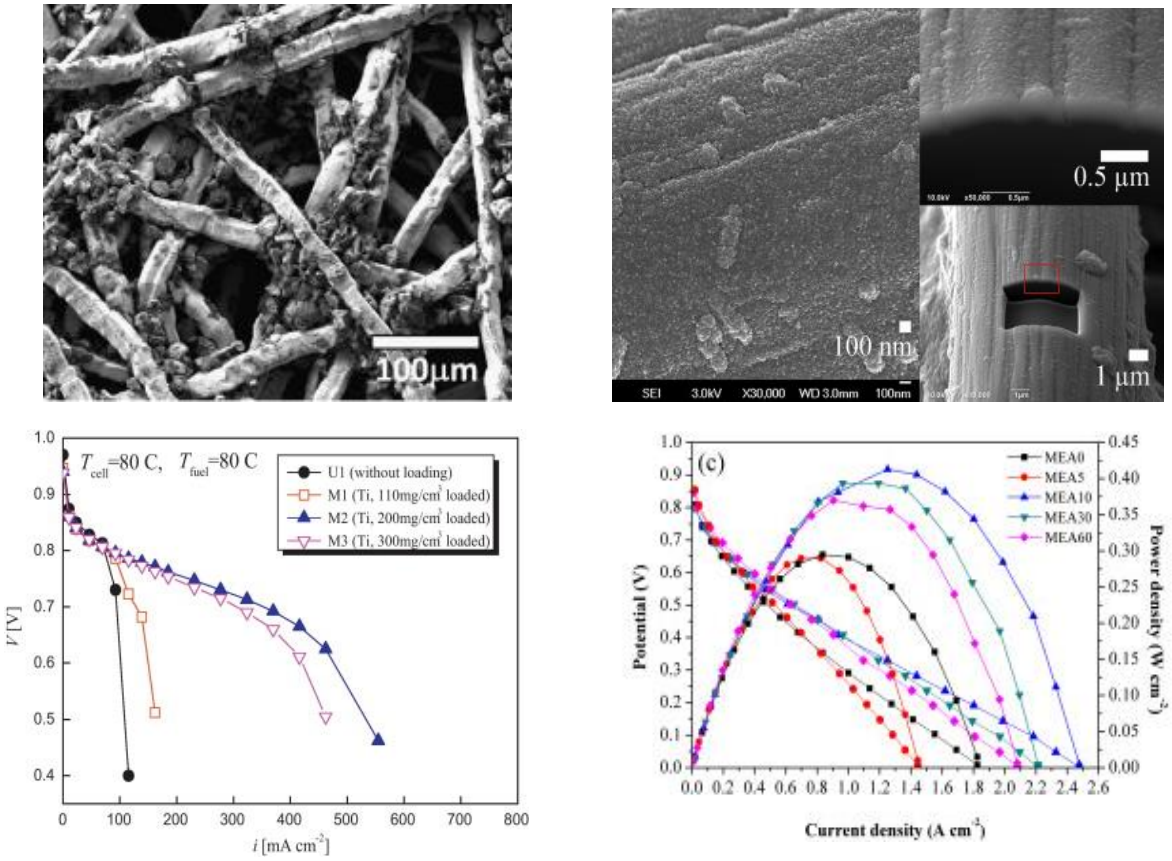

Figure 2-18: Titanium coated GDL. (Left) SEM micrograph of the Ti felt substrate surface with Ti powder (300 mg cm^{-3}) (top) and polarisation curve of Ti substrate with different Ti loading, 80ºC (bottom) (Right) SGL 10BA after 10 minutes Ti spluttering (top), and the polarisation curve and power density of GDL with varying Ti spluttering time, 65ºC (bottom) [176].

Free-standing MPLs

Several research groups have researched a free-standing MPL with varying success [62, 254, 255]: Bauder et al. produced in-house non-woven synthetic support for a carbon black/PTFE MPL with 20% and 40% wt. PTFE content, they exhibited lower contact angle and through-plane resistances (particularly 40% wt. PTFE) than the commercial MPL. By increasing the thickness of the 20% wt. MPL, they found comparable power densities to SGL 25BC. However, at high RH flooding caused mass transport losses. The use of EIS and synchrotron radiography allowed the group to see the cause of resistance losses and to assess liquid water distribution in operando. Ito et al. produced a free-standing MPL sheet from acetylene black and PTFE which was applied to Toray TGP-H090 and H060 carbon substrates and left as a free-standing MPL with no backing substrate (the thickness of all was maintained at ~300 μm) [62]. Fig. 2.19 is the polarisation curve of the MPLs, the standalone MPL (GDL 5 in figure) produced higher peak power density than when applied to the carbon substrate, particularly at high current densities and at all relative humidities. This was attributed to the low thermal conductivity of the MPL which hindered liquid water accumulation in the bulk MPL as it could be transported by vapour diffusion without hindering O_2 diffusion. Interestingly the pore size distribution of the fabricated MPL was highly micro and meso-porous, having very few macropores. Macro-pores are believed to be the pathway for gas diffusion, although if water is in the vapour state, then it might be that the reactant gas is able to travel through the micro and meso pores as they are not filled by liquid water. However, as the stand alone MPL lacked the mechanical strength and flexibility it is likely to have a very low lifespan if subjected to durability testing.

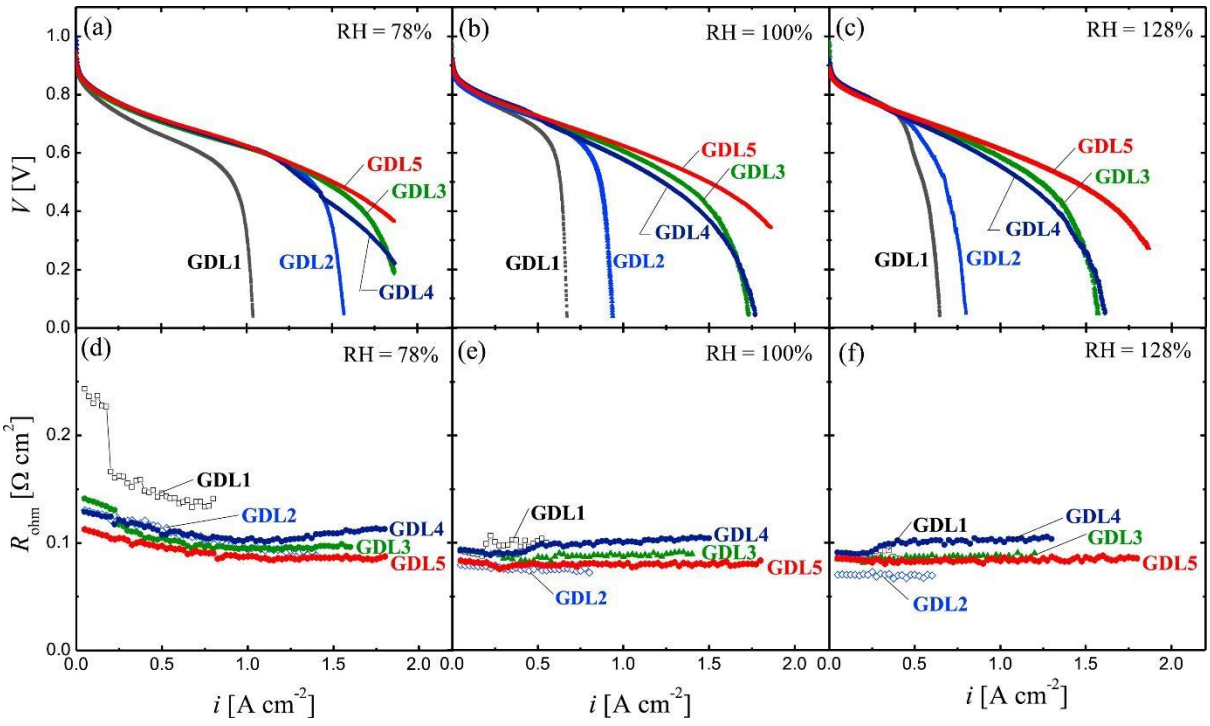

Figure 2-19:Polarisation curve and ohmic resistance of fuel cell set ups with different MPL thicknesses applied to Toray H-060 GDL substrate (GDL 5 is free standing MPL) [62].

Duan et al. [255] electro spun a carbon nanofiber sheet which possessed good electrical conductivity and hydrophobicity, and when applied as an MPL exhibited a higher permeability than conventional coated GDL. When tested as the cathodic GDL, a high peak power density (321 mW $cm^{-2)}$ was achieved corresponding to 23% higher to the conventional MPL at the cathodic GDL. Their work did not however, asses the durability of the MPL material.

2.5.1 Alternatives to PTFE in the MPL

Conventionally the carbon black in the microporous layer is mixed with PTFE as a hydrophobic binder, in order to prevent flooding of the porous media during fuel cell operation, especially at high current densities. However, the use of PTFE as a hydrophobic agent has an adverse effect on the physical, microstructural and transport characteristics of the MPL. To this end, a large volume of research has been conducted into alternative means of preventing flooding.

Fluorinated Polymers

Super hydrophobicity is achieved when the contact angle of a material exceeds 150˚. One branch of research is focused on improving the hydrophobicity of the microporous layer using similar materials to PTFE, aiming to increase the contact angle whilst also reducing ohmic and mass transfer losses. For example, a significant amount of research has also been conducted into the viability of polyvinylidene fluoride (PVDF) as a replacement binder for use in the porous media of PEMFC. For example, Su et al. [74] fabricated gas diffusion electrodes using 15% wt. PVDF as the catalyst layer binder. They concluded that polyvinylidene fluoride improved surface morphology, and improved distribution of catalyst particles on the surface, increasing the availability of active sites. A peak power density to 0.56 W cm^{-2} was measured compared to 0.20 W cm^{-2} using Nafion as a binder. Zhang et al. [256] investigated PVDF for the anion exchange membrane fuel cells; similarly they found that using PVDF as a binder in the MPL increases the catalytic activity.

Meanwhile, Park et al. [257] fabricated a polyvinylidene fluoride-based MPL from a slurry with carbon black, which was applied to a carbon cloth GDL using the doctor blade method. MPLs with various ratios of PVDF and carbon black were compared with a PTFE-based MPL, and uncoated GDLs. SEM images revealed that the surface morphology of the PVDF-based MPL had greater uniformity than the PTFE-based MPL. The large cracks that are characteristic of PTFE-based MPLs were not present for PVDF; which was instead characterised by small pores. The use of PVDF as a binder resulted in significantly higher fuel cell power density, which they attributed to the appropriate in-plane and through-plane microstructure observed in the SEM images. However, hydrophobicity of the MPL could also have been highly influential, as the untreated GDL only reached a maximum current density 0.3 A cm^{-2} compared to the 1.2 A cm^{-2} for the PVDF-based MPL. Since no contact angle measurements were performed and the relative humidity of the fuel cell tests was not recorded, it is difficult to draw conclusions from this study.

Bottino et al. [258] produced MPLs using phase inversion technique by immersion in a water bath of a mixture of either polyvinylidene fluoride or sulfonated polyvinylidene fluoride and using Vulcan XC-

72 carbon black and Timrex HSAG 300 graphite as the electroconductive filler. The exposure time of the cast MPL prior to immersion in the coagulation bath was varied, from 0.5 minutes to 8 minutes as was the solvent used, N-methyl-2-pyrrolidone (NMP) and Dimethyl sulfoxide (DMSO). The MPL from DMSO solvent, PVDF, and an 8-minute expose time measured the highest contact angle at 130º. The PVDFS MPL produced the highest cell performance, at 0.60 A cm^{-2} a voltage of 0.60 V was recorded compared to 0.43 V for the PVDF.

Ong et al. [259] also prepared a PVDF-based MPL via phase-inversion of PVDF and Vulcan XC-72 carbon black, which was then applied to a commercial wet-proofed cloth E-TEK GDL which was exposed for 30s and then immersed in a water bath. Increasing the PVDF content of the MPL from 5-10% wt. decreased the permeability significantly from 23.99 to 0.57 $\times 10^{-4}$ mol s^{-1} Pa^{-1} m^{-2} and whereas the increase in resistivity of MPL is insignificant (0.50 to 0.52 Ω). Two PVDF solutions were prepared for the carbon black dispersion, using different solvents: N,N-dimethylformamide (DMF) and N-methyl-2-pyrrolidone (NMP). The DMF cast MPL measured a higher resistance (0.062 Ω) than the NMP cast MPL (0.053 Ω), though the permeability values did not vary. The PVDF MPL GDL produced a higher limiting current density and greater peak power density (0.33 W cm^{-2}) than the blank and the 40% wt. PTFE MPL (0.25 W cm^{-2}). The difference in potential was particularly higher in current densities > 0.3 A cm^{-2} thus having superior mass transport properties at higher current densities. This was attributed to the microstructure of the PVDF MPL being an asymmetric porous structure with cavities, in which the in-plane and through-plane mass transport is enhanced. As this GDL was not subject to heat treatment or sintering, a comparison of the surface morphology of the PVDF MPL heat treated and immersed would prove interesting, especially when combined with in-situ imaging of water distribution. Phase immersion may produce a smoother, more homogeneous PVDF coating, yielding different results to when the MPL is heat treated.

In addition, perfluoropolyether-based microporous layers have been studied [232, 260]. PFPE binds strongly with carbon black due to its high surface area and porosity, allowing for the ease of adsorption of PFPE. Moreover, perfluoropolyethers can be chemically linked to the carbon black producing PFPE-functionalised carbons which are highly stable and can reach the super-hydrophobic threshold (157º at

8% wt.) [261]. PFPE-functionalised carbon blacks offer a promising alternative to carbon black-PTFE composites as unlike PTFE, the conductivity is preserved in the PFPE-modified carbon black because the electrical continuity of the conductive carbon network is maintained [262].Where Vulcan XC-72 has been chemically functionalised with 10% wt. peroxide PFPE the resistivity remains very close to the value of the pristine carbon black [260, 262].

Experiments conducted by Navarrini et al. [260] into functionalised-PFPE carbon blacks in the MPL indicated that 1% wt functionalised-PFPE has better performance in the mass transport zone than 10% wt. PTFE, where the voltage drop occurs at 1.30 A cm^{-2} rather than 1.0 A cm^{-2}. Thus a 30% increase in current density was achieved by the substitution of PTFE with functionalised-PFPE. The peak density was increased from around 0.42 W cm^{-2} to 0.45 W cm^{-2}, which was attributed to better reactant diffusion due to improved water management and higher gas permeability. Likewise, a recent study by Latorrata et al. [263] concluded that a 10% higher power density can be obtained using PFPE-functionalised Vulcan XC-72 in the MPL in the place of conventional PTFE at 80°C and RH 60%.A peak power density of 460 mW cm^{-2} was achieved at 80°C and 100% (Fig. 2.20 (right)). Fig. 2.20 (left) shows the mass transfer or diffusion resistance of the different MPL-coated GDLs, where at 60°C and 100% RH the PTFE MPL experiences mass transport losses at high current density. This indicates the inferior water management of the conventional PTFE MPL.

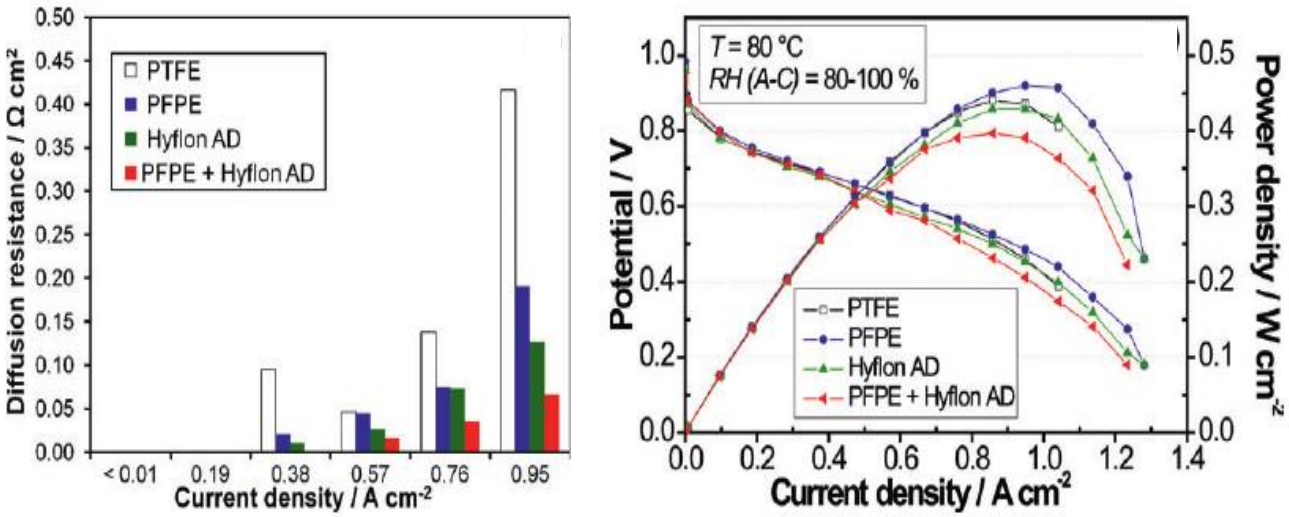

Figure 2-20: The diffusion resistance of the GDLs with MPL different compositions (60º C, 80-100% RH). (Right) Polarisation curve of MEAs with the differing MPL compositions (80 º C and 80-100% RH). [189].

Balzarotti et al. [232] used a high molecular weight PFPE-based MPL (i.e. Fluorolink® P56) with different wt.%, which was applied to B1-A, E-TEK carbon cloth GDL. A contact angle of 149° was achieved with 12% wt. PFPE, whilst the value was 154º for 6 wt%. PFPE. A higher power density was also achieved for 6% wt. PFPE compared to the 12% wt., 0.59 W cm^{-2} and 0.53 W cm^{-2} respectively. The authors' explanation was that the larger cracks in the MPL surface improved permeability and diffusive properties of the MPL, however this is not conducive with other findings as larger cracks increase the resistance at the MPL and catalyst layer interface. It is more likely that the increase in PFPE concentration reduced the available pore space and thus limited reactant diffusion.

The characterisation of fluorinated polymers in the MPL by Latorrata et al. [75] is highly informative. The work compared PTFE with alternative fluorinated polymer binders, namely fluorinated ethylene polymer (FEP), perfluoropolyether (PFPE), and perfluoroalcoxy (PFA). The FEP-based MPL was reported to have the highest contact angle of 160º, whilst the PTFE-based MPL had the lowest contact angle, making it the least hydrophobic. Correspondingly, the fluorinated ethylene polymer -based MPL had the highest maximum power density, and the lowest mass transport losses in fuel cell tests. For example, at 1.0 A cm^{-2}, the FEP-based MPL was measured to have a potential of 1.0 V, compared to

0.8 V for the PTFE-based MPL (Fig. 2.20). The same group [264] then conducted further experiments into the stability and durability of FEP-based MPLs, with minimal difference in fuel cell performance after 1000 h of mechanical and chemical accelerated stress testing.

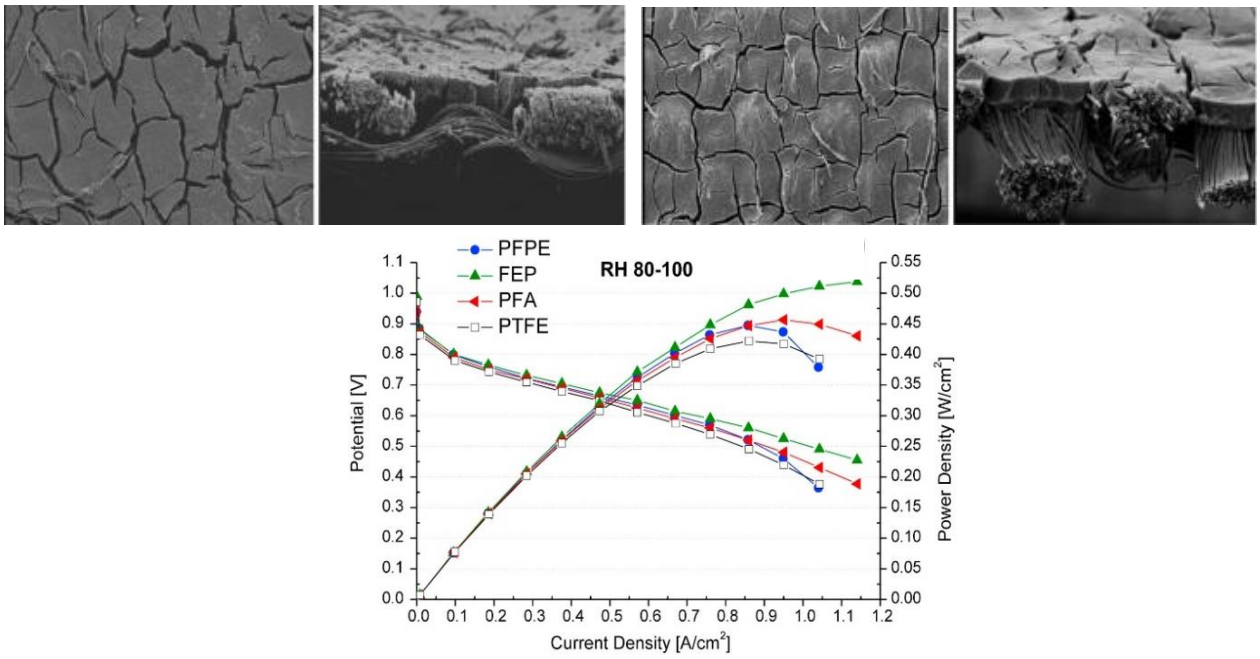

Figure 2-21: (Top) SEM images of the surface and cross section of the MPL (left) FEP, (right) PTFE. (Bottom) MPLs fabricated with different hydrophobic agents at RH 80–100 [190].

Park et al. [265] also conducted research into 10% wt. FEP-based MPLs deposited on Toray carbon cloth, and reached similar conclusions. The use of FEP resulted in a higher water contact angle (145°) compared with PTFE-based microporous layers (141°C), which may have increased the water-repelling capability of the MPL. The FEP-based MPL produced a more precise and uniform pore size distribution than PTFE-based MPL due to the smaller particle size, moreover, an absence of large pores and crude cracks on the MPL surface was observed. These two factors are believed to reduce the contact resistance between the MPL and catalyst layer, however, contact resistance measurements were not conducted. In fuel cell performance tests, the fluorinated ethylene polymer-based MPL produced a higher power density of ~ 0.3 W cm^{-2}, compared to ~ 0.25 W cm^{-2} for the PTFE-based MPL.

Meanwhile, Yan et al. [237] found that 30 wt.% of FEP in the MPL was optimal for minimising flooding and improving the fuel cell performance, and obtained a maximum power density of 1.4 W cm^{-2}. Moreover, they compared different MPL coating methods (i.e., spray coating and screen printing), concluding that screen printing resulted in better cell performance. This was attributed to the formation of cracks in the spray-coated MPL coating, reducing the contact area between the electrocatalyst layer and the MPL, thus increasing the contact resistance.

Hydrophilic and Mixed-wettability MPLs

Another branch of research is directed towards the study of hydrophilic MPLs. Instead of conventional hydrophobic MPLs, where the aim is to push water through and out of the fuel cell, hydrophilic MPLs aim to pull water out of the electrocatalyst layer. The potential of hydrophilic MPLs to mitigate water flooding at high current densities has been reported in several studies [266-269]. For example, Aoyama et al. [269] compared hydrophobic and hydrophilic MPLs of various thicknesses, conducting polarisation measurements in fully humidified conditions. They reported that hydrophobic MPLs had the highest cell resistance and that the hydrophilic carbon fibre MPL produced a higher voltage than the hydrophobic carbon black MPL at high current densities (0.4 V and 0.3 V respectively at 1.6 A cm^{-2}). It was deduced that the hydrophilic MPL surface allows water to spread across the MPL surface and promotes evaporation within the large pores and thus the thick hydrophilic MPLs may be more effective when there is more liquid water produced. Similarly, Tanuma et al. [252] also developed a novel hydrophilic MPL composed of vapour-grown carbon fibres with hydrophilic ionomer, resulting in MEAs with higher power density compared to those with hydrophobic MPLs, across a range of different relative humidities. Different MPL architectures were more influential at different relative humidities; where at low RH (30%) the mean pore diameter was the largest factor, and conversely at high RH (100%) pore volume was the greatest contributor to power density. The greatest power density (0.75 W cm^{-2}) was achieved at 30% RH.

The majority of research into PEMFC is targeted at improving MEA performance in high humidity conditions; however, it is also necessary to optimise PEMFC design for low humidity conditions> this is because PEMFCs are to be applied to a broad spectrum of applications (aerospace, stationary and portable applications) and these have different operating requirements and reactant feeds. In low relative humidity conditions, maintaining membrane hydration for optimal ionic conductivity is the largest challenge. To this end, investigations on how to create hydrophilic MPLs allowing for PE.MFC self-humidification have been conducted [270, 271]. A hydrophilic anodic was produced by Guo et al.[270] by ultraviolet treatment of TiO_2 particles, to reduce the membrane resistance in low humidity conditions. The hydrophilic MPL reportedly decreased both the charge transfer resistance at low current densities, and the ohmic and mass transport resistance at high current densities, improving performance at both low (100 mA cm^{-2} and high (1200 mA cm^{-2}) current densities. Other works have used UV treatment of the MPL to create hydrophilic regions to produce a GDL with graded hydrophobicity for the diversion of liquid water away from the catalyst layer [272]. The UV treatment leads to the formation of OH radicals on of the gas flow channel side of the GDL, thus reducing the hydrophobicity and creating a GDL with graded wettability from the catalyst layer to the gas flow channel [272].

To provide a deeper understanding of how hydrophilic regions in the MPLs facilitate liquid water transport in MEAs, Mukundan et al. [136] used neutron radiography to visualise the liquid water distribution *i*n-situ. An MPL was produced by incorporating 10% hydrophilic alumosilicate fibres into a conventional hydrophobic carbon black MPL slurry and applied to an SGL 24AA GDL, and a comparison was made with a commercial SGL 25BC. The addition of the hydrophilic fibres increased voltage by 150 mV at 2 A cm^{-2}, increasing power density by 30%. Liquid water distribution was analysed to understand the difference in power density. The water profile across a cross-section of the cell operating at 1.0 A cm^{-2} was obtained by neutron imaging (Fig. 2.22). In the hydrophobic MPL, indicated by the red line, the peak indicates that liquid water saturation is concentrated close to the cathode catalyst layer, moreover, the MPL has a low water content as can be seen by the drop when moving away from the MEA. In contrast, the MPL with hydrophilic fibres, shown by the blue line, has more liquid

water in the MPL region evidenced by the steadier water content profile. Additionally, there is no peak at the cathode catalyst area, indicating that liquid water saturation is lower at the cathode catalyst layer, thus, indicating that liquid water saturation is lower at the cathode catalyst layer, thus, indicating that the loss in power of the hydrophobic 25BC were mass transport losses due to liquid water saturation.

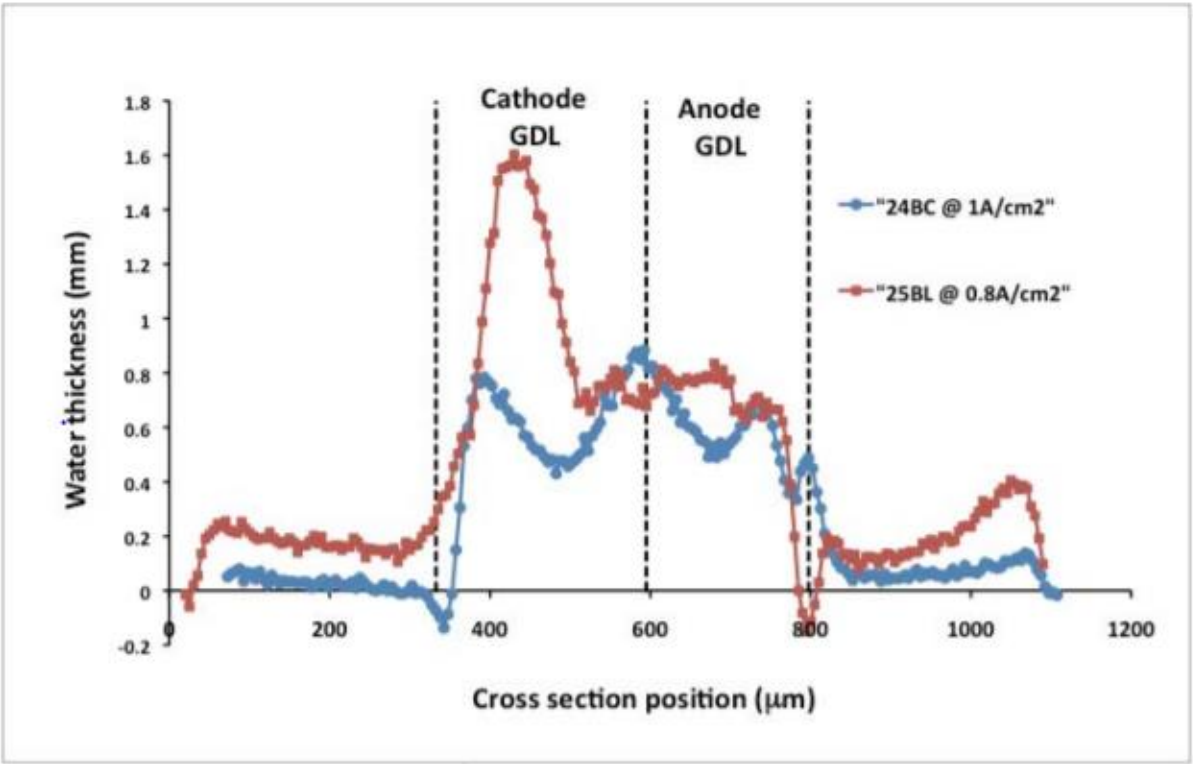

Figure 2-22: Water profiles at 2.5 cm^{2}at 80ºC and 100% RH using the 2 GDLs. 25BL (10% hydrophilic fibres in MPL) and 25BC (hydrophobic MPL) [199].

Furthermore, the addition of alumosilicate and hydrophilic fibres into the hydrophobic MPL improved the mean pore diameter. The increased pore diameter facilitated the movement of liquid water away from the MPL/ catalyst interface, where the hydrophilic pores provided pathways in the MPL, wicking the water away from the cathode.

Additionally, Aoyama et al. [269, 273] and Nozaki et al. [268] used cryogenic scanning electron microscopy of cross-sections of the cathode side microporous layer to visualise the liquid water distribution inside hydrophilic and hydrophobic MPLs. They found that much less liquid water was

present in a thick hydrophilic MPL compared to a thin hydrophilic MPL or a conventional hydrophobic MPL. They postulated that thick hydrophilic MPLs facilitate the passage of liquid water, which is then able to more rapidly into the gaseous phase to be transported effectively through the porous media.

Multi-layer MPLs

An innovative dual-layer MPL was developed by Kitahara et al. [274, 275], with a thin hydrophilic MPL deposited directly onto a conventional hydrophobic MPL, for low relative humidity operation. The hydrophilic MPLs were composed of 95% carbon black mixed with 5% polyvinyl alcohol (PVA) or TiO_2 (titanium dioxide). They reported that the hydrophilic MPL preserves the membrane humidity, whilst the hydrophobic layer prevents the removal of water from the hydrophilic MPL by evaporation. The dual-layer hydrophilic/hydrophobic (5 wt. % PVA) MPL produced greater power than the hydrophobic PTFE MPL, particularly in the mass transport region, where at 1.2 A cm^{-2} the voltage was 0.5 V and 0.3 V respectively. Further performance enhancements were done by optimising the PTFE content, and thus the hydrophobicity of the hydrophobic layer [274]. A further innovation was the development of a triple-layer MPL by Kitahara et al. [276] where, the substrate was coated in a hydrophobic MPL (10 wt.% PTFE), followed by another hydrophobic MPL (30 wt.% PTFE), and finally a hydrophilic PVA-based MPL (Fig. 2.23). This resulted in further improvements in the fuel cell performance, which was attributed to the hydrophobic gradient which successfully expelled liquid water from the electrocatalyst layer at high relative humidity. The most influential aspect of this group's work is the introduction of the concept of graduated MPLs, rather than limiting the design to one single layer with a homogeneous microstructure.

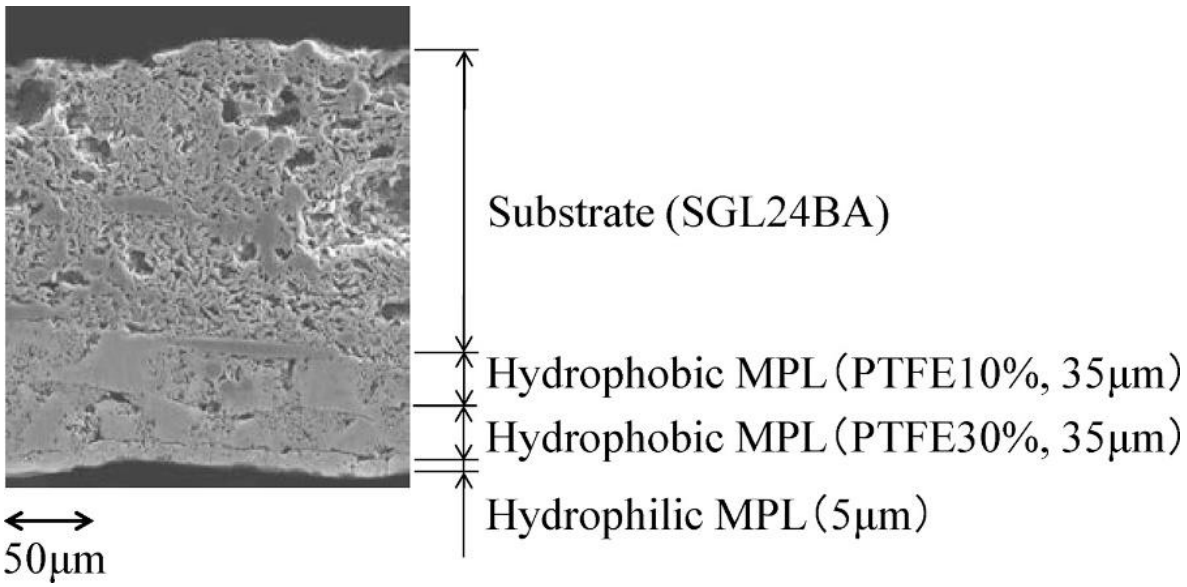

Figure 2-23: Cross-sectional SEM micrograph of a triple-layer MPL-coated GDL [202].

2.5.2 Summary of Material and Design Enhancements to the Microporous Layer

Novel MPL materials present an exciting future in fuel cell engineering, especially the application of carbons with differing aspects to conventional carbon black, e.g., graphene platelets and carbon nanotubes. The material basis of the MPL determines the morphology and microstructure of the porous media and thus influences the reactant pathways and water management in the MPL and the MEA as a whole. Due to its unique MPL micro-structure, graphene-based MPLs are becoming an extremely popular research area. Moreover, composite MPLs formed of carbons with different aspects have a synergetic effect on the MPL morphology, where reactant transport and liquid water are better managed than the single material-based MPL. This opens up a multitude of possibilities for MPL material compositions, the optimisation of which can be greatly accelerated by the use of micro-scale modelling. Current MPL research is limited by a lack of consistency, which makes comparison of the effect of the materials themselves highly difficult. For example, characterisation methods vary between papers making it hard to establish the cause for high/low power density or good/bad water transport phenomena. Furthermore, these findings are drawn from in-house MPLs where the method of application of the MPL to the substrate is variable. It has been remarked that the application method

can affect the microstructural properties of the whole GDL, particularly the substrate MPL/ interface [237]. This is largely disregarded, and conclusions are drawn based on the material composition of the applied layer.

The optimisation of liquid water displacement in the microporous layer and the membrane electrode assembly as a whole will lead to significant increases in fuel cell efficiency. The superhydrophobic threshold of the MPL is easily achieved with alternative fluorinated polymers and by plasma deposition of smaller wt.% than conventional PTFE. The lower polymer content equates to small reductions in pore size and conductivity, thus increasing the capability of the MPL for two-phase and electron transport. Moreover, in particular, the PFPE-functionalised carbon black, or even other carbon materials, can rectify many of the problems encountered with the conventional PTFE adsorption on carbon black, such as increased durability and minimal impact on MPL pore size distribution.

Innovative MPL architectures with mixed wettabilities have been shown to improve power density, where hydrophilic regions act as pathways to push liquid water away from the cathode electrocatalyst area. Further research is needed to improve these hydrophilic/ hydrophobic MPLs by optimising the ratio of hydrophilic: hydrophobic areas, as well as their correct profile, shape, and distribution.

2.6 Summary of the Literature

Over the past two decades, a substantial body of work has been dedicated to the methods of characterisation of the gas diffusion layer. The literature on the porous media of the PEMFC is expansive, where the gas diffusion layers have been widely studied through experimental methods and computational models. The experimental data has helped to validate and contradict the application of existing equations for the transport properties of the porous media.

Experimental visualisations of the PEMFC GDLs using nano and micro-scale methods have become a hot topic of research over the last decade. In addition, X-ray computed tomography and FIB-SEM have allowed for imaging of the internal structure of the gas diffusion layers, and from these 3D images, computational models have been used to solve equations to calculate the transport properties. X-ray computed tomography is now a well-established technique that has been used for both ex-situ and in-operando studies of PEMFC. Whilst SEM has been used extremely successfully to support the findings from in-situ and ex-situ measurements and for the visualisation of the surface morphology of the GDL, which is of great importance for the visualisation of the liquid waterfront.

Although significant work has been carried out on liquid water transport and management in the gas diffusion layers, it is evident that it is still one of the largest limiting factors for PEMFC power generation. The majority of studies on the GDL have largely focused on the evaluation of the performance and the characterisation of existing commercial GDLs. Characterisation of commercial GDLs has been researched at great length, and the link between the GDL structure and the transport properties of the GDL has been well-established. However, it has been noticed that few research papers have actually used these findings to develop innovative in-house GDL designs, using alternative materials, though the suggestion has been raised by several researchers. Moreover, the porous layers of the PEMFC (the MPL, catalyst layers, and the GDL) are routinely investigated as either individual components or as the whole fuel cell. There is definitively a lack of a holistic approach to these components, although their optimum operation is dependent on each other. It is therefore important that more work is performed on the porous media and MEA as a whole.

The focus of this research is to optimise the current MPL-coated gas diffusion layer as a means to reduce water saturation in the porous media whilst maintaining high conductivity, diffusivity, and permeability. In addition, the GDL architecture and microstructure will be optimised to promote two-phase flow at high current densities. In order to do so, carefully selected non-conventional materials will be prepared, characterised, and compared with conventional GDL materials.

2.7 The Knowledge Gap

Having undertaken a detailed summary of the literature on the gas diffusion layer and microporous layer of the polymer electrolyte membrane fuel cell, a clear gap in knowledge has emerged. Recent design modifications to the materials and architecture of the microporous layer have improved cell performance although it is clear that further optimisation is needed to increase the range of operating conditions at which the PEM fuel cell can perform.

From the literature, there are a few salient points that should be observed. Firstly, the addition of materials other than carbon black to the microporous layer produces an MPL of much different physical and microstructure properties to the conventional. These properties have had a positive influence on the transport properties and by extension cell performance.

Secondly, the influence of the pore size and its distribution in the microporous layer has shown that the inclusion of mesopores and small macropores in the layer has improved fuel cell performance at higher current densities and higher humidity conditions. Thus, implying that the presence of these larger pores reduces the mass transport losses and helps to mitigate liquid water saturation.

Lastly, the recent development of novel pore architectures in the MPL, such as graduated pore size from the catalyst layer to the substrate, has resulted in increased limiting current densities and higher power densities. This improves upon the initial purpose of the MPL being an intermediary between the gas diffusion layer and the catalyst layer and enhances its capability for water management.

Within these research topics lies the basis of this thesis, as there is a defined gap in knowledge in these three topics. Initially, this research addresses the knowledge gap regarding alternative materials; graphene has proven itself to be a potentially beneficial material in the microporous layer. However, the optimisation of the graphene content of the microporous layer has not been thoroughly investigated, this is explored in Chapter 4.

Previous studies have shown the benefits of the presence of large pore sizes in the microporous layer resulting from the use of alternative carbons, such as carbon nanotubes and carbon fibres. Graphene foam, a recent discovery, has received very little research attention, although it can hold significant

potential as an MPL material. A novel graphene foam derived from the pyrolysis of sodium ethoxide is produced and its viability in PEM fuel cells is investigated. This material has not previously been investigated in the microporous layer.

Finally, Chapter 6 explores innovative microporous layer architectures by the fabrication of MPLs with a pore gradient. By applying layers of different carbon materials (carbon black, large graphene, and small graphene) it is possible to produce microporous layers with a custom pore gradient. The results of this investigation are found in Chapter 6.

Chapters 7 and 8 conclude this thesis summarising the findings and the impacts of this work, as well as suggested trajectories for future projects and continuation on this topic.

Chapter 3: Experimental Methods

3.1 Introduction to Methods

The role of the microporous layer in the fuel cell MEA is manifold, enabling efficient thermal and electron transfer whilst simultaneously ensuring the transport of reactants to and water away from the catalyst layer. Thus, enhancement of microporous layer design is complicated as it requires the optimisation several physical and electrochemical properties. The desirable characteristics and the methods of characterisation of the gas diffusion layer and microporous layer were detailed in the literature review, found in Chapter 2 of the thesis. In this chapter the chosen characterisation methods are explained, with summaries of the experimental procedure and details of the equipment including the manufacturer and model numbers.

3.2. Material Synthesis

Chapter 5 was the product of a research collaboration between the University of Sheffield and Kyushu University in Japan. At Kyushu University they have been synthesising novel graphene foams for use as a platinum support, and as a non-precious metal catalyst when doped with nitrogen and iron. The graphene foams have an open pore structure and graphene thin walls which lends an extremely high surface area and could reduce resistance to mass transfer in the microporous layer. Equally, the high carbon purity and low oxygen content of the material results in a high electron conductivity which is another desirable property for the MPL. To this end, graphene foams were synthesised and MPLs were fabricated in order to gauge if the material could be used for both the catalyst layer and the microporous layer or as a multifunctional layer.

Graphene foams were fabricated using the two-step pyrolysis methodology developed by Speyer et al. [277], in this method sodium ethoxide is used as the precursor to produce the graphene foams. The sodium ethoxide is pyrolised in a box furnace under a flow of nitrogen gas (75 ml/min) to produce the initial carbonaceous foam. The temperature was increased by 5°C / minute until a temperature of 725°C was reached, the temperature was then held at 725°C for 2 hours.

The resulting product was then stirred overnight in deionised water, before washing with 5 litres of water and vacuum filtered to remove any residual sodium impurities. The resulting product was then dried in a vacuum oven at 80°C and separated into two batches for the second pyrolysis step; one of which was pyrolised at 1000°C in a nitrogen atmosphere (100 ml/min) which was then labelled N graphene foam, the other sample was pyrolised at 1000°C in an atmosphere of 95% nitrogen and 5% hydrogen (100 ml/ min) which was then labelled NH graphene foam. Fig. 3.1 shows the two-step pyrolysis process, graphene foams can be seen as the resulting product. Both graphene foams appear as a black powder like substance similar in appearance to carbon black, however the physical properties differ as the graphene foams are less dense and tend to flocculate when agitated.

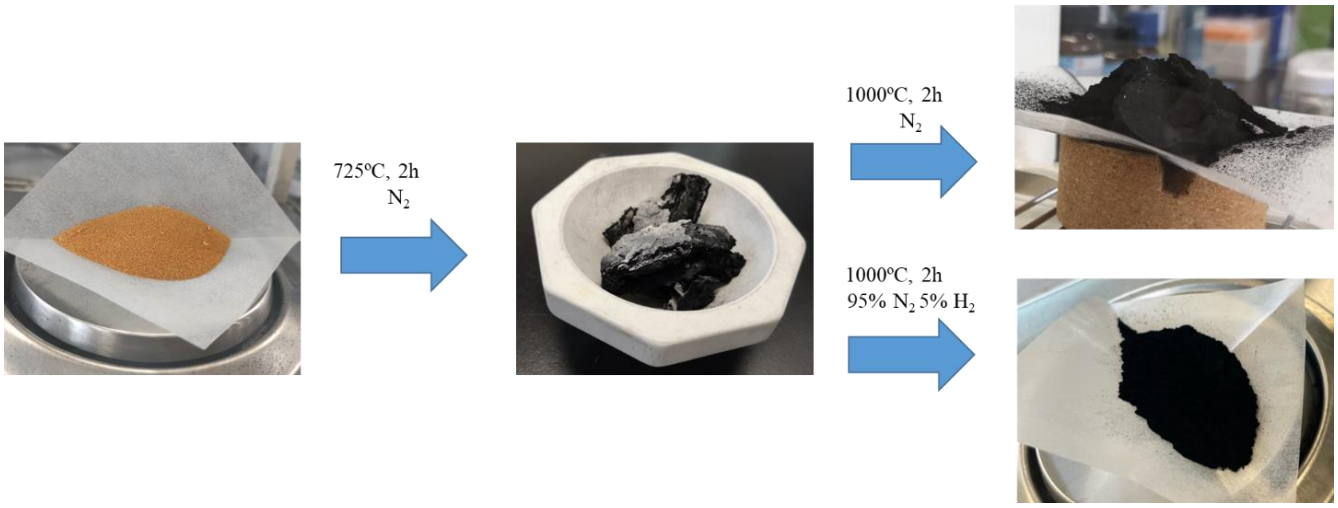

Figure 3-1: Schematic of the two-step pyrolysis process to produce the nitrogen-graphene foam and the nitrogen-hydrogen graphene foam.

3.3. Elemental Analysis of Carbon Foams

3.3.1 X-ray Photoelectron Spectroscopy

X-ray Photoelectron Spectroscopy, or XPS, is a non-destructive technique which is widely used for the analysis of the surface chemistry of samples. XPS reveals information about the elemental composition structure of the sample to a depth of 10 nm, where elements are detected from the binding energies of the photoelectrons with the exception hydrogen and helium. Elemental analysis of the carbon foams, nitrogen-graphene foam and the nitrogen-hydrogen-graphene foam was determined by X-ray photoelectron spectroscopy (XPS). All the elemental analysis was conducted at Kyushu University on a PHI 5000 Vera Probe II (ULVAC-PHI, INC.).

3.4. Characterisation of Microporous Layers

3.4.1. Morphology and Microstructure

Porosity/ Pore Size Distribution

Mercury intrusion porosimetry (MIP) is a widely used technique to measure the total pore volume and pore diameters of porous media, and as such it can be used to determine the bulk porosity and pore size distribution of the gas diffusion layer. MIP is based on the application of gradually increasing external pressure to a porous sample which is immersed in a non-wetting fluid, typically mercury. The volume of intruded mercury into the pores is recorded at each pressure step. At low pressure the mercury is able to fill the larger (macro) pores of the GDL as there is less resistance as less surface tension needs to be overcome, as the pressure increases the smaller pores are penetrated. Fig. 3.2 shows the pore size distribution of an uncoated carbon paper GDL, an MPL-coated carbon paper GDL and a novel composite GDL obtained using MIP. The data for the pore size distribution of the MPL is shown in conjunction with the pore size of the GDL, as the layer is applied to the GDL it is characterised together. In this regard it is not possible to say with definite certainty that all of the pores in the microporous region are those of the MPL as the GDL substrate data is also present. This becomes more difficult if the pore sizes in the MPL are the in the mesoporous and microporous region, which occur with frequency in the GDL substrate. This is a recurrent difficulty with research and innovation into the MPL as it occurs in conjunction with the GDL it is difficult to characterise. Moreover, as ex-situ

characterisation of the MPL properties occurs in isolation to the other properties, the enhancement of one characteristic of the MPL may have a detrimental effect on another. This can only be realised through cell performance testing.

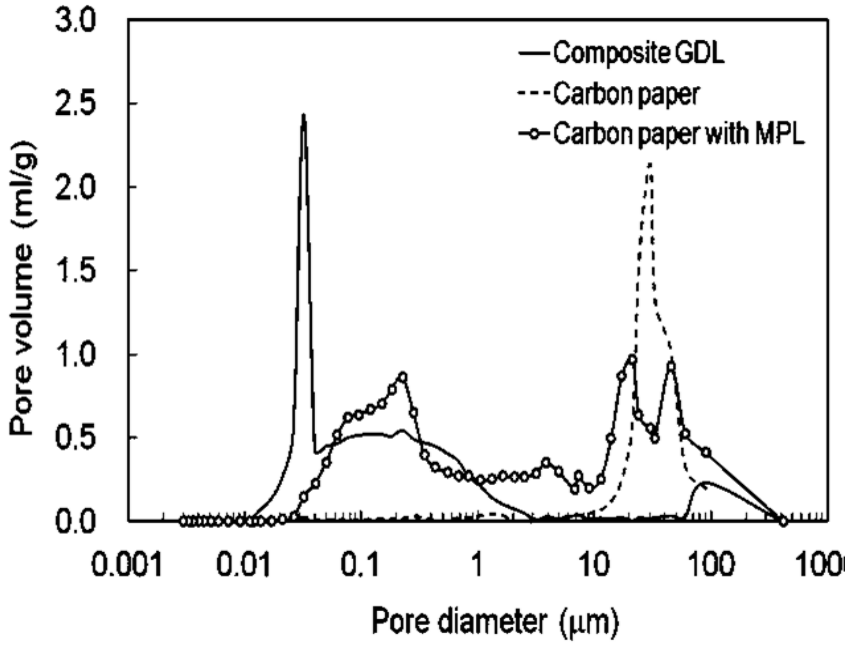

Figure 3-2: The pore size distribution of an uncoated carbon paper GDL, an MPL-coated carbon paper GDL, and a composite GDL produced using carbon black [9].

MIP measurements are based on the Washburn equation (equation 3.1) which relates the pressure of the gas to the pore size of the medium; the pressure needed to enable mercury intrusion is related to the pore diameter.

$$P_L - P_G = \frac{4\sigma cos\theta}{D_P} \tag{3.1}$$

Where, P_L is the pressure of the liquid, P_G is the pressure of the gas, σ is the surface tension of the liquid θ is the contact angle of the intrusion liquid, and D_P is the pore diameter.

Mercury intrusion porosimetry was used to determine the pore characteristics of the blank and coated GDLs (pore size distribution, mean pore diameter and porosity). In this instance the measurements were conducted using a MicroActive AutoPore V 9600 V, where the intrusion pressure of the mercury was

then gradually increased from 0 to 421 MPa. The intruded volume of mercury (log differential intrusion [mL/g]) was recorded at each pressure step, from which the pore size distribution could be defined.

3.4.2 Scanning Electron Microscopy (SEM) imaging

Scanning electron microscopy (SEM) is an established technique to obtain clear, high-resolution images of the surface of a material. SEM images are produced by scanning a focused beam of high energy electrons across the surface of a sample. The interactions between electrons and the atoms of the sample produce a signal which reveals information about the composition, morphology, and physical structure of the sample. The morphological characteristics and microstructure of the GDLs were observed using scanning electron microscopy which was performed on a JEOL instrument (Model JSM-6010LA). The samples were adhered to the sample holder using a double-sided, conductive carbon tape. To obtain the cross-sectional images, the samples were placed vertically using a cross-sectional sample holder enabling the observation of the top view of the sample edges. Thus, the thickness of the MPL could be determined with accuracy. Imaging of the carbon materials (Vulcan carbon black, Nanene graphene nanoplatelets, and the graphene foams) was performed on a higher resolution scanning electron microscope (FEI Inspect F), and the samples were splutter coated in gold prior to visualisation in order to reduce the electron excitement of the carbon. Double-sided adhesive carbon disks were used to stick the prepared powder samples on to the sample holder. The carbon powders were applied to the carbon disks using a small spatula, pressurised nitrogen was used to remove excess (poorly adhered) particles and to obtain the correct sample height.

3.4.3. Physical Properties

3.4.3.1 Contact Angle

Contact angle measurements can be used to determine the hydrophobic and hydrophilic characteristics of the surface of a sample. A droplet of water is placed on the surface of a sample, and the angle between the sample and the line tangent to the edge of the droplet is measured (Fig. 3.3). This is known as the contact angle, the size of which indicates the wettability of the surface. If the contact angle measured is larger than 90° then the surface is considered to be hydrophobic, whereas angles lower than 90° are

hydrophilic. The principle behind this is based on the intermolecular interactions between the surface and the water droplet, and is expressed mathematically in Young's equation (equation 3.2):

$$cos\theta = \frac{\gamma_{sv} - \gamma_{ls}}{\gamma_{lv}} \tag{3.2}$$

Where, θ is the contact angle, γ_{sv} is the surface energy of the solid-vapour interface, γ_{ls} is the surface energy of the liquid- solid interface, and γ_{lv} is the surface energy of the liquid-vapour interface (surface tension).

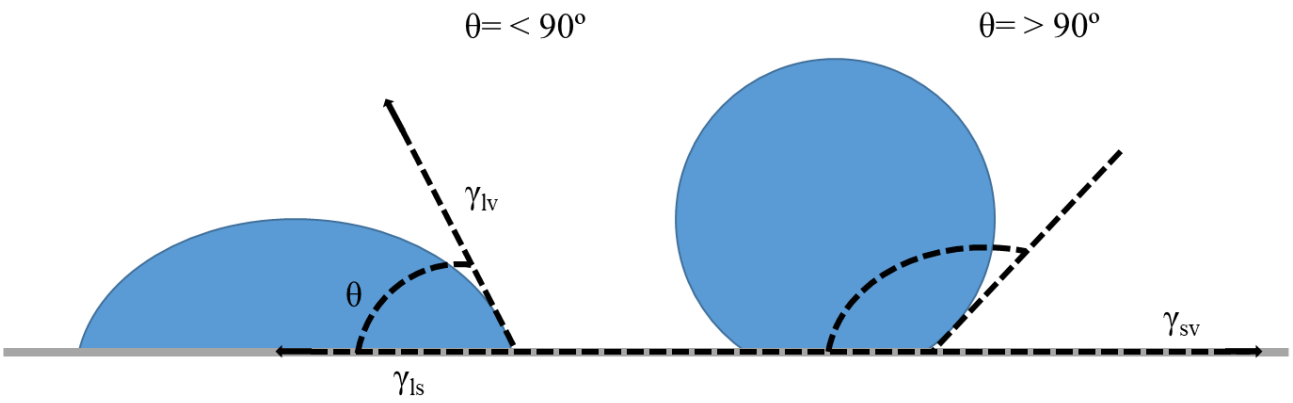

Figure 3-3: Diagram showing the contact angles on a hydrophilic (left) and hydrophobic surface (right).

In this investigation, the water contact angle of the GDL surfaces was measured using a video drop shape system FTA200 goniometer (First Ten Angstroms, USA). Owing to the slight inhomogeneity of the GDL surface, the contact angle measurements were taken at several positions on the surface of the sample to ensure a realistic representation of the average value of the contact angle. As such the contact angle was measured at 7 positions on the GDL sample, and the average value and the 95% confidence interval were then calculated.

3.4.3.2 Through-plane Permeability

Permeability is the ability of a porous material to allow fluid through its pores, as such the permeability of a porous medium is extremely influential in determining the fluid flow rate through the pores. A high permeability of GDL is important as it allows for a greater reactant flow to the catalyst layer, additionally it allows water produced at the catalyst layer to be directed to the fluid flow channels to prevent electrode flooding. Low permeability increases the reactant transport resistances and creates a higher pressure gradient, it increases the necessary power input to maintain the flow rate of the reactant gases.

The coefficient of gas permeability is usually measured experimentally according to Darcy's law by measuring the pressure drop at specific flow rates across the sample [91, 92, 93]. Darcy's law is an approximation of the Navier-Stokes equation, which is valid for only laminar flow rates, where the velocity of flow can be assumed to be Stokes flow. Darcy's Law states that the flow rate through a porous body is equal to the product of the permeability and the pressure gradient across the porous body divided by the viscosity of the fluid. It is calculated from the following [70]:

$$\frac{\Delta P}{L} = \frac{\mu}{k} v \tag{3.3}$$

$$v = \frac{Q}{\pi D^2/4} \tag{3.4}$$

Where, ΔP is the pressure drop across the sample, L is the measured thickness of the samples, μ is the dynamic viscosity of the flowing gas (for nitrogen at 20°C is about 1.8×10^5 Pa s), k is the gas permeability of the sample, v is the velocity of the flowing gas, Q is the volumetric flow rate and D is the diameter of the sample exposed to the flow, respectively. As the MPL and substrate are layered in the coated GDL, the pressure drop can be viewed as:

$$\Delta P_{GDL} = \Delta P_{substrate} + \Delta P_{MPL} \tag{3.5}$$

Where, ΔP_{GDL} , $\Delta P_{substrate}$ and ΔP_{MPL} are the pressure drops across the coated GDL, substrate and MPL respectively. Combining Equations (3.3) and (3.5) gives the following:

$$\frac{\mu L_{GDL}}{k_{GDL}} v = \frac{\mu L_{substrate}}{k_{substrate}} v + \frac{\mu L_{MPL}}{k_{MPL}} v \tag{3.6}$$

where, μL_{GDL} $\mu L_{substrate}$ and μL_{MPL} are the lengths of the coated GDL substrate, the substrate and MPL respectively, and k_{GDL} , $k_{substrate}$ and k_{MPL} are the permeability coefficients of the coated GDL, substrate and MPL, respectively. Thus, the permeability of the MPL can be solved by equation (3.7):

$$k_{MPL} = \frac{L_{MPL}}{\frac{L_{GDL}}{k_{GDL}} - \frac{L_{substrate}}{k_{substrate}}} \tag{3.7}$$

The experimental setup used was contrived by Ismail et al. [7] (Fig. 3.4), and consists of lower and upper fixtures, where a circular GDL sample of 25.4 mm is diameter is placed and tightened between these two fixtures. Nitrogen gas is forced to flow through the sample, and the pressure drop is measured across the GDL for 7 flowrates. A flow controller (HFC-202, Teledyne Hastings, UK) with a range of 0.0–0.1 SLPM is used to control the flowrate of the nitrogen gas. A differential pressure sensor (PX653, Omega, UK) with a range of ±12.5 Pa, was used to measure the pressure difference across the GDL sample.

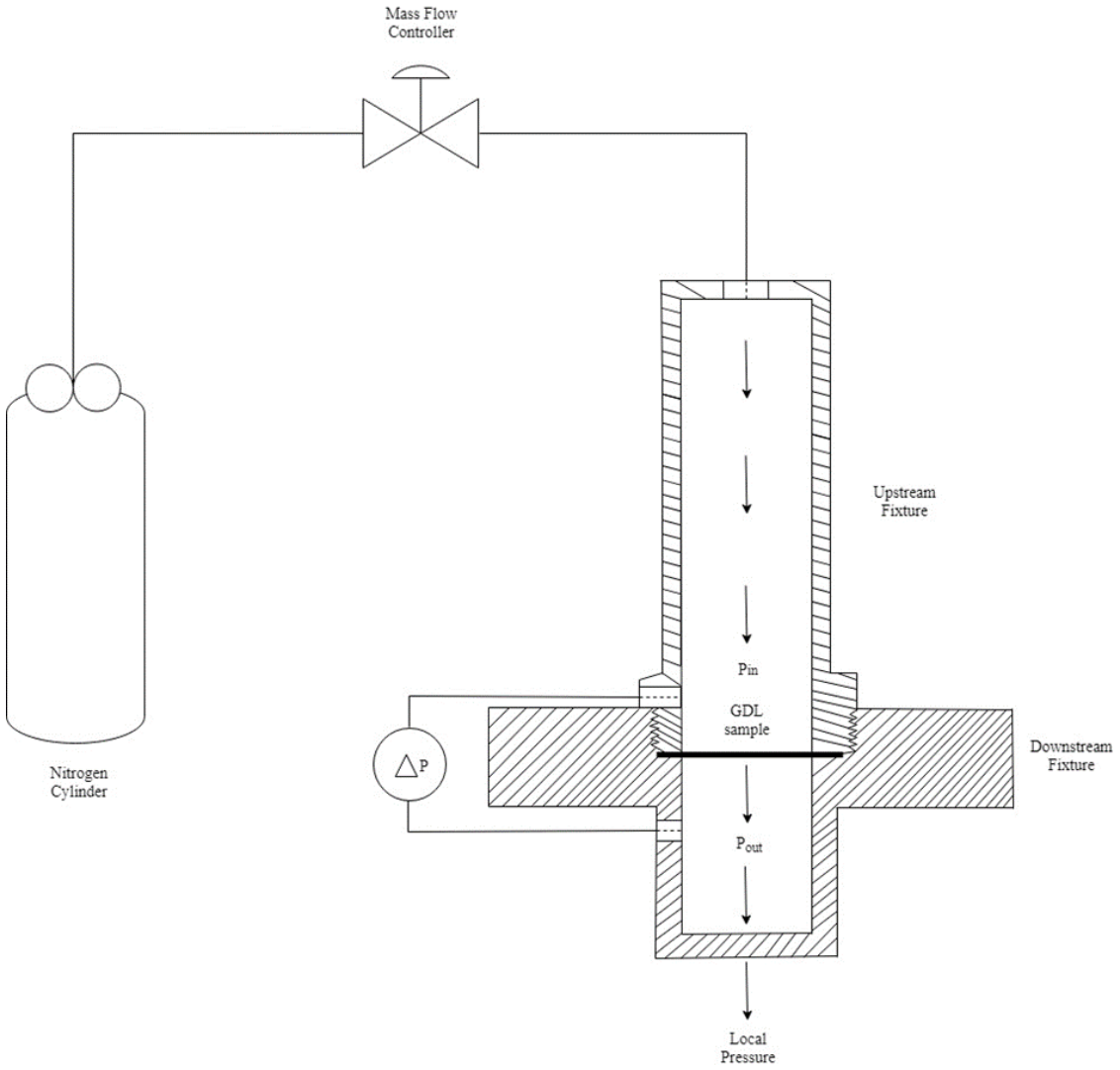

Figure 3-4: Schematic diagram of the in-house setup used to measure the through-plane permeability of the GDL samples [7].

3.4.3.3 In-plane Electrical Conductivity

The in-plane electrical conductivity of the GDL samples was measured using the 4-probe method outlined by Smits et al. [278] and adapted by Ismail et al. [8], where a geometry-dependant correction factor is employed for thin sheets. According to Smits' method, the correction factor is dependent on the dimensions of the GDLs samples and the spacing between the probes. Essentially, it is derived from two ratios, being the length of the GDL to its width (a/d), and the width of the GDL to the spacing between the probes (d/s). The ratios were calculated as 1 (a/d) and 1 (d/s) for samples used. Thus, from Smits tables the correction factor has a value of 1. The electrical resistivity, ρ, can be then calculated using the following formula [278]:

$$\rho = CtR \tag{3.8}$$

where, C is the correction factor, t is the thickness of the GDL, and R is the measured electrical resistance. The electrical conductivity (σ) is the reciprocal of the electrical resistivity (ρ) as thus is calculated by:

$$\sigma = \frac{1}{\rho} \tag{3.9}$$

The experimental procedure (Fig. 3.5) was derived from the in-plane conductivity setup as described by Ismail et al.[8]. The GDL sample was positioned on an insulating polycarbonate plate. The thickness of the GDL samples averaged from 5 measurements taken at equally spaced positions. The electrical resistance was measured by an RS Pro 804 Ohmmeter (RS Components), which has a resolution of 0.01 mΩ. The micro-ohmmeter provides a current which flows across the samples via the current leads and measures the voltage using the voltage leads. Thus, the resistance is then calculated using Ohm's Law. As the distance between the two voltage probes must be kept constant they are housed in a plastic body, where spacing of which is equal to the width of the GDL sample (20 mm). Finally, adhering to Smit's method the spacing between each probe and the adjacent electrode was the same as the spacing between

the two probes. The in-plane conductivity of 5 samples was measured, where each GDL sample was measured 5 times. The individual values of the resistance were then averaged.

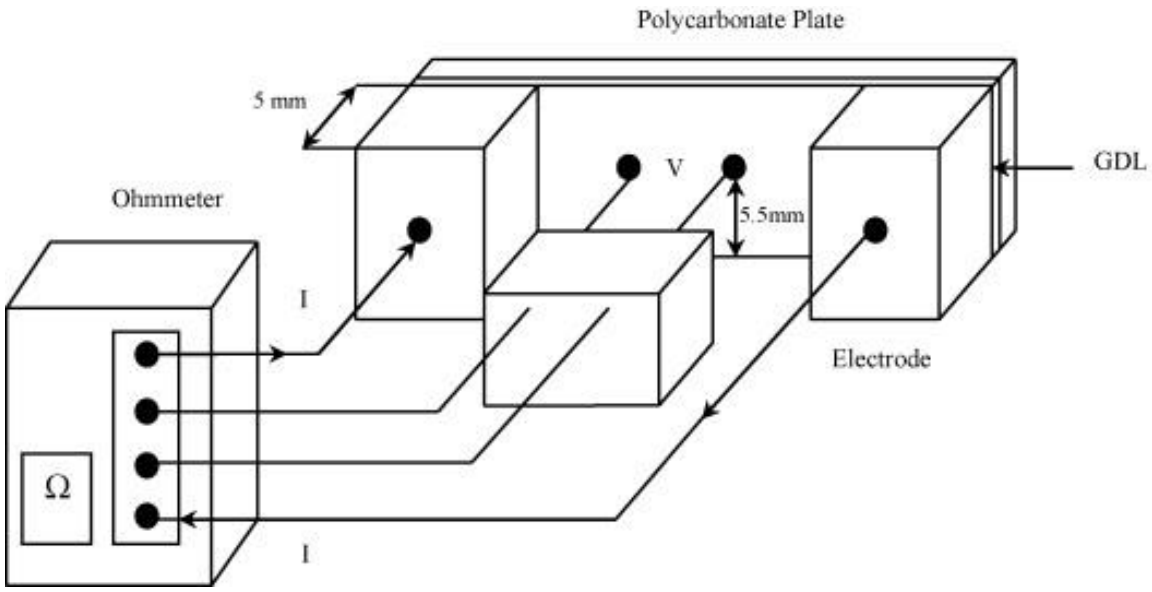

Figure 3-5: Schematic diagram of the setup to measure the in-plane electrical conductivity [8].

3.4.5. Electrochemical Characterisation of Microporous Layers

3.4.5.1 PEMFC Performance Testing

Polarisation curves, or IV curves, are the main electrochemical performance tests of PEM fuel cells; they show the cell voltage output plotted against the current density. By multiplying the voltage by the current at each point the cell power density can be obtained. This is then plotted against the cell current density in order to produce a power density curve. The polarisation curve is a powerful tool that can be used to determine the sources of loss in the cell, a detailed explanation of these losses and how they can be derived from the polarisation curve is given in Chapter 1, Section 1.4.6.

The MEA was assembled using a C2 Freudenberg carbon substrate as the anode GDL, where fabricated dual-layer GDLs were used as the cathode GDL. The MEA utilised a catalyst coated membrane as received produced from Nafion 212 (Fuel Cell Earth), where a platinum loading at both the cathode and anode was 0.5 mg cm-^{2} or 0.3 mg cm^{-2}. The single cell measurements were conducted on a commercial fuel cell test station (Scriber, or Biologic) with an electrode active area of 500 mm^{2}. For each of the MEAs assembled PEMFC performance measurements were taken at 80°C at a range of air and hydrogen relative humidity conditions (from 25% RH to 100% RH), measurements were also taken with oxygen and hydrogen at 50% RH. The inlet pressure for the anode and cathode back pressure applied was 250 kPa and 230 kPa respectively in accordance with the EU test protocols for single cell measurements for PEMFC [279].

3.4.5.2 Electrochemical Impedance Spectroscopy

Electrochemical impedance spectroscopy (EIS) is a valuable technique which is used to analyse the sources of performance losses in fuel cells and other electrochemical devices. Voltage loss in the fuel cell originates from three main sources: activation or charge transfer losses; ion transport or ohmic losses; and concentration or mass transport losses. By producing an equivalent model circuit where the physiochemical processes which occur in the fuel cell are represented by capacitors, resistors, and inductors (Fig. 3.6), one is able to determine the sources of impedance within the fuel cell.

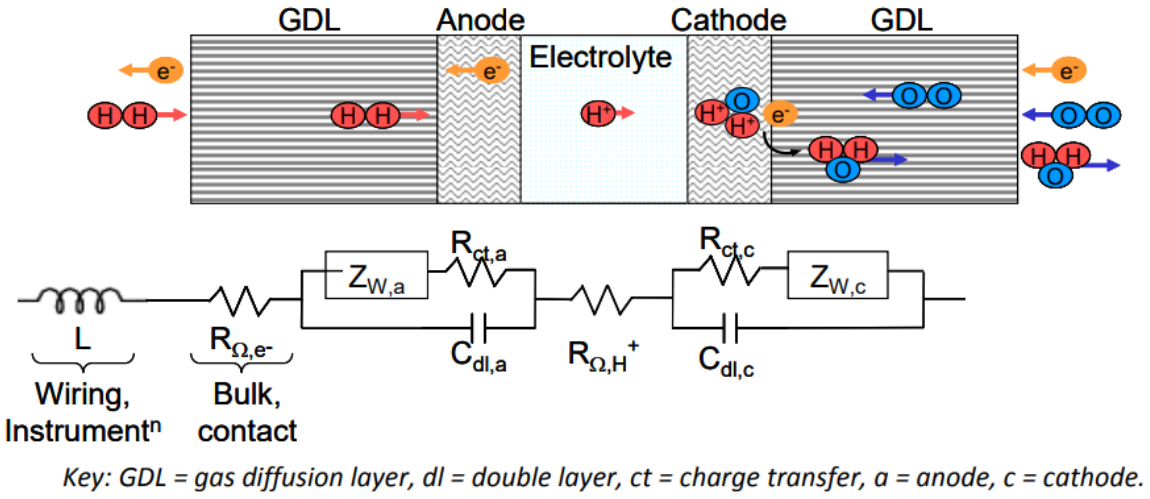

Figure 3-6: The equivalent circuit model used to represent the membrane electrode assembly components (ideal resistors (R), capacitors (C), and inductors (L)). in EIS analysis. Zw is the Warburg element used to represent diffusion or mass transport impedance [2].

In the equivalent circuit, the resistors represent the pathways for electron and ion transfer, and therefore represent the bulk resistances of the material to ion transfer i.e., the membrane electrolyte resistance to ion transfer, or the resistance of the GDL to electron transfer. The capacitors and inductors represent polarisation regions, such as the reaction processes at the catalyst layers. EIS data is typically presented in the form of Nyquist plots (Fig. 3.7) where the real voltage (x-axis) is plotted against the imaginary voltage (y-axis), which is indicative of the capacitive and inductive character of the cell. The shape of the impedance arc and its intercept with the x-axis provide insight into possible mechanisms of impendence. Fig 3.7 is an example of a Nyquist plot where the sources of impedance have been identified. The intercept with the x-axis corresponds to the ohmic resistance, the first semicircle relates to the charge transfer resistance, and finally, the second semi-circle is the mass transport resistance. In this research project, EIS measurements were taken at 0.6 V for each of the test conditions, and the data is presented as Nyquist plots.

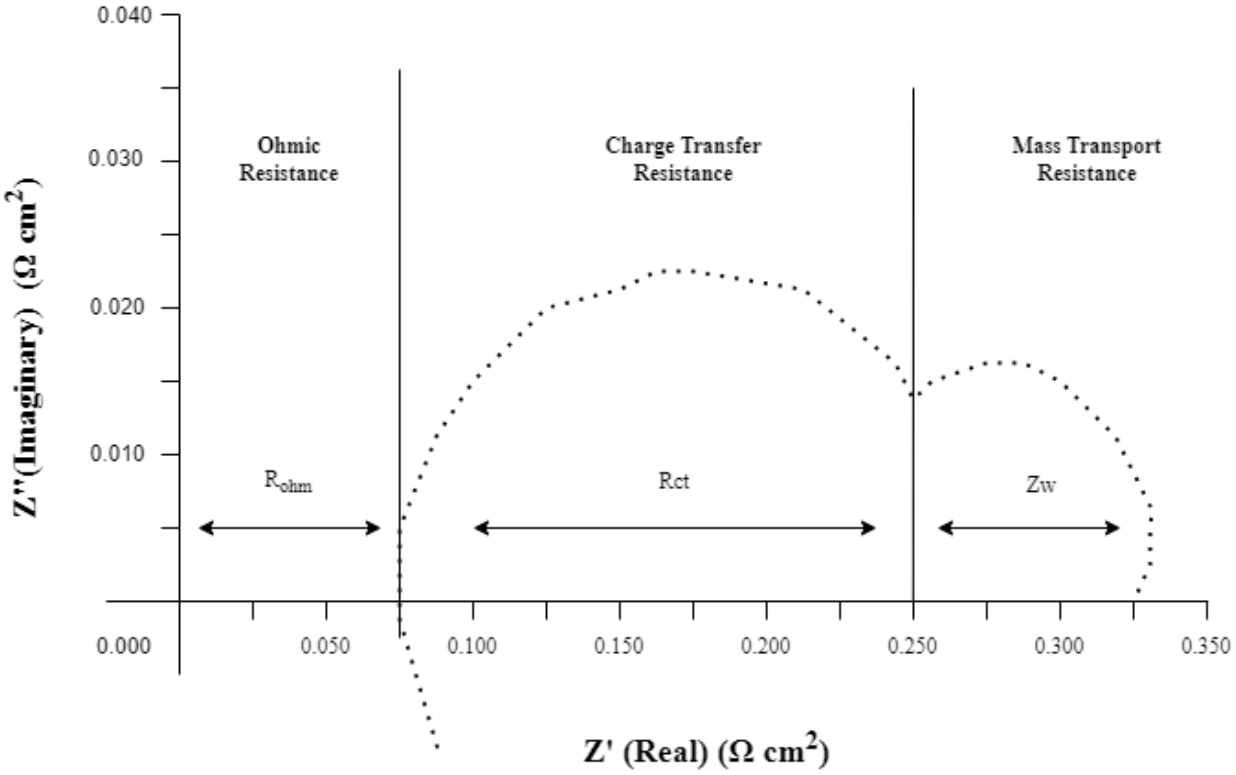

Figure 3-7: The Nyquist plot indicating the sources of internal resistive loss within the cell. Adapted from [1][2].

Chapter 4: Optimisation and Characterisation of Graphene-based Microporous Layers for Polymer Electrolyte Membrane Fuel Cells

4.1 Abstract

The viability of graphene-based microporous layers (MPLs) for polymer electrolyte membrane fuel cells is critically assessed through detailed characterisation of the morphology, microstructure, and transport properties. Microporous layer composition was optimised by the fabrication of several hybrid MPLs produced from various ratios of graphene to Vulcan carbon black. Single cell tests were performed at various relative humidity conditions between 25% and 100% at 80°C, in order to provide a detailed understanding of the effect of the graphene-based MPL composition on the MEA performance, with a specific focus on the ohmic and mass transport regions. The inclusion of graphene in the MPL alters the pore size distribution of the layer and results in the formation of mesopores and macropores. The inclusion of graphene at 50 wt.% affects the transport properties of the layer by reducing the gas permeability but increasing the electrical contact resistance, contact angle and in-plane conductivity. Polarisation curves indicate that a small addition of graphene 30 wt.% in the microporous layer optimises cell performance in low humidity conditions and when air is used as the oxidant. In higher humidity conditions ≥ 50% relative humidity, where mass transport losses dominate, 50 wt.% graphene and greater leads to improved cell performance. Graphene inclusion is optimal at 50 wt.% graphene where air is used as the oxidant.

4.2 Introduction

Water management remains one of the largest barriers limiting fuel cell efficiency, especially at high current density; due to the dual problem of liquid water accumulation in the electrode which limits reactant transport [281, 282], and membrane dehydration leading to a loss of proton conductivity [221, 283]. The microporous layer (MPL) within the gas diffusion layer (GDL) of PEMFC is widely acknowledged as a crucial performance-enhancing component [217, 284]; improving cell efficiency and durability, largely by the improved management of the flow of water and reactants [284]. The role of the MPL in the fuel cell MEA is complex, as it serves as a conduit for the transport of heat, electrons,

and mass. Therefore, MPL enhancement poses a challenge to researchers as it requires the optimisation of several parameters. Alternations to the microstructural, physical, or electrochemical properties may be extremely beneficial in terms of one characteristic but detrimental in another, and as a result, negatively impact cell performance. For this reason, characteristics must not be assessed in isolation, as performance enhancements may be the result of a compromise of one characteristic in favour of another. The MPL itself is a testament to the necessity of prioritising one characteristic over another, i.e., although the extra layer at the GDL/catalyst interface increases resistance to the transport of mass and electrical charge, these losses are deemed negligible considering the performance enhancements gained from the addition of the layer.

The purpose of this research is to develop a greater understanding of how composition affects MPL microstructure and morphology, and ultimately identify strategies to improve fuel cell efficiency. The synergetic effect of different types of carbon has been explored by several researchers. Early research investigated the interactions of different types of carbon black when used together in the MPL, and the effects imparted on MPL morphology gas transmission and liquid water saturation [3, 230]. Numerous studies have examined the synergy between carbon nanotubes and high-purity carbon black in the microporous layer; inclusions of multi-wall carbon nanotubes have influenced the microstructure and pore size distribution of the layer and improved the mass transport phenomena, particularly in saturated conditions [241, 249, 251, 281]. Similar studies have been undertaken using graphene as an additive in the microporous layer [244, 253], these demonstrated that the addition of graphene can lead to significant improvements in MEA performance, resulting in higher power densities and limiting current densities. Although the performance enhancements with graphene were strongly influenced by the cell operating conditions, notably the temperature and relative humidity.

A recent trend has seen graphene being explored as an alternative to carbon black in the MPL. Graphene is a two-dimensional monolayer of graphitic carbon atoms, with good mechanical stiffness and elasticity, as well as extremely high electrical conductivity and thermal conductivity [285]. Graphene has previously been explored as an MPL material by a few researchers both as a freestanding MPL [244] and conventionally applied to carbon substrates [242, 243, 245, 253]. Leeuwner et al. [244]

fabricated a free-standing MPL for the cathode GDL from commercially available compressed 3D freestanding graphene foam. However, the lack of treatment with a hydrophobic agent and inhomogeneous surface limited the power density at higher current densities (>1500 mA cm^{-2}) due to flooding. Ozden et al. [242] characterised MPLs from Grade DU25 graphene. The in-house graphene-based MPL exhibited a higher peak power density than the Vulcan-based MPLs at relative humidity ranging between 40 to 100%. However, their research was limited by the use of a single material, pure graphene for the fabrication of the MPLs, composite MPLs produced from graphene and carbon black were not considered. Whereas Mariani et al. [243] characterised microporous layers produced from various-sized graphene platelets to ascertain the optimum platelet size for the MPL. 25µm sized platelets produced the highest power density, yet their results suggest that a combination of graphene and carbon black (1:1 ratio) in the microporous layer may have a complimentary effect. Similar studies using exfoliated graphene [253], reduced graphene oxide, and natural graphite [245] indicated that composite MPLs produced from graphene and carbon black result in a higher current density, particularly at higher relative humidity operation.

Although these works further our understanding of how graphene can be used in the MPL, they have not explored the optimisation of the ratio of graphene platelets to carbon black. Mixing graphene with carbon black, or a mixture of graphene with different morphologies has the potential for a synergetic effect on MPL morphology and microstructure, thus optimising cell performance. Here we present the fabrication and characterisation of novel MPLs produced from graphene-based materials. The microporous layers were produced from Nanene (2D Tech, Cheltenham) a high-purity graphene, Vulcan XR 72 C carbon black, and a combination of the two materials. The MPLs were then characterised for their morphology, physical properties, and fuel cell performance.

4.3 Methodology

4.3.1 Materials

The fabricated dual-layer GDLs were used at the cathode. The carbon substrate used to produce the dual-layer GDLs was Toray TGP H-60 carbon paper (10% wt. PTFE treated, Fisher Scientific). The carbon powder used in the MPL ink was Vulcan XC 72 R (Sigma Aldrich®, BET surface area: 238 $m^2 g^{-1}$ [286] whereas the few-layer graphene (FLG) powder used in this study was Nanene (2-DTech Ltd., part of Versarien plc., UK). Nanene is produced using a mechanochemical process with BET surface area: 45 $m^2 g^{-1}$. The hydrophobicity of the layer was achieved by the addition of 60 wt.% polytetrafluoroethylene dispersion (PTFE, Sigma-Aldrich®).

MPLs were produced from a viscous ink consisting of carbon and PTFE. Distilled water was used as the solvent for the MPL ink. Triton X-100 (Sigma Aldrich®) and methyl cellulose (Sigma Aldrich®) were added to improve the dispersibility and the rheology of the MPL ink [287].The MPL was applied to commercial Toray TGP-H-60 GDL (10 wt.% PTFE) using a micrometre applicator (Industrial Physics) with a heated plate at 80°C.

The MPL-coated GDLs were heat treated in a tube furnace to thermally decompose the Triton X100 and methyl cellulose, and to uniformly distribute the PTFE particles throughout the MPL. The temperature profile was 120°C for 1 hour, 280°C for 30 minutes and finally sintered at 350°C for 30 minutes [83]. Table 1 lists all the MPL compositions investigated in the study following initial drying and thermal treatment. The MPL composition by weight remained unchanged consisting of 80% carbon and 20% PTFE. The carbon loading was kept constant at 2.0 mg cm^{-2} in all inks as in [83].

Table 4-1: The compositions of the microporous layer inks.

MPL	**Vulcan (wt.%)**	**Nanene (wt.%)**	**PTFE (wt.%)**
G0	80	0	20
G30	56	24	20
G50	40	40	20
G70	24	56	20
G100	0	80	20

The thickness of each of the GDL samples was measured using a micrometre before and after the MPL coating was applied. Each sample was measured at 5 equally spaced positions within it to provide a representative average value of the thickness.

4.4 Results and Discussion

4.4.1 Morphology

The morphology and the surface structure of the carbon substrate and the MPLs were visualised by scanning electron microscopy (SEM). Fig. 4.1 is a series of SEM micrographs showing the surface structure of the MPL-coated and the uncoated Toray substrates. Notable differences can be seen between the surface structure and morphology of the carbon black MPL and those derived from graphene. This morphological difference depends on the physical characteristics and the behaviour of the MPL material. The particle size of the two materials differs greatly; where the Nanene graphene nanoplates are several orders of magnitude larger than the Vulcan carbon black particles, 10 μm and 50 nm respectively.

Due to van der Waals forces carbon black nanoparticles agglomerate in the MPL to form a microporous structure. The agglomeration of the carbon black particles results in the distinctive micro-cracks which characterise the surface of G0 (Fig 4.1(b)), the carbon black MPL, these are the result of shrinkage caused by solvent evaporation in the thermal treatment phase. The presence of these cracks is typical of carbon black based MPLs and is frequently noted in the literature. However, they are absent from all the graphene containing MPLs regardless of carbon black content (Fig. 4.1(c-f)). The visible cracking on the surface of the G0 and its absence in the other samples indicates that this phenomenon is present in MPLs comprised of a smaller particle size, and the inclusion of particles with larger dimensions prevents its occurrence. One of the key roles of the MPL is to maintain the correct balance of liquid water in the catalyst layer and the membrane; where the membrane requires hydration to reduce ohmic resistive losses, but excess water leads to insufficient reactant distribution at the surface of the catalyst layer, causing mass transport losses. As such the MPL structure must simultaneously be able to retain

liquid water in low humidity conditions and remove water at high humidity conditions or high current density operation. The presence of cracks on the MPL surface have been shown to promote the transport of liquid water away from the catalyst layer in high humidity conditions by acting as liquid phase pathways diverting the water from the catalyst layer [150, 288]. Certainly, the crack-free morphology of the graphene containing MPLs visually appear to have a much lower permeability than the carbon black MPL as there are no clear routes for the fluids to permeate the MPL. The SEM images suggest that liquid water may stagnate on the graphene containing MPL surfaces rather than being channelled away, and that they provide a higher resistance to reactant transport. Like with many of the contradicting physical properties of the MPL, surface cracking presents problems as it has also been related to reduced mechanical durability of the layer [289]. Improvements in fluid transport need to be balanced against strength durability of the component.

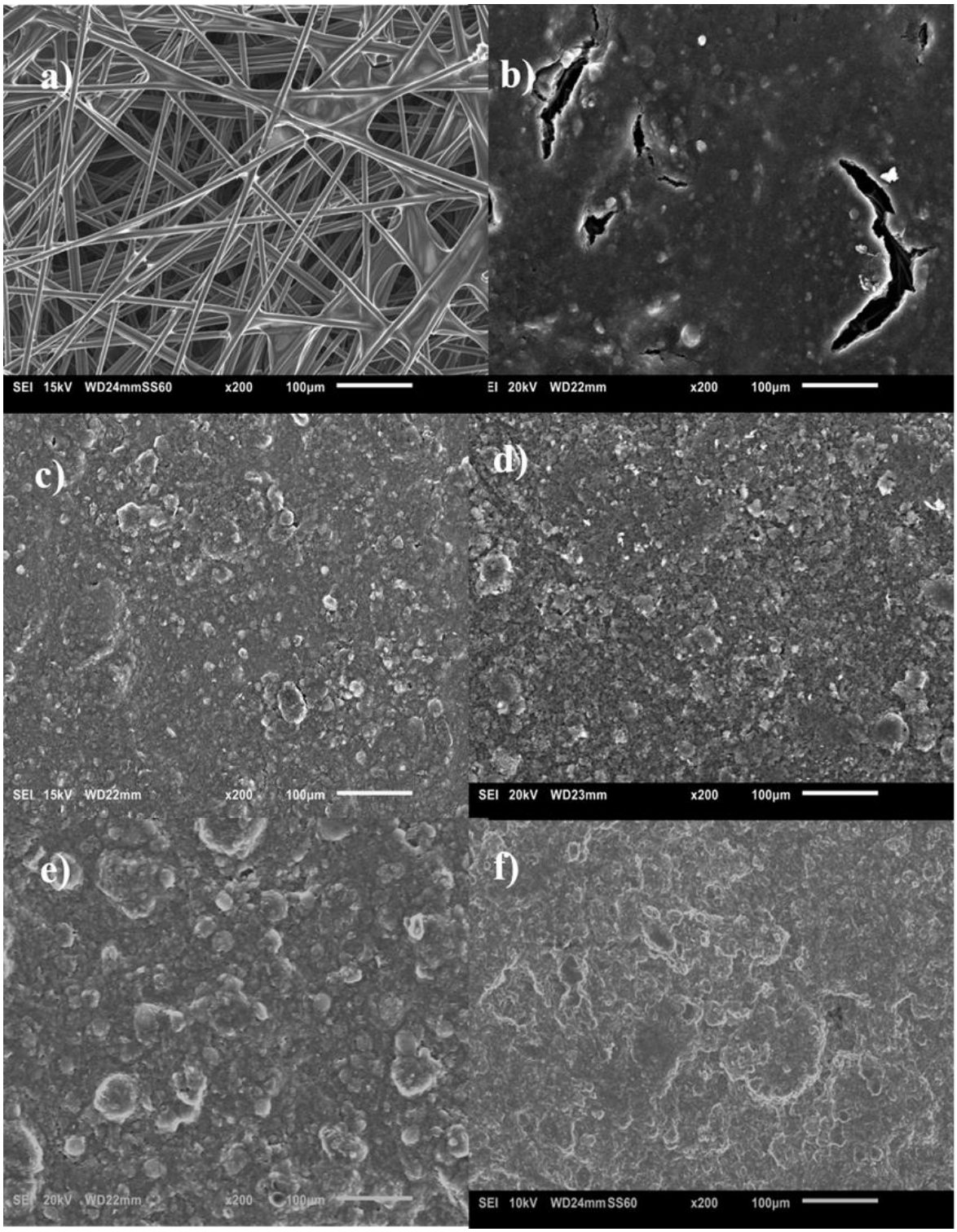

Figure 4-1: SEM micrographs of the dual-layer MPL-coated and the uncoated GDLs (from top left to bottom right: Toray H-060, G0, G30, G50, G70 and G100). The number after the letter "G" represent the weight fraction of graphene in the MPL.

The micrographs of G30, G50, and 70 (Figs. 4.1 (c-e)) indicate that the mixed compositions result in a similar morphology and microstructure, where the graphene nanoplates are encompassed in a conductive filler formed of the carbon black agglomerates. The graphene containing microporous layers appears to have a smoother surface than the pure carbon black owing to the dominant graphene which is decorated with the carbon black agglomerates. G30 (Fig. 4.1(c)) can be seen as being more densely packed than G50 and G70 (Figs. 4.1 (d and e)) owing to the greater percentage of small particles in its composition. This influences the mean pore size and the pore size distribution through the MPL, as can be seen in the following section (Fig. 4.3). G100 (Fig. 4.1(f)) is distinguishable from the other MPLs with a graphene inclusion due to its lack of conductive filler which results in a much larger pore size visible from the micrographs.

4.4.2 Pore Size Distribution

The porosity and pore size distribution of the MPLs were obtained using mercury intrusion porosimetry (MIP). For ease of identification and discussion of the microstructure, the pores of the single and dual-layer GDLs are classified into 3 groups according to their size, where: pores smaller than 0.07 μm are identified as micropores, mesopores range between 0.07 –5 μm in size, and finally the pores larger than 5 μm are identified as macropores. The determination of these groups is based on the mechanism for gas diffusion inside the pores, which differs depending on their size. Knudsen diffusion is the prevailing mechanism in the micropores whose dimensions are comparable to the gas mean free path, whereas bulk diffusion dominates in macropores. In mesopores, both bulk diffusion and Knudsen diffusion are present [290].

The dual function of the MPL for the transport of reactants to the catalyst layer and the removal of water in the opposite direction means that the MPL has two conflicting roles. The pore size and microstructural properties of the MPL greatly influence the ability of the component to carry out these roles as the transport of the two fluids (reactant gas and liquid water) takes place in pores of different sizes. Mesopores are important for maintaining gas transmission in saturated conditions [218]. As the transport of liquid water typically takes place in pores larger than 20 μm [235], and due to the high capillary pressure the hydrophobic micropores become occupied by liquid water. Thus, for the reactant

gas to maintain free transmission, it must pass through the mesopores of the GDL. As such, the presence of mesopores in the GDL enhances the mass transport capabilities at higher current densities and in higher relative humidity conditions [218]. According to this principle, an MPL with both micropores and mesopores

Fig. 4.2 shows the pore size distribution for the dual-layer GDLs. Unsurprisingly, the uncoated GDL is mainly comprised of macropores which can be seen as the large peak after 10 µm, whereas the addition of the microporous layer to the GDL leads to the addition of micropores and mesopores to the pore profile. The composition of the microporous layers influences the pore profiles of the coated GDLs, where the mean pore size of the MPL increases with the increasing inclusion of graphene. The pore size distribution and porosity of the coated GDLs are mainly governed by the macroporous substrate and as such Fig. 4.2 (b) was produced for ease of comparison of the microporous layers. This figure shows the distribution of the micropores and the mesopores and thus provides greater clarity when determining the variation in pore sizes in the microporous layer. The Toray 60 carbon substrate was used as the baseline, which is represented by the black line in Fig 4.2 (b). Due to the infrequency of meso and micropores in the substrate, pores smaller than 1000 nm in the MPL-coated GDLs were assumed to be the microporous layer. G0 (the Vulcan MPL) has the typical pore profile of the conventional microporous layer, where the majority of the pores are in the microporous region with a sharp peak at 50nm. Conversely, G100 (the pure graphene MPL) has a larger average pore size, with most pores occurring in the mesoporous region and the peak occurring at 500 nm. The two materials were visualised using SEM and the average particle size was found to be 20–80 nm for Vulcan carbon black and 0.5–5 µm for graphene, both of which are within the range of the manufacturer's specifications. Given the average particle size of the two materials, it is unsurprising that the average pore size of G100 is an order of magnitude larger than that of G0.

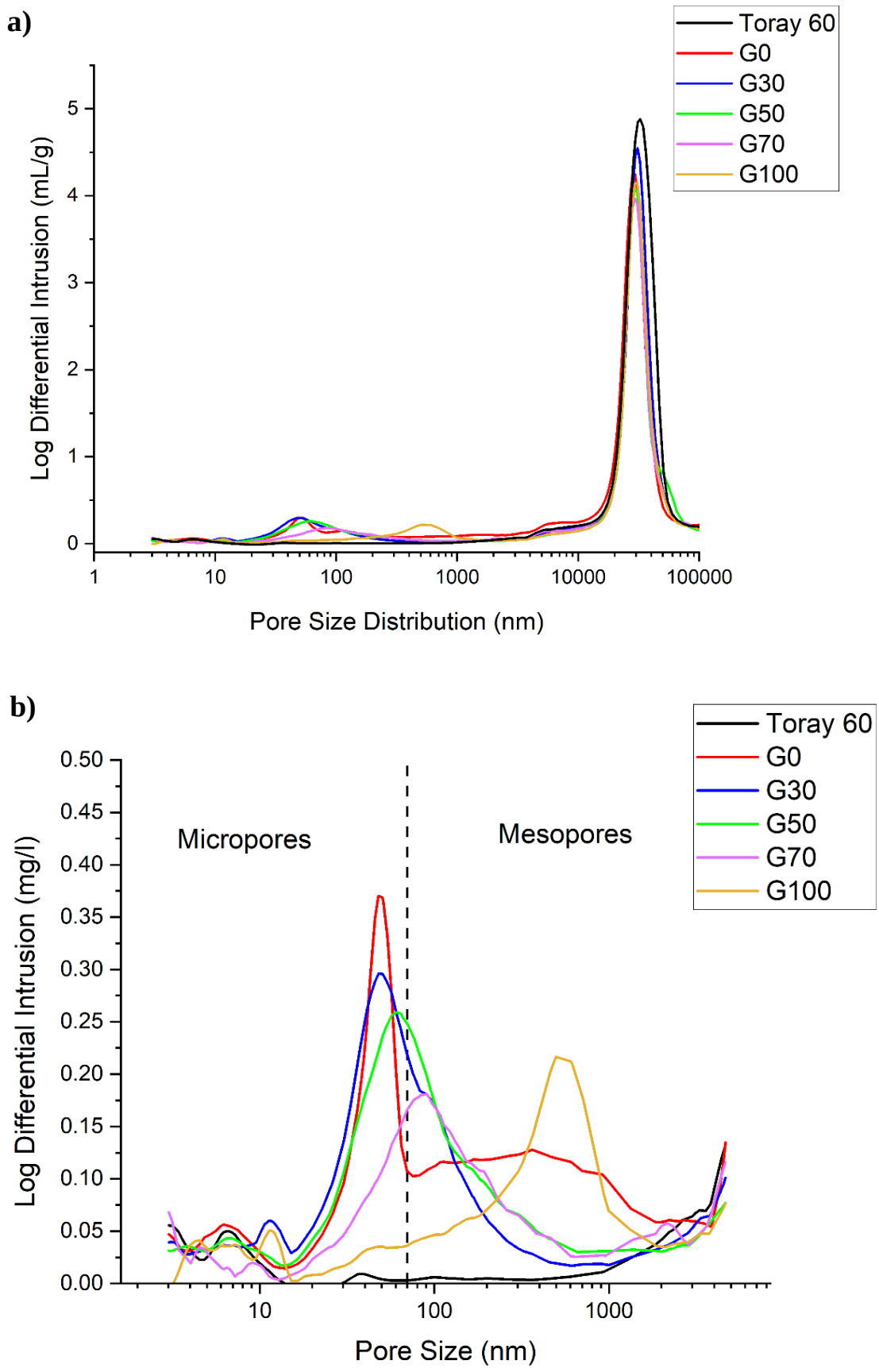

Figure 4-2: Pore size distribution of the uncoated and coated GDLs obtained by mercury intrusion porosimetry (MIP). Micropores are defined by < 70nm, whereas mesopores are defined as >70nm and <5000nm.

The inclusion of GNP to the MPL composition increases the average pore sizes in the MPL and leads to the formation of small mesopores in the layer. Interestingly, for the mixed composition MPLs, Vulcan is the dominant material in determining the average pore size, as can be seen in Table 4.2 and in Fig. 4.2 (b). This is in line with the SEM micrographs which show that voids between the larger GNP are occupied by the smaller carbon black particles, Figs. 4.1 (c) and 4.1 (d) reveal the pore space between the GNP is filled with carbon black conductive filler. As such this leads to the formation of micropores and reduction of mesoporous void space. Although G70 is largely comprised of graphene, its modal average pore size is 83 nm, which is more similar to the G0 (50 nm) rather than G100 (500 nm). Likewise, G50 and G30 are characterised by micropores, with the most frequent pore size being the same for G30 (50 nm) as for G0. However, the distribution is more evenly weighted for G30, due to the inclusion of GNP. As G30 has a higher percentage of carbon black filler than G50 and G70, it has a larger number of micropores in the MPL. G50 MPL has a desirable pore size distribution with an average pore size of 61 nm. G50 has an even distribution of micropores and small mesopores and this may lead to enhanced performance at high relative humidity operation and current densities; enabling the simultaneous capillary wicking of liquid water to mitigate flooding at the cathode and improve reactant diffusion to the catalyst [252, 291].

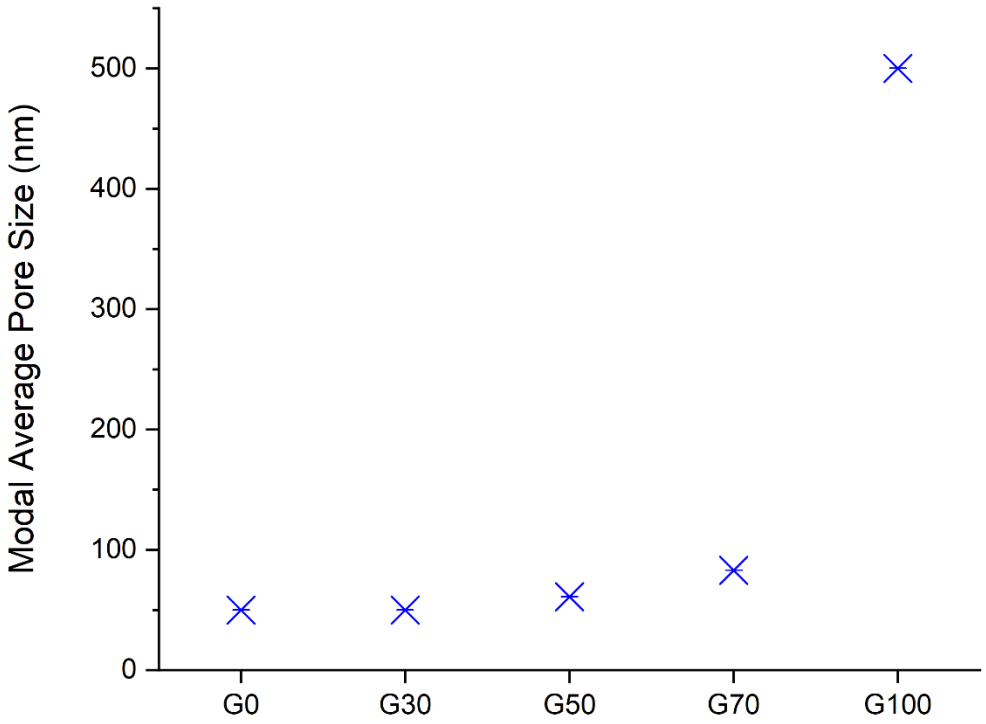

Figure 4-3: Modal average pore size (nm) of the MPL-coated GDLs.

Table 4.2 shows the cumulative pore volume of the investigated MPL-coated GDLs. It can be observed that G0 has the largest cumulative pore volume (1.82 ml g^{-1}) compared to the other samples. This is determined not only the presence of micropores (which form as a result of agglomeration of carbon black particles) but also due the cracks which were clearly visible in Fig. 4.1 (b). Table 4.2 also shows that the cumulative pore volume in general decreases with increasing graphene content; increasing graphene content in the MPL from 30% (G30) or 50% (G50) to 100% (G100) decreases the cumulative pore volume from 1.71 to 1.56 ml g^{-1}.

Table 4-2: The porosity and pore volume of the MPL-coated GDLs.

Gas Diffusion Layer	Porosity	Total Pore Volume (ml g^{-1})	Mean Pore Size (nm)
G0	74%	1.82	50
G30	72%	1.71	50
G50	72%	1.71	61
G70	72%	1.62	83
G100	71%	1.56	500

The porosity is an important physical property as the porosity and diffusivity of the GDL determine its effective diffusivity. This is significant as diffusion is the main mode of gas transport in the GDL. G0 has the highest porosity of the MPL-coated GDLs and as such is likely to have a greater effective gas diffusivity than the other MPLs, and subsequently have a higher performance when tested in the fuel cell. However, porosity and pore volume are just one of the physical properties that determine the effect of the MPL on cell performance, moreover, the reported pore volume and porosity values do not account for either the presence of the cracks nor the influence of liquid water which would obstruct diffusive pathways and precipitate mass transport loss.

4.4.3 Contact Angle

The wettability, or hydrophobicity/ hydrophilicity of the MPLs is dependent on the physical properties of the material and the surface structure. This determines the strength of the interactions between the surface and the water molecules. Static contact angle measurements were used to investigate the wettability characteristics of the microporous layer surfaces. All of the GDL surfaces investigated were found to be hydrophobic, exhibiting a contact angle greater than 90˚. The value of the contact angle of the uncoated carbon substrate (Toray 60) (131˚) shows that the surface of the uncoated substrate is moderately hydrophobic. This is in good agreement with those reported in the literature (129 ± 9˚) [44]. The inclusion of 10 wt.% of PTFE increases the hydrophobicity of the substrates compared to pure carbon fibre substrates.

Referring to Fig. 4.4, the addition of the microporous layers increases the contact angle of the uncoated Toray carbon substrate. This is largely due to the inclusion of PTFE (20 wt.%) in their composition, though the change in surface roughness from the MPL also increased the hydrophobicity of the layer. The roughness of a surface impacts on the contact angle; where the rougher the surface, the larger the contact angle [44].

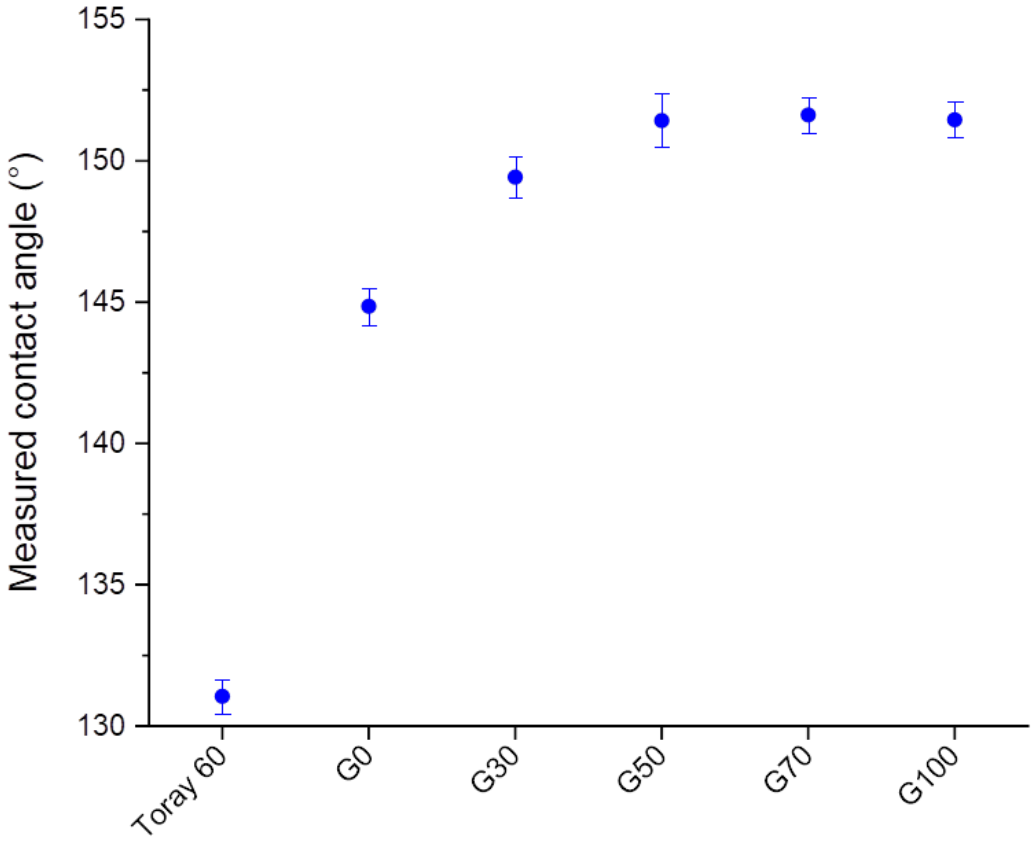

Figure 4-4: The measured static contact angle of water droplets on the coated and uncoated GDL.

The highest contact angle was measured on the G50, G70, and G100 MPLs, this indicates that at 50 wt.% graphene a plateau was reached. Therefore, there would be no benefit to MPL hydrophobicity by increasing the graphene concentration above 50% in the MPL. These improvements to the wettability correspond to approximately a 15% increase in the contact angle of the uncoated Toray substrate. Moreover, G30 indicates that a 13% increase in the hydrophobicity of the GDL can be achieved with even a small addition of graphene (30%) to the MPL. The inclusion of graphene into the MPL

composition results in an increase in the hydrophobicity of the surface compared to the single material Vulcan MPL, an increase of 3% for G30 and 5% for G50, G70, and G100, respectively.

The hydrophobicity of a surface is determined by the physical characteristics and the morphology of the surface. As previously mentioned, the graphene nanoplatelets exhibit a stacking behaviour in the MPL, the slight increase in the hydrophobicity of the MPLs composed with graphene is attributed to this stacked graphene morphology. This indicates that there are fewer pathways for the removal of water from the surface, moreover, the surface morphology of G0 is characterised by cracks that serve as channels for water penetration.

However, as there is minor variation in the measured contact angles of the surfaces it can be understood that the dominating factor in their wettability is the PTFE content, which is kept constant, and not the microstructural properties which varies greatly between the samples.

4.4.4 Through-Plane Permeability

Fig. 4.5 shows the through-plane permeability measurements of the uncoated and MPL-coated GDLs. As can be expected, the uncoated carbon substrate has the highest through-plane permeability of those measured, which decreases by 70% with the addition of the microporous layer. A significant drop in the through-plane permeability with the addition of the MPL has been widely observed in the literature [83, 292]. It is clear from the SEM micrographs (Fig. 4.1) why the addition of the MPL increases the resistance to the flow of mass, as the highly porous structure of the gas diffusion layer fibre is covered with a compact layer of carbon particles. A high permeability is desirable as it governs the reactant flow to the catalyst layer, and allows water produced at the catalyst to be directed to the fluid flow channels to prevent electrode flooding. Low permeability increases reactant transport resistance and creates a higher pressure gradient, thus increasing the necessary power input to maintain the correct stoichiometry of the reactant gases.

The permeability of the gas diffusion layer is dependent on its physical structure and morphology, notably the porosity and the pore size distribution. As was previously noted, these microstructural properties varied greatly between the different MPL compositions, where the highest pore volume was reported with G0, and decreased with the addition of graphene to the layer. When comparing the microporous layers, it is important to emphasise that the wt.% PTFE and carbon loading of the MPL was kept consistent at 20 wt.% and 2.0 mg cm^{-1} respectively, as is typically used in the literature. The carbon loading and the PTFE have both reportedly negatively impacted the flow of air through the MPL [83].

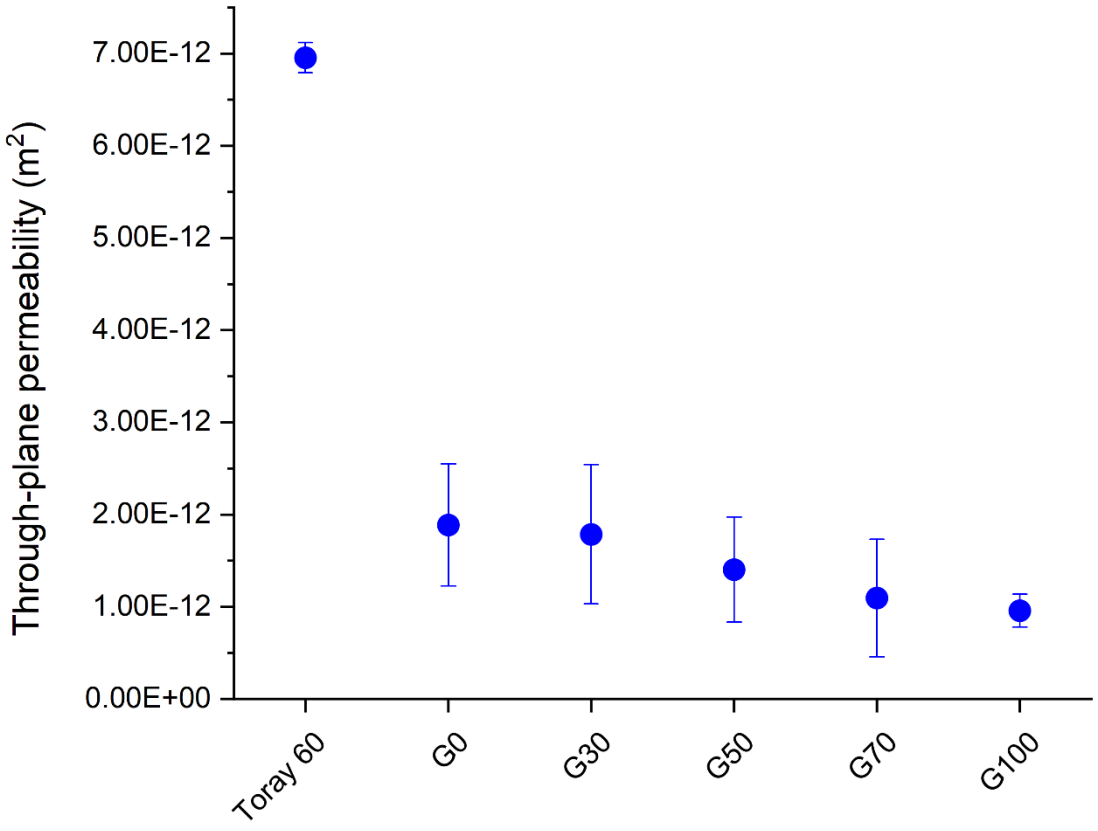

Figure 4-5: The through plane permeability measurements for the uncoated and MPL-coated GDLs.

The addition of graphene to the MPL leads to a step-change in the through-plane permeability, which becomes more prominent with the increase in wt.% graphene in the composition. Notably, G30 has a minimal decrease in permeability amounting to a 1.5% reduction compared with the conventional MPL

(G0), whereas G70 and G100 exhibit a much greater 48% and 55% decrease in permeability, respectively. As the Vulcan particles and graphene flakes are in equal weight there is variation in the dominant material across the samples, diversifying the microstructure of the layer and thus the capability for airflow. This reduction in through-plane permeability of the graphene-based MPLs indicates that the inclusion of graphene in the MPL leads to greater resistance to airflow. This reduction in air flow can be attributed to the morphology of the graphene flakes which differs greatly from that of the Vulcan carbon black particles. The graphene flakes have a 2-dimensional geometry as opposed to the spherical morphology of the carbon black particles. This 2-dimensional geometry lends to dense, horizontal stacking of the graphene flakes in the MPL, which forms a sheet-like structure that obstructs airflow in the through-plane direction. Moreover, the increase in graphene concentration is associated with a reduction in total pore volume which limits the availability of pore space for gas transport through the MPL. This is likely the reason for the reduction in the through-plane permeability associated with the increase in graphene in the microporous layer. This is in agreement with [242] who reported a lower through-plane permeability for single-material graphene MPL than those derived from carbon black.

For the mixed composition MPLs, it is apparent that up to a 50 wt.% graphene inclusion in the MPL leads to carbon black being the dominant material, as there is minimal reduction in the airflow compared with G0 (0 wt.% graphene). However, at 70 wt.% graphene (G70) the graphene platelets govern the microstructure, and a significant reduction in through-plane permeability is observed from the stacking of the graphene platelets obstructing the airflow. The single material MPLs have the smallest variation in permeability, again this is attributed to the homogeneity of the microstructure.

4.4.5 In-plane Electrical Resistivity

The in-plane electrical resistivity measurements indicate that G100, the graphene based MPL has a much lower in-plane resistivity than G0, the carbon black MPL, at 5.6 mΩ cm and 8.0 mΩ cm respectively. These values are in good agreement with those reported in [245] in which a similar grade of graphene nanoplates was used.

The excellent electron conductivity of graphene is widely acknowledged and reported in the literature, where single-layer graphene has an exceptionally high electrical conductivity (6×10^5 S m^{-1}) [293]. The electrical conductivity of the graphene nanoplatelets is thus greatly influenced by the number of graphene layers, the lateral size, and the purity of the material**.** To this end, few layer graphene has been used in a number of investigations involving nanoelectronics, ultracapacitors, gas sensors, catalyst supports.

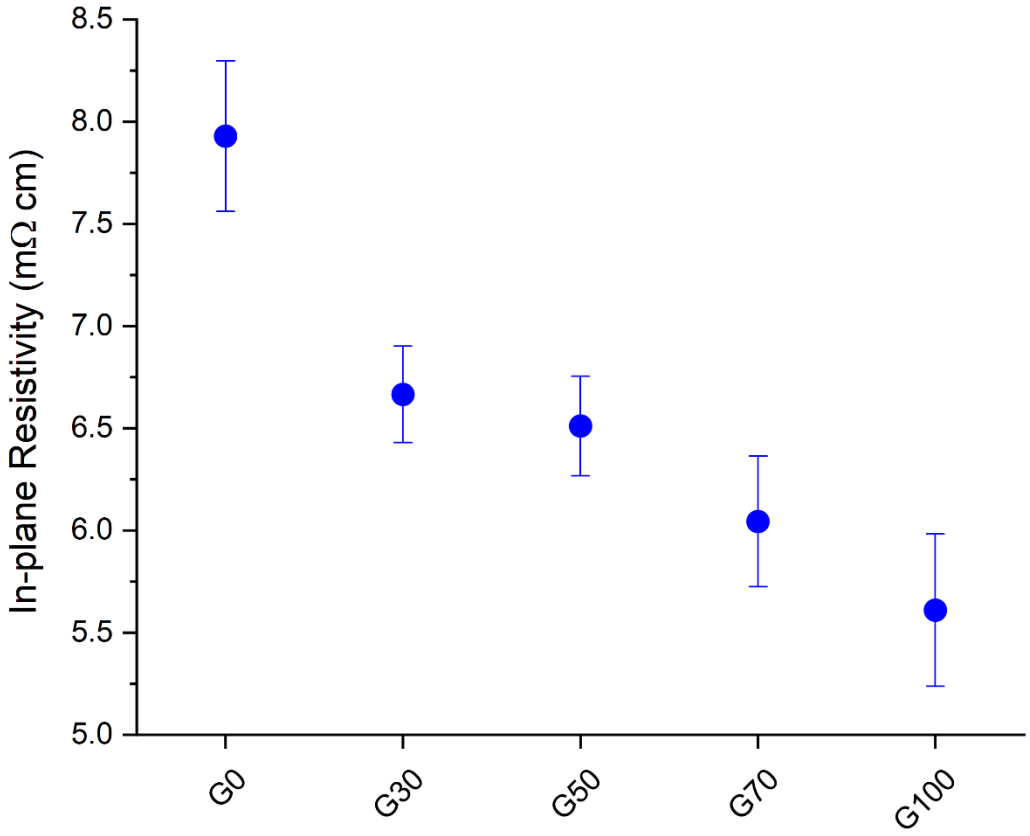

Figure 4-6: The measured in-plane resistivity of the MPL-coated GDLs.

The Nanene graphene nanoplates used in this investigation have a high 98% purity and notably few layers (< 5); the electrical conductivity of which exceeds that of the Vulcan XC 72 R carbon black used (~277 S m^{-1}) [286, 294]. As the resistivity of the MPL is dependent on the physical properties of the carbon material and the electrical conductivity when it has adhered to the PTFE, it is therefore unsurprising that the inclusion of graphene nanoplatelets in the MPL composition increases the conductivity of the surface for all MPLs tested. The measured resistivity G30 indicates that even a small inclusion of graphene in the MPL (30%) has marked improvements in the electron transfer properties of the layer, equating to a 20% reduction in resistivity from the conventional carbon black MPL. Higher inclusions of graphene lead to greater improvements in the electron transfer capabilities of the MPL, where G50 and G70 have a 23% and 32% reduction in resistivity, respectively.

4.4.6 Fuel Cell Performance

Single-cell electrochemical performance tests were conducted under different humidity conditions, from low humidity operation (RH = 25%) to high humidity operation (RH = 100%). High humidity operation can result in liquid water formation and accumulation, leading to what is conventionally known as ‘water flooding’ which impedes oxygen supply to the cathode catalyst layer, leading to mass transport losses and reduced catalyst efficiency [282, 295]. On the other hand, low humidity conditions lead to membrane electrolyte dehydration, reducing ionic resistance of the membrane electrolyte and leading to increased ohmic losses [221, 283, 296]. Varying operating conditions enables the assessment of the dominant mechanisms and phenomena for water transport in the MPL, thus enabling the optimisation of the MPL for cell efficiency. It is from the polarisation curves generated and the single-cell measurements that the viability of an innovative MPL can truly be assessed. Although the MPLs were characterised ex-situ in terms of their microstructural, physical, and electrochemical characteristics these were measured as stand-alone parameters and without the influence of other factors which occur in the fuel cell, such as mechanical and chemical stresses. For this reason, ex-situ analysis alone cannot be used to determine the effectiveness of an MPL in an operational fuel cell.

Polarisation curves were taken at 25%, 50%, 75%, and 100% relative humidity conditions in air, and also at 50% relative humidity in oxygen (Figs. 4.7 (a-e)), at a constant temperature of 80°C; this allowed for the assessment of the viability of the graphene-based MPLs under actual operating conditions. The MPL-coated GDLs perform better than the uncoated Toray-60 GDL in all conditions, which is consistent with previous research findings; as the addition of the MPL reduces membrane dehydration in low humidity conditions [297, 298] and at high humidity conditions reduces liquid water saturation at the catalyst layer GDL interface [284, 299]. Fig 4.7 (a) shows the polarisation curve of the GDLs at 25% relative humidity operation. In these conditions, the G30 MPL outperforms all the other MPLs. Under low-humidity operating conditions, the ohmic losses caused by the membrane dry-out are the prevailing factor behind the low performance of the fuel cell. The high performance exhibited by G30 indicates that it is better than the other MPLs at retaining liquid water and preventing membrane dry-out, particularly G100 which achieves a noticeably lower potential (0.57 V and 0.46 V at 1.6 A cm^{-2}, respectively).

However, at 50% RH (Fig 4.7 (b)) G30 and the commercial G0 MPL start to experience significant potential drops at relatively low current density (~ 1.2 A cm^{-2}). This could be attributed to the inability of the above MPLs to reject excess liquid water produced at the cathode catalyst layer. This trend continues at 75% and 100% RH operation, where liquid water is more prevalent, thus it is clear that these performance losses are due to the inability of G0 and G30 to sufficiently divert liquid water away from the cathode catalyst layer.

Larger inclusions of graphene in the MPL composition produce a higher limiting current density and greater power density in more humidified conditions (50%, 75%, and 100% RH). Figs. 4.10 (b-d) indicate that G50, G70, and G100 do not suffer the same potential drops that G0 and G30 experience in these conditions. It can be concluded that, under intermediate or high humidity conditions, the addition of 50% or above of graphene to the MPL has a positive impact on the fuel cell performance as evidenced by the lower mass transport losses and the increased limiting current density of the fuel cell. G100 in particular has the lowest limiting current density in the 25% RH humidity operation at 1.97 A cm^{-2} but exhibits the highest in the 100% RH humidity condition, 2.17 A cm^{-2}. There is a slight power drop

between 100% RH from 75% RH where the peak power point of 0.90 W cm^{-2} reached 1.6 A cm^{-2}, greatly exceeding that of G0 and G30 in these conditions (0.64 W cm^{-2} and 0.49 W cm^{-2}) and higher than G70 and G50 at 0.85 W cm^{-2} and 0.87 W cm^{-2}, respectively. G50 performs well overall and records the highest power density at 50% RH, 0.91 W cm^{-2} at 1.9 A cm^{-2}. Although, notably, G50 continues to perform well in higher relative humidity conditions, at 75% RH it reaches the highest limiting current density of 2.25 A cm^{-2}. Furthermore, it produces the highest power density of all MPLs in 100% RH (0.88 W cm^{-2} at 1.7 A cm^{-2}). The pore size distribution data indicates why this is the case. When graphene makes up 50% or greater of the MPL composition, it leads to the formation of mesopores in the MPL which are very slightly present in the 30% wt. graphene MPL (Fig. 4.3). The presence of these mesopores enhances the removal of liquid water away from the catalyst layer which explains why G50, G70, and G100 do not experience the same potential drops at high current densities that G30 and G0 experience.

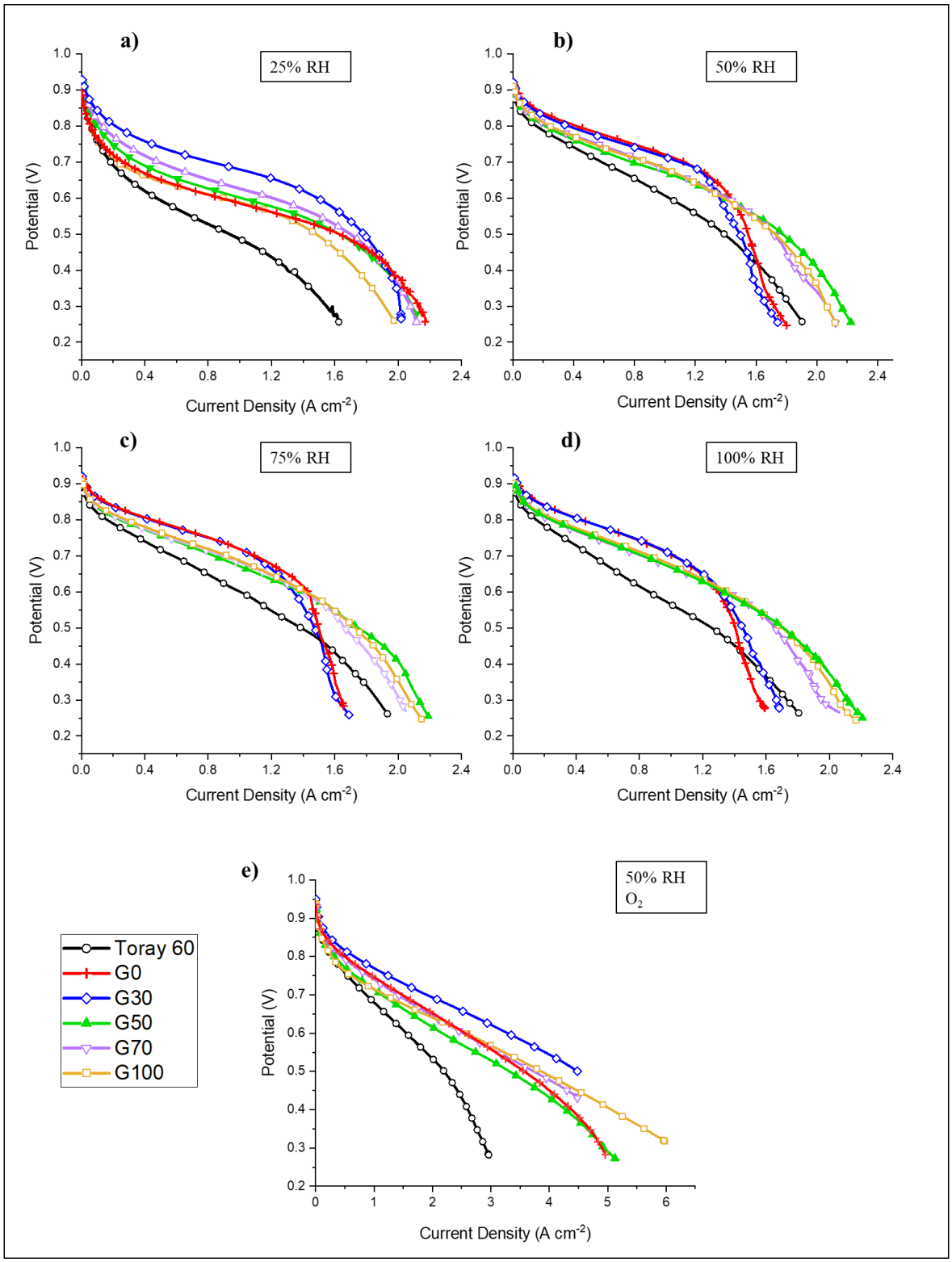

Figure 4-7: Polarisation curves of the MPL-coated and uncoated GDLs at (a-e) 25%, 50%, 75% and 100% relative humidity in air, and 50% relative humidity in pure oxygen.

Similar findings have been reported when other carbon-based materials have been mixed with carbon black in the microporous layer, such as graphene [242, 243, 245], and multiwall carbon nanotubes [161, 241, 249, 291] which have led to the presence of mesopores in the microporous layer and have reduced mass transport losses at high current densities in high relative humidity operations.

Fig 4.7 (e) shows the polarisation curve at 50% relative humidity where pure oxygen was used as the oxidant, this significantly reduces the effect of mass transport losses and reveals the impact of resistance on cell performance. In these conditions, G30 performs very well and has the lowest resistance of all of the GDLs resulting from a well-hydrated membrane and good GDL conductivity. This is confirmed by the EIS results which can be seen in the following section (Fig 4.9 (e)). G50, G70, and G100 behave similarly in terms of resistance and cell performance is similar in this condition.

Overall, G50 is the optimal MPL composition under the commonly used intermediate and high humidity conditions as it produces high fuel cell performance with a relatively low amount of graphene that is much more expensive than carbon black.

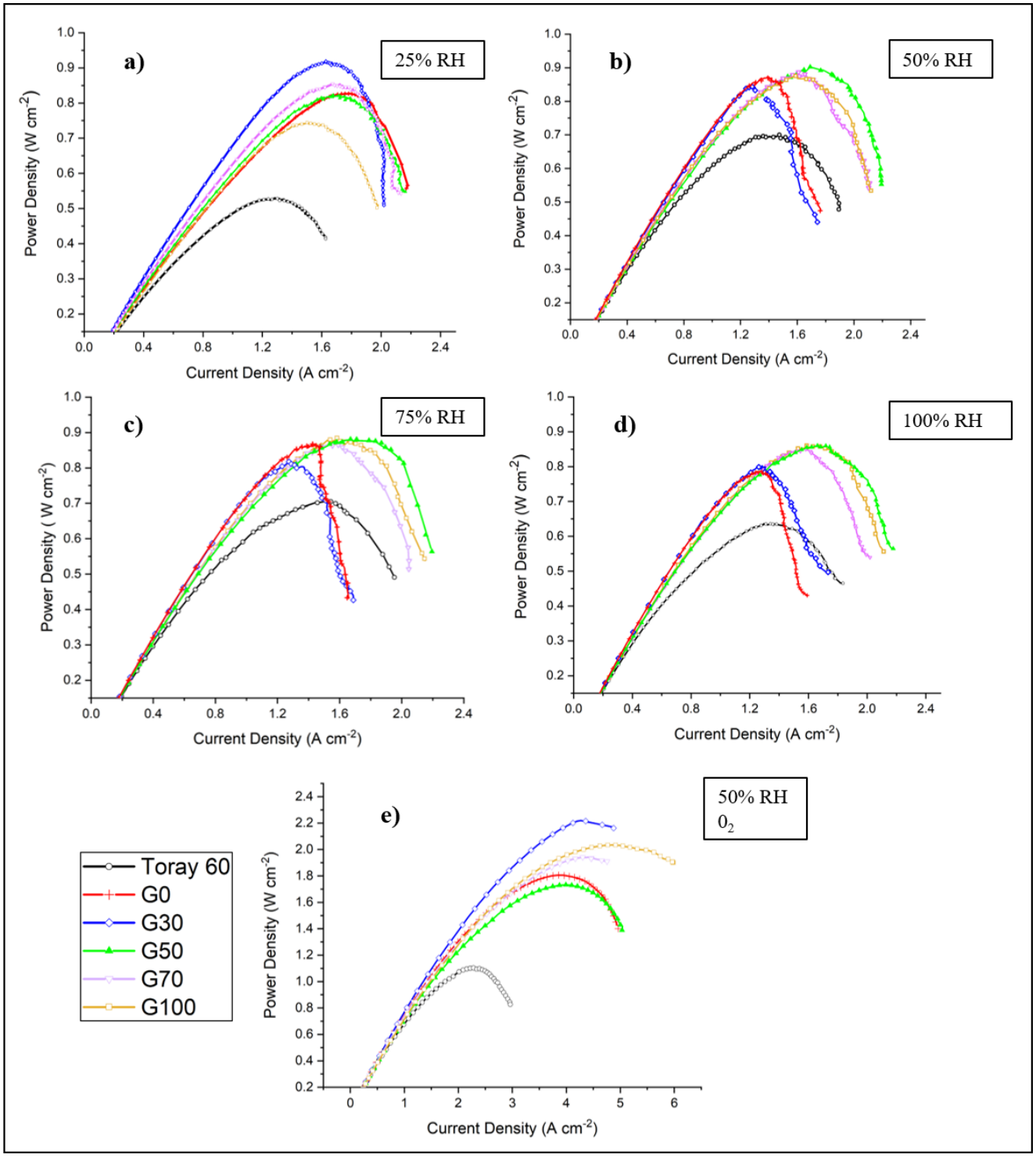

Figure 4-8: Power density measurements of the MPL-coated gas diffusion layers in different conditions (a-e) 25%, 50%, 75% and 100% relative humidity.

4.4.7 Electrical Impedance Spectrometry (EIS)

Electrical Impedance Spectrometry was performed at 0.6 V. Fig. 4.9 shows the results for the EIS measurements for the MEAs at 25%, 50%, 75%, and 100% RH in air, as well as 50% RH in O_2. The results of the EIS correspond well with those obtained from the IV curves (Fig. 4.7 and 4.8). Figs. 4.9 (a-d) indicates that for the fuel cell operating in the air, the ohmic losses are comparable for all of the MPL-coated GDLs. As the intercept with the x-axis is similar for each of the MPL-coated GDLs, whereas the uncoated GDL intercepts with the x-axis at a high value, equating to a higher measured resistance, this is especially seen at the 25% relative humidity condition. Ohmic resistance is determined by the contact resistance between the components and the bulk material resistance [300]. Typically, the membrane resistance accounts for the majority of this, which in turn, is largely dependent on the internal humidification of the polymer membrane. Thus, the uncoated GDL reduces the capability of the membrane to retain water and limits the contact between the GDL and the catalyst layer. The ability of the MPL to enhance these two properties with the addition of the MPL is well reported in the literature [61, 223, 227, 301-303].

The use of pure oxygen as the oxidant significantly reduces the dominating effect of oxygen mass transport losses, in doing so it allows for the analysis of ohmic and activation resistances. EIS results where pure oxygen was used as the oxidant can be seen in Fig. 4.9 (e). Unsurprisingly, the uncoated Toray GDL is characterised by a large semi-circle which indicates much greater charge transfer resistance and a later intercept with the x-axis indicating high ohmic resistance than the MPL-coated GDLs as was seen in Fig 4.9 (a) (25% RH). Moreover, larger semi-circles are observed with a corresponding increase in graphene concentration in the MPL, this demonstrates that G30 promotes better contact with the catalyst layer and is better at maintaining membrane hydration in comparison, to the MPLs with a higher inclusion of graphene. This may be due to the conditions at the triple phase boundary, where the ionomer in the catalyst is dry which promotes charge transfer resistance. G30 has the smallest semi-circle and the earliest intercept with the x-axis indicating the lowest charge transfer and ohmic resistance.

However, it is clear from Fig. 4.12 that there is a noticeable increase in the size of the semi-circle with an increase in humidification for the G0 and G30 MPLs. Fig. 4.9 (a), taken at 25% RH produces comparable resistances to the other GDLs, however Figs. 4.9 (b-d) show a huge growth in the circle size indicating slower reaction kinetics and pronounced mass transport limitations. This is in accordance with the polarisation curves (Fig. 4.7), where large potential drops highlight oxygen mass transport losses at relatively low current densities (~1.2 A cm^{-2}) (Figs. 4.7 (b-d)). For the MPLs with higher inclusions of graphene (G50, G70, and G100) these changes in the semi-circle size cannot be observed signifying that the graphene-based MPLs do not suffer from oxygen mass transport losses and therefore are more capable of reducing liquid water saturation in the MEA. This allows for the higher limiting current densities and maximum power densities that can be seen in Fig. 4.8.

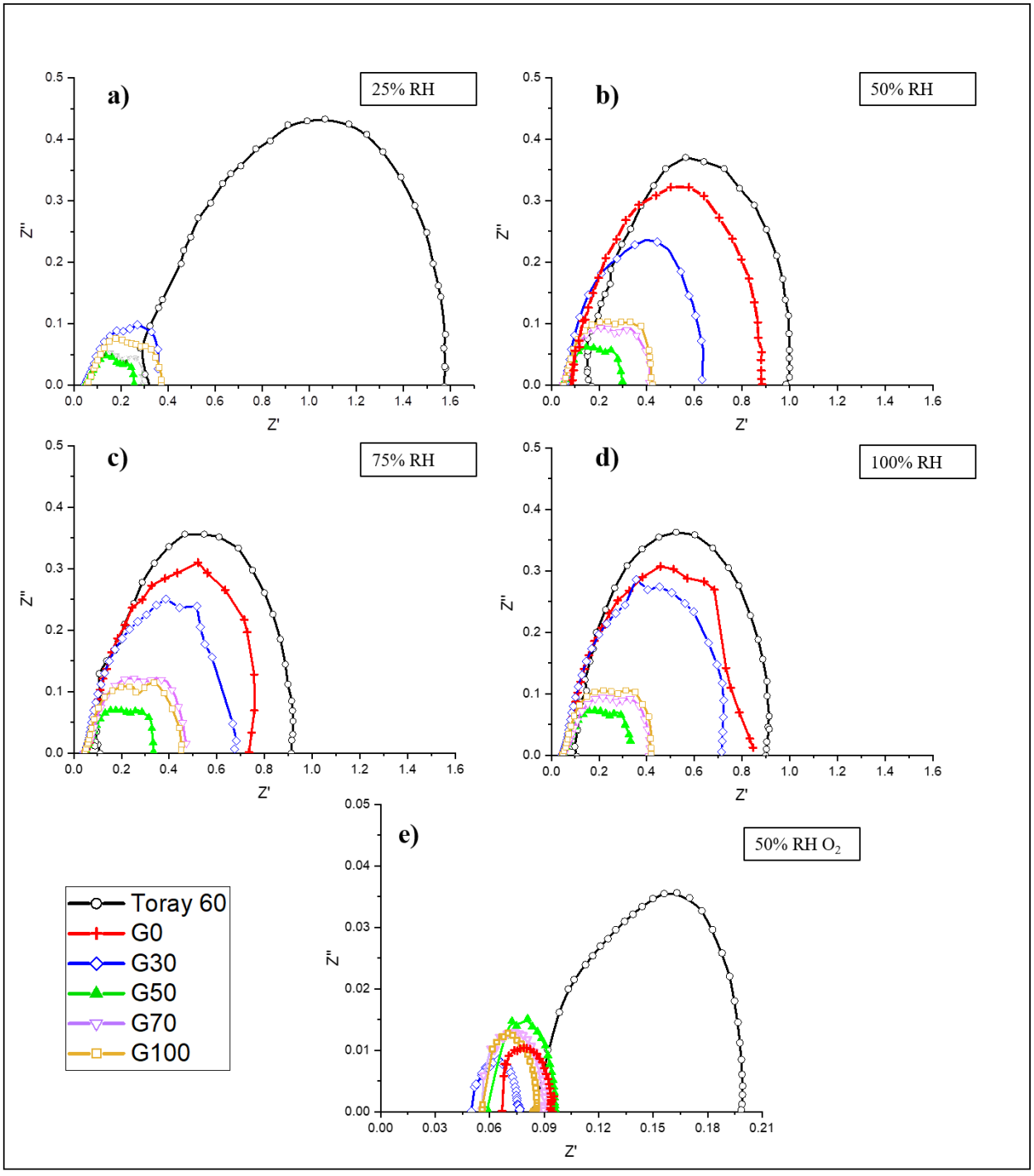

Figure 4-9: Electrical Impedance Spectrometry measurements taken at 0.6V for the MPL-coated and uncoated GDLs at (a-e) 25%, 50%, 75% and 100% relative humidity in air, and 50% relative humidity in pure oxygen.

4.5 Conclusions

Microporous layers produced from graphene and carbon black in varying concentrations were applied to carbon paper GDLs. The concentration of graphene in the MPL was varied to enhance MEA performance and to optimise their design for water management in high humidity conditions. Below are the main findings of the study:

- The polymer electrolyte fuel cell was found to perform better with relatively low graphene content in the cathode MPL (≤ 30%) under low humidity conditions (e.g., 0 or 25% RH) and this is due to the availability of a high amount of micropores that assist in retaining water needed to humidify the membrane electrolyte and the membrane phase in the catalyst layer.
- Larger amounts of graphene (≥ 50%) are needed to be added to the cathode MPL for the fuel cells operating with intermediate or high humidity conditions (50, 75, or 100% RH). Such amounts are necessary to obtain a sufficient amount of mesopores required to drive excess water away from the MEA and subsequently mitigate water flooding.
- Expectedly, the electrical conductivity of the MPL increases with increasing graphene content and this is evidently due to the substantially higher electrical conductivity of graphene compared to carbon black. On the other hand, the gas permeability of the MPL-coated GDL was found to decrease with increasing graphene content; this is attributed to the sheet-like structure of the graphene used which hinders the flow of the gases.

Chapter 5: An Assessment of Novel Graphene Foam Microporous Layers for Polymer Electrolyte Fuel Cells: Fabrication and Characterisation.

5.1 Abstract

Graphene foam was synthesised from the pyrolysis of sodium ethoxide, the resulting carbon was then subject to pyrolysis in different atmospheres to enhance the conductivity. The graphene foams underwent characterisation by electron microscopy and x-ray fluorescence which showed high carbon purity open foams with micron-scale pores and graphene-thin walls. Microporous layers were then produced from these graphene foams, commercial graphene, and carbon black; they were then characterised ex-situ and through polarisation curves.

Ex-situ characterisation of the microporous layers was used to determine the micro-structural and physical properties, as well as its ability to repel liquid water and conduct electron and mass transfer. Electron microscopy and mercury intrusion porosimetry enabled the analysis of morphology and microstructure, and the transport properties of the layer were determined through permeability, electrical conductivity, and contact angle measurements. Polarisation curves were performed at low and high relative humidity conditions to understand the capability of these microporous layers in a range of operating conditions.

5.2 Introduction

Recent research attention has focused on the gas diffusion layer and in particular the microporous layer and its vital role in liquid water management [61, 72, 161, 166, 168, 232, 258, 263, 273, 304-310]. Significant improvements in fuel cell performance have been achieved by optimisation of the physical structure of the MPL such as its morphology, pore size and thickness, and its constituent materials i.e. the wettability [136, 168, 269, 273, 276, 304, 311, 312], carbon type [161, 249, 308], and carbon loading [83, 226]. Thanks to this, noteworthy conclusions have been drawn about the beneficial physical properties of the layer, where the presence of meso and macropores within the MPL has been shown to enhance cell performance

[161, 249, 252, 313, 314]. Control over the pore size of the MPL has been achieved by the use of pore-forming agents [238, 315] and by material selection, i.e. varying the type of carbon black, and inclusion of carbon materials aside from carbon blacks such as carbon nanotubes [247, 291, 308] and graphene [242-245].

The fabrication of graphene foams from a sodium ethoxide pre-cursor has been the subject of recent research interest, where sodium ethoxide has been combusted in air [316], or pyrolised in nitrogen atmosphere [277]. Graphene foams are a promising novel material with an attractive microstructure, consisting of a porous open foam with graphene thin cell wells. This unique physical structure has led to its usage in several applications in hydrogen engineering systems, particularly non–Pt catalysts PEMFC [317] and hydrogen storage [318]. The study of graphene-foam-based microporous layers is extremely limited [244, 319, 320], whereas Leeuwner et al. [244] used a commercial graphene foam as a stand-alone microporous layer. The porous microstructure of the graphene foam suffered under compression and its performance was limited by its lack of wet-proofing. Chen et al. [319] also used a commercial graphene foam to produce an MPL though this circumstance a slurry was produced akin to the conventional method using carbon black and PTFE, this was then applied to a Toray TGP- H 060 GDL. Previous studies have both used commercial graphene foams, however, the graphene foams in this research were produced in-house using the initial stages of the non-precious metal catalyst preparation. This study was undertaken in conjunction with the research partners at Kyushu University who have been developing graphene foams for use as Pt catalyst support, and as a non-precious metal catalyst when doped with iron and nitrogen. The highly porous structure of the foams results in a material with an extremely high surface area which could reduce resistance to mass transfer in the MPL. Moreover, the foams have a low oxygen content and high carbon purity which is associated with good electrical conductivity, another physical property that is important in the MPL. This study aims to assess the potential of graphene foams to improve MPL performance and to gauge if a single material can be used for both the MPL and the catalyst support, this could simplify the manufacturing process and reduce costs.

In this study graphene foams were produced from sodium ethoxide which were pyrolised in different conditions; pure nitrogen and a mixed atmosphere of 95% nitrogen and 5% hydrogen by volume. The resulting foams were then characterised using SEM and XPS to understand the effect of pyrolysis conditions on elemental composition, microstructure, and level of graphitisation. Subsequently, microporous layers were produced from the graphene foams alongside commercial graphene nanoplates and Vulcan 72-XC R carbon black for reference. These microporous layers underwent ex-situ characterisation of their morphology and microstructure and their ability to conduct the transport of mass and electrons. Finally, polarisation curves and EIS measurements were taken at various relative humidity conditions to determine the appropriate operating conditions for their use and their suitability in PEMFC.

5.3 Results and Discussion

5.3.1 Characterisation of Graphene Foams

Table 5.1 shows the different physical and chemical properties of the carbons used in the MPLs. The atomic concentration data for the commercial graphene nanoplates and carbon black was supplied by the manufacturers (2D Tech, Cheltenham, and Cabot Corporation respectively). Whereas the elemental analysis of the graphene foams was carried out using X-ray Photoelectron Spectroscopy (XPS) at Kyushu University. As outlined in Chapter 3.1 fabrication of the graphene foams, sodium ethoxide was pyrolised in a nitrogen atmosphere, the resulting product was washed to remove the sodium salts, dried, and was subject to a second pyrolysis stage. The carbon was divided into two batches prior to pyrolysis, where one was pyrolysed under nitrogen flow and the other was pyrolysed under a flow of 95 vol.% N_2 and 5 vol.% H_2. The resulting products were weighed, placed in a sample tube, and labeled N-GF and NH-GF respectively. The NH-GF graphene foam was fabricated to ascertain if pyrolysis in an atmosphere with hydrogen would reduce the O_2 content and increase the carbon purity of the graphene foam. The XPS results indicate that pyrolysis under N_2/H_2 flow produced a high concentration of O_2 in the sample with an atomic concentration of 10% as opposed to 5% in the sample pyrolised in the pure N_2 atmosphere. Similarly, there is a larger percentage of impurities

(residual Na) in the NH-GF compared to the N-GF, combined with the higher concentration of O_2 resulting in a lower carbon purity in the NH-GF rather than the N-GF foam (85% and 93% respectively). A high carbon purity results in an increased electrical conductivity and a high electron mobility, and thus would result in an MPL with a higher bulk conductivity. The manufacturers report a higher carbon purity for the commercial materials than was achieved with the foams that were synthesised.

Table 5-1: The characteristics of the tested carbons: Vulcan 72 XC-R, Graphene Nanoplates and the Graphene Foams

.

	Surface Area[1]	Pore Size[1]	Particle Size[2]	Atomic Concentration (%)[3]			
				C	N	O	Other
N-GF	258 $m^2 g^{-1}$	2.67 nm	50 μm	93.11	0.36	5.25	1.28
NH-GF	273 $m^2 g^{-1}$	2.30 nm	50 μm	85.34	0.58	10.29	3.79
Graphene NP	45 $m^2 g^{-1}$	N/A	0.5-5 μm	98.00	0.03	2.00	1.00
Vulcan 72 XC-R	241 $m^2 g^{-1}$ [321]	< 3.00 nm [322]	0.02-0.08 μm	98.30 [322]	0.00 [322]	1.40 [322]	0.30 [322]

[1] *Obtained by BET for graphene foams, manufacturer's data for commercial products.*

[2] *Obtained by SEM*

[3] *Obtained by XPS*

Morphology

The microstructure of the materials was characterised by SEM, as can be seen in Figs. 5.1 and 5.2. The SEM micrographs enable the analysis of the morphology and physical structure of the materials prior to their use as a microporous layer material. Figs. 5.1 (a-c) shows the commercial graphene nanoplates (Nanene); a distinctive structure formed from layered platelet-shaped graphene nanoparticles. Fig. 5.1(a) confirms densely packed regions of graphene platelets surrounded by void. This can be further understood from an examination of Fig. 5.1 (c), where it is revealed that the graphene nanoplatelets preferentially stack in the in-plane directions. This tendency to stack in this direction creates an almost 2-dimensional microstructure. However, Fig. 5.1 (c) shows some graphene nanoplates stacked in the through-plane direction; this exposes the number of graphene layers that make up the material. According to the manufacturers, this is a few-layer graphene, meaning that there are 2-5 layers of stacked nano-particles [323], and indeed less than 10 layers are countable. This is of particular importance as the limited stacking of the graphene nanoplates results in higher electron mobility [323-325].

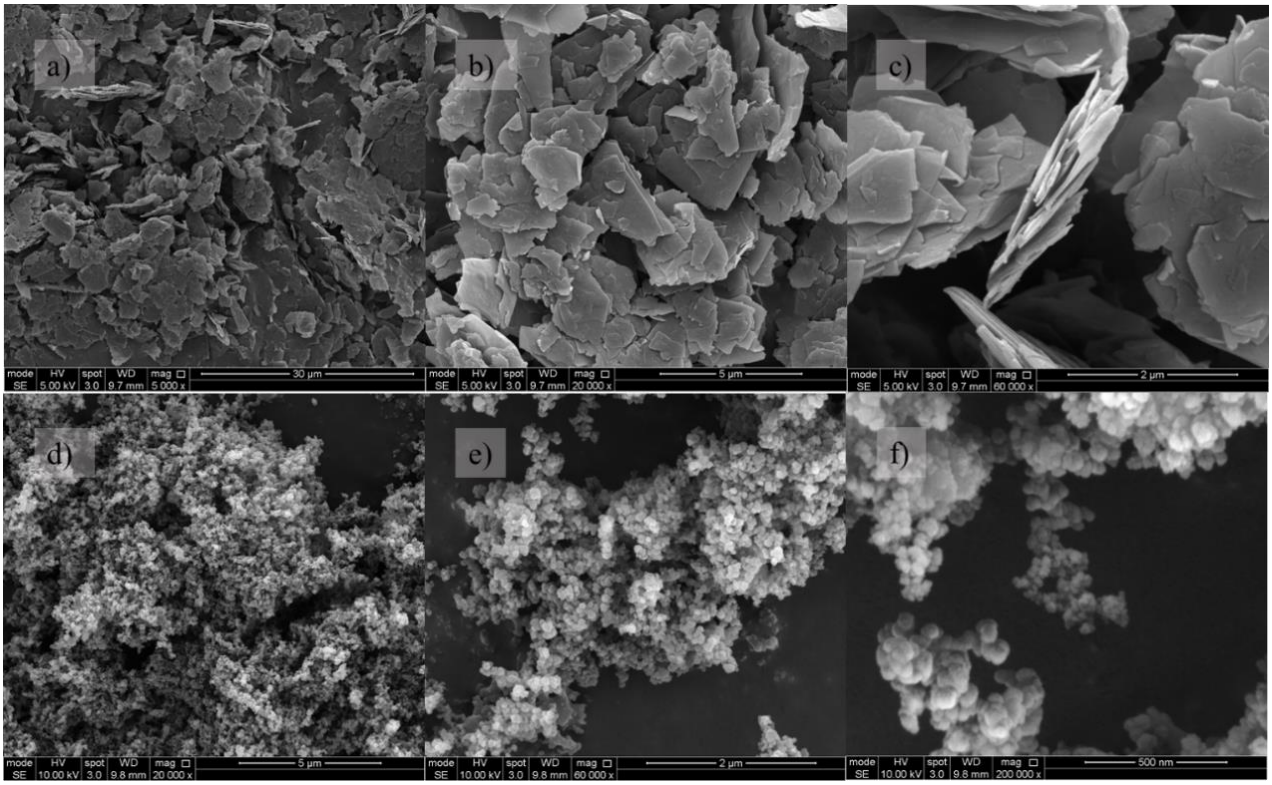

Figure 5-1: Nanene graphene nanoplatelets: at (a) 5000x, (b) 20000x, and (c) 60000x magnifications. Vulcan carbon black at (d) 20000x, (e) 60000x, and (f) 200000x magnifications.

Figs. 5.1 (d-f) shows the microstructure of Vulcan XC-72R carbon black. The morphological characterisation of carbon blacks has been extensively researched [229, 326-331] due to its very good physical and chemical characteristics and its wide usage in electrochemical applications. Vulcan XC-72R is typical of high-purity carbon blacks which are comprised of individual ~ 50 nm spherical nanoparticles, known as "primary particles" [326]. From the current SEM images, these were found to be in the range from 20 nm to 80 nm (Fig. 5.1 (f)). These primary particles then fuse together via Van der Waals forces to form an aggregate in the region of 200 to 800 nm [328, 329] as can be seen clearly in Figs. 5.1 (e) and 5.1 (f). Smaller primary particles (~20 nm) tend to form smaller aggregates (~ 250 nm), whereas larger particles (~ 50 nm) form larger aggregates (~ 600 nm) [326, 328, 331]. The SEM images of the carbon black aggregates unveil a microstructure which is entirely different from the graphene nanoplates; the 3-dimensional aggregates formed by the primary particles produce a different solid-to-void relationship than the almost 2-dimensional physical structure of the graphene nanoplates. There is a higher frequency of smaller void pockets between the carbon black aggregates than the graphene particles, and thus it can be expected to have a greater number of micropores in the physical structure than the graphene nanoplates as will be shown later in the pore size distribution section (Section 5.3.2).

Highly porous, three-dimensional carbon structures are visible in Fig. 5.2; these are the graphene foams: N-GF (Figs. 5.2 (a-c)) and NH-GF (Figs. 5.2 (d-f)), respectively. Without magnification the graphene foams visually resemble the carbon black as they are a fine black powder that tends to flocculate; however, the microstructure of the foam particles differs greatly from the carbon black spherical particles. Their microstructure bears similarities to the commercial graphene (Nanene graphene nanoplatelets) as the distinctive platelet-shape nanoparticles can be discerned (Figs. 5.2 (a and d)); however, for the carbon foams these serve as the carbon framework for the micron-scale macropores (Figs. 5.2 (c and f)) which are present throughout the structure. The SEM micrographs confirm that there is no discernible difference in the microstructure of the two foams, where both methods of pyrolysis produce a three-dimensional open pore structure. This interconnected pore structure prevents the restacking of graphene sheets and thus maintains a large surface area. This results in the formation

of large mesopores and small macropores in the MPL. The pore size distribution is an important morphological and physical property in determining the ability of the microporous layer to manage the transport of reactants and products to mitigate flooding and reduce mass transport losses. A greater frequency of micron-size macropores in the graphene foams, may in turn enhance the mass transfer of reactants and products across the microporous layer. The pore size distribution of the microporous layers is discussed in detail in Section 2.1.1, which focuses on the morphology of the MPL.

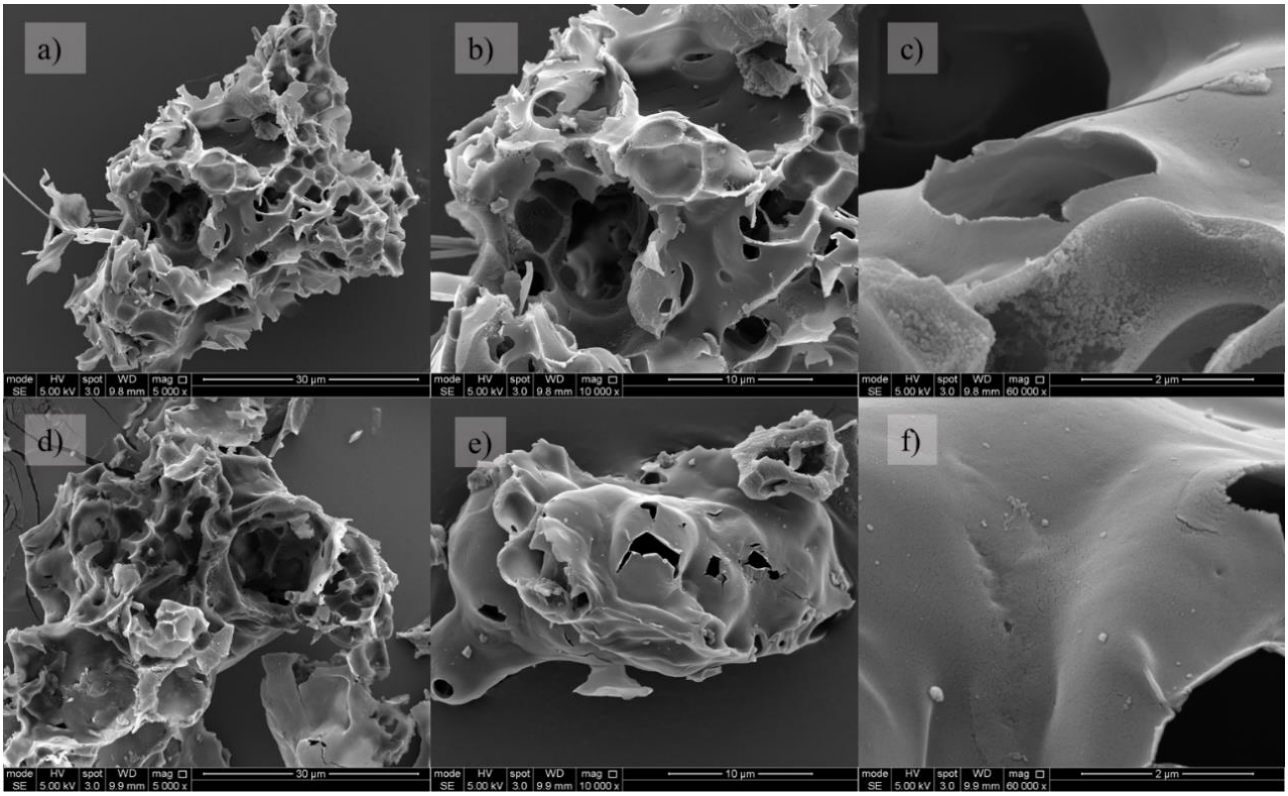

Figure 5-2: SEM micrographs of the graphene foams. N-GF at (a) 5000x, (b) 10000x and (c) 60000x magnifications, and NH-GF at: (d) 5000x, (e) 10000x and (f) 60000x magnifications.

5.3.2 Characterisation of the Microporous Layers

5.3.2.1 Morphology

Fig. 5.3 shows the SEM micrographs showing the surface morphology of the fabricated MPLs. The morphology of the MPLs varies greatly depending on the physical structure and the morphology of the constituent materials. The graphene nanoplate MPL can be seen in Fig. 5.3 (a); in this micrograph, the horizontally stacked formation of the graphene flakes is revealed. An undulating crack-free surface is produced with little visible void space at this resolution indicating that the pore sizes are on the sub-micron scale (<1 μm). The morphology of the carbon black MPL (Fig. 5.3 (b)) is typical of the commercial MPL, with the appearance of an even homogenous surface with micropores. The SEM micrographs show few cracks across the surface of the carbon black MPL. These mud-like cracks are particularly associated with carbon black-based microporous layers and are well noted in the literature [47, 52, 332-334]. However, they are much more clearly shown in Fig. 4.1 in Section 4.4.1. They are a result of the carbon black agglomeration process, where island-like structures form from the migration of isolated carbon particles [334]. The formation of these cracks is related to the thermal treatment of the MPL and in particular the evaporation of solvent [335, 336]. The microstructure of the graphene foam MPLs (Figs. 5.3 (c and d)) shows a much more porous structure than the graphene platelets and the Vulcan where void space is clearly visible indicating that the pores are much larger than the other two materials. There is little discernment between the two graphene foams as both have retained the characteristic open foam structure, indicating that the method of fabrication of the ink and the application of the microporous layers to the substrate does not damage the unique microstructure of the graphene foams.

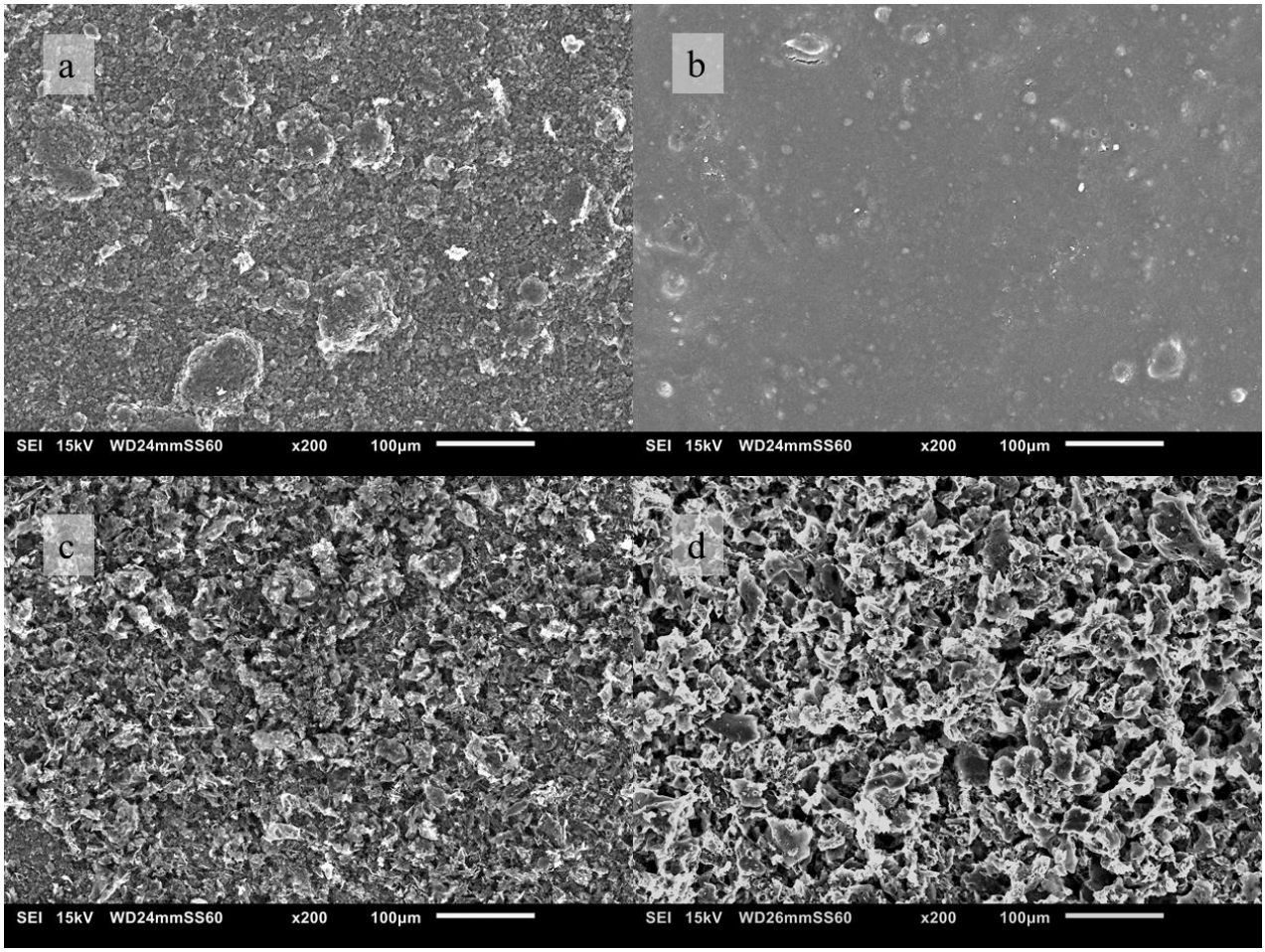

Figure 5-3: SEM micrographs of the surface of the MPL-coated GDLs (a-d: graphene nanoplates, Vulcan, N-graphene foam and NH-graphene foam)

5.3.2.2 Porosity and Pore Size Distribution

The carbon material used for the fabrication of the microporous layer determines its microstructure and morphology as can be seen from the SEM micrographs, thus defining the pore size and consequentially its ability to conduct mass transfer. As previously discussed in Chapter 4, there are three categories of pore size in the MPL-coated gas diffusion layer; the smallest being micropores < 0.07 µm, mesopores range from 0.07–5 µm in size, and finally macropores are the largest being pores ≥ 5 µm [337]. The differentiation of pore size is determined by the diffusion mechanism of gas transport within the pores. In micropores, where the pore diameter is comparable to the mean free path of the gas (λ air ~ 70 nm), gas transport occurs through Knudsen diffusion whereas bulk diffusion is the prevailing mechanism in macropores which are 2 orders of magnitude larger than the micropores [292]. In mesopores, both

mechanisms of gas transport occur [292]. As the transport of fluid through a material is determined by the size of the pores, it is important to understand the pore size distribution in the MPL to ascertain its capabilities. The MPL has the dual purpose of enabling the flow of mass towards the catalyst layer and liquid water away from the catalyst, therefore the optimal pore size distribution of the MPL should allow for the transport of both liquid and gas. However, a high porosity and pore size distribution are not the only factors in determining the ability of the MPL to manage two-phase flow in the cell; it is also important to consider the tortuosity and hydrophobicity of the material and the mechanical stability of the layer.

The pore size distribution of the fabricated MPLs was obtained by mercury intrusion porosimetry and can be seen in Fig. 5.4. From the data one can see that the pore sizes of the MPLs vary dramatically from small microporous region to micron scale pores depending on the material used. The MPL produced from Vulcan carbon black has a predominantly microporous physical structure with a smaller number of pores occurring in the mesoporous region; the peak indicates that the majority of pores present in the carbon black agglomerates are ~50 nm in size. This corresponds with the average particle size of the carbon black primary particles which were measured using SEM to be in the range of ~ 20 nm to ~ 80 nm.

The MIP data generated exposes the pore size distribution and the dominant pore size of the MPL-coated gas diffusion layer. The Vulcan carbon black GDL has the greatest percentage of micropores (5%) compared to the graphene nanoplates (2%), and the graphene foams N-GF (2.5%) and HN-GF (3%). The pore profile of the graphene foam and graphene-based microporous layers does not fall in the microporous region; instead, more pores occur in the mesoporous region, 10%, 13%, and 15% for the graphene and the graphene foams (N-GF and HN-GF) respectively in comparison to 9% in the Vulcan GDL. The SEM micrographs of the graphene foams (Fig. 5.2) reveal micron-scale pores throughout the carbon structure which were visibly preserved in the formation of the microporous layer (Figs. 5.3 (c and d)). The results of the mercury intrusion porosimetry of the graphene foam MPLs (Fig. 5.4 (b)) confirm that the mesopores are the most abundant pores in the layer.

The porosity and pore profile of the layer influence its ability the transport of mass, as the main mechanism for reactant transport (i.e., diffusion) depends on these structural properties of the MPL. The mercury intrusion porosimetry results confirm that the N-GF and the NH-GF GDLs have a higher porosity (75%) than the Vulcan (74%) and graphene nanoplates (71%) they probably have a greater ability to conduct mass transport in dry conditions, however, this does not consider the tortuosity of the material. However, the absence of micropores and the largely macroporous nature of N-GF and NH-GF layers may lead to water stagnation and pore saturation in high humidity conditions as the pressure gradient between the microporous layer and the gas diffusion substrate is relatively low [129, 338].

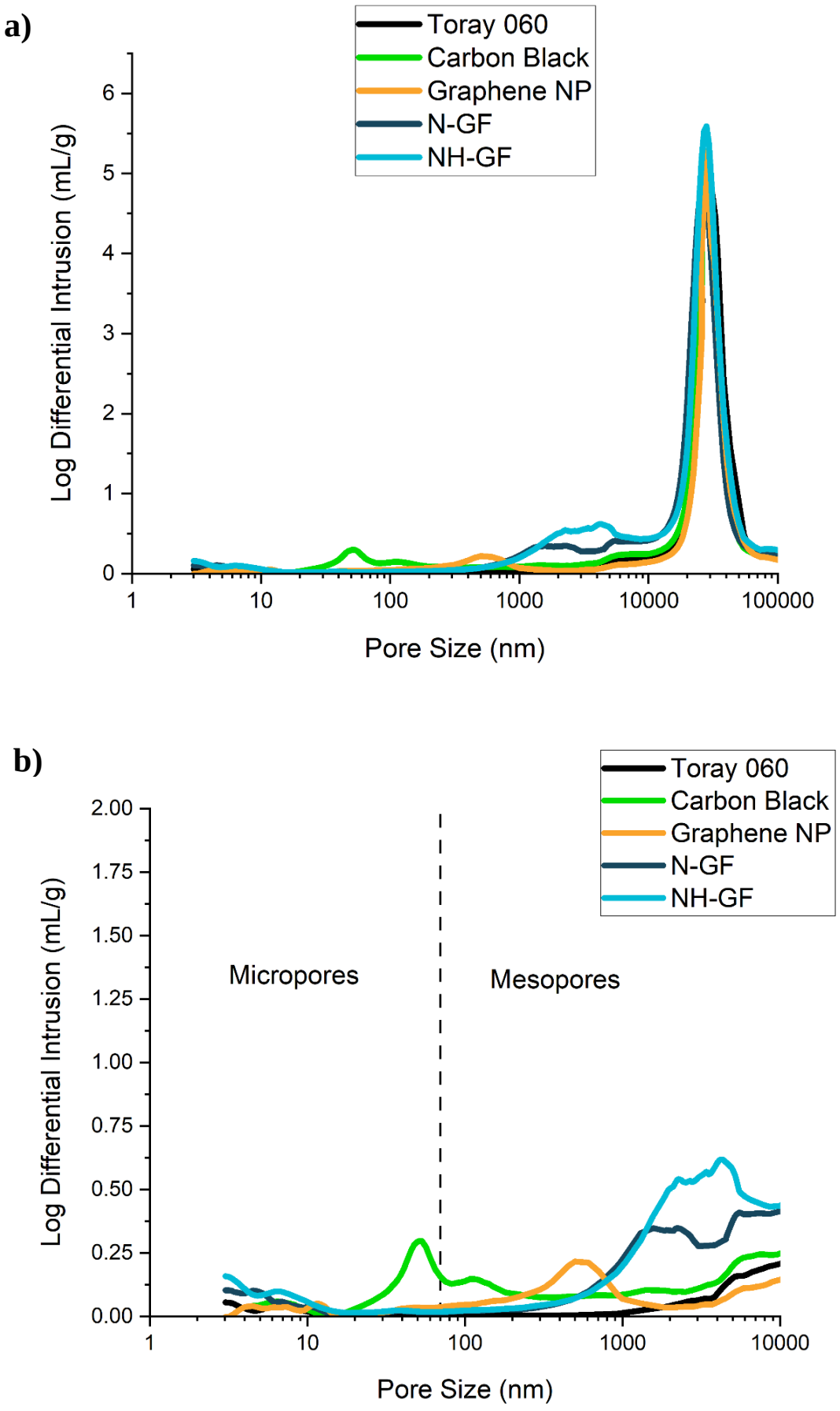

Figure 5-4: The pore size distribution of the investigated coated GDLs, (b) focuses on the microporous layer.

5.3.2.3 Contact Angle

The static contact angle measurements indicate the hydrophobicity of the MPL surface. The contact angle results of the MPL-coated GDLs indicate that the composition of the microporous layers influences the wettability. The highest contact angle was measured on the surface of the GNP MPL (151°); lower contact angles were recorded from the two graphene foams and the Vulcan, 143°, 142°, and 145° respectively. The greater hydrophobicity of the GNP MPL is attributed to the compactness of these layers and the stacking of the graphene plates in the horizontal plane. This is in line with values reported by Ozden et al. [242] and Mariani et al. [243] who report that the graphene nanoplates produced an MPL with a higher contact angle. This results in a crack-free surface morphology with a microscopic roughness produced from the vertical stacking of the graphene nanoplates as can be seen in the SEM micrograph (Fig. 5.3 (a)). This ultimately increases the contact angle of the respective MPL. In contrast to this, the surface of the N-GF and NH-GF GDLs is less densely packed and has a reduced mechanical stability compared to the other two materials' surfaces; this may have led to lower contact angle values compared to that of GNP GDL. This indicates that the N-GF and NH-GF MPLs most likely have, compared to GNP MPL, less tendency to trap water produced at the catalyst layer that is most needed for membrane-phase humidification under low-humidity conditions. An MPL with a higher contact angle has been shown to enhance electrochemical performance in single-cell measurements [52, 280, 312, 339-341]

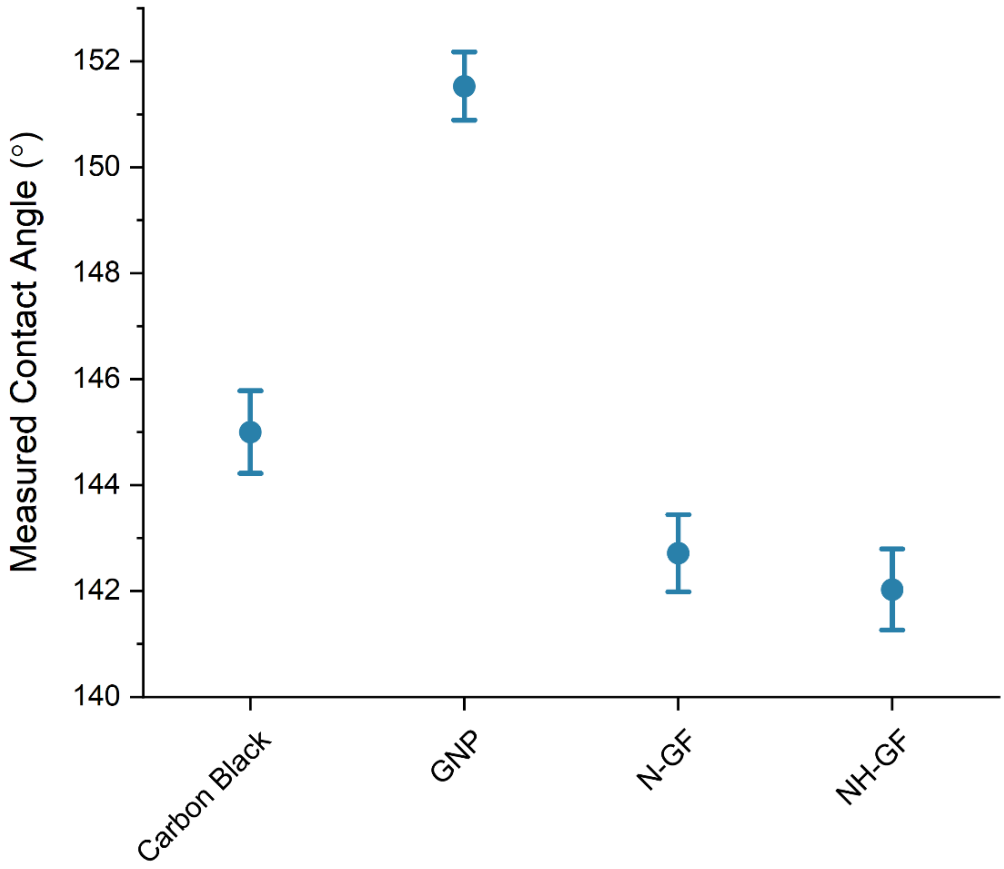

Figure 5-5: The measured contact angle of the MPL-coated GDLs.

5.3.2.4 Through-plane Permeability

The through-plane permeability of the gas diffusion layers reduces with the addition of a microporous layer to the carbon substrate. This is widely noted in literature: the uncoated Toray TGP-H060 has the highest permeability. The carbon component of the MPL has a large influence on the permeability of the gas diffusion layers, where the graphene foam microporous layers record the highest permeability followed by the carbon black.

There is a clear link between the porosity of the layers and their permeability; this is well established in the literature as a higher porosity of material allows for greater airflow and less resistance to the flowing gas. This correlates well with the data as the MPLs produced from the graphene foams allows for the greatest gas permeability and have the highest porosity (75%). However, given the hollow 3-

dimensional open structure of the graphene foams, a higher permeability than the measured value was anticipated, this may be due to other physical properties, such as the tortuosity of the material.

The error bars of the carbon black MPL indicate a greater variation in permeability between samples compared to the other materials; this is probably due to an uneven distribution of the cracks in the MPL (Fig. 4.1 (d)). Conversely, the microporous layers derived from graphene nanoplatelets have small error bars indicating a smaller degree of variation between the samples compared to the other materials. This is likely due to the horizontal stacking of graphene nanoplates creating a more uniform, crack-free surface. However, the graphene MPL has the lowest through-plane permeability of the samples which matches the porosity which was lower than the other materials (71% compared to 75% for GF). Moreover, the 2D physical structure of the graphene nanoplatelets gave rise to stacking in the microporous layer forming a layer that is mostly perpendicular to the flow of gas, thus providing resistance to the flow of gas and reducing the permeability of the layer.

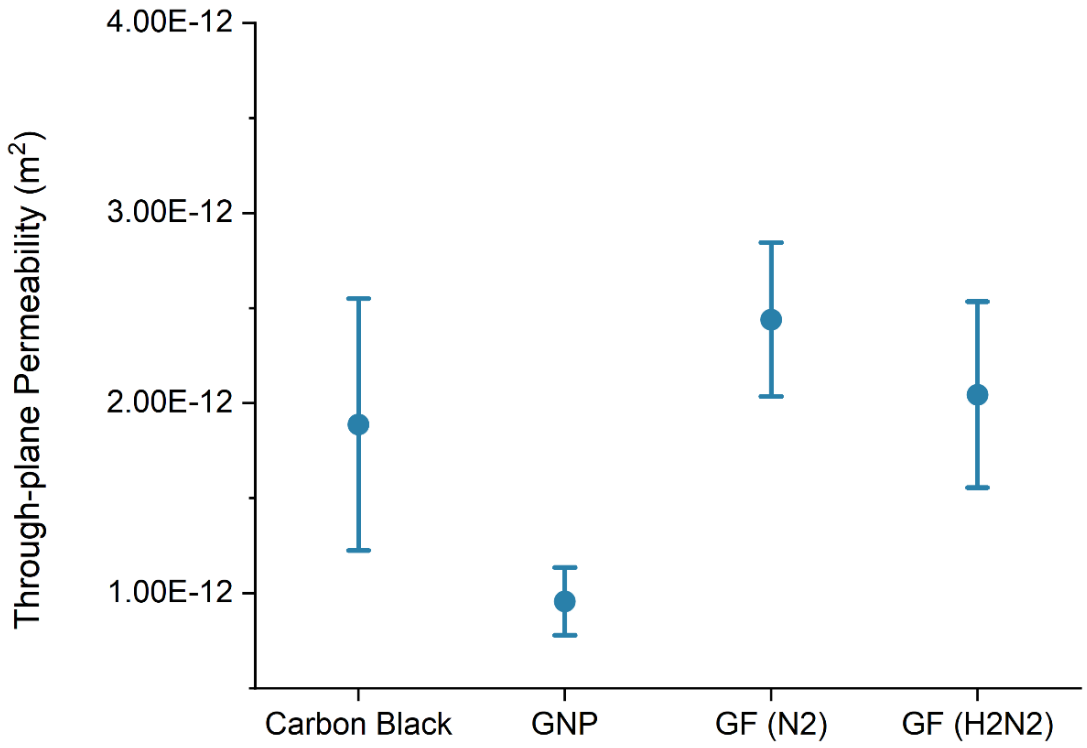

Figure 5-6: The measured through-plane permeability of the MPL-coated GDLs.

5.3.2.5 In-Plane Electrical Resistivity

The in-plane electrical resistivity of the samples was measured and can be seen in Fig. 5.7. The GNP MPL recorded the lowest in-plane resistivity, whereas the Vulcan carbon black MPL was the least conductive. The resistivity of the MPLs is determined by morphology and physical structure of the layer itself, as well as the physio-chemical properties of the composite materials and their interactions, i.e. the electro-conductivity of the carbon particles, the quantity of polymer (PTFE) [8], and the type of hydrophobic polymer used [257, 265]. The unique electron conductivity of graphene is well documented from an array of experimental studies [342-346]; Bolotin et al. reported an exceptionally high conductivity of 230 000 $cm^2\ V^{-1}\ s^{-1}$ at room temperature for single-layer graphene [346]. For graphene, the electrical conductivity is solely based on the defects in the material and the number of layers, the fewer of both are better (12, 14); single-layer graphene has the highest electron conductivity, followed by few layers and finally multilayer. The high electron mobility of few-layer graphene explains the low resistivity of the MPLs derived from graphene nanoplates. As this is a high carbon purity (98%) and few-layer graphene, it is unsurprising that the resistivity is low for this MPL although it is invertible that a degree restacking of the plates occurs in the fabrication of the layer.

Notably, the N-GF has a lower in-plane resistivity than the NH-GF; this can be explained by the XPS elemental analysis which showed that the graphene foam pyrolised in pure nitrogen conditions (N-GF) has a higher carbon purity (93%) than that subject to pyrolysis in the nitrogen and hydrogen atmosphere (85%). The pyrolysis in a pure nitrogen atmosphere was able to enhance the purity (i.e., remove oxygen and sodium) and graphitise the carbon foam to produce a graphitic structure more effectively than pyrolysis in a 5% hydrogen atmosphere. This resulted in a graphene foam with a higher electrical conductivity.

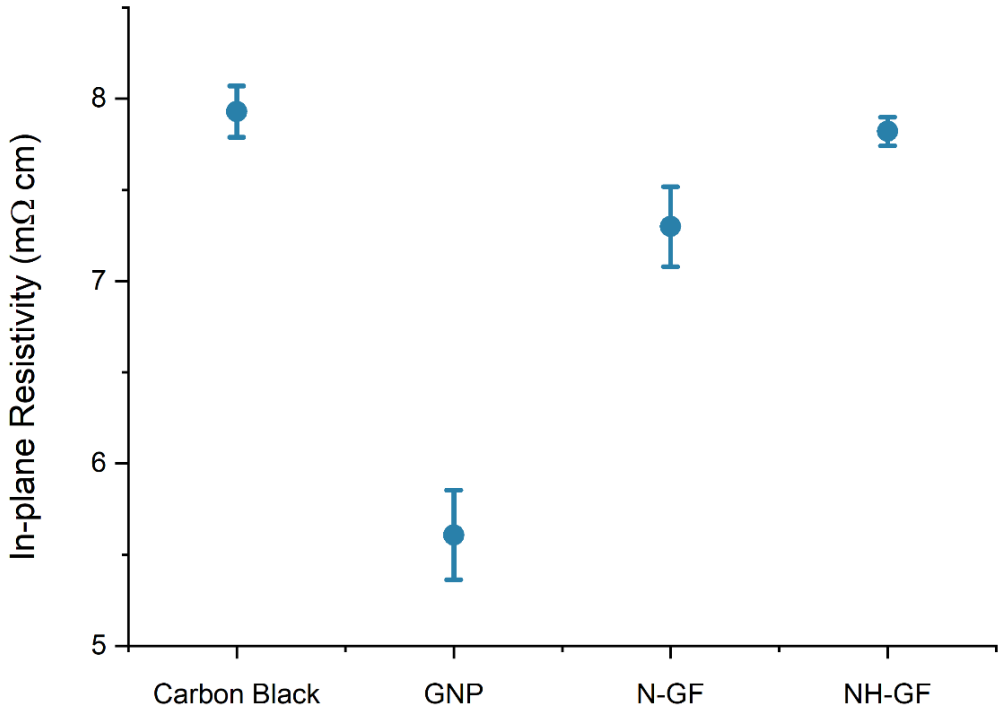

Figure 5-7: The in-plane electrical resistivity of the coated GDLs.

5.3.3 Fuel Cell Performance

Fig. 5.8 shows the performance of the MPL-coated GDLs in a range of different relative humidity conditions. Single-cell measurements were taken from low humidity (25% RH) to high humidity conditions (100 RH%) to understand the ideal operating conditions for the GDLs. Both low-humidity and high-humidity operations have limitations that lead to power losses in the fuel cell. Low relative humidity conditions are problematic as the membrane must be sufficiently hydrated to allow effective proton conduction. While operating under low humidity conditions, the membrane can dry out which reduces the ionic conductivity, increasing ohmic losses. Contrarily, high humidity conditions potentially pose a different problem stemming from excess water. This excess water can saturate the pores of the porous media: the GDL, MPL, and the catalyst later, which restricts reactant flow and reduces catalyst active site availability. These mass transport losses are particularly prevalent at high current density operations where the oxygen reduction reaction is occurring at a faster rate and thus a greater amount of water is being produced and less oxygen is being supplied to the catalyst layer. Polarisation curves were taken at 25%, 50%, 75%, and 100% relative humidity operation in the air at a

constant temperature of 80º C (Figs. 5.8 (a-d)). From this, it was possible to emulate real-life operating conditions and to determine in which conditions the graphene foam microporous layers exhibited the greatest performance and suffered the least losses.

The GNP MPL exhibits similar performance to that shown in Fig. 4.8, suffering from the greatest activation losses and encounters ohmic resistivity, particularly in low humidity conditions (25% and 50% RH). However, the GNP MPL shows superior oxygen mass transport characteristics with excellent performance in high humidity conditions (75% and 100% RH) and the high current density region where liquid water saturation limits oxygen diffusivity. Fig 5.8 shows that, under all the humidity conditions, the fuel cell performs better with the commercial materials (graphene nanoplates and Vulcan carbon black) than with the graphene foam as evidenced by the highest limiting current density and the highest peak power density featured by the former MPL. This could be mainly attributed to the ability of the carbon black MPL to retain more water required to humidify the ionomer phase in the catalyst layer. As shown in Fig. 5.4, Vulcan carbon black MPL features a higher amount of micropores, which are required to retain water, especially under low humidity conditions, compared to graphene foam samples. This argument is evidenced by the corresponding EIS curves at 0.6 V (Fig. 5.10) that show the charge transfer resistance (the right intercept of the semicircle with the x-axis) of the fuel cell with carbon black is always lower than those of the graphene foams, thus indicating better hydration is attained for the ionic phase of the catalyst layer. Expectedly, the fuel cell performance degrades under high humidity conditions (RH = 75% and 100%) and this is due to water flooding that manifests itself through the sharp decline in performance at high current densities and subsequently reduced limiting current densities. Notably, the fuel cell with N-GF MPL performs better than with NH-GF MPL; this could be attributed to the higher carbon content (Table 5.1) and subsequently higher electrical conductivity (Fig. 5.7) demonstrated by the former graphene foam MPL. For graphene foams to be a viable material for the microporous layer the ohmic and activation losses need to be overcome, this would require further control and optimisation of the pore size of the foam structure. They maintain a high carbon purity in the material.

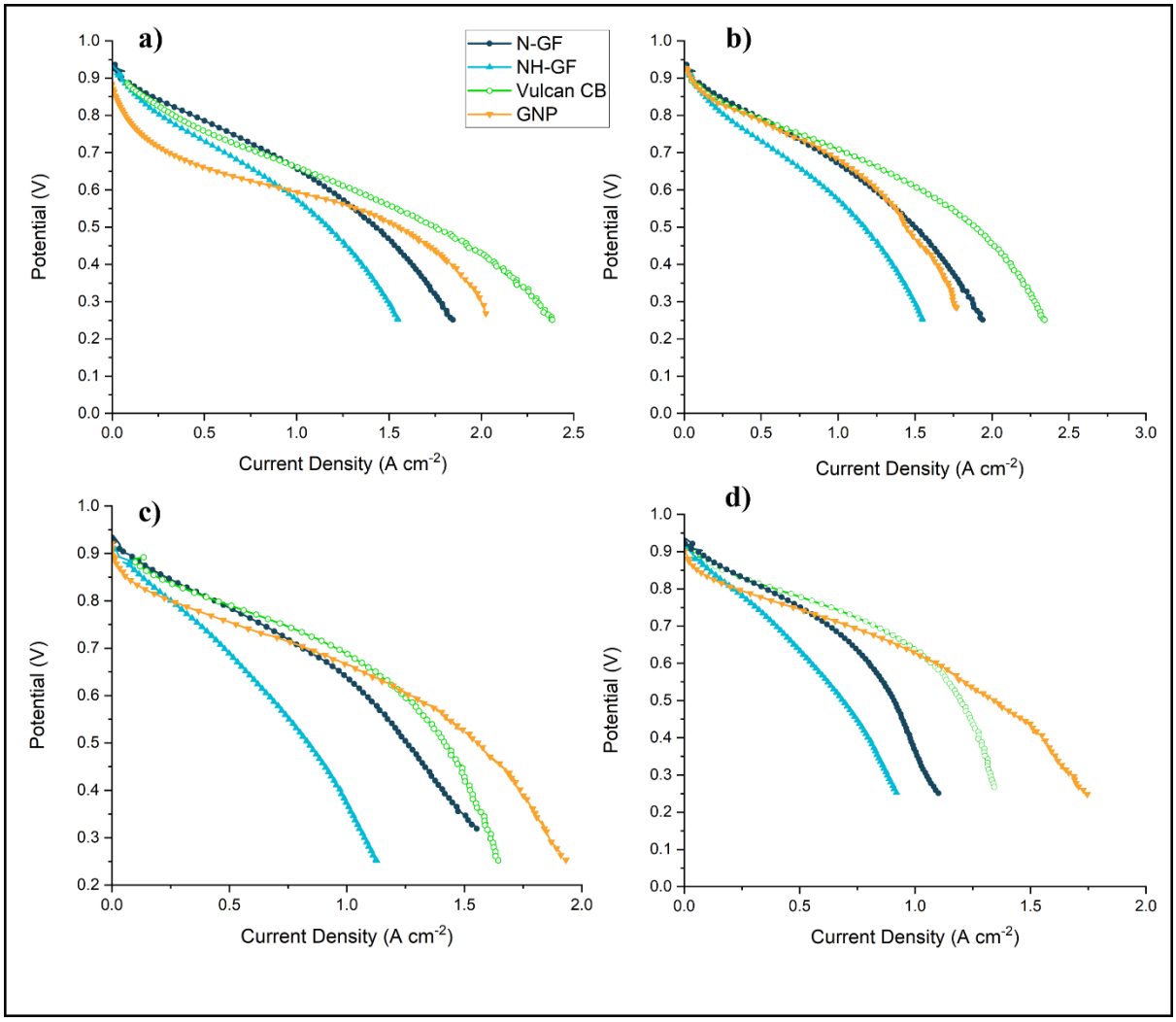

Figure 5-8: IV curves of the N-GF, NH-GF, GNP graphene nanoplates and Vulcan carbon black GDLs. Taken at (a-d) 25%, 50%, 75% and 100% relative humidity in air at 80ºC.

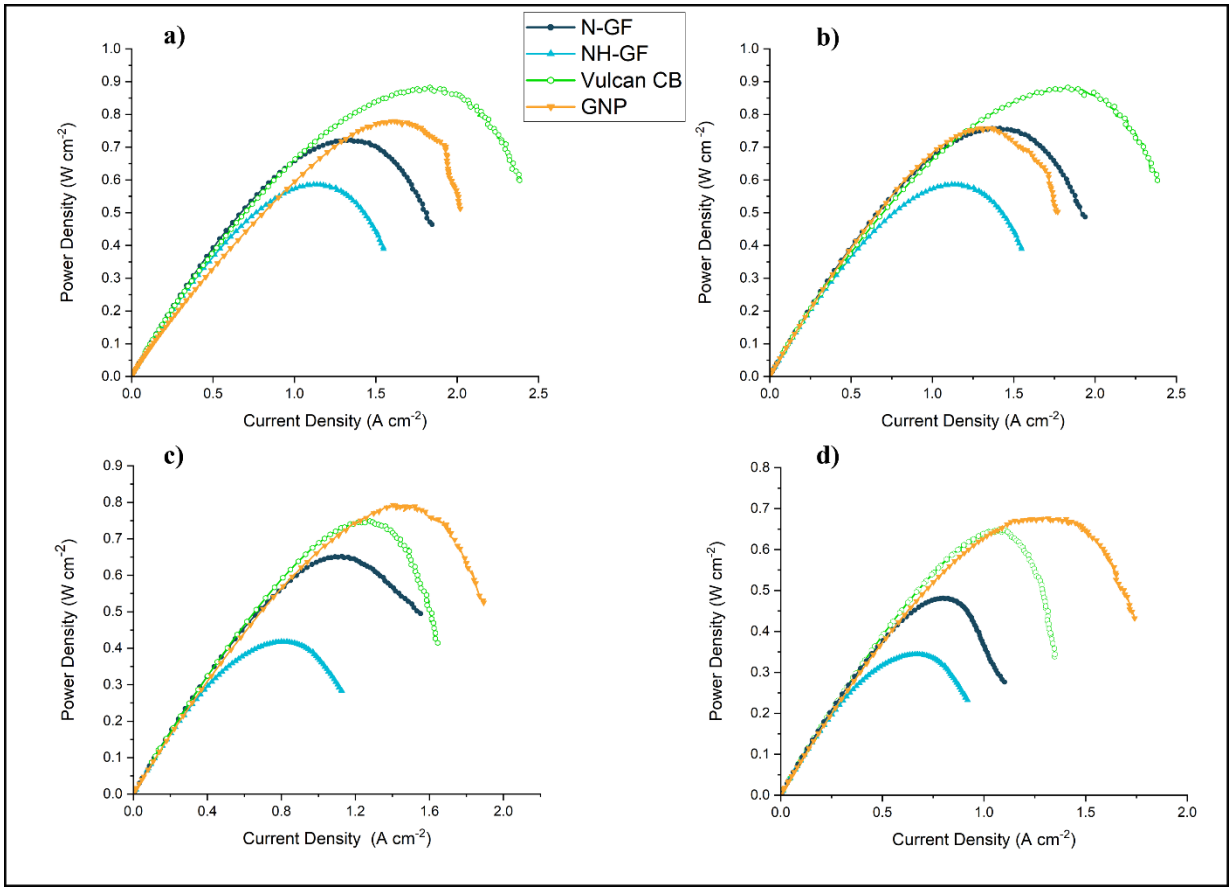

Figure 5-9: Power curves of the N-GF, NH-GF, GNP Graphene nanoplates, and Vulcan carbon black GDLs. Taken at (a-d) 25%, 50%, 75% and 100% relative humidity in air at 80ºC.

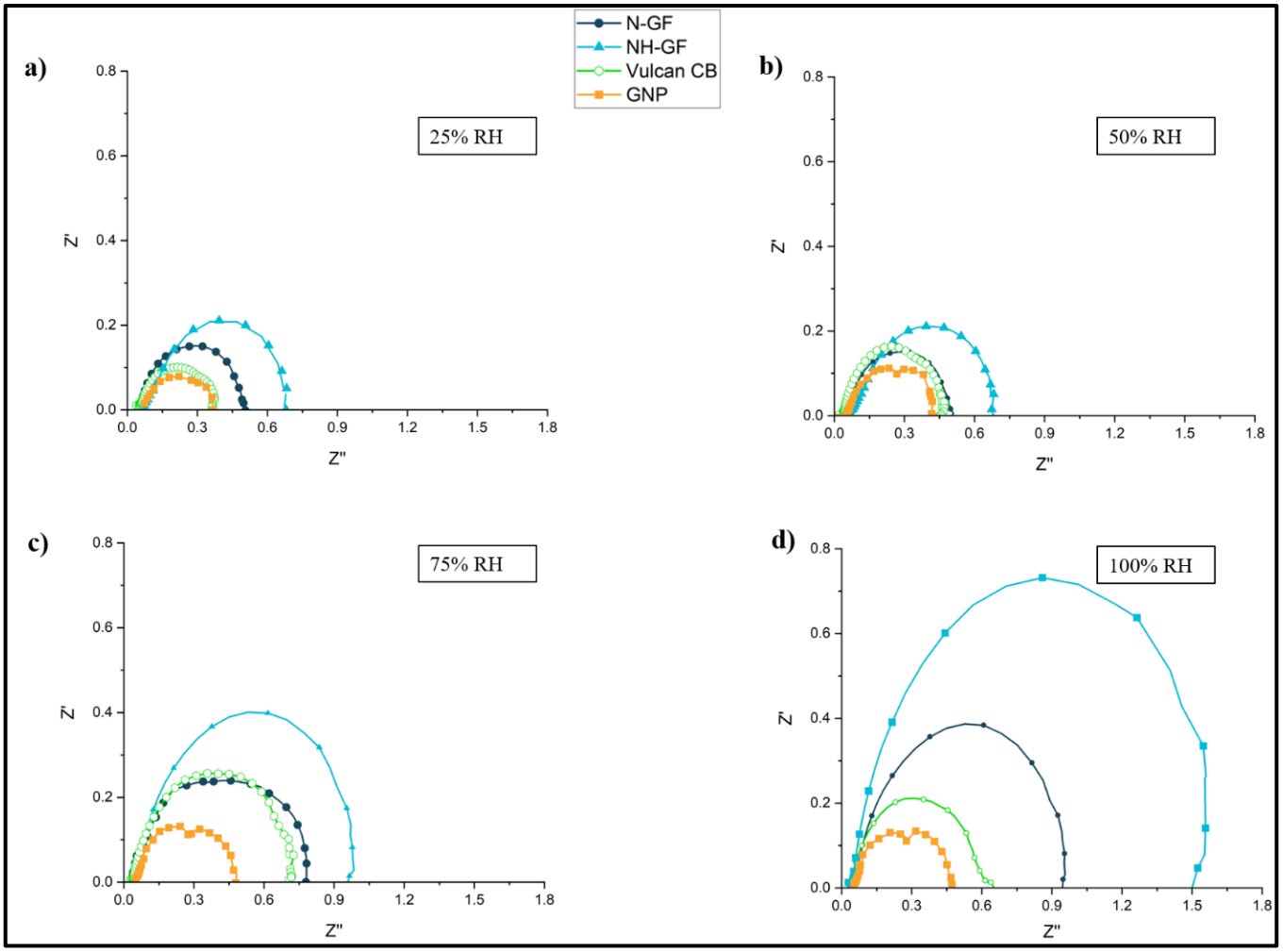

Figure 5-10: EIS results of the N-GF, NH-GF, GNP graphene nanoplates and Vulcan carbon black GDLs. Taken at (a-d) 25%, 50%, 75% and 100% relative humidity in air at 80ºC. Taken at 0.6 V.

5.4 Conclusions

Graphene foams were fabricated from the pyrolysis of sodium ethoxide in two different atmospheres to produce N-GF and NH-GF. Microporous layers were produced from the N-GF and NH-GF graphene foams which were then characterised alongside MPLs produced from carbon black and graphene nanoplates. The N-GF MPL exhibited favourable characteristics for mass and electron transport in ex-situ tests, moreover, polarisation curves showed that it is competitive with carbon black in the mid-current density region and at 50% and 75% relative humidity operation. This investigation shows that in the current graphene foam, there is no potential for graphene foam as a microporous layer material, however, the morphology and the hydrophobicity of the MPL require optimisation to improve performance in high humidity operation.

- The atmospheric composition during pyrolysis affects the physio-chemical properties of graphene foams. Graphene foam produced in the pure nitrogen atmosphere (100 vol.% N_2) had a greater carbon purity than the foam produced from pyrolysis in nitrogen and hydrogen atmosphere (95 vol.% N_2: 5 vol.% H_2).
- The pore size distribution of the graphene foam MPLs falls into the large mesoporous region with an absence of small mesopores and micropores. The peak pore size of the N-GF and NH-GF are 1-2 μm and 4 μm, respectively.
- The N-GF exhibited more desirable physical and electrical characteristics than the NH-GF. A higher electron conductivity was measured with the N-GF MPL which is attributed to the higher percentage of carbon in the foam. A higher through-plane permeability was also recorded on the N-GF, although the wettability of the two foams was comparable.
- The N-GF exhibits similar performance to the carbon black MPL in the low current density region, however at higher current densities and fully humified conditions it suffers from mass transport losses.
- This is attributed to a combination of the large pore size in the layer and the reduced electrical conductivity of the foam.

- NH-GF struggles in all conditions and is uncompetitive, suffering from both ohmic losses and mass transport losses. This is particularly apparent at 100% relative humidity operation.
- The graphene MPL benefits from the presence of water in the porous media. This is increased humidification, and better performance in higher humidity conditions (75% and 100 % relative humidity) and in the higher current density region.
- In low humidity conditions (25% and 50%) the graphene MPL is limited by ohmic and activation losses from insufficient membrane hydration and increased contact resistance with the catalyst layer.

Chapter 6: Rethinking Microporous Design: Fabrication and Characterisation of Bi-layer Pore Graded Microporous Layers

6.1 Introduction

Numerous studies have shown that the performance of gas diffusion layers is enhanced with the addition of a microporous layer that is typically comprised of carbon black and a hydrophobic agent (PTFE). Conventional microporous layer design consists of a single layer with a continuous microstructure and physical properties [1, 39, 217, 220, 222, 232, 267]. In this chapter, the novel design of a bi-layered microporous layer is fabricated and characterised alongside the conventional single-layer microporous layer to investigate the potential for further enhancement of cell performance.

In the bi-layer MPL, the microporous layer consists of two layers with individual physical properties, notably a different microstructure and pore profile from the previous layer. Therefore, producing a pore gradient through the MPL from the catalyst layer interface to the gas diffusion layer interface. The idea behind this design is that it will further enhance the water removal properties of the microporous layer in high current density operation and high humidity conditions. The capillary pressure is the mechanism by which liquid water is removed from the catalyst layer interface through the gas diffusion layer [53, 87, 127, 347, 348]. Research indicates that the presence of micropores in the MPL at the catalyst layer/ MPL interface promotes stronger capillary pressure through the GDL substrate to the outlet, thus aiding the removal of accumulated liquid water [166, 170, 219, 238, 315, 349-351]. Theoretically, an MPL with a graded pore size from the catalyst layer interface to the gas diffusion layer interface maintains the pressure through the MPL and results in enhanced liquid water removal capabilities. Indeed, a pore-graded MPL is an enhancement of the original purpose and design of the MPL, to enable the capillary mechanism for liquid water removal.

Various research groups have experimentally investigated pore-graded gas diffusion substrates, which have been shown to reduce liquid water accumulation and improve cell performance, particularly in the high current density region [166, 170, 315]. Balakrishnan et al. [166, 170] produced a pore-graded GDL substrate from electrospinning, which mitigated liquid water saturation and reduced mass transport

losses in fully humidified conditions (100% RH). A significant volume of work has been carried out on modelling the MPL microstructure and the effect of pore size and structure [219, 352-354]. Notably, Zhan et al. produced a 3D pore network model to investigate the effect that a pore-graded MPL has on liquid water saturation, relative oxygen effective diffusivity and limiting current density [219]. They found that a graded porosity reduced liquid water saturation at the catalyst layer interface and increased oxygen diffusivity. Similarly, Wong et al. [352] modelled the pore network of the MPL-coated GDL using X-ray CT reconstructions to simulate the water saturation behaviour and oxygen mass transport.

Experimental work on the pore-graded microporous layer is limited, though it has yielded significant results in terms of improving our knowledge of the optimisation of MPL microstructure. Bi-layer microporous layers have been produced by several researchers who have investigated the graded hydrophobicity in the MPL [274, 275, 350, 355]. Influential work undertaken by Tang et al. [238] investigated the effect of a pore-graded triple-layer MPL. NH_4Cl pore former was used to produce an MPL with decreasing pore size from the catalyst layer interface to the GDL interface. They report that the pore-graded MPL enhanced MEA performance, particularly in high current density operation as it provided additional capillary pressure from the catalyst layer to GDL promoting liquid water removal. Gas diffusion layers with a pore-graded MPL were produced by Chun et al. [230] and by Lin et al. [349] by using different carbons for the two layers of the MPL. Chun et al. [230] used thermally expanded graphite, whereas Lin et al. [349] used acetylene black and Vulcan 72-XC, to manipulate the pore gradient from the catalyst layer interface to the GDL interface. Their findings support those of Tang et al., as they report that the pore-graded MPL promoted liquid water removal and enhanced cell performance in high current densities.

In this investigation, bi-layer pore-graded MPLs were produced and characterised to see the effect of a graduated pore structure on the GDL characteristics and cell performance. To control the pore size of the layers and to achieve layers with differing pore structures, MPL ink was produced from different carbons (large graphene nanoplates, small graphene nanoplates and carbon black). In Chapter 4, it was demonstrated that substituting carbon black with graphene nanoplates led to an increase in pore size and the formation of mesopores in the microporous layers. Thus, in this research chapter, the pore size

of the layers was controlled simply by the type of carbon used. Pore-graded microporous layers were fabricated by stratifying two MPL inks produced from different carbons. Both MPL layers have distinct microstructures and pore profiles and therefore form a pore size gradient through the MPL. The order in which the inks were applied to the GDL substrate was alternated to produce MPLs with both increasing and decreasing pore sizes from the GDL to the catalyst layer interface. This enables greater conclusions to be drawn about the effects of the individual layers rather than the bulk MPL.

6.2 Methodology

6.2.1 Preparation of the Microporous Layers

Bi-layered microporous layers were fabricated from Vulcan XC 72-R carbon black (Sigma Aldrich, UK) and from graphene nanoplates of two different sizes (Fischer Scientific, UK) which are referred to as small graphene (SG) and large graphene (LG). The physical properties of which are listed in Table 6.1, note that the physical properties differ from the graphene used in the previous chapters (4 and 5).

Table 6-1: The physical properties of the carbon materials.

Material	**Particle Size (nm)**	**Surface Area (m^2/g)****
Vulcan XC 72-R	20-80 nm*	241 m^2/g
Small Graphene	2000 nm**	750 m^2/g
Large Graphene	500-5000 nm	150 m^2/g

*- Measured using SEM
**- Manufacturer's data

The bi-layer microporous layers were produced by applying an initial coating of 100µm, this was then dried on a hot plate at 70° before a second layer of 50 µm was applied. This was then dried on a hot plate at 70° and finally sintered in a furnace at 120° for 60 minutes, followed by 280° for 30 minutes and finally at 350° at 30 minutes to sinter the PTFE. Table 6.2 shows the compositions of the bi-layer microporous layers, where the initial layer was applied to the substrate first. The MPL thickness corresponds to the thickness of the dried layer.

Table 6-2: The compositions of the microporous layers.

Sample	**Initial Layer**	**Secondary Layer**	**Initial Layer Thickness (µm)**	**Secondary Layer Thickness (µm)**
CB	Vulcan	Vulcan	90	
LG	Large Graphene	Large Graphene	90	
CBLG	Vulcan	Large Graphene	60	30
LGCB	Large Graphene	Vulcan	60	30
SGCB	Small Graphene	Vulcan	60	30
LGSG	Large Graphene	Small Graphene	60	30

6.3 Results and Discussion

6.3.1 Morphology

The surface structures and morphology of the microporous layers are revealed in the SEM micrographs shown in Fig. 6.1 and Fig 6.2. The flattest or smoothest MPL is the single layer of Vulcan carbon black (Fig 6.1 (a)), which has fewer cracks than the typical aforementioned characteristic surface of carbon black microporous layers [288, 289, 334, 335, 356]. Whereas the MPLs produced from the large graphene nanoplates (Fig 6.1 (c)) are revealed to have a rougher surface owing to their relatively greater size resulting in a microscopic roughness. The MPL composed of the small graphene platelets has a greater degree of undulation and roughness than the carbon black though less so than the large graphene.

Regarding the bi-layer MPLs, one can see that the variation in materials and their order of application determines the appearance and physical structure of the MPL surfaces, i.e., the surface of LGCB (Fig. 6.2 (a)) is entirely different from CBLG (Fig. 6.2 (b)). The LGCB in particular Fig. 6.2 (a) has a remarkably similar morphology to the single layer MPL where carbon black is applied to the carbon substrate. This is likely due to the larger nanoplatelets providing a more supportive layer to the carbon black agglomerates, akin to the carbon substrate. Likewise, the surface morphology of the CBLG resembles the single material large graphene MPL. Interestingly, where the outermost layer is carbon black (LGCB and SGCB, or Figs 6.2 (a) and (c)) the MPL surface is characterised by distinct cracking, which is usually typical in the single layer of carbon black. This is most clearly visible in Chapter 4, Fig. 4.1 (b). There is a greater degree of cracking where carbon black is the secondary layer compared to the single material carbon black MPL. Cracking of the MPL occurs during the coating and drying process due to particle agglomeration [334, 335]. Previous research indicates that liquid water intrudes the MPL through these cracks and that they serve as low capillary barrier conduits for the macroscale transport of liquid water [352]. The location of these cracks on the MPL surface determines the liquid water saturation patterns in the GDL substrate [288, 309]. Therefore, the MPLs which have a carbon black layer at the catalyst layer interface such as LGCB, SGCB and CB, may benefit from enhanced liquid water removal as the surface cracks aid with the mitigation of liquid water.

Where the two graphene nanoplates are used (LGSG, Fig. 6.2 (d)) the small graphene nanoplates are visible on the surface of the large graphene structure. Individual formations of stacked graphene nanoplates are revealed in varying sizes. The observable larger platelets are likely to be from the initial layer of large graphene, although they may be from inconsistencies in the dimensions of the small graphene nanoplates as can be seen in the single material small graphene MPL (Fig. 6.1 (b)).

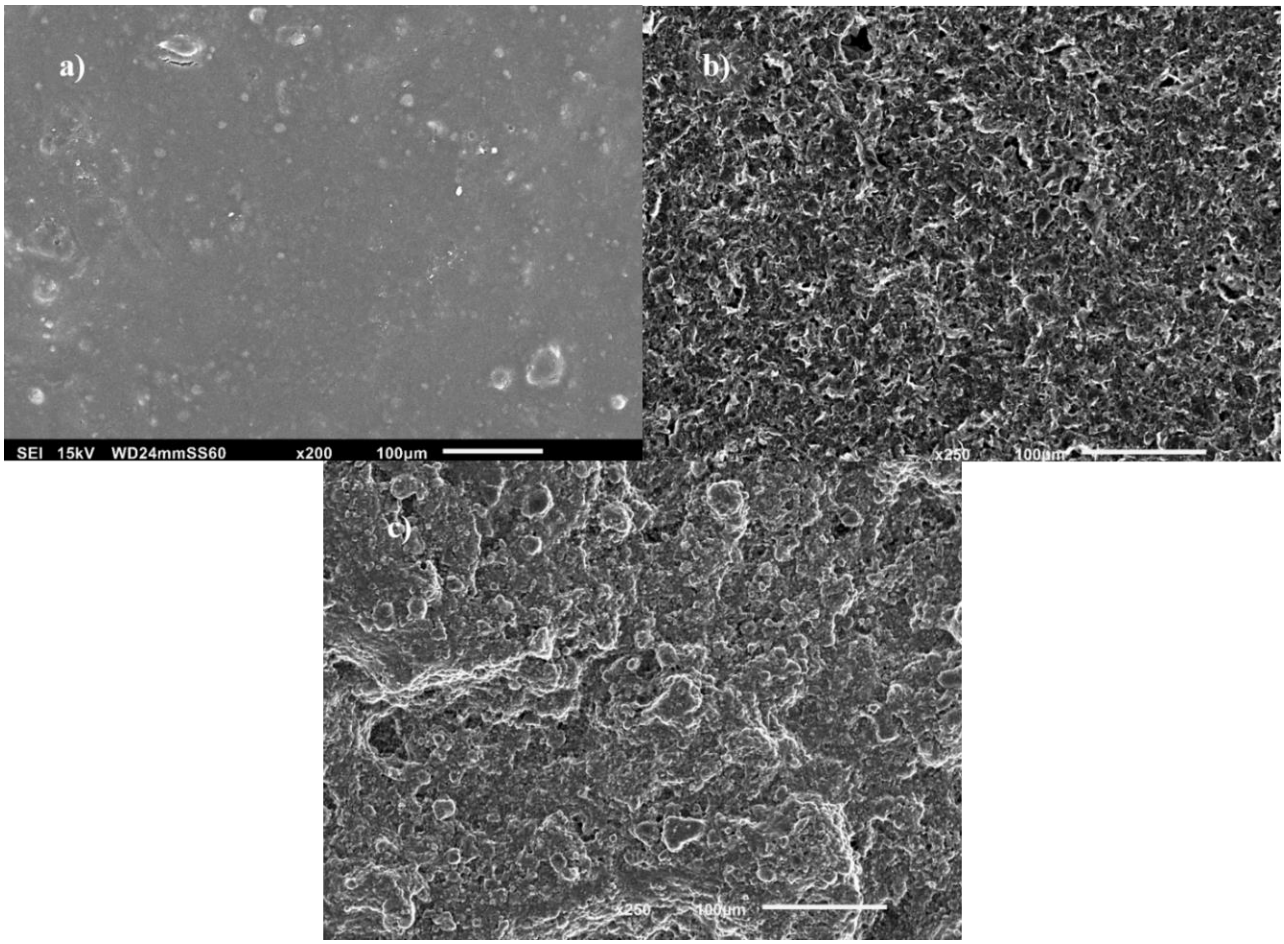

Figure 6-1: SEM images of microporous layers produced from a single material (a-c) carbon black, small graphene, and large graphene.

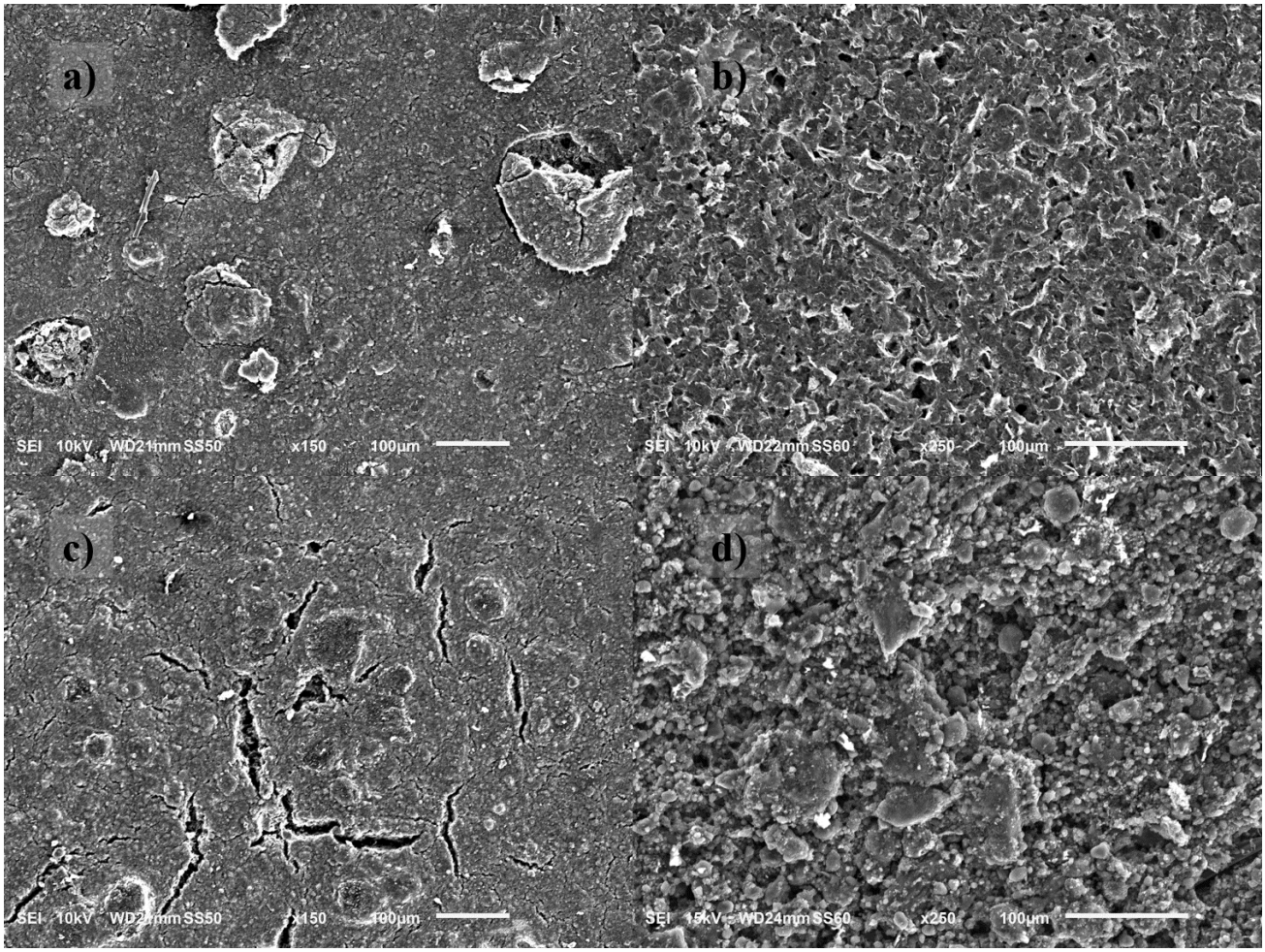

Figure 6-2: SEM micrographs of the layered MPLs from (a-d) LGCB, CBLG, SGCB and SGLG.

6.3.2 Porosity and Pore Size Distribution

The pore size distribution of the MPL-coated gas diffusion is an important physical property as it determines the mechanism for the transport of the reactants through the MPL. There are three prevailing pore sizes in the MPL and GDL: micropores, mesopores, and macropores. Micropores are defined as being smaller than 0.07 µm in diameter, whereas macropores are pores larger than 5µm, mesopores lie in between micro and macropores being from 0.07 µm to 5 µm in diameter [52]. The classification of pore size is based on the mechanism for gas transport where the Knudsen diffusion occurs in micropores, and bulk diffusion is the dominant mechanism in macropores. In mesopores, both bulk and Knudsen diffusion prevail [3, 143, 357]. Several research papers support the conclusions drawn in

Chapter 4, that the inclusion of large mesopores in the MPL enhances its ability to transport liquid water and reactants simultaneously.

Porosity and pore size distribution data of the MPL-coated gas diffusion layers, which can be seen in Fig 6.3, was obtained from mercury intrusion porosimetry. Fig 6.3 (b) is a rescaled image of the pore size distribution data in Fig. 6.3(a), which focuses on the microporous and mesoporous regions. Fig 6.3 (b) enables examination and comparison of the pore size distributions of the microporous layers with greater ease.

Fig 6.3 (b) reveals that in the microporous layers containing carbon black (LGCB, CBLG, and SGCB), there is an initial peak in the pore size distribution at 50 nm. The high frequency of pores of this size is due to the carbon black layer that is present in these MPLs, as can be seen from the results of the pure carbon black MPL which also peaks at 50 nm. However, the bi-layer MPLs exhibit two peaks in pore size: for example, the presence of the large graphene in the LGCB, CBLG, and LGSG microporous layers results in the formation of a large number of pores of ~ 1200 nm in size. These large mesopores are formed from the large graphene nanoplates. As the large graphene nanoplates are roughly two orders of magnitude greater than the carbon black particles in size (CB φ= 20-80 nm and LG φ= 500-5000 nm, respectively) these 1200 nm pores are a clear sign of a layer of large graphene. As mentioned in the methodology this is a different material used to the previous two chapters, hence the larger pore size produced. It is not surprising that the pore size distribution of the LGCB and the CBLG MPLs are very similar with both having visible peaks at 70 nm and 1200 nm to account for the carbon black and large graphene layers.

The small graphene layer results in a pore size of 500 nm being formed, this can be seen in Fig. 6.3 (b) where the SGCB has a secondary peak at 500 nm, after the initial peak at 70 nm from the carbon black layer. This is less well defined with the LGSG MPL where instead of two distinct peaks, one large peak can be seen occupying the region of 500-1200 nm. This is likely due to the similar pore sizes of the layers of small graphene and large graphene which results in an overlap in the pore size distribution of the overall MPL.

In general, the presence of two clear peaks in the pore size distribution of the MPLs indicates the successful fabrication of an MPL consisting of two distinct material layers with their morphology and microstructure. A high degree of material mixing would have resulted in the formation of a new dominant pore size as can be seen in Chapter 4 where graphene was mixed into the same layer of carbon black (Figs. 4.1 and 4.2). The purpose of this research is to produce pore-graded MPLs formed of two layers with differing morphologies and pore sizes. The results of the pore size data are shown in Figs. 6.3 signal that this was successfully achieved by using both carbon black and graphene nanoplates to produce separate inks and applying them in layers to the GDL substrate.

The pore size distribution of the bi-layer MPLs is all the more important due to the synergetic effect of the microstructure of the two layers. From an initial coating of large graphene and a subsequent layer of carbon black, the LGCB GDL has a pore gradient in which the pore size increases from the catalyst layer to the gas diffusion substrate. This may have enhanced capabilities for the removal of liquid water in high humidity conditions and a high current density operation [87, 142, 219, 230, 333, 349]. The increase in pore size through the MPL from the catalyst layer interface to the GDL interface results in an increased pressure gradient which may promote liquid water removal via capillary wicking [127, 347, 348, 350, 358]. This may also be demonstrated with the SGCB GDL, however, the difference in pore size between the two layers is not as apparent as in the LGCB MPL. Conversely, where carbon black is used as the initial layer and graphene is at the catalyst layer interface the pore size decreases from the catalyst layer to the gas diffusion substrate, this may hinder performance as the macropores of the graphene layer may retain liquid water rather than repel it [87]. Moreover, the graphene nanoplates may have reduced contact with the catalyst layer compared to the carbon black which can result in activation and ohmic losses.

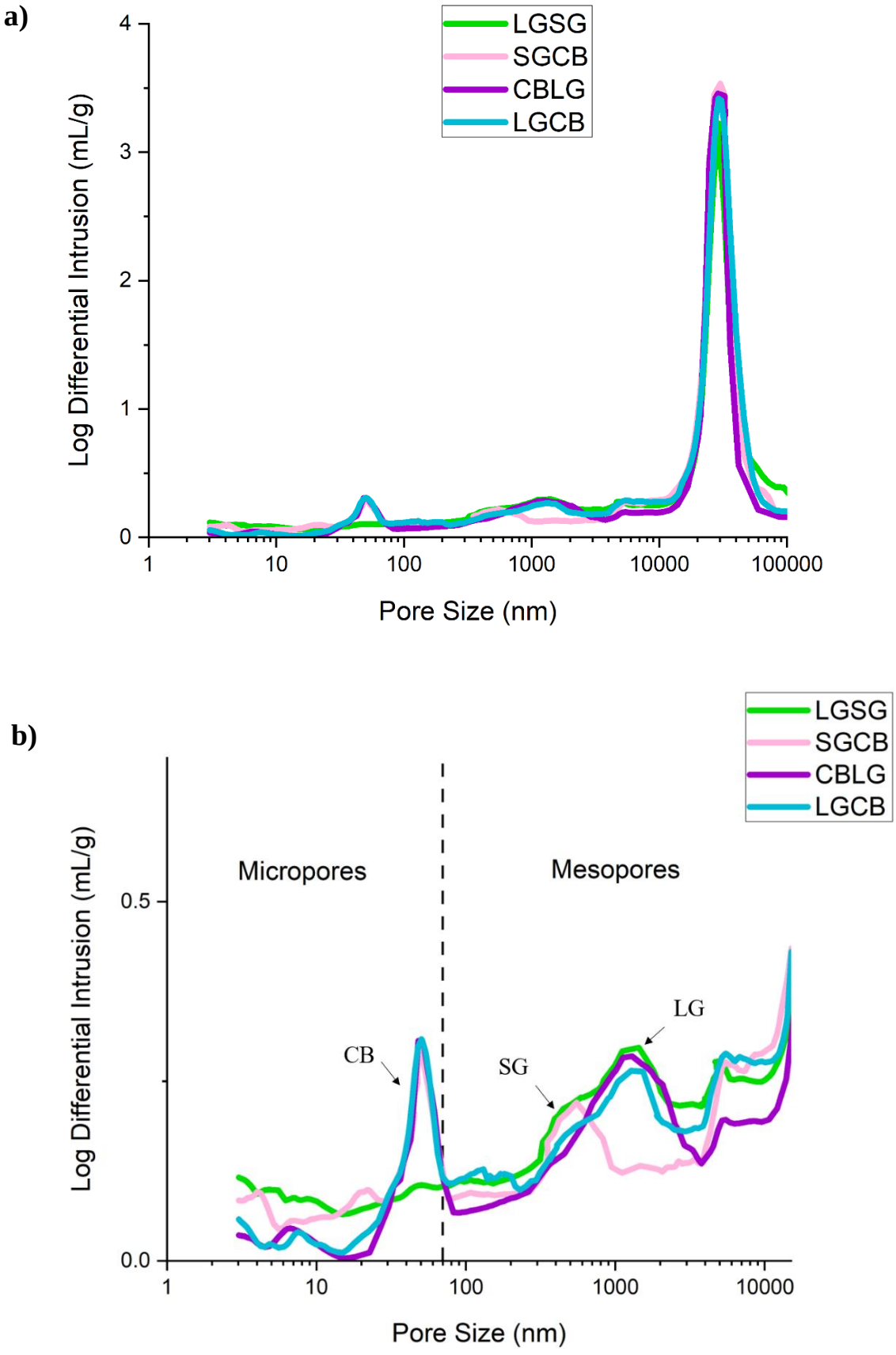

Figure 6-3: The pore size distribution of the bi-layer MPL-coated gas diffusion layers (Pores are defined as: micropores = <70 nm and mesopores= 70 nm-5000 nm), (b) is focused on the microporous region.

6.3.3 Contact Angle

The wettability of a surface indicates the ability of a liquid to interact with the solid surface and other liquids. Contact angle measurements, which measure the angle between the solid-liquid interface and the gas-liquid interface, are used to measure the wettability of the surface [222, 347, 359]. A contact angle > 90° indicates a hydrophobic surface, and for the gas diffusion and microporous layers generally, a more hydrophobic surface is desirable for its water-repelling properties [52, 53, 347, 360].

Fig. 6.4 is a plot of the contact angles measured on the surfaces of the microporous layers. The highest contact angle (151°) was recorded on the surface of the MPL comprised of large graphene nanoplates (GNP), whereas the lowest contact angle (145°) was recorded on the single material carbon black MPLs (CB). For the bi-layered MPLs, the results indicate that the contact angle is largely determined by the material that makes up the top layer; to an extent, this is predictable as it is this surface on which the droplet is being measured. However, the hydrophobicity of this layer is seemingly influenced by the initial coating layer, as can be seen with the CBLG microporous layer. The measured contact angle of the CBLG is slightly lower than the single material LG microporous layer, 150.4° and 151.5° respectively. Although the difference in the two values is small, the same trend is apparent with the MPLs with carbon black as the external surface (LGCB and SGCB), where the bi-layer MPLs have higher contact angle (145.7° and 145.1°) than the single material carbon black (144.9°).

In terms of wettability, the surface of the small graphene nanoplates has similar physicochemical properties to carbon black rather than the large graphene nanoplates. The microporous layer with a surface coating of small graphene (LGSG) measured a contact angle comparable to those with carbon black, being 5° lower than the bi-layer MPL with a large graphene surface. This is attributed to the smaller particle size, in this case nanoplates, producing an MPL with a lower surface roughness leading to a lower degree of wettability [305].

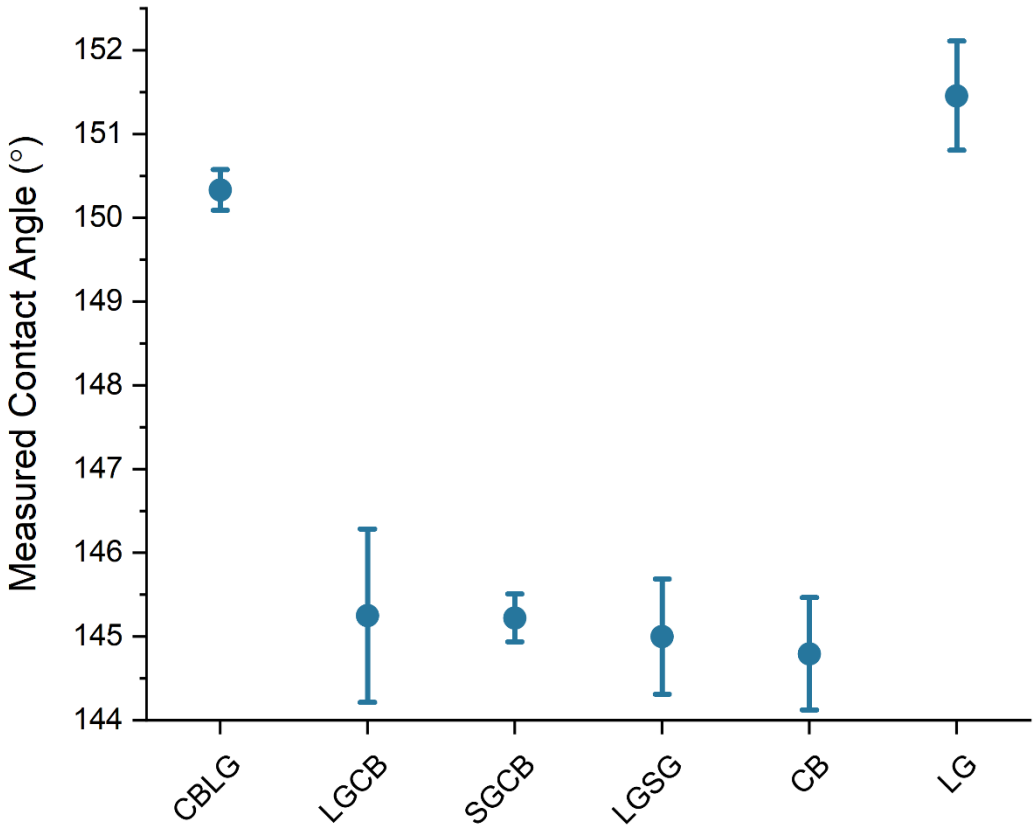

Figure 6-4: The measured contact angle of water droplets on the surface of the MPLs.

6.3.4 Through-plane Permeability

The single-layer carbon black MPL has the highest through-plane permeability of all of the samples. It has also the greatest degree of variation, which was seen in the previous investigations, and as before it is attributed to surface cracking from the drying process and the agglomeration process. The SGCB MPL has a similar surface morphology to the pure carbon black (Fig 6.1) and is characterised by a high degree of cracking. This may explain the large error bars with these samples.

Of the bi-layer MPLs their permeability is determined by both of their constituent materials for all MPLs their permeability was measured between the extremes of carbon black and large graphene. It is clear that a layer of large graphene nanoplates in the MPL reduces the gas flow through the GDL in the through-plane direction, as the lowest permeability is recorded with the LGCB, CBLG, and LGSG microporous layers. The results shown in Fig 6.5 indicate that the material of the initial coating layer is the largest factor in the overall permeability of the microporous layer. As the bi-layer MPLs comprised

of large graphene and carbon black have a lower permeability when the large graphene is the initial layer as in LGCB. Where the large graphene is the top layer then there is less resistance to the gas flow.

Unlike the MPLs containing large graphene, the small graphene MPLs exhibit similar properties to the carbon black in terms of gas permeability. The SGCB and the pure carbon black MPL have the highest through-plane permeabilities of the MPLs at 2.06 $x10^{-12}$ and 2.08 $x10^{-12}$, respectively. This is likely due to the high surface area of the small graphene nanoplates, and the smaller relative size compared to the large graphene nanoplates. The SEM micrographs in Fig. 6.2 reveal that the MPLs with a layer of small graphene have a porous structure compared to the MPLs formed from carbon black and large graphene.

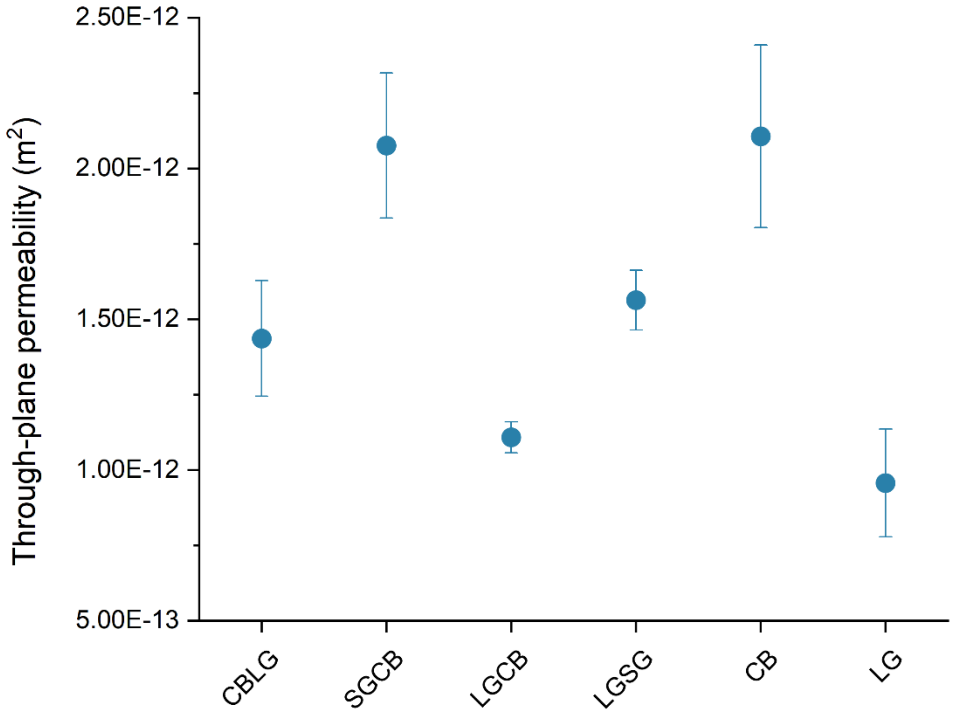

Figure 6-5: The through-plane permeability measurements of the MPL-coated GDLs.

6.3.5 In-plane Electrical Resistivity

A low electron resistivity is an essential characteristic for the MPL-coated GDL as one of its primary functions is to ensure the effective transport of electrons between the catalyst layer and the flow-field plates [1]. Resistance within the MPL-coated gas diffusion layer and contact resistance with the catalyst layer and current collector corresponds to ohmic losses leading to reduced cell performance. It is therefore important that the resistivity of the GDL is minimised. The electrical resistivity of the MPL is determined by the conductivity of its consistent materials; the carbon and the PTFE, and their interactions [44, 70, 360], i.e. the MPL produced from a material with a higher conductivity has a higher bulk conductivity than one produced from a less conductive material.

The measured values for the in-plane electrical resistivity of the GDLs can be seen in Fig. 6.6. The bi-layer MPLs have the lowest measured resistivity of the GDLs, where the lowest resistivity was measured on the bi-layered MPLs LGCB and SGCB, 4.89 mΩ cm and 5.19 mΩ cm, respectively. Notably, both of these MPLs have carbon black as the top layer, this external carbon black layer may enhance the conductivity of the MPL by reducing the contact resistance with the probes. Moreover, the CBLG MPL is comprised of the same constituent layers as LGCB, but the order of the layers is inverted. It is noteworthy that the resistivity of the CBLG is slightly higher than the LGCB MPL, this supports the idea that the contact resistance between the probes and the carbon black is less than between the large graphene and the carbon black. The MPLs which have carbon black as the top layer may have greater contact with the catalyst layer compared to those where graphene nanoplates are in contact with the catalyst layer. This may be due to the spherical particles and 3D carbon black agglomerate structure compared to the 2D graphene nanoplates (Chapter 5, Fig 5.1). The lowest resistivity of the LGCB may result from a synergetic effect of a lower bulk resistivity from the large graphene nanoplates and a reduced contact resistance from the carbon black particles. The external carbon black layer on the LGCB reduced the resistivity of the LG MPL by 12% from 5.6 mΩ cm to 4.91 mΩ cm. Whereas an external layer of the small graphene nanoplates as in LGSG increases the resistivity of the MPL by 3% this may be to do with the bulk resistivity of the small graphene being greater than the large graphene

and similar contact resistances with the large graphene. There are no benefits in terms of electron conductivity from layering the two graphene materials.

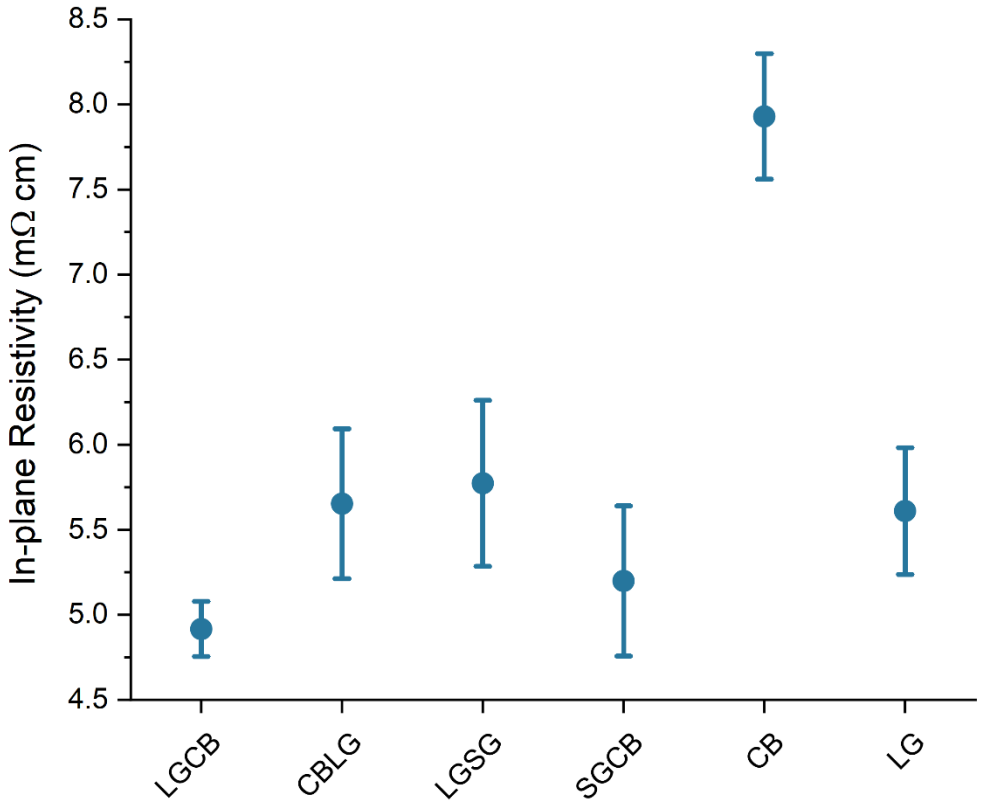

Figure 6-6: The measured in-plane electrical resistivity of the MPL-coated GDLs.

6.3.6 Fuel Cell Performance Testing

To assess the viability of the bi-layered MPLs for the cathode gas diffusion layer, polarisation curves were performed on the MPL-coated GDLs. Cell potential and current measurements were taken in varying cell conditions of 25%, 50%, 75%, and 100% relative humidity, alongside EIS measurements taken at 0.6 V. These two performance tests allow for the comparison of the MPLs in terms of their power density output and the sources of impedance within the operational fuel cell.

Fig. 6.7 shows the polarisation curves of the tested microporous layers, from the ex-situ experiments three of the dual-layer MPL-coated GDLs were tested (LGCB, CBLG, and LGSG) alongside carbon

black and graphene. These three samples were selected to understand if performance enhancement could be achieved by layering two materials with different physical and electrochemical properties. Previous experiments in Chapter 4 (Fig 4.7- 4.9) indicated the MPL produced from graphene exhibits a better performance than carbon black in the mass transport region although it produced greater ohmic impedance. In contrast to this, the carbon black MPL is less subject to ohmic resistance and instead experiences mass transport resistance. Thus, the idea of material layering was developed to overcome the limitations of the two materials. The variation in the physical and electrochemical characteristics of the microporous layers results in trends in single-cell testing.

The low relative humidity condition (25% RH Fig 6.7 (a)) sees favourable performances from the LGCB, the CBLG, and the carbon black MPLs. Of which the LGCB MPL produces the highest peak power density and reaches the highest limiting current density (1.6 A cm^{-2}, Fig. 6.8 (a)). In particular, this MPL performs well in the low-to-mid current density regions, where losses originate from ohmic impedance, due to dehydration of the membrane leading to reduced hydrogen crossover, and the bulk resistance of the components. This indicates that the LGCB and pure carbon black MPL are more able to maintain membrane hydration in drier conditions than the MPLs where graphene is at the interface with the catalyst layer. Carbon black at this interface promotes contact with the catalyst layer, reducing interfacial resistance; for the bi-layer MPL the effect of the two materials is synergetic where the carbon black reduces the contact resistance, and the large graphene reduces the bulk resistivity of the MPL. Conversely, the LGSG MPL produces a much lower power density than the other two samples in this condition. The slope of the graph indicates that this muted performance is due to ohmic resistance, most likely due to insufficient hydration of the membrane and activation losses at the cathode catalyst layer. This can be confirmed by the EIS results shown in Fig. 6.9 (a), where the 45° angle of the semi-circular arc and the delayed initial intercept with the x-axis indicate ohmic impedance. Similarly, the relatively large size of the semi-circular arc is representative of high activation losses in this MPL. Referring to the polarisation curves (Fig. 4.7 (a)) and EIS results (Fig. 4.9 (a)) of Chapter 4, the pure graphene (G100) MPLs exhibited increased ohmic and activation resistance similar to the layered LGSG. The

addition of a layer of small graphene is unable to increase or promote membrane hydration and contact with the catalyst layer.

In high humidity operation (75% and 100% relative humidity), the performance of the fuel cell is limited by the presence of liquid water which occupies the available pore space and thus reduces the diffusion pathways for reactants. An MPL-coated GDL which performs well in these conditions can mitigate the flooding phenomenon and maintain the supply of reactants to the catalyst layer. Figs. 6.8 (c and d) show the power density curves measured at 75% and 100% relative humidity respectively, the CBLG MPL is unable to produce a high-power density in these conditions and suffers mass transport losses at 0.6 A cm^{-2}. The large two-part semi-circle shown in the EIS results in Fig. 6.9 (c and d) indicates that these current limitations occur due to charge transfer and diffusion impedance. Examination of Fig 6.9 (b) reveals that this is starting to occur at 50%, although the potential drop does not occur until the fuel cell is stressed at 75% and 100% relative humidity operation (Fig. 6.9 (c-d)).

Of the layered MPLs, the LGCB and LGSG demonstrate an enhanced performance over the single material carbon black MPL. The highest power density was achieved with the LGCB MPL which excels in the low to mid-current density regions, at higher current densities can maintain higher voltages than the carbon black, although evidently suffers mass transport losses. In contrast to the LGCB MPL, the LGSG is visibly limited by ohmic resistance in the low current density region however exhibits an excellent performance when producing high current densities. This is confirmed by the EIS results (Fig. 6.9 (d)) where the radius of the LGSG arc is smaller than the other MPLs meaning that there is little evidence of charge transfer or mass transport impedance. The enhanced performance in high humidity conditions and in the high current density region indicates that the LGSG can mitigate liquid water saturation and maintain the concentration of reactants at the catalyst layer despite the increased humidity. Figs. 6.7 and 6.9 indicate that the bi-layer graphene MPL, LGSG, can relieve liquid saturation than the single material large graphene MPL, where at 100% relative humidity it produces a higher power density and limiting current density (1.3 A cm^{-2} and1.1 A cm^{-2} respectively). The most plausible explanation for this is the incremental pore size from the catalyst layer to the GDL substrate which enhances the predisposition of the graphene material to eject liquid water from the MPL/catalyst layer

interface. However, in operating conditions where less liquid water is present, such as when the reactant gases are partially humidified or whilst operating in lower current densities, the single material graphene offers a better performance and there is no benefit from the bi-layer MPL.

The polarisation curves and EIS results indicate that power enhancements can be achieved with the bi-layer MPLs and that there is a synergetic relationship between the two materials. The physical and electrochemical properties of the two materials mean that the performance of the MPL is determined by the material at the catalyst interface and the interface with the substrate. The LGCB MPL is more capable than the CBLG MPL at reducing the bulk and interfacial resistance and is better able to maintain a flow of reactants to the catalyst layer when more liquid water is present in the fuel cell. This indicates that the order in which the materials are applied to the MPL corresponds to its ability to enhance performance, be it in terms of electron conductivity or diffusivity. Overall, the layered MPLs enhanced the performance of the single-material MPLs. The choice of the composition of the MPL should be determined by the operating conditions which the MPL will be operating under. Maximum power density can be achieved by using a primary layer of large graphene and a secondary layer of carbon black at the catalyst layer interface, whereas when operating in conditions where the oxidant is likely to be saturated with water the LGSG would be able to sustain the highest potential.

.

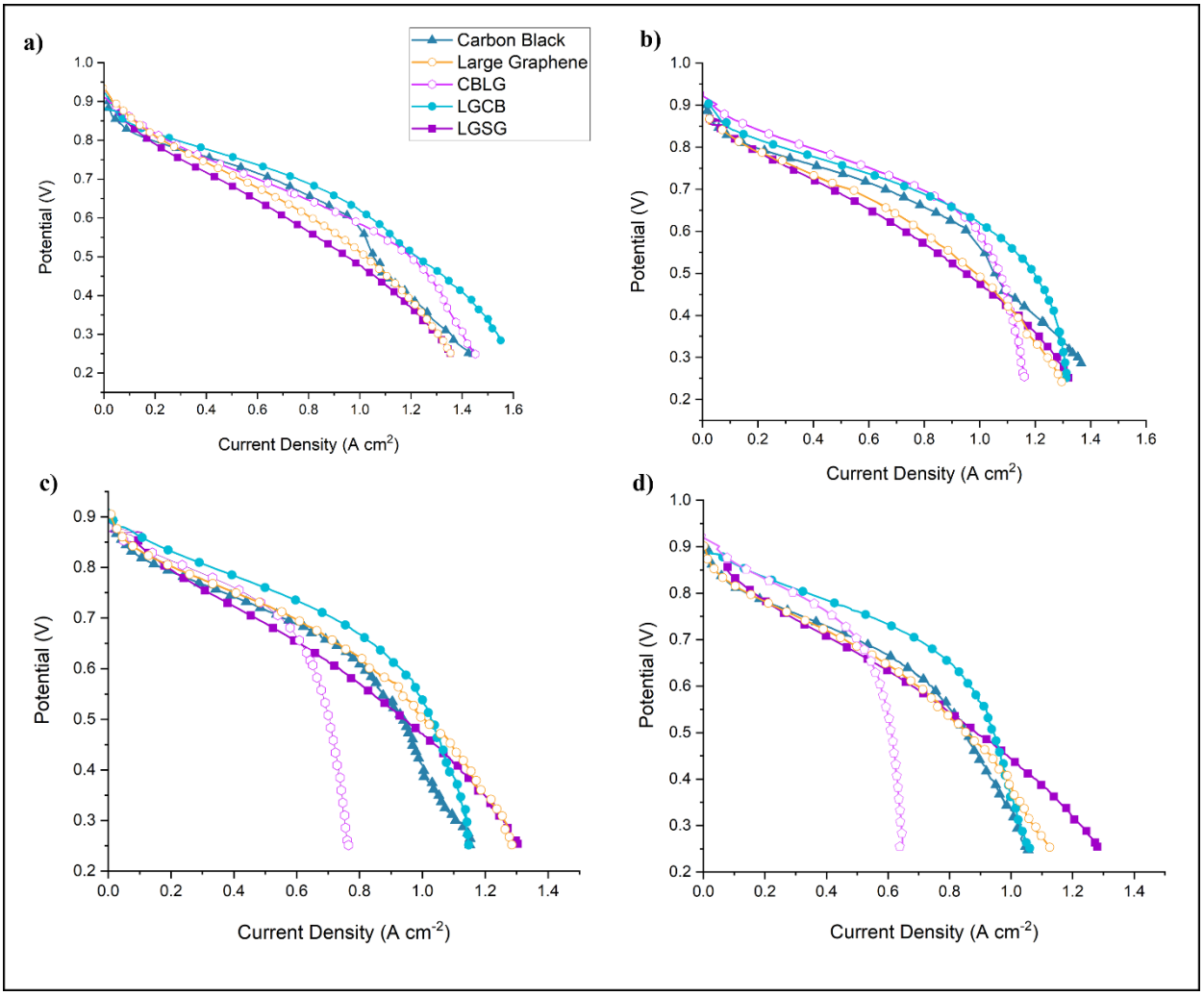

Figure 6-7:The IV curves from the single cell measurements of the MPL-coated GDLs for carbon black, graphene, CBLG, LGCB and LGSG. Taken at (a-d) 25%, 50%, 75% and 100% relative humidity in air at 80ºC.

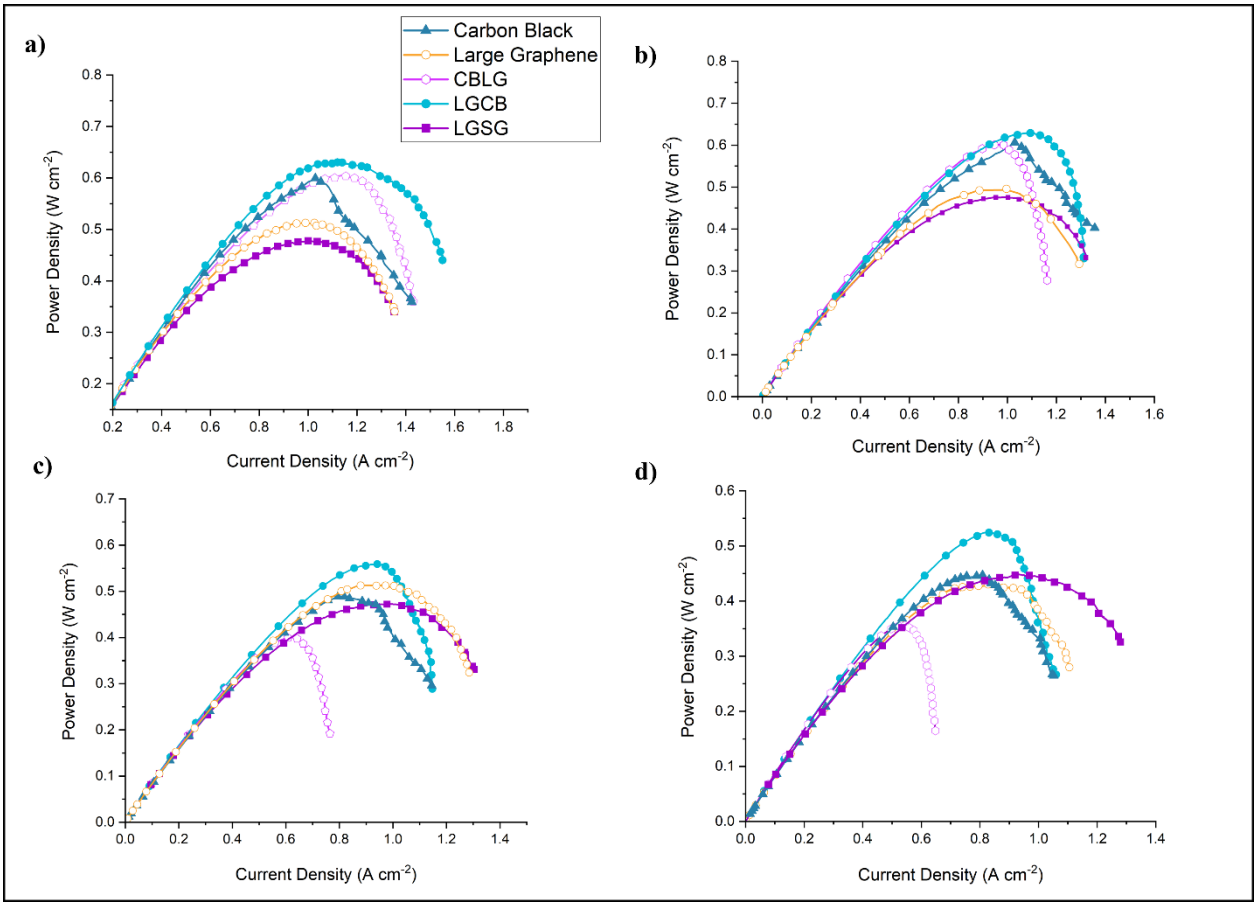

Figure 6-8: The polarisation curves from the single cell measurements of the MPL-coated GDLs for carbon black, graphene, CBLG, LGCB and LGSG. Taken at (a-d) 25%, 50%, 75% and 100% relative humidity in air at 80ºC.

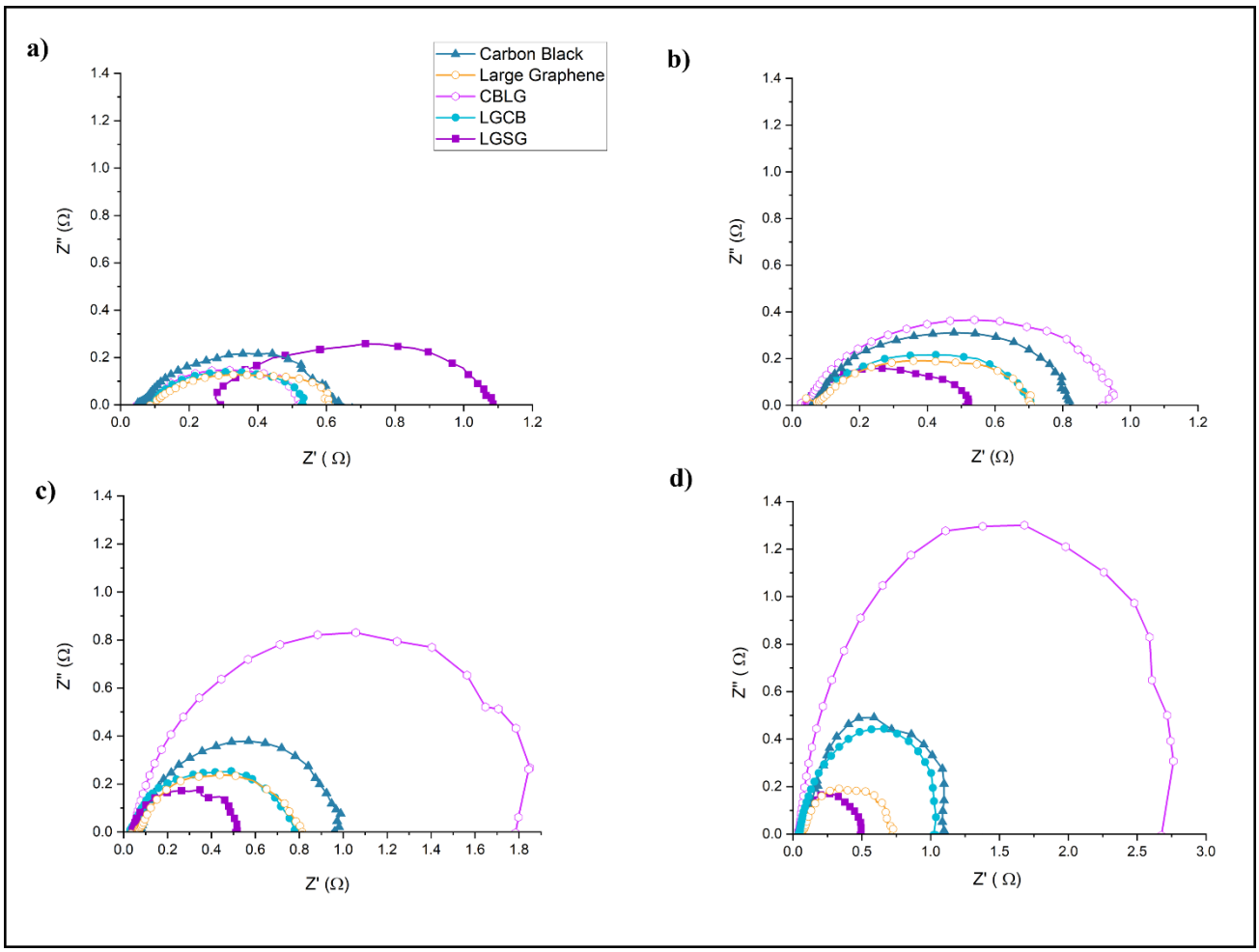

Figure 6-9: The EIS measurements from the single cell measurements of the MPL-coated GDLs for carbon black, graphene, CBLG, LGCB and LGSG. Taken at (a-d) 25%, 50%, 75% and 100% RH.

6.4 Conclusions

Bi-layered microporous layers with a graduated pore structure were prepared. By using Vulcan 72XC and graphene nanoplates for the layers of the MPL the microstructure and pore size could be manipulated. Their microstructure and electrochemical properties were characterised alongside the conventional single-layer MPLs for their potential use as a cathodic gas diffusion material. The SEM micrographs and pore size distribution data indicate the successful fabrication of an MPL with two distinct layers. The bi-layer MPLs exhibit enhanced performance compared to the single layer materials, particularly the LGCB which achieves the high power density in all conditions. The MPL comprised of

two types of graphene (LGSG) has excellent water mitigation properties and suffers the least diffusion impedance.

The salient points from this study are as follows:

- Fabrication of a pore-graded MPL is achievable by applying layers of MPL ink formed of graphene nanoplates and carbon black. The layer of graphene nanoplates was characterised by large mesopores, whereas the carbon black layer produced micropores.
- The electrical conductivity of the bi-layer MPLs was greater than the single material graphene and carbon black. This likely results from the synergetic reduction in contact resistivity and enhanced bulk conductivity.
- For the bi-layer MPLs, the wettability of the surface is largely determined by the external MPL layer applied, although the initial layer has a minor impact on the contact angle.
- The single-cell measurements showed that the bi-layered MPLs produced higher power densities and reached higher operational current compared to the single-layer carbon black MPL except the CBLG MPL which failed to compete with the mixed material and single material MPLs in conditions greater than 50 % relative humidity.
- The bi-layered microporous layer produced from large graphene and carbon black (LGCB) produced a higher peak power density in every condition. In particular, the ohmic and activation losses were significantly reduced, although mass transport limitations were also improved.
- The microporous layer produced from layered graphene (LGSG) excelled in the high current density region (> 1 cm^{-2}) and in high humidity operation, with minimal diffusion impedance. Whilst operating in lower humidity conditions (25% and 50% relative humidity) and at lower current densities (>1 cm^{-2}), the LGSG experienced higher ohmic impedance than the MPLs containing carbon black, regardless of composition.

Chapter 7: Concluding Remarks

The microporous layer (MPL) is an often-overlooked component of the polymer electrolyte membrane fuel cell, yet it plays a significant role in the optimisation of cell performance. In particular, its role in the management of liquid water within in the fuel cell; the MPL helps to simultaneously maintain the membrane hydration and prevent liquid water flooding at the catalyst layer.

The purpose of this thesis is to explore the potential of novel materials and architectures for the MPL, and their ability to enhance cell performance. To meet this research objective, microporous layers were produced from non-conventional materials and were subsequently characterised alongside conventional MPLs. The three research chapters built on our understanding of the impact of novel materials on these properties of the microporous layers. The microporous layers were characterised in terms of their morphology and microstructure, and physical and electrochemical properties. The physical and electrochemical characteristics which were measured ex-situ were electron conductivity (in-plane resistivity), wettability (contact angle), and gas permeability. The morphology and microstructure were revealed through SEM imaging and MIP for the pore size distribution of the layers. Finally, single cell measurements were taken to produce polarisation curves and EIS data these helped determine the suitability of these layers as the cathode gas diffusion layer.

In Chapter 4, the potential use of graphene nanoplates an MPL material was explored, where microporous layers were fabricated from graphene nanoplates and carbon black, and from hybrids of the two materials. This chapter lays the foundation of the thesis as it revealed the impact of the inclusion of a different carbon, i.e., graphene, on the physical and electro-chemical properties of the layer. This was then to be manipulated in Chapter 6 with the fabrication of pore graded microporous layers. Chapter 5 investigated a completely novel MPL material, graphene foams. These foams were fabricated in-house during a research visit to Kyushu University, Japan and then characterised in terms of their elemental composition (XPS) and microstructure (high resolution SEM). Microporous layers were produced, and they underwent the same characterisation tests as the previous chapter. Chapter 6 drew on the findings of the previous chapters notably that the material composition of the layer determines its microstructural and electro-chemical properties. Instead of combining the two materials as in Chapter

4, the materials were applied as separate layers in order to produce MPLs with a planned pore architecture. These microporous layers were then characterised using the previous ex-situ methods and in the operational fuel cell to determine their potential in mitigating of liquid water saturation at the cathode GDL. The bi-layer MPLs exhibited excellent performance characteristics from the synergetic relationship between the two materials.

The key findings of the technical chapters (Chapters 4, 5 and 6) are summarised in the following bullet points:

- The polymer electrolyte fuel cell was found to perform better with relatively low graphene content in the cathode MPL (≤ 30%) under low humidity conditions (e.g., 0 or 25% RH) and this is due the availability of high amount of micropores that assist in retaining water needed to humidify the membrane electrolyte and the membrane phase in the catalyst layer.
- Larger amounts of graphene (≥ 50%) are needed to be added to the cathode MPL for the fuel cells operating with intermediate or high humidity conditions (50, 75 or 100% RH). Such amounts are necessary to obtain sufficient amount of mesopores required to drive excess water away from the MEA and subsequently mitigate water flooding.
- Expectedly, the electrical conductivity of the MPL increases with increasing graphene content and this is evidently due to substantially higher electrical conductivity of graphene compared to carbon black. On the other hand, the gas permeability of the MPL-coated GDL was found to decreases with increasing graphene content; this is attributed to the sheet-like structure of the graphene used which hiders the flow of the gases.
- The atmospheric composition during pyrolysis affects the physio-chemical properties of graphene foams. Graphene foam produced in the pure nitrogen atmosphere (100 vol.% N_2) had a greater carbon purity than the foam produced from pyrolysis in nitrogen and hydrogen atmosphere (95 vol.% N_2: 5 vol.% H_2).

- The pore size distribution of the graphene foam MPLs fall into the large mesoporous region with an absence of small mesopores and micropores. The peak pore size of the N-GF and NH-GF are 1-2 μm and 4 μm, respectively.
- The NH-GF exhibited more desirable physical and electrical characteristics than the NH-GF. A higher electron conductivity was measured with the N-GF MPL which is attributed to the higher percentage of carbon in the foam. A higher through-plane permeability was also recorded on the N-GF, although the wettability of the two foams was comparable.
- The N-GF exhibits a similar performance to the carbon black MPL in the low current density region, however at higher current densities and fully humified conditions it suffers from mass transport losses. This is likely due to the absence of small mesopores and micropores in the layer.
- NH-GF struggles in all conditions and is uncompetitive, suffering from both ohmic losses and mass transport losses. This is particularly apparent at 100%relative humidity operation. This is attributed to a combination of the large pore size in the layer and the reduced electrical conductivity of the foam.
- The fabrication of a bi-layer pore graded MPL is achievable by applying separate layers of MPL ink formed of graphene nanoplates and carbon black. Both layers had their individual microstructure and physical properties. The layer of graphene nanoplates was characterised by large mesopores, whereas the carbon black layer produced micropores.
- The electrical conductivity of the bi-layer MPLs was greater than the single material graphene and carbon black. This likely results from synergetic reduction in contact resistivity and enhanced bulk conductivity. The inclusion of the graphene layer in the microporous layer results in the
- Unsurprisingly, for the bi-layer MPLs the wettability of the surface is largely determined by the external MPL layer applied, although the initial layer has a minor impact on the contact angle.

- The single cell measurements showed that the bi-layered MPLs produced higher power densities and reached higher operational current compared to the single layer carbon black MPL with the exception of the CBLG MPL which failed to compete with the mixed material and single material MPLs in conditions greater than 50 % relative humidity.
- The bi-layered microporous layer produced from large graphene and carbon black (LGCB) produced the higher peak power density in every condition. In particular, the ohmic and activation losses were significantly reduced, although mass transport limitations were also improved.
- The microporous layer produced from layered graphene (LGSG) excelled in the high current density region (> 1 cm^{-2}) and in high humidity operation, with minimal diffusion impedance. Whilst operating in lower humidity conditions (25% and 50% relative humidity) and at lower current densities (>1 cm^{-2}), the LGSG experienced higher ohmic impedance than the MPLs containing carbon black, regardless of composition.

Chapter 8: Recommendations for Future Work

There are several potential areas for research into MPL optimisation and the implementation of new designs into the commercial PEM fuel cell. Recommended topics for study and suggestions to elevate the impact of the research are listed below:

- Gas diffusion and microporous layers with an optimised design can potentially enhance PEM fuel cell performance particularly in the high current density region and in high humidity conditions. Microporous layers with a porosity gradient in the direction of the catalyst layer to the gas diffusion substrate in particular have achieved improved cell performance by increasing the limiting current density and reducing mass transport losses. The pore graded MPL has a greater capability to mitigate liquid water saturation at the catalyst later MPL interface. In order to further enhance cell performance, the pore size and structure of the component layers should be optimised by comparing MPLs with the same pore size gradient (large to small: GDL to catalyst layer) but with different pore sizes.
- A significant body of research has been taken into graduated hydrophobicity in the MPL. Key research findings report that inhomogeneous wettability in the MPL can improve cell performance by the formation of corridors for the preferential transport of liquid water. Future work can be undertaken designing MPLs with different wettability profiles. More studies can be conducted on the patterned wettability of the MPL surface in order to optimise liquid water removal.
- Greater research needs to be taken into the optimisation of the foam structure if carbons foams are be used as an MPL material. Failing this, there is room for research into mixed material MPLs with carbon foams providing a cheaper alternative to graphene nanoplates for the formation of macropores.
- Research into novel materials has been successful with performance enhancements achieved with alternative materials to carbon black. However, the true potential of these materials and designs in the commercial fuel cell is limited by the lack of durability testing.

Increased durability testing which investigates the degradation rate of new designs against the conventional will give a better indication of their applicability for commercialisation.

- It is important that research into fuel cell components remains relevant to the commercial fuel cell industry and their applicability to real applications. Although, many pioneering performance improvements have been achieved from modifications of one of the key fuel cell components (GDLs), very few of these are elevated from the single cell laboratory scale, or subject to durability testing. A greater emphasis should be placed on the scalability of the technology, and the feasibility of designs and application methodology for a commercially viable product. A focus on these areas would attract greater investment into the sector, and thus accelerate the development of fuel cell technology and infrastructure. Additionally, there should be greater research emphasis placed on the cost of materials and manufacturing of microporous layers and ink deposition, this will provide a holistic view of the financial impact and overall price per Watt.
- Although a significant breadth of material has been published on non-conventional microporous layers, in terms of their optimised wettability and microstructure. However, in terms of methodology, improvements could be made generally: provision of detailed information about the carbon material used, this would help understand the characteristics of the microporous layers produced; clarification over PEMFC test definitions, as low relative humidity is taken to mean 0% RH to 50% RH conditions.

References

[1] F. Barbir, PEM fuel cells : theory and practice. Academic Press, 2013, pp. 518-518.

[2] Scribner Associates. "Electrochemical Impedance Spectroscopy (EIS): A Powerful and Cost-Effective Tool for Fuel Cell Diagnostics." http://www.scribner.com/wp-content/uploads/2017/06/Scribner-Associates-Electrochemical-Impedance-Spectroscopy-for-Fuel-Cell-Research.pdf (accessed 05/01, 2022).

[3] G. Lin, S.Liu, G. Qu, Y. Song, T. Li, F. Liu and Yafei Hu , "Effect of pore size distribution in the gas diffusion layer adjusted by composite carbon black on fuel cell performance," 2020, doi: 10.1002/er.6350.

[4] N. Alhazmi, D. B. Ingham, M. S. Ismail, K. J. Hughes, L. Ma, and M. Pourkashanian, "Effect of the anisotropic thermal conductivity of GDL on the performance of PEM fuel cells," International Journal of Hydrogen Energy, vol. 38, no. 1, pp. 603-611, 1 11 2013.

[5] J. M. Tang, M. E. Itkis, C. Wang, X. Wang, Y. Yan, and R. C. Haddon, "Carbon nanotube free-standing membrane as gas diffusion layer in hydrogen fuel cells," Micro & Nano Letters, vol. 1, no. 1, pp. 62-62, 2006, doi: 10.1049/mnl:20065030.

[6] M. S. Ismail, D. B. Ingham, K. J. Hughes, L. Ma, and M. Pourkashanian, "Effective diffusivity of polymer electrolyte fuel cell gas diffusion layers: An overview and numerical study," International Journal of Hydrogen Energy, vol. 40, no. 34, pp. 10994-11010, 9 14 2015.

[7] M. S. Ismail, D. B. Ingham, K. J. Hughes, L. Ma, and M. Pourkashanian, "Through-plane permeability for untreated and PTFE-treated gas diffusion layers in proton exchange membrane fuel cells," Journal of Fuel Cell Science and Technology, vol. 7, no. 5, pp. 0510161-0510167, 2010/10// 2010, doi: 10.1115/1.4000685.

[8] M. S. Ismail, T. Damjanovic, D. B. Ingham, M. Pourkashanian, and A. Westwood, "Effect of polytetrafluoroethylene-treatment and microporous layer-coating on the electrical conductivity of gas diffusion layers used in proton exchange membrane fuel cells," Journal of Power Sources, vol. 195, no. 9, pp. 2700-2708, 2010/5// 2010, doi: 10.1016/j.jpowsour.2009.11.069.

[9] J.-P. Shim, C.-S. Han, H.-J. Sun, G.-S. Park, J.-J. Lee, and H.-K. Lee, "Preparation and Characterization for Carbon Composite Gas Diffusion Layer on Polymer Electrolyte Membrane Fuel Cells," Transactions of the Korean hydrogen and new energy society, vol. 23, no. 1, pp. 34-42, 2012/2// 2012, doi: 10.7316/khnes.2012.23.1.034.

[10] S-Y. Fang, L. G. Teoh, R-H. Huang, K-L. Hsueh, K-H. Yang, W-K. Chao and F-S. Shieu, "Enhancement of proton exchange membrane fuel cell performance by titanium-coated anode gas diffusion layer," International Journal of Hydrogen Energy, vol. 39, no. 36, pp. 21177-21184, 2014/12// 2014, doi: 10.1016/j.ijhydene.2014.10.055.

[11] M. S. Ismail, K. J. Hughes, D. B. Ingham, L. Ma, and M. Pourkashanian, "Effects of anisotropic permeability and electrical conductivity of gas diffusion layers on the performance of proton exchange membrane fuel cells," Applied Energy, vol. 95, pp. 50-63, 2012/7// 2012, doi: 10.1016/j.apenergy.2012.02.003.
[12] International Energy Association, "Technology Roadmap Hydrogen and Fuel Cells." [Online]. Available: www.iea.org/t&c/ (Accessed 05/01, 2022)
[13] J. Howes, "Hydrogen and Fuel Cells: Opportunities for Growth A Roadmap for the UK E4tech and Element Energy," 2016.
[14] I. Staffell, D. Scamman, A. V. Abad, P. Balcombe, P. E. Dodds, P. Ekins, N. Shahd and K. R. Ward, "The role of hydrogen and fuel cells in the global energy system," in Energy and Environmental Science vol. 12, ed: Royal Society of Chemistry, 2019, pp. 463-491.
[15] M. Salimi, M. Hosseinpour, and T. N.Borhani, "The Role of Clean Hydrogen Value Chain in a Successful Energy Transition of Japan," Energies, vol. 15, no. 16, 2022/8// 2022, doi: 10.3390/en15166064.
[16] Department for Energy Security and Net Zero and Department for Business, Energy & Industrial Strategy, "UK Hydrogen Strategy".. [Online]. Available: https://www.gov.uk/government/publications/uk-hydrogen-strategy. (Accessed 16/06/2023)
[17] R. M. Uriu, "Betting on Hydrogen: Japan's Green Industrial Policy for Hydrogen and Fuel Cells," in International Political Economy Series, 2021.
[18] Department for Transport, Office for Low Emission Vehicles, and The Rt Hon John Hayes CBE MP "£23 million boost for hydrogen-powered vehicles and infrastructure," in gov.uk, ed, 18/03/2017.[Online] Available: https://www.gov.uk/government/news/23-million-boost-for-hydrogen-powered-vehicles-and-infrastructure#:~:text=change%20and%20energy-,%C2%A323%20million%20boost%20for%20hydrogen%2Dpowered%20vehicles%20and%20infrastructure,of%20hydrogen%20vehicles%20and%20infrastructure.&text=A%20new%20%C2%A323%20million,today%20(18%20March%202017). (Accessed: 16/06/2023).
[19] Vattenfall, "Press Release March 29, 2022 11:59 GMT 2 MIN New polling shows UK consumers want a renewables-led Energy Supply Strategy," 22/3/ 2022.[Online] Available: https://group.vattenfall.com/uk/newsroom/pressreleases/2022/new-polling-shows-uk-consumers-want-a-renewables-led-energy-supply-strategy#:~:text=More%20than%20three%20in%20five,and%20nuclear%20generation%20(23%25). (Accessed:16/06/2023).
[20] United States Department of Energy, "Fuel cell comparison chart." [Online]. Available: https://www.energy.gov/eere/fuelcells/comparison-fuel-cell-technologies. (Accessed: 16/06/2023)
[21] S. H. Siyal, D. Mentis, U. Mörtberg, S. R. Samo, and M. Howells, "A preliminary assessment of wind generated hydrogen production potential to reduce the gasoline fuel used in road transport sector of Sweden," International Journal of Hydrogen Energy, vol. 40, no. 20, pp. 6501-6511, 2015/6// 2015, doi: 10.1016/j.ijhydene.2015.03.108.

[22] S. H. Siyal, D. Mentis, and M. Howells, "Economic analysis of standalone wind-powered hydrogen refueling stations for road transport at selected sites in Sweden," International Journal of Hydrogen Energy, vol. 40, no. 32, pp. 9855-9865, 2015/8// 2015, doi: 10.1016/j.ijhydene.2015.05.021.
[23] V. Uusitalo, S. Väisänen, E. Inkeri, and R. Soukka, "Potential for greenhouse gas emission reductions using surplus electricity in hydrogen, methane and methanol production via electrolysis," Energy Conversion and Management, vol. 134, pp. 125-134, 2017/2// 2017, doi: 10.1016/j.enconman.2016.12.031.
[24] G. Pleßmann, M. Erdmann, M. Hlusiak, and C. Breyer, "Global energy storage demand for a 100% renewable electricity supply," in Energy Procedia, 2014, vol. 46: Elsevier Ltd, pp. 22-31, doi: 10.1016/j.egypro.2014.01.154.
[25] H. Boeriu, "BMW to produce a low-volume hydrogen fuel-cell car in 2021," in BMW Blog, ed, 2017.
[26] Z. Lu, J. Waldecker, M. Tam, and M. Cimenti, "Influence of MPL Structure Modification on Fuel Cell Oxygen Transport Resistance," ECS Transactions, vol. 69, no. 17, pp. 1341-1353, 2015/9// 2015, doi: 10.1149/06917.1341ecst.
[27] A. Maruta, "Japan's ENE-FARM programme," Fuel cells: Why is Austria not taking off, 2016.
[28] H. Jung, K. T. Park, M. N. Gueye, S. H. So, and C. R. Park, "Bio-inspired graphene foam decorated with Pt nanoparticles for hydrogen storage at room temperature," International Journal of Hydrogen Energy, vol. 41, no. 9, pp. 5019-5027, 2016/3// 2016, doi: 10.1016/j.ijhydene.2015.12.016.
[29] J. Larminie and A. Dicks, Fuel Cell Systems Explained. West Sussex, England: John Wiley & Sons, Ltd,. 2003.
[30] J. Zhang, PEM Fuel Cell Electrocatalysts and Catalyst Layers. London: Springer, 2008.
[31] P. Muthu, R. P. O'Hayre, W. G. Colella, and R. H. Adams, "Fuel Cell Fundamentals". West Sussex, England: John Wiley & Sons, Ltd,. 2009.
[32] M. F. Mathias, J. Roth, J. Fleming and W. Lehnert, Handbook of Fuel Cells, Fundamentals, Technology and Applications., vol. 3 (Fuel Cell Technology and Applications). New York: John Wiley & Sons, 2003, pp. 517-537.
[33] D. Harvey, J. G. Pharoah, and K. Karan, "A comparison of different approaches to modelling the PEMFC catalyst layer," Journal of Power Sources, vol. 179, no. 1, pp. 209-219, 2008/4// 2008, doi: 10.1016/J.JPOWSOUR.2007.12.077.
[34] S. Li, J. Yuan, M. Andersson, G. Xie, and B. Sundén, "Influence of anisotropic gas diffusion layers on transport phenomena in a proton exchange membrane fuel cell," International Journal of Energy Research, vol. 41, no. 14, pp. 2034-2050, 11 1 2017.
[35] D. Todd and W. Mérida, "Synthesis of transport layers with controlled anisotropy and application thereof to study proton exchange membrane fuel cell performance," Journal of Power Sources, vol. 311, pp. 182-187, 4 15 2016.
[36] P. Rama, Y. Liu, R. Chen, H. Ostadi, K. Jiang, Y. Gao, X. Zhang, D. Brivio and P. Grassini, "A numerical study of structural change and anisotropic permeability in compressed carbon cloth polymer electrolyte fuel cell gas diffusion layers," Fuel Cells, vol. 11, no. 2, pp. 274-285, 4 2011.

[37] J. G. Pharoah, K. Karan, and W. Sun, "On effective transport coefficients in PEM fuel cell electrodes: Anisotropy of the porous transport layers," Journal of Power Sources, vol. 161, no. 1, pp. 214-224, 10 20 2006.
[38] H. Meng, "A simplified method for solving anisotropic transport phenomena in PEM fuel cells," Journal of Power Sources, vol. 161, no. 1, pp. 466-469, 10 20 2006.
[39] Z. Qi and A. Kaufman, "Improvement of water management by a microporous sublayer for PEM fuel cells," Journal of Power Sources, 2002, doi: 10.1016/S0378-7753(02)00058-7.
[40] X. G. Yang, Q. Ye, and P. Cheng, "Matching of water and temperature fields in proton exchange membrane fuel cells with non-uniform distributions," International Journal of Hydrogen Energy, vol. 36, no. 19, pp. 12524-12537, 9 2011.
[41] N. Kulkarni, Matt D.R. Kok, Rhodri Jervis, F. Iacoviello, Q. Meyer, P. R. Shearing and D. J.L. Brett, "The effect of non-uniform compression and flow-field arrangements on membrane electrode assemblies - X-ray computed tomography characterisation and effective parameter determination," Journal of Power Sources, vol. 426, pp. 97-110, 2019/6// 2019, doi: 10.1016/j.jpowsour.2019.04.018.
[42] S. Hasanpour, M. Hoorfar, and A. B. Phillion, "Different methods for determining porosity of gas diffusion layer using X-ray microtomography," Electrochimica Acta, vol. 185, pp. 34-39, 12 10 2015.
[43] I. V. Zenyuk, D. Y. Parkinson, L. G. Connolly, and A. Z. Weber, "Gas-diffusion-layer structural properties under compression via X-ray tomography," Journal of Power Sources, vol. 328, pp. 364-376, 10 1 2016.
[44] A. El-kharouf, T. J. Mason, D. J. L. Brett, and B. G. Pollet, "Ex-situ characterisation of gas diffusion layers for proton exchange membrane fuel cells," Journal of Power Sources, vol. 218, pp. 393-404, 2012/11// 2012, doi: 10.1016/J.JPOWSOUR.2012.06.099.
[45] F. N. Buechi, R. Flückiger, D. Tehlar, F. Marone, and M. Stampanoni, "Determination of Liquid Water Distribution in Porous Transport Layers," 2008: The Electrochemical Society, pp. 587-592.
[46] E. A. Wargo, V. P. Schulz, A. Çeçen, S. R. Kalidindi, and E. C. Kumbur, "Resolving macro- and micro-porous layer interaction in polymer electrolyte fuel cells using focused ion beam and X-ray computed tomography," Electrochimica Acta, vol. 87, pp. 201-212, 1 1 2013.
[47] C. S. Kong, D. Y. Kim, H. K. Lee, Y. G. Shul, and T. H. Lee, "Influence of pore-size distribution of diffusion layer on mass-transport problems of proton exchange membrane fuel cells," Journal of Power Sources, 2002, doi: 10.1016/S0378-7753(02)00028-9.
[48] S. Malik, L. Smith, J. Sharman, E. M. Holt, and S. P. Rigby, "Pore Structural Characterization of Fuel Cell Layers Using Integrated Mercury Porosimetry and Computerized X-ray Tomography," Industrial and Engineering Chemistry Research, vol. 55, no. 41, pp. 10850-10859, 10 19 2016.
[49] N. Khajeh-Hosseini-Dalasm, T. Sasabe, T. Tokumasu, and U. Pasaogullari, "Effects of polytetrafluoroethylene treatment and compression on gas diffusion

layer microstructure using high-resolution X-ray computed tomography," Journal of Power Sources, vol. 266, pp. 213-221, 11 15 2014.
[50] J. Wackerl, "Analytics oPhysical Properties of Low-Temperature Fuel Cells.," in Fuel Cell Science and Engineering: Materials, Processes, Systems and Technology, , D. S. a. B. Emont Ed., J. Wackerl, Ed.: John Wiley & Sons Inc., 2012.
[51] J. T. Gostick, M. W. Fowler, M. D. Pritzker, M. A. Ioannidis, and L. M. Behra, "In-plane and through-plane gas permeability of carbon fiber electrode backing layers," Journal of Power Sources, vol. 162, no. 1, pp. 228-238, 2006/11// 2006, doi: 10.1016/J.JPOWSOUR.2006.06.096.
[52] S. Park, J.-W. Lee, and B. N. Popov, "A review of gas diffusion layer in PEM fuel cells: Materials and designs," International Journal of Hydrogen Energy, vol. 37, no. 7, pp. 5850-5865, 2012/4// 2012, doi: 10.1016/J.IJHYDENE.2011.12.148.
[53] A. Ozden, S. Shahgaldi, X. Li, and F. Hamdullahpur, "A review of gas diffusion layers for proton exchange membrane fuel cells—With a focus on characteristics, characterization techniques, materials and designs," Progress in Energy and Combustion Science, vol. 74, pp. 50-102, 2019/9// 2019, doi: 10.1016/J.PECS.2019.05.002.
[54] M. A. Ioannidis, M. J. Kwiecien, and I. Chatzis, "Statistical analysis of the porous microstructure as a method for estimating reservoir permeability," 0920.4105/96, 1996.
[55] J. J. a. M. Beaudoin, J, Handbook of Analytical Techniques in Concrete Science and Technology. 2001.
[56] N. Zamel, N. G.C. Astrath, X. Li, J. Shen, J. Zhou, F. B.G. Astrath, H Wang and Z-S. Liu, "Experimental measurements of effective diffusion coefficient of oxygen–nitrogen mixture in PEM fuel cell diffusion media," Chemical Engineering Science, vol. 65, no. 2, pp. 931-937, 1 16 2010.
[57] W. Chen and F. Jiang, "Impact of PTFE content and distribution on liquid-gas flow in PEMFC carbon paper gas distribution layer: 3D lattice Boltzmann simulations," International Journal of Hydrogen Energy, vol. 41, no. 20, pp. 8550-8562, 6 1 2016.
[58] J. Hinebaugh, Z. Fishman, and A. Bazylak, "Unstructured Pore Network Modeling with Heterogeneous PEMFC GDL Porosity Distributions," Journal of The Electrochemical Society, vol. 157, no. 11, p. B1651, 2010.
[59] L. Holzer, O. Pecho, J. Schumacher, Ph. Marmet, O. Stenzel, F.N. Büchi, A. Lamibrac and B. Münch , "Microstructure-property relationships in a gas diffusion layer (GDL) for Polymer Electrolyte Fuel Cells, Part I: effect of compression and anisotropy of dry GDL," Electrochimica Acta, vol. 227, pp. 419-434, 2 10 2017.
[60] D. Muirhead, R. Banerjee, M. G. George, N. Ge, P. Shrestha, H. Liu, J. Lee and A. Bazylak, "Liquid water saturation and oxygen transport resistance in polymer electrolyte membrane fuel cell gas diffusion layers," Electrochimica Acta, vol. 274, pp. 250-265, 6 1 2018.
[61] G.-G. Park, Y.-J. Sohn, T.-H. Yang, Y.-G. Yoon, W.-Y. Lee, and C.-S. Kim, "Effect of PTFE contents in the gas diffusion media on the performance of

PEMFC," Journal of Power Sources, vol. 131, no. 1-2, pp. 182-187, 2004/5// 2004, doi: 10.1016/j.jpowsour.2003.12.037.
[62] H. Ito, Y. Heo, M. Ishida, A. Nakano, S. Someya, and T. Munakata, "Application of a self-supporting microporous layer to gas diffusion layers of proton exchange membrane fuel cells," Journal of Power Sources, vol. 342, pp. 393-404, 2017/2// 2017, doi: 10.1016/j.jpowsour.2016.12.064.
[63] S. Didari, A. Asadi, Y. Wang, and T. A. L. Harris, "Modeling of composite fibrous porous diffusion media," International Journal of Hydrogen Energy, vol. 39, no. 17, pp. 9375-9386, 6 5 2014.
[64] L. Pisani, "Simple Expression for the Tortuosity of Porous Media," Transport in Porous Media, vol. 88, no. 2, pp. 193-203, 6 2011.
[65] M. M. Tomadakis and T. J. Robertson, "Viscous permeability of random fiber structures: Comparison of electrical and diffusional estimates with experimental and analytical results," Journal of Composite Materials, vol. 39, no. 2, pp. 163-188, 2005.
[66] Z. Fishman and A. Bazylak, "Heterogeneous through-plane porosity distributions for treated PEMFC GDLs I. PTFE effect," Journal of the Electrochemical Society, vol. 158, no. 8, 8 2011.
[67] J. H. Nam and M. Kaviany, "Effective diffusivity and water-saturation distribution in single- and two-layer PEMFC diffusion medium," International Journal of Heat and Mass Transfer, vol. 46, no. 24, pp. 4595-4611, 2003.
[68] M. Espinoza, M. Andersson, J. Yuan, and B. Sundén, "Compress effects on porosity, gas-phase tortuosity, and gas permeability in a simulated PEM gas diffusion layer," International Journal of Energy Research, vol. 39, no. 11, pp. 1528-1536, 9 1 2015.
[69] O. Chapuis, M. Prat, M. Quintard, E. Chane-Kane, O. Guillot, and N. Mayer, "Two-phase flow and evaporation in model fibrous media. Application to the gas diffusion layer of PEM fuel cells," Journal of Power Sources, vol. 178, no. 1, pp. 258-268, 3 15 2008.
[70] V. Gurau, M. J. Bluemle, E. S. De Castro, Y.-M. Tsou, T. A. Zawodzinski, and J. A. Mann, "Characterization of transport properties in gas diffusion layers for proton exchange membrane fuel cells: 2. Absolute permeability," Journal of Power Sources, vol. 165, no. 2, pp. 793-802, 3 20 2007.
[71] N. Alhazmi, D. B. Ingham, M. S. Ismail, K. Hughes, L. Ma, and M. Pourkashanian, "The through-plane thermal conductivity and the contact resistance of the components of the membrane electrode assembly and gas diffusion layer in proton exchange membrane fuel cells," Journal of Power Sources, vol. 270, pp. 59-67, 12 15 2014.
[72] G. Velayutham, J. Kaushik, N. Rajalakshmi, and K. S. Dhathathreyan, "Effect of PTFE content in gas diffusion media and microlayer on the performance of PEMFC tested under ambient pressure," Fuel Cells, vol. 7, no. 4, pp. 314-318, 2007/8// 2007, doi: 10.1002/fuce.200600032.
[73] J. Chen, T. Matsuura, and M. Hori, "Novel gas diffusion layer with water management function for PEMFC," Journal of Power Sources, vol. 131, no. 1, pp. 155-161, 2004, doi: 10.1016/j.jpowsour.2004.01.007.

[74] H. Su, S. Pasupathi, B. Bladergroen, V. Linkov, and B. G. Pollet, "Optimization of gas diffusion electrode for polybenzimidazole-based high temperature proton exchange membrane fuel cell: Evaluation of polymer binders in catalyst layer," International Journal of Hydrogen Energy, vol. 38, no. 26, pp. 11370-11378, 2013/8// 2013, doi: 10.1016/J.IJHYDENE.2013.06.107.
[75] S. Latorrata, P. Gallo Stampino, C. Cristiani, and G. Dotelli, "Novel superhydrophobic microporous layers for enhanced performance and efficient water management in PEM fuel cells," International Journal of Hydrogen Energy, vol. 39, no. 10, pp. 5350-5357, 2014/3// 2014, doi: 10.1016/J.IJHYDENE.2013.12.199.
[76] N. Zamel and X. Li, "Effective transport properties for polymer electrolyte membrane fuel cells - With a focus on the gas diffusion layer," in Progress in Energy and Combustion Science vol. 39, ed, 2013, pp. 111-146.
[77] H. Taira and H. Liu, "In-situ measurements of GDL effective permeability and under-land cross-flow in a PEM fuel cell," in International Journal of Hydrogen Energy, 2012, vol. 37, pp. 13725-13730.
[78] I. S. Hussaini and C. Y. Wang, "Measurement of relative permeability of fuel cell diffusion media," Journal of Power Sources, vol. 195, no. 12, pp. 3830-3840, 6 15 2010.
[79] J. Zhao, S. Shahgaldi, I. Alaefour, Q. Xu, and X. Li, "Gas permeability of catalyzed electrodes in polymer electrolyte membrane fuel cells," Applied Energy, vol. 209, pp. 203-210, 1 1 2018.
[80] J. Ihonen, M. Mikkola, and G. Lindbergh, "Flooding of Gas Diffusion Backing in PEFCs," Journal of The Electrochemical Society, vol. 151, no. 8, p. A1152, 2004.
[81] M. Hossain, S. Z. Islam, and P. Pollard, "Numerical study of the effect of effective diffusivity and permeability of the gas diffusion layer on fuel cell performance," Proceedings of the Institution of Mechanical Engineers, Part A: Journal of Power and Energy, vol. 226, no. 7, pp. 907-921, 2012/11/01 2012, doi: 10.1177/0957650912454402.
[82] M. Prasanna, H. Y. Ha, E. A. Cho, S. A. Hong, and I. H. Oh, "Influence of cathode gas diffusion media on the performance of the PEMFCs," Journal of Power Sources, vol. 131, no. 1-2, pp. 147-154, 5 14 2004.
[83] O. M. Orogbemi, D. B. Ingham, M. S. Ismail, K. J. Hughes, L. Ma, and M. Pourkashanian, "Through-plane gas permeability of gas diffusion layers and microporous layer: Effects of carbon loading and sintering," Journal of the Energy Institute, vol. 91, no. 2, pp. 270-278, 2018/4// 2018, doi: 10.1016/J.JOEI.2016.11.008.
[84] M. V. Williams, H. R. Kunz, and J. M. Fenton, "Influence of Convection Through Gas-Diffusion Layers on Limiting Current in PEM FCs Using a Serpentine Flow Field," Journal of The Electrochemical Society, vol. 151, no. 10, p. A1617, 2004.
[85] H. Oh, Y. i. Lee, G. Lee, K. Min, and J. S. Yi, "Experimental dissection of oxygen transport resistance in the components of a polymer electrolyte

membrane fuel cell," Journal of Power Sources, vol. 345, pp. 67-77, 2017, doi: 10.1016/j.jpowsour.2017.01.087.
[86] J. R. Kim, J. S. Yi, and T. W. Song, "Investigation of degradation mechanisms of a high-temperature polymer-electrolyte-membrane fuel cell stack by electrochemical impedance spectroscopy," Journal of Power Sources, vol. 220, pp. 54-64, 12 15 2012.
[87] J. Park, H. Oh, Y. I. Lee, K. Min, E. Lee, and J.-Y. Jyoung, "Effect of the pore size variation in the substrate of the gas diffusion layer on water management and fuel cell performance," Applied Energy, vol. 171, pp. 200-212, 2016/6// 2016, doi: 10.1016/J.APENERGY.2016.02.132.
[88] J. Cho, H. S. Kim, and K. Min, "Transient response of a unit proton-exchange membrane fuel cell under various operating conditions," Journal of Power Sources, vol. 185, no. 1, pp. 118-128, 10 15 2008.
[89] R. R. Rashapov and J. T. Gostick, "In-Plane Effective Diffusivity in PEMFC Gas Diffusion Layers," Transport in Porous Media, vol. 115, no. 3, pp. 411-433, 12 1 2016.
[90] G. S. Hwang and A. Z. Weber, "Effective-Diffusivity Measurement of Partially-Saturated Fuel-Cell Gas-Diffusion Layers," Journal of The Electrochemical Society, vol. 159, no. 11, pp. F683-F692, 2012.
[91] Y. Utaka, Y. Tasaki, S. Wang, T. Ishiji, and S. Uchikoshi, "Method of measuring oxygen diffusivity in microporous media," International Journal of Heat and Mass Transfer, vol. 52, no. 15-16, pp. 3685-3692, 7 2009.
[92] S. Chevalier, N. Lavielle, B. D. Hatton, and A. Bazylak, "Novel electrospun gas diffusion layers for polymer electrolyte membrane fuel cells: Part I. Fabrication, morphological characterization, and in situ performance," Journal of Power Sources, vol. 352, pp. 272-280, 6 1 2017.
[93] D. Kramer, S. A. Freunberger, R. Flückiger, I. A. Schneider, A. Wokaun, F. N. Büchi and G. G. Scherer, "Electrochemical diffusimetry of fuel cell gas diffusion layers," Journal of Electroanalytical Chemistry, vol. 612, no. 1, pp. 63-77, 1 1 2008.
[94] R. Flückiger, S. A. Freunberger, D. Kramer, A. Wokaun, G. G. Scherer, and F. N. Büchi, "Anisotropic, effective diffusivity of porous gas diffusion layer materials for PEFC," Electrochimica Acta, vol. 54, no. 2, pp. 551-559, 12 30 2008.
[95] P. Mangal, L.M. Pant, N. Carrigy, M. Dumontier, V. Zingan, S. Mitra and M. Secanell, "Experimental study of mass transport in PEMFCs: Through plane permeability and molecular diffusivity in GDLs," Electrochimica Acta, vol. 167, pp. 160-171, 6 10 2015.
[96] N. B. Carrigy, L. M. Pant, S. Mitra, and M. Secanell, "Knudsen Diffusivity and Permeability of PEMFC Microporous Coated Gas Diffusion Layers for Different Polytetrafluoroethylene Loadings," Journal of The Electrochemical Society, vol. 160, no. 2, pp. F81-F89, 2013.
[97] R. Koresawa and Y. Utaka, "Improvement of oxygen diffusion characteristic in gas diffusion layer with planar-distributed wettability for polymer electrolyte fuel cell," Journal of Power Sources, vol. 271, pp. 16-24, 8 19 2014.

[98] R. Wu, Q. Liao, X. Zhu, and H. Wang, "Pore network modeling of cathode catalyst layer of proton exchange membrane fuel cell," International Journal of Hydrogen Energy, vol. 37, no. 15, pp. 11255-11267, 8 2012.
[99] T. Rosén, J. Eller, J. Kang, N. I. Prasianakis, J. Mantzaras, and F. N. Büchi, "Saturation Dependent Effective Transport Properties of PEFC Gas Diffusion Layers," Journal of The Electrochemical Society, vol. 159, no. 9, pp. F536-F544, 2012.
[100] P. A. García-Salaberri, J. T. Gostick, G. Hwang, A. Z. Weber, and M. Vera, "Effective diffusivity in partially-saturated carbon-fiber gas diffusion layers: Effect of local saturation and application to macroscopic continuum models," Journal of Power Sources, vol. 296, pp. 440-453, 8 6 2015.
[101] D. Froning, J.Yu, G. Gaiselmann, U. Reimer, I. Manke, V. Schmidt and W. Lehnert, "Impact of compression on gas transport in non-woven gas diffusion layers of high temperature polymer electrolyte fuel cells," Journal of Power Sources, vol. 318, pp. 26-34, 6 30 2016.
[102] P. Zhou and C. W. Wu, "Numerical study on the compression effect of gas diffusion layer on PEMFC performance," Journal of Power Sources, vol. 170, no. 1, pp. 93-100, 6 30 2007.
[103] J. P. Owejan, T. A. Trabold, and M. M. Mench, "Oxygen transport resistance correlated to liquid water saturation in the gas diffusion layer of PEM fuel cells," International Journal of Heat and Mass Transfer, vol. 71, pp. 585-592, 4 2014.
[104] M. Mench, M., Fuel Cell Engines. John Wiley & Sons Inc., 2008.
[105] Y. Wang, K. S. Chen, J. Mishler, S. C. Cho, and X. C. Adroher, "A review of polymer electrolyte membrane fuel cells: Technology, applications, and needs on fundamental research," in Applied Energy vol. 88, ed: Elsevier Ltd, 2011, pp. 981-1007.
[106] A. Pfrang, D. Veyret, F. Sieker, and G. Tsotridis, "X-ray computed tomography of gas diffusion layers of PEM fuel cells: Calculation of thermal conductivity," International Journal of Hydrogen Energy, vol. 35, no. 8, pp. 3751-3757, 4 2010.
[107] H. Sadeghifar, N. Djilali, and M. Bahrami, "A new model for thermal contact resistance between fuel cell gas diffusion layers and bipolar plates," Journal of Power Sources, vol. 266, pp. 51-59, 2014/11// 2014, doi: 10.1016/J.JPOWSOUR.2014.04.149.
[108] G. Xu, J. M. Lamanna, J. T. Clement, and M. M. Mench, "Direct measurement of through-plane thermal conductivity of partially saturated fuel cell diffusion media," Journal of Power Sources, vol. 256, pp. 212-219, 6 15 2014.
[109] O. S. Burheim, J. G. Pharoah, H. Lampert, P. J. S. Vie, and S. Kjelstrup, "Through-plane thermal conductivity of PEMFC porous transport layers," Journal of Fuel Cell Science and Technology, vol. 8, no. 2, 2011.
[110] P. Teertstra, G. Karimi, and X. Li, "Measurement of in-plane effective thermal conductivity in PEM fuel cell diffusion media," Electrochimica Acta, vol. 56, no. 3, pp. 1670-1675, 2011/1// 2011, doi: 10.1016/J.ELECTACTA.2010.06.043.

[111] J. Yablecki and A. Bazylak, "Determining the effective thermal conductivity of compressed PEMFC GDLs through thermal resistance modelling," Journal of Power Sources, vol. 217, pp. 470-478, 2012/11// 2012, doi: 10.1016/J.JPOWSOUR.2012.06.011.
[112] H. Sadeghifar, N. Djilali, and M. Bahrami, "Effect of Polytetrafluoroethylene (PTFE) and micro porous layer (MPL) on thermal conductivity of fuel cell gas diffusion layers: Modeling and experiments," Journal of Power Sources, vol. 248, pp. 632-641, 2014.
[113] G. Karimi, X. Li, and P. Teertstra, "Measurement of through-plane effective thermal conductivity and contact resistance in PEM fuel cell diffusion media," Electrochimica Acta, vol. 55, no. 5, pp. 1619-1625, 2 1 2010.
[114] I. Nitta, O. Himanen, and M. Mikkola, "Thermal conductivity and contact resistance of compressed gas diffusion layer of PEM fuel cell," Fuel Cells, vol. 8, no. 2, pp. 111-119, 4 2008.
[115] P. Roy Chowdhury, A. Vikram, R. K. Phillips, and M. Hoorfar, "Measurement of effective bulk and contact resistance of gas diffusion layer under inhomogeneous compression - Part II: Thermal conductivity," Journal of Power Sources, vol. 320, pp. 222-230, 7 15 2016.
[116] M. Hamour, J. C. Grandidier, A. Ouibrahim, and S. Martemianov, "Electrical conductivity of PEMFC under loading," Journal of Power Sources, vol. 289, pp. 160-167, 5 19 2015.
[117] T. Ioroi, T. Oku, K. Yasuda, N. Kumagai, and Y. Miyazaki, "Influence of PTFE coating on gas diffusion backing for unitized regenerative polymer electrolyte fuel cells," Journal of Power Sources, vol. 124, no. 2, pp. 385-389, 2003/11// 2003, doi: 10.1016/S0378-7753(03)00795-X.
[118] Aydin, M. Zedda, and N. Zamel, "Challenges Associated with Measuring the Intrinsic Electrical Conductivity of Carbon Paper Diffusion Media," Fuel Cells, vol. 15, no. 3, pp. 537-544, 6 1 2015.
[119] J. Kleemann, F. Finsterwalder, and W. Tillmetz, "Characterisation of mechanical behaviour and coupled electrical properties of polymer electrolyte membrane fuel cell gas diffusion layers," Journal of Power Sources, vol. 190, no. 1, pp. 92-102, 5 1 2009.
[120] W. R. Chang, J. J. Hwang, F. B. Weng, and S. H. Chan, "Effect of clamping pressure on the performance of a PEM fuel cell," Journal of Power Sources, vol. 166, no. 1, pp. 149-154, 2007/3// 2007, doi: 10.1016/J.JPOWSOUR.2007.01.015.
[121] V. Mishra, F. Yang, and R. Pitchumani, "Measurement and Prediction of Electrical Contact Resistance Between Gas Diffusion Layers and Bipolar Plate for Applications to PEM Fuel Cells," Journal of Fuel Cell Science vol. 1, no. 1, pp. 2-9, 2004.
[122] S. E. Oualid, R. Lachat, D. Candusso, and Y. Meyer, "Characterization process to measure the electrical contact resistance of Gas Diffusion Layers under mechanical static compressive loads," International Journal of Hydrogen Energy, vol. 42, no. 37, 2017.
[123] W. Y. Hsu and T. D. Gierke, "ION TRANSPORT AND CLUSTERING IN NAFION* PERFLUORINATED MEMBRANES**," 1983.

[124] Q. Dong, J. Kull, and M. M. Mench, "Real-time water distribution in a polymer electrolyte fuel cell," Journal of Power Sources, vol. 139, no. 1-2, pp. 106-114, 1 4 2005.
[125] K. Ruksawong, R. Songprakorp, V. Monyakul, N. A. David, P. C. Sui, and N. Djilali, "Investigation of PEMFC under Static Magnetic Field: Temperature, Relative Humidity and Performance," Journal of The Electrochemical Society, vol. 164, no. 2, pp. F1-F8, 2017.
[126] A. Z. Weber and J. Newman, "Effects of Microporous Layers in Polymer Electrolyte Fuel Cells," Journal of The Electrochemical Society, vol. 152, no. 4, p. A677, 2005.
[127] J. T. Gostick, M. W. Fowler, M. A. Ioannidis, M. D. Pritzker, Y. M. Volfkovich, and A. Sakars, "Capillary pressure and hydrophilic porosity in gas diffusion layers for polymer electrolyte fuel cells," Journal of Power Sources, vol. 156, no. 2, pp. 375-387, 6 1 2006.
[128] J. Hinebaugh and A. Bazylak, "ESFuelCell2012-91466 Pore Network Modeling to Study the Effects of Common Assumptions in GDL Liquid Water Invasion Studies," 2012.
[129] J. H. Nam, K. J. Lee, G. S. Hwang, C. J. Kim, and M. Kaviany, "Microporous layer for water morphology control in PEMFC," International Journal of Heat and Mass Transfer, 2009, doi: 10.1016/j.ijheatmasstransfer.2009.01.002.
[130] U. Pasaogullari, C.-Y. Wang, and K. S. Chen, "LIQUID WATER TRANSPORT IN POLYMER ELECTROLYTE FUEL CELLS WITH MULTI-LAYER DIFFUSION MEDIA," 2004.
[131] S. Litster, C. R. Buie, T. Fabian, J. K. Eaton, and J. G. Santiago, "Active water management for PEM fuel cells," Journal of the Electrochemical Society, vol. 154, no. 10, 2007, doi: 10.1149/1.2766650.
[132] A. Bazylak, D. Sinton, and N. Djilali, "Dynamic water transport and droplet emergence in PEMFC gas diffusion layers," Journal of Power Sources, vol. 176, no. 1, pp. 240-246, 1 21 2008.
[133] I. Manke, Ch. Hartnig, M. Grünerbel, W. Lehnert, N. Kardjilov, A. Haibel, A. Hilger, J. Banhart and H. Riesemeier, "Investigation of water evolution and transport in fuel cells with high resolution synchrotron x-ray radiography," Applied Physics Letters, vol. 90, no. 17, 2007.
[134] S. Litster, D. Sinton, and N. Djilali, "Ex situ visualization of liquid water transport in PEM fuel cell gas diffusion layers," Journal of Power Sources, vol. 154, no. 1, pp. 95-105, 3 9 2006.
[135] G. Lin and T. V. Nguyen, "Effect of Thickness and Hydrophobic Polymer Content of the Gas Diffusion Layer on Electrode Flooding Level in a PEMFC," Journal of The Electrochemical Society, vol. 152, no. 10, p. A1942, 2005.
[136] R. Mukundan, J.Davey, J. D. Fairweather, D. Spernjak, J. S. Spendelow, D. S. Hussey, D. Jacobson, P. Wilde, R. Schweiss and R. L. Borup, "Effect of hydrophilic treatment of microporous layer on fuel cell performance," in ECS Transactions, 2010, vol. 33, 1 PART 2 ed., pp. 1109-1114, doi: 10.1149/1.3484604.
[137] P. Deevanhxay, T. Sasabe, S. Tsushima, and S. Hirai, "Effect of liquid water distribution in gas diffusion media with and without microporous layer on PEM

fuel cell performance," Electrochemistry Communications, vol. 34, pp. 239-241, 2013.
[138] P. Oberholzer, P. Boillat, R. Siegrist, A. Kästner, E.H. Lehmann, G.G. Scherer, and A. Wokaun, "Simultaneous neutron imaging of six operating PEFCs: Experimental set-up and study of the MPL effect," Electrochemistry Communications, vol. 20, no. 1, pp. 67-70, 7 2012.
[139] A. Turhan, K. Heller, J. S. Brenizer, and M. M. Mench, "Quantification of liquid water accumulation and distribution in a polymer electrolyte fuel cell using neutron imaging," Journal of Power Sources, vol. 160, no. 2 SPEC. ISS., pp. 1195-1203, 10 6 2006.
[140] Z. Fishman and A. Bazylak, "Heterogeneous Through-Plane Porosity Distributions for Treated PEMFC GDLs. II. Effect of MPL Cracks," Journal of The Electrochemical Society, vol. 158, no. 8, p. B846, 2011.
[141] Y. Wang, S. Basu, and C. Y. Wang, "Modeling two-phase flow in PEM fuel cell channels," Journal of Power Sources, vol. 179, no. 2, pp. 603-617, 5 1 2008.
[142] R. Wu, X. Zhu, Q. Liao, H. Wang, Y-d. Ding, J. Li and D-d. Ye, "A pore network study on the role of micro-porous layer in control of liquid water distribution in gas diffusion layer," International Journal of Hydrogen Energy, vol. 35, no. 14, pp. 7588-7593, 7 2010.
[143] F. A. L. Dullien, Porous Media. Fluid Transport and Pore Structure. London: Academic Press Limited, 1992.
[144] Benjamin Straubhaar, M. Prat and J. Pauchet, "Présentée et soutenue par : pore network modelling of condensation in gas diffusion layers of proton exchange membrane fuel cells directeur(s) de Thèse : Rapporteurs : Membre(s) du jury," 2015.
[145] Y. Gao, X. Zhang, P. Rama, Y. Liu, R. Chen, H. Ostadi and K. Jiang, "Calculating the Anisotropic Permeability of Porous Media Using the Lattice Boltzmann Method and X-ray Computed Tomography," Transport in Porous Media, vol. 92, no. 2, pp. 457-472, 3 2012.
[146] B. Han and H. Meng, "Numerical studies of interfacial phenomena in liquid water transport in polymer electrolyte membrane fuel cells using the lattice Boltzmann method," International Journal of Hydrogen Energy, vol. 38, no. 12, pp. 5053-5059, 4 22 2013.
[147] G. R. Molaeimanesh and M. H. Akbari, "A three-dimensional pore-scale model of the cathode electrode in polymer-electrolyte membrane fuel cell by lattice Boltzmann method," Journal of Power Sources, vol. 258, pp. 89-97, 7 15 2014.
[148] K. T. Cho and M. M. Mench, "Fundamental characterization of evaporative water removal from fuel cell diffusion media," Journal of Power Sources, vol. 195, no. 12, pp. 3858-3869, 6 15 2010.
[149] J. Roth, J. Eller, F. Marone, and F. N. Büchi, "Investigation of the representative area of the water saturation in gas diffusion layers of polymer electrolyte fuel cells," Journal of Physical Chemistry C, vol. 117, no. 49, pp. 25991-25999, 12 12 2013.
[150] H. Markötter, R. Alink, J. Haußmann, K. Dittmann, T. Arlt, F. Wieder, C. Tötzke, M. Klages, C. Reiter, H. Riesemeier, J. Scholta, D. Gerteisen, J.

Banhart and I. Manke, "Visualization of the water distribution in perforated gas diffusion layers by means of synchrotron X-ray radiography," International Journal of Hydrogen Energy, vol. 37, no. 9, pp. 7757-7761, 2012/5// 2012, doi: 10.1016/j.ijhydene.2012.01.141.

[151] J. Eller, T. Rosén, F. Marone, M. Stampanoni, A. Wokaun, and F. N. Büchi, "Progress in In Situ X-Ray Tomographic Microscopy of Liquid Water in Gas Diffusion Layers of PEFC," Journal of The Electrochemical Society, vol. 158, no. 8, p. B963, 2011.

[152] Y.-S. Chen, H. Peng, D. S. Hussey, D. L. Jacobson, D. T. Tran, T. Abdel-Baset and M. Biernacki, "Water distribution measurement for a PEMFC through neutron radiography," 2007.

[153] H. Murakawa, K. Sugimoto, K. Miyata, H. Asano, N. Takenaka, and Y. Saito, "Visualization of water behavior in the in-plane and through-plane directions in a PEFC using a neutron image intensifier," in Physics Procedia, 2013, vol. 43: Elsevier B.V., pp. 277-281.

[154] N. J. Cooper, A. D. Santamaria, M. K. Becton, and J. W. Park, "Neutron radiography measurements of in-situ PEMFC liquid water saturation in 2D & 3D morphology gas diffusion layers," International Journal of Hydrogen Energy, vol. 42, no. 25, pp. 16269-16278, 6 22 2017.

[155] M. A. Hoeh, T. Arlt, I. Manke, J. Banhart, D. L. Fritz, W. Maier and W. Lehnert, "In operando synchrotron X-ray radiography studies of polymer electrolyte membrane water electrolyzers," Electrochemistry Communications, vol. 55, pp. 55-59, 6 1 2015.

[156] J. Lee, J. Hinebaugh, and A. Bazylak, "Synchrotron X-ray radiographic investigations of liquid water transport behavior in a PEMFC with MPL-coated GDLs," Journal of Power Sources, vol. 227, pp. 123-130, 2013/4// 2013, doi: 10.1016/j.jpowsour.2012.11.006.

[157] Y. Wang, C. Y. Wang, and K. S. Chen, "Elucidating differences between carbon paper and carbon cloth in polymer electrolyte fuel cells," Electrochimica Acta, 2007, doi: 10.1016/j.electacta.2006.11.012.

[158] A. Pfrang, S. Didas, and G. Tsotridis, "X-ray computed tomography of gas diffusion layers of PEM fuel cells: Segmentation of the microporous layer," Journal of Power Sources, vol. 235, pp. 81-86, 2013/8// 2013, doi: 10.1016/j.jpowsour.2013.01.179.

[159] K. S. S. Naing, Y. Tabe, and T. Chikahisa, "Performance and liquid water distribution in PEFCs with different anisotropic fiber directions of the GDL," Journal of Power Sources, vol. 196, no. 5, pp. 2584-2594, 2011/3// 2011, doi: 10.1016/j.jpowsour.2010.10.080.

[160] S. Karvonen, T. Hottinen, J. Ihonen, and H. Uusalo, "Modeling of polymer electrolyte membrane fuel stack end plates," Journal of Fuel Cell Science and Technology, vol. 5, no. 4, 2008/11// 2008, doi: 10.1115/1.2930775.

[161] J. Lee, R. Banerjee, M. G. George, D. Muirhead, P. Shrestha, H. Liu, N. Ge, S. Chevalier and A. Bazylak, "Multiwall carbon nanotube-based microporous layers for polymer electrolyte membrane fuel cells," Journal of the Electrochemical Society, vol. 164, no. 12, pp. F1149-F1157, 2017, doi: 10.1149/2.0861712jes.

[162] J. Eller, T. Rosén, F. Marone, M. Stampanoni, A. Wokaun, and F. N. Bchi, "Progress in in situ X-ray tomographic microscopy of liquid water in gas diffusion layers of PEFC," Journal of the Electrochemical Society, vol. 158, no. 8, 2011/8// 2011, doi: 10.1149/1.3596556.
[163] Q. Meyer, S.Ashton, P. Boillat, M. Cochet , E. Engebretsen, D. P. Finegan, X. Lu, J. J. Bailey, N. Mansor, R. Abdulaziz, O. O. Taiwo, R. Jervis, S. Torija, P. Benson, S.Foster, P. Adcock, P. R. Shearing and D. J.L. Brett , "Effect of gas diffusion layer properties on water distribution across air-cooled, open-cathode polymer electrolyte fuel cells: A combined ex-situ X-ray tomography and in-operando neutron imaging study," Electrochimica Acta, vol. 211, pp. 478-487, 2016/9// 2016, doi: 10.1016/j.electacta.2016.06.068.
[164] P. Shrestha, C. Lee, K. F. Fahy, M. Balakrishnan, N. Ge, and A. Bazylak, "Pore-Scale Liquid Water Visualization for Understanding Water Transport in Operating Fuel Cells," ECS Transactions, vol. 92, no. 8, pp. 61-69, 2019/7// 2019, doi: 10.1149/09208.0061ecst.
[165] R. Jose Varghese, E. H. M. Sakho, S. Parani, S. Thomas, O. S. Oluwafemi, and J. Wu, "Introduction to nanomaterials: synthesis and applications," Nanomaterials for Solar Cell Applications, pp. 75-95, 2019/1// 2019, doi: 10.1016/B978-0-12-813337-8.00003-5.
[166] M. Balakrishnan, P. Shrestha, N. Ge, C-H. Lee, K.F. Fahy, R. Zeis, V. P. Schulz, B.D. Hatton, and Aimy Bazylak, "Designing Tailored Gas Diffusion Layers with Pore Size Gradients via Electrospinning for Polymer Electrolyte Membrane Fuel Cells," ACS Applied Energy Materials, vol. 3, no. 3, pp. 2695-2707, 2020/3// 2020, doi: 10.1021/acsaem.9b02371.
[167] Ö. Delikaya, N. Bevilacqua, L. Eifert, U. Kunz, R. Zeis, and C. Roth, "Porous electrospun carbon nanofibers network as an integrated electrode@gas diffusion layer for high temperature polymer electrolyte membrane fuel cells," Electrochimica Acta, vol. 345, pp. 136192-136192, 2020/6// 2020, doi: 10.1016/j.electacta.2020.136192.
[168] G. Ren, Z. Qu, X. Wang, and J. Zhang, "Liquid water transport and mechanical performance of electrospun gas diffusion layers," International Journal of Green Energy, vol. 19, no. 2, pp. 210-218, 2022, doi: 10.1080/15435075.2021.1941046.
[169] S. Chevalier, N. Ge, J. Lee, M. G. George, H. Liu, P. Shrestha, D. Muirhead, N. Lavielle, B. D. Hatton, and A. Bazylak, , "Novel electrospun gas diffusion layers for polymer electrolyte membrane fuel cells: Part II. In operando synchrotron imaging for microscale liquid water transport characterization," Journal of Power Sources, vol. 352, pp. 281-290, 2017/6// 2017, doi: 10.1016/j.jpowsour.2017.01.114.
[170] M. Balakrishnan, P. Shrestha, CH. Lee, N. Ge, K.F. Fahy, M. Messerschmidt, J. Scholta, L. Eifert, J. Maibach, R. Zeis, B. D. Hatton, and A. Bazylak, "Degradation Characteristics of Electrospun Gas Diffusion Layers with Custom Pore Structures for Polymer Electrolyte Membrane Fuel Cells," ACS Applied Materials and Interfaces, vol. 13, no. 2, pp. 2414-2427, 2021/1// 2021, doi: 10.1021/acsami.0c15324.

[171] W. Z. Fang, Y. Q. Tang, L. Chen, Q. J. Kang, and W. Q. Tao, "Influences of the perforation on effective transport properties of gas diffusion layers," International Journal of Heat and Mass Transfer, vol. 126, pp. 243-255, 2018/11// 2018, doi: 10.1016/j.ijheatmasstransfer.2018.05.016.
[172] D. Gerteisen, T. Heilmann, and C. Ziegler, "Enhancing liquid water transport by laser perforation of a GDL in a PEM fuel cell," Journal of Power Sources, vol. 177, no. 2, pp. 348-354, 2008/3// 2008, doi: 10.1016/j.jpowsour.2007.11.080.
[173] D. Gerteisen and C. Sadeler, "Stability and performance improvement of a polymer electrolyte membrane fuel cell stack by laser perforation of gas diffusion layers," Journal of Power Sources, vol. 195, no. 16, pp. 5252-5257, 2010/8// 2010, doi: 10.1016/j.jpowsour.2010.03.021.
[174] J. Haußmann, H. Markötter, R. Alink, A. Bauder, K. Dittmann, I. Manke and J. Scholta, "Synchrotron radiography and tomography of water transport in perforated gas diffusion media," Journal of Power Sources, vol. 239, pp. 611-622, 2013/10// 2013, doi: 10.1016/j.jpowsour.2013.02.014.
[175] Z. Niu, J. Wu, Z. Bao, Y. Wang, Y. Yin, and K. Jiao, "Two-phase flow and oxygen transport in the perforated gas diffusion layer of proton exchange membrane fuel cell," International Journal of Heat and Mass Transfer, vol. 139, pp. 58-68, 2019/8// 2019, doi: 10.1016/j.ijheatmasstransfer.2019.05.008.
[176] G. Okuhata, T. Tonoike, K. Nishida, S. Tsushima, and S. Hirai, "Effect of Perforation Structure of Cathode GDL on Liquid Water Removal in PEFC," ECS Transactions, vol. 58, no. 1, pp. 1047-1057, 2013/8// 2013, doi: 10.1149/05801.1047ecst.
[177] X. Wang, S. Chen, Z.Fan, W. Li, S. Wang, X. Li, Y. Zhao, T. Zhu and X. Xie, "Laser-perforated gas diffusion layer for promoting liquid water transport in a proton exchange membrane fuel cell," International Journal of Hydrogen Energy, vol. 42, no. 50, pp. 29995-30003, 2017/12// 2017, doi: 10.1016/j.ijhydene.2017.08.131.
[178] R. Alink, J. Haußmann, H. Markötter, M. Schwager, I. Manke, and D. Gerteisen, "The influence of porous transport layer modifications on the water management in polymer electrolyte membrane fuel cells," Journal of Power Sources, vol. 233, pp. 358-368, 2013/7// 2013, doi: 10.1016/j.jpowsour.2013.01.085.
[179] M. P. Manahan and M. M. Mench, "Laser Perforated Fuel Cell Diffusion Media: Engineered Interfaces for Improved Ionic and Oxygen Transport," Journal of The Electrochemical Society, vol. 159, no. 7, pp. F322-F330, 2012, doi: 10.1149/2.084207jes.
[180] S. Kaushal, P. Negi, A. K. Sahu, and S. R. Dhakate, "Upshot of natural graphite inclusion on the performance of porous conducting carbon fiber paper in a polymer electrolyte membrane fuel cell," Materials Research Express, vol. 4, no. 9, 2017/9// 2017, doi: 10.1088/2053-1591/aa8517.
[181] V. Gurau, T. Zawodzinski, and R. Wayne, "In-Situ Characterization of GRAFCELL® Flexible Graphite Film as Gas Diffusion Layers for PEMFCs," 2008/10// 2008: The Electrochemical Society, pp. 1651-1659, doi: 10.1149/1.2982006.

[182] R. Zhang, Q. Wen, W. Qian, D. S. Su, Q. Zhang, and F. Wei, "Superstrong ultralong carbon nanotubes for mechanical energy storage," Advanced Materials, vol. 23, no. 30, pp. 3387-3391, 2011/8// 2011, doi: 10.1002/adma.201100344.
[183] B. Peng, M. Locascio, P. Zapol, S. Li, S. L. Mielke, G. C. Schatz and H. D. Espinosa , "Measurements of near-ultimate strength for multiwalled carbon nanotubes and irradiation-induced crosslinking improvements," Nature Nanotechnology, vol. 3, no. 10, pp. 626-631, 2008, doi: 10.1038/nnano.2008.211.
[184] Q. Zhao, M. B. Nardelli, and J. Bernholc, "Ultimate strength of carbon nanotubes: A theoretical study," Physical Review B - Condensed Matter and Materials Physics, vol. 65, no. 14, pp. 1-6, 2002, doi: 10.1103/PhysRevB.65.144105.
[185] A. Caradonna, C. Badini, E. Padovano, and M. Pietroluongo, "Electrical and thermal conductivity of epoxy-carbon filler composites processed by calendaring," Materials, vol. 12, no. 9, 2019, doi: 10.3390/ma12091522.
[186] P. Kim, L. Shi, A. Majumdar, and P. L. McEuen, "Thermal transport measurements of individual multiwalled nanotubes," Physical Review Letters, vol. 87, no. 21, pp. 215502-4, 2001/11// 2001, doi: 10.1103/PhysRevLett.87.215502.
[187] P. H. Maheshwari, C. Gupta, V. Selvaganesh, and R. B. Mathur, "CNT membrane as a free standing electrode for PEM fuel cell," Journal of the Electrochemical Society, vol. 161, no. 12, pp. F1146-F1153, 2014, doi: 10.1149/2.0201412jes.
[188] Y. Gao, G. Q. Sun, S. L. Wang, and S. Zhu, "Carbon nanotubes based gas diffusion layers in direct methanol fuel cells," Energy, vol. 35, no. 3, pp. 1455-1459, 2010/3// 2010, doi: 10.1016/j.energy.2009.11.031.
[189] H. Deng, Y. Zhang, X. Zheng, Y. Li, X. Zhang, and X. Liu, "A CNT (carbon nanotube) paper as cathode gas diffusion electrode for water management of passive μ-DMFC (micro-direct methanol fuel cell) with highly concentrated methanol," Energy, vol. 82, pp. 236-241, 2015/3// 2015, doi: 10.1016/j.energy.2015.01.034.
[190] S. Ghobadi, L. Işlkel Şanll, R. Bakhtiari, and S. Alkan Gürsel, "Green Composite Papers via Use of Natural Binders and Graphene for PEM Fuel Cell Electrodes," ACS Sustainable Chemistry and Engineering, vol. 5, no. 9, pp. 8407-8415, 2017/9// 2017, doi: 10.1021/acssuschemeng.7b02207.
[191] B. Yarar Kaplan, L. Işıkel Şanlı, and S. Alkan Gürsel, "Flexible carbon–cellulose fiber-based composite gas diffusion layer for polymer electrolyte membrane fuel cells," Journal of Materials Science, vol. 52, no. 9, pp. 4968-4976, 2017/5// 2017, doi: 10.1007/s10853-016-0734-6.
[192] T. Kinumoto, T. Matsumura, K. Yamaguchi, M. Matsuoka, T. Tsumura, and M. Toyoda, "Material Processing of Bamboo for Use as a Gas Diffusion Layer in Proton Exchange Membrane Fuel Cells," ACS Sustainable Chemical Engineering, vol. 3, no. 7, pp. 1374-1380, 2015.
[193] T. Matsumura, T. Kinumoto, M. Matsuoka, T. Tsumura, and M. Toyoda, "Preparation of Carbonaceous Fiber Sheets Derived from Bamboo and

Application to Gas Diffusion Layer of Proton Exchange Membrane Fuel Cells," ECS Transactions, vol. 64, no. 45, 2015.
[194] F. Destyorini, Y. Irmawati, H. Widodo, D. S. Khaerudini, and N. Indayaningsih, "Properties and performance of gas diffusion layer PEMFC derived from coconut coir," Journal of Engineering and Technological Sciences, vol. 50, no. 3, pp. 409-419, 2018, doi: 10.5614/j.eng.technol.sci.2018.50.3.7.
[195] N. Indayaningsih, A. Zulfia, D. Priadi, and S. Hendrana, "Preparation of carbon composite from coconut fiber for gas diffusion layer," Ionics, vol. 22, no. 8, pp. 1445-1449, 2016/8// 2016, doi: 10.1007/s11581-016-1657-6.
[196] Y.-J. Heo, M. Park, W.-S. Kang, K. Y. Rhee, and S.-J. Park, "Preparation and characterization of carbon black/pitch-based carbon fiber paper composites for gas diffusion layers," Composites Part B: Engineering, vol. 159, pp. 362-368, 2019/2// 2019, doi: 10.1016/j.compositesb.2018.09.108.
[197] M. Glora, M. Wiener, R. Petričević, H. Pröbstle, and J. Fricke, "Integration of carbon aerogels in PEM fuel cells," Journal of Non-Crystalline Solids, vol. 285, no. 1-3, pp. 283-287, 2001/6// 2001, doi: 10.1016/S0022-3093(01)00468-9.
[198] J. Wang, R. Petricevic, R. Saliger, H. Proebstle, and J. Fricke, "Carbon Cloth Reinforced Carbon Aerogel Films Derived from Resorcinol Formaldehyde," in "Journal of Porous Materials," 2001, vol. 8.
[199] A. M. I. Trefilov, A. Tiliakos, Elena C. Serban, C. Ceaus, S. M. Iordache, S. Voinea and A. Balan, "Carbon xerogel as gas diffusion layer in PEM fuel cells," International Journal of Hydrogen Energy, vol. 42, no. 15, pp. 10448-10454, 2017/4// 2017, doi: 10.1016/j.ijhydene.2017.03.016.
[200] T. Bystron, M. Vesely, M. Paidar, G. Papakonstantinou, K. Sundmacher, B. Bensmann, R. Hanke-Rauschenbach and K. Bouzek, "Enhancing PEM water electrolysis efficiency by reducing the extent of Ti gas diffusion layer passivation," Journal of Applied Electrochemistry, vol. 48, no. 6, pp. 713-723, 2018/6// 2018, doi: 10.1007/s10800-018-1174-6.
[201] H. Choi, O. H. Kim, M. Kim, H. Choe, Y. H. Cho, and Y. E. Sung, "Next-generation polymer-electrolyte-membrane fuel cells using titanium foam as gas diffusion layer," ACS Applied Materials and Interfaces, vol. 6, no. 10, pp. 7665-7671, 2014/5// 2014, doi: 10.1021/am500962h.
[202] K. Fushinobu, D. Takahashi, and K. Okazaki, "Micromachined metallic thin films for the gas diffusion layer of PEFCs," Journal of Power Sources, vol. 158, no. 2, pp. 1240-1245, 2006/8// 2006, doi: 10.1016/J.JPOWSOUR.2005.10.080.
[203] T. Hottinen, M. Mikkola, T. Mennola, and P. Lund, "Titanium sinter as gas diffusion backing in PEMFC," Journal of Power Sources, vol. 118, no. 1-2, pp. 183-188, 2003/5// 2003, doi: 10.1016/S0378-7753(03)00087-9.
[204] N. Wan, C. Wang, and Z. Mao, "Titanium substrate based micro-PEMFC operating under ambient conditions," Electrochemistry Communications, vol. 9, no. 3, pp. 511-516, 2007/3// 2007, doi: 10.1016/j.elecom.2006.10.025.
[205] P. Patel, P. P. Bhingole, and D. Makwana, "Manufacturing, characterization and applications of lightweight metallic foams for structural applications: Review," Materials Today: Proceedings, vol. 5, no. 9, pp. 20391-20402, 2018/1// 2018, doi: 10.1016/j.matpr.2018.06.414.

[206] T. Matsushita, S. Fujibayashi, and T. Kokubo, "Titanium foam for bone tissue engineering," Metallic Foam Bone, pp. 111-130, 2017/1// 2017, doi: 10.1016/B978-0-08-101289-5.00004-4.
[207] J. Banhart, "Aluminum Foams: On the Road to Real Applications," MRS Bulletin, vol. 28, no. 4, pp. 290-295, 2003/4// 2003, doi: 10.1557/mrs2003.83.
[208] S. Arisetty, A. K. Prasad, and S. G. Advani, "Metal foams as flow field and gas diffusion layer in direct methanol fuel cells," Journal of Power Sources, vol. 165, no. 1, pp. 49-57, 2007/2// 2007, doi: 10.1016/J.JPOWSOUR.2006.12.008.
[209] A. Fly, D. Butcher, Q. Meyer, M. Whiteley, A. Spencer, C. Kim, P.R. Shearing, D.J.L. Brett and R. Chen, "Characterisation of the diffusion properties of metal foam hybrid flow-fields for fuel cells using optical flow visualisation and X-ray computed tomography," Journal of Power Sources, vol. 395, pp. 171-178, 2018/8// 2018, doi: 10.1016/j.jpowsour.2018.05.070.
[210] A. Fly, Q. Meyer, M. Whiteley, F. Iacoviello, T. Neville P.R. Shearing, D.J.L. Brett, C. Kim, and R. Chen, "X-ray tomography and modelling study on the mechanical behaviour and performance of metal foam flow-fields for polymer electrolyte fuel cells," International Journal of Hydrogen Energy, vol. 44, no. 14, pp. 7583-7595, 2019/3// 2019, doi: 10.1016/j.ijhydene.2019.01.206.
[211] W. Yuan, Y. Tang, X. Yang, and Z. Wan, "Porous metal materials for polymer electrolyte membrane fuel cells – A review," Applied Energy, vol. 94, pp. 309-329, 2012/6// 2012, doi: 10.1016/j.apenergy.2012.01.073.
[212] D. Modroukas, V. Modi, and L. G. Fréchette, "Micromachined silicon structures for free-convection PEM fuel cells," Journal of Micromechanics and Microengineering, vol. 15, no. 9, pp. S193-S201, 2005/9// 2005, doi: 10.1088/0960-1317/15/9/S04.
[213] F. Y. Zhang, S. G. Advani, and A. K. Prasad, "Performance of a metallic gas diffusion layer for PEM fuel cells," Journal of Power Sources, vol. 176, no. 1, pp. 293-298, 2008/1// 2008, doi: 10.1016/j.jpowsour.2007.10.055.
[214] P. Liu, G. P. Yin, and Q. Z. Lai, "Gold-plated Ni mesh as the gas diffusion medium for air-breathing direct methanol fuel cell," International Journal of Energy Research, vol. 33, no. 1, pp. 1-7, 2009, doi: 10.1002/er.1463.
[215] A. Jayakumar, P. Candidate, M. Ramos, and A. Al-Jumaily, "a novel 3d printing technique to synthesise gas diffusion layer for pem fuel cell application," 2016. [Online]. Available: https://asmedigitalcollection.asme.org/IMECE/proceedings-pdf/IMECE2016/50596/V06BT08A021/2496781/v06bt08a021-imece2016-65554.pdf
[216] Q. Meyer, N. Mansor, F. Iacoviello, P.L. Cullen, R. Jervis, D. Finegan, C. Tan, J. Bailey, P.R. Shearing and D.J.L. Brett, "Investigation of Hot Pressed Polymer Electrolyte Fuel Cell Assemblies via X-ray Computed Tomography," Electrochimica Acta, vol. 242, pp. 125-136, 2017/7// 2017, doi: 10.1016/j.electacta.2017.05.028.
[217] J. Zhou, S. Shukla, A. Putz, and M. Secanell, "Analysis of the role of the microporous layer in improving polymer electrolyte fuel cell performance," Electrochimica Acta, vol. 268, pp. 366-382, 2018/4// 2018, doi: 10.1016/j.electacta.2018.02.100.

[218] J. Chen, H. Xu, H. Zhang, and B. Yi, "Facilitating mass transport in gas diffusion layer of PEMFC by fabricating micro-porous layer with dry layer preparation," Journal of Power Sources, vol. 182, no. 2, pp. 531-539, 2008/8// 2008, doi: 10.1016/j.jpowsour.2008.04.031.
[219] N. Zhan, W. Wu, and S. Wang, "Pore network modeling of liquid water and oxygen transport through the porosity-graded bilayer gas diffusion layer of polymer electrolyte membrane fuel cells," Electrochimica Acta, vol. 306, pp. 264-276, 2019/5// 2019, doi: 10.1016/j.electacta.2019.03.115.
[220] Y. Yang, X. Zhou, B. Li, and C. Zhang, "Recent progress of the gas diffusion layer in proton exchange membrane fuel cells: Material and structure designs of microporous layer," International Journal of Hydrogen Energy, vol. 46, no. 5, pp. 4259-4282, 2021/1// 2021, doi: 10.1016/J.IJHYDENE.2020.10.185.
[221] Q. Yan, H. Toghiani, and J. Wu, "Investigation of water transport through membrane in a PEM fuel cell by water balance experiments," Journal of Power Sources, vol. 158, no. 1, pp. 316-325, 2006/7// 2006, doi: 10.1016/j.jpowsour.2005.09.013.
[222] G. Velayutham, "Effect of micro-layer PTFE on the performance of PEM fuel cell electrodes," International Journal of Hydrogen Energy, vol. 36, no. 22, pp. 14845-14850, 2011/11// 2011, doi: 10.1016/J.IJHYDENE.2011.03.037.
[223] A. Z. Weber, "Improved modeling and understanding of diffusion-media wettability on polymer-electrolyte-fuel-cell performance," Journal of Power Sources, 2010, doi: 10.1016/j.jpowsour.2010.03.011.
[224] Y. Wang, S. Al Shakhshir and X. Li, "Fabrication of Hydrophobic coating on GDL with silicone based materials," in "Environ. Sci. Technol," 1980, vol. 22.
[225] H.-M. Chang, C.-W. Lin, M.-H. Chang, H.-R. Shiu, W.-C. Chang, and F.-H. Tsau, "Optimization of polytetrafluoroethylene content in cathode gas diffusion layer by the evaluation of compression effect on the performance of a proton exchange membrane fuel cell," Journal of Power Sources, vol. 196, no. 8, pp. 3773-3780, 2011/4// 2011, doi: 10.1016/J.JPOWSOUR.2010.12.090.
[226] L. R. Jordan, A. K. Shukla, T. Behrsing, N. R. Avery, B. C. Muddle, and M. Forsyth, "Diffusion layer parameters influencing optimal fuel cell performance," Journal of Power Sources, 2000, doi: 10.1016/S0378-7753(99)00489-9.
[227] S. Park, J.-W. Lee, and B. N. Popov, "Effect of carbon loading in microporous layer on PEM fuel cell performance," Journal of Power Sources, vol. 163, no. 1, pp. 357-363, 2006/12// 2006, doi: 10.1016/J.JPOWSOUR.2006.09.020.
[228] E. Antolini, R. R. Passos, and E. A. Ticianelli, "Effects of the carbon powder characteristics in the cathode gas diffusion layer on the performance of polymer electrolyte fuel cells," Journal of Power Sources, vol. 109, no. 2, pp. 477-482, 2002, doi: 10.1016/S0378-7753(02)00112-X.
[229] J. Yu, M. N. Islam, T. Matsuura, M. Tamano, Y. Hayashi, and M. Hori, "Improving the performance of a PEMFC with Ketjenblack EC-600JD carbon black as the material of the microporous layer," Electrochemical and Solid-State Letters, vol. 8, no. 6, 2005, doi: 10.1149/1.1904504.
[230] X. Wang, H.Zhang, J. Zhang, H.Xu, X. Zhu, J. Chen and B. Yi, "A bi-functional micro-porous layer with composite carbon black for PEM fuel

cells," Journal of Power Sources, vol. 162, no. 1, pp. 474-479, 2006/11// 2006, doi: 10.1016/j.jpowsour.2006.06.064.
[231] E. Carcadea, H. Ene, D.B. Ingham, R. Lazar, L. Ma, M. Pourkashanian and I. Stefanescu, "A computational fluid dynamics analysis of a PEM fuel cell system for power generation," International Journal of Numerical Methods for Heat and Fluid Flow, vol. 17, no. 3, pp. 302-312, 2007, doi: 10.1108/09615530710730166.
[232] R. Balzarotti, S. Latorrata, P. G. Stampino, C. Cristiani, and G. Dotelli, "Development and characterization of non-conventional micro-porous layers for PEM fuel cells," Energies, vol. 8, no. 7, pp. 7070-7083, 2015, doi: 10.3390/en8077070.
[233] B. Millington, V. Whipple, and B. G. Pollet, "A novel method for preparing proton exchange membrane fuel cell electrodes by the ultrasonic-spray technique," Journal of Power Sources, vol. 196, no. 20, pp. 8500-8508, 2011/10// 2011, doi: 10.1016/j.jpowsour.2011.06.024.
[234] Y.-S. Kim, D.-H. Peck, S.-K. Kim, D.-H. Jung, S. Lim, and S.-H. Kim, "Effects of the microstructure and powder compositions of a micro-porous layer for the anode on the performance of high concentration methanol fuel cell," International Journal of Hydrogen Energy, vol. 38, no. 17, pp. 7159-7168, 2013/6// 2013, doi: 10.1016/j.ijhydene.2013.04.003.
[235] T. Li, K. Wang, J. Wang, Y.Liu, Y.Han, J.Song, H. Hu, G. Lin and Y. Liu, "Preparation of hierarchical-pore gas diffusion layer for fuel cell," Journal of Materials Scienc, vol. 55, pp.4558–4569, doi: 10.1007/s10853-019-04323-9.
[236] J. H. Chun, K. T. Park, D. H. Jo, J. Y. Lee, S. G. Kim, E. S. Lee b, J-Y. Jyoung and S. H. Kim, "Determination of the pore size distribution of micro porous layer in PEMFC using pore forming agents under various drying conditions," International Journal of Hydrogen Energy, vol. 35, no. 20, pp. 11148-11153, 2010/10// 2010, doi: 10.1016/j.ijhydene.2010.07.056.
[237] W. M. Yan, C. Y. Hsueh, C. Y. Soong, F. Chen, C. H. Cheng, and S. C. Mei, "Effects of fabrication processes and material parameters of GDL on cell performance of PEM fuel cell," International Journal of Hydrogen Energy, vol. 32, no. 17, pp. 4452-4458, 2007/12// 2007, doi: 10.1016/j.ijhydene.2007.02.003.
[238] H. Tang, S. Wang, M. Pan, and R. Yuan, "Porosity-graded micro-porous layers for polymer electrolyte membrane fuel cells," Journal of Power Sources, 2007, doi: 10.1016/j.jpowsour.2007.01.021.
[239] Z. Tang, C. K. Poh, Z. Tian, J. Lin, H. Y. Ng, and D. H. C. Chua, "In situ grown carbon nanotubes on carbon paper as integrated gas diffusion and catalyst layer for proton exchange membrane fuel cells," Electrochimica Acta, vol. 56, no. 11, pp. 4327-4334, 2011/4// 2011, doi: 10.1016/J.ELECTACTA.2011.01.035.
[240] R. Schweiss, M. Steeb, P. M. Wilde, and T. Schubert, "Enhancement of proton exchange membrane fuel cell performance by doping microporous layers of gas diffusion layers with multiwall carbon nanotubes," Journal of Power Sources, vol. 220, pp. 79-83, 2012/12// 2012, doi: 10.1016/J.JPOWSOUR.2012.07.078.

[241] S.-Y. Lin and M.-H. Chang, "Effect of microporous layer composed of carbon nanotube and acetylene black on polymer electrolyte membrane fuel cell performance," International Journal of Hydrogen Energy, vol. 40, no. 24, pp. 7879-7885, 2015/6// 2015, doi: 10.1016/J.IJHYDENE.2014.10.146.
[242] A. Ozden, S. Shahgaldi, J. Zhao, X. Li, and F. Hamdullahpur, "Assessment of graphene as an alternative microporous layer material for proton exchange membrane fuel cells," Fuel, vol. 215, pp. 726-734, 2018/3// 2018, doi: 10.1016/J.FUEL.2017.11.109.
[243] M. Mariani, S. Latorrata, S. Patrignani, P. Gallo Stampino, and G. Dotelli, "Characterization of novel graphene-based microporous layers for Polymer Electrolyte Membrane Fuel Cells operating under low humidity and high temperature," International Journal of Hydrogen Energy, vol. 45, no. 11, pp. 7046-7058, 2020/2// 2020, doi: 10.1016/j.ijhydene.2019.12.213.
[244] M. J. Leeuwner, D. P. Wilkinson, and E. L. Gyenge, "Novel Graphene Foam Microporous Layers for PEM Fuel Cells: Interfacial Characteristics and Comparative Performance," Fuel Cells, vol. 15, no. 6, pp. 790-801, 2015/12// 2015, doi: 10.1002/fuce.201500031.
[245] M. J. Leeuwner, A. Patra, D. P. Wilkinson, and E. L. Gyenge, "Graphene and reduced graphene oxide based microporous layers for high-performance proton-exchange membrane fuel cells under varied humidity operation," Journal of Power Sources, vol. 423, pp. 192-202, 2019/5// 2019, doi: 10.1016/J.JPOWSOUR.2019.03.048.
[246] R. Sandström, J. Ekspong, A. Annamalai, T. Sharifi, A. Klechikov, and T. Wågberg, "Fabrication of microporous layer-free hierarchical gas diffusion electrode as a low Pt-loading PEMFC cathode by direct growth of helical carbon nanofibers," RSC Advances, vol. 8, no. 72, pp. 41566-41574, 2018, doi: 10.1039/c8ra07569g.
[247] J. Kim, H. Kim, H. Song, D. Kim, G. H. Kim, D. I , Y. Jeong and T.Park, "Carbon nanotube sheet as a microporous layer for proton exchange membrane fuel cells," Energy, vol. 227, pp. 120459-120459, 2021/7// 2021, doi: 10.1016/j.energy.2021.120459.
[248] A. M. Kannan, P. Kanagala, and V. Veedu, "Development of carbon nanotubes based gas diffusion layers by in situ chemical vapor deposition process for proton exchange membrane fuel cells," Journal of Power Sources, 2009, doi: 10.1016/j.jpowsour.2009.03.022.
[249] H. Gharibi, M. Javaheri, and R. A. Mirzaie, "The synergy between multi-wall carbon nanotubes and Vulcan XC72R in microporous layers," International Journal of Hydrogen Energy, vol. 35, no. 17, pp. 9241-9251, 2010/9// 2010, doi: 10.1016/J.IJHYDENE.2009.08.092.
[250] A. M. Kannan and L. Munukutla, "Carbon nano-chain and carbon nano-fibers based gas diffusion layers for proton exchange membrane fuel cells," Journal of Power Sources, vol. 167, no. 2, pp. 330-335, 2007/5// 2007, doi: 10.1016/J.JPOWSOUR.2007.02.064.
[251] P. Gallo Stampino, L. Omati, C. Cristiani, and G. Dotelli, "Characterisation of nanocarbon-based gas diffusion media by electrochemical impedance

spectroscopy," in Fuel Cells, 2010/4// 2010, vol. 10, 2 ed., pp. 270-277, doi: 10.1002/fuce.200900126.
[252] T. Tanuma, M. Kawamoto, and S. Kinoshita, "Effect of properties of hydrophilic microporous layer (MPL) on PEFC performance," Journal of the Electrochemical Society, vol. 164, no. 6, pp. F499-F503, 2017, doi: 10.1149/2.0371706jes.
[253] A. T. Najafab, M. J. Leeuwner, D. P. Wilkinson, and E. L. Gyenge, "Electrochemically Produced Graphene for MicroporousLayers in Fuel Cells," ChemSusChem, vol. 9, pp. 1689 –1697-1689 –1697, 2016.
[254] A. Bauder, K. A. Friedrich, J. Haußmann, H. Markötter, I. Manke, R. Alink and J. Scholta, "Self-Supporting Microporous Layers (MPLs) for PEM Fuel Cells," ECS Transactions, vol. 58, no. 1, pp. 1391-1399, 2013/8// 2013, doi: 10.1149/05801.1391ecst.
[255] Q. Duan, B. Wang, J. Wang, H. Wang, and Y. Lu, "Fabrication of a carbon nanofiber sheet as a micro-porous layer for proton exchange membrane fuel cells," Journal of Power Sources, vol. 195, no. 24, pp. 8189-8193, 2010/12// 2010, doi: 10.1016/J.JPOWSOUR.2010.07.032.
[256] F. Zhang, H. Zhang, C. Qu, and J. Ren, "Poly(vinylidene fluoride) based anion conductive ionomer as a catalyst binder for application in anion exchange membrane fuel cell," Journal of Power Sources, vol. 196, no. 6, pp. 3099-3103, 2011/3// 2011, doi: 10.1016/J.JPOWSOUR.2010.11.102.
[257] S. B. Park, S. Kim, Y. I. Park, and M. H. Oh, "Fabrication of GDL microporous layer using PVDF for PEMFCs," in Journal of Physics: Conference Series, 2009, vol. 165: Institute of Physics Publishing, doi: 10.1088/1742-6596/165/1/012046.
[258] A. Bottino, G. Capannelli, A. Comite, C. Costa, and A. L. Ong, "Microporous layers based on poly(vinylidene fluoride) and sulfonated poly(vinylidene fluoride)," International Journal of Hydrogen Energy, vol. 40, no. 42, pp. 14690-14698, 2015/11// 2015, doi: 10.1016/J.IJHYDENE.2015.08.099.
[259] A. L. Ong, A. Bottino, G. Capannelli, and A. Comite, "Effect of preparative parameters on the characteristic of poly(vinylidene fluoride)-based microporous layer for proton exchange membrane fuel cells," Journal of Power Sources, vol. 183, no. 1, pp. 62-68, 2008/8// 2008, doi: 10.1016/J.JPOWSOUR.2008.04.064.
[260] W. Navarrini, M. Sansotera, M. V. Diamanti, M. P. Pedeferri, M. Gola, and G. Dotelli, "Perfluoropolyethers as superhydrophobizing agents for carbon-based surfaces of fuel cell gas diffusion layers."
[261] M. Sansotera, W. Navarrini, M. Gola, C. L. Bianchi, P. Wormald, A.Famulari and M.Avataneo, "Peroxidic perfluoropolyether for the covalent binding of perfluoropolyether chains on carbon black surface," Journal of Fluorine Chemistry, vol. 132, no. 12, pp. 1254-1261, 2011/12// 2011, doi: 10.1016/J.jfluchem.2011.07.018.
[262] M. Sansotera, M. Gola, G. Dotelli, and W. Navarrini, "The Role of Perfluoropolyethers in the Development of Polymeric Proton Exchange Membrane Fuel Cells," in Fluorinated Polymers: Applications: Volume 2, B.

Ameduri and H. Sawada Eds. Cambridge: Royal Society of Chemistry, 2016, pp. 158-178.
[263] S. Latorrata, M. Sansotera, M. Gola, P. G. Stampino, W. Navarrini, and G. Dotelli, "Innovative Perfluoropolyether-Functionalized Gas Diffusion Layers with Enhanced Performance in Polymer Electrolyte Membrane Fuel Cells," Fuel Cells, vol. 20, no. 2, pp. 166-175, 2020/4// 2020, doi: 10.1002/fuce.201900169.
[264] S. Latorrata, P. G. Stampino, C. Cristiani, and G. Dotelli, "Performance evaluation and durability enhancement of FEP-based gas diffusion media for PEM fuel cells," Energies, vol. 10, no. 12, 2017, doi: 10.3390/en10122063.
[265] S. B. Park, J. Eon Kim, and M.-H. Oh, "Fabrication of GDL Microporous Layer Using FEP for PEMFCs," in "Semiconductors and Superlattices," Gordon and Breach Science Pub, 2000, vol. 9.
[266] R. Schweiss, M. Steeb, and P. M. Wilde, "Mitigation of water management in PEM fuel cell cathodes by hydrophilic wicking microporous layers," Fuel Cells, vol. 10, no. 6, pp. 1176-1180, 2010/12// 2010, doi: 10.1002/fuce.201000003.
[267] T. Tanuma and S. Kinoshita, "Impact of gas diffusion layers (GDLs) on water transport in PEFCs," Journal of the Electrochemical Society, vol. 159, no. 2, 2012, doi: 10.1149/2.054202jes.
[268] R. Nozaki, Y. Tabe, T. Chikahisa, and T. Tanuma, "Analysis of Oxygen Transport Resistance Components and Water Transport Phenomena with Hydrophilic and Hydrophobic MPL in PEFC," ECS Transactions, vol. 80, no. 8, pp. 335-344, 2017.
[269] Y. Aoyama, K. Suzuki, Y. Tabe, T. Chikahisa, and T. Tanuma, "Effect of hydrophilic micro-porous layer structure on microscopic water distribution and cell performance in PEFC," in ECS Transactions, 2015, vol. 69: Electrochemical Society Inc., 17 ed., pp. 743-752, doi: 10.1149/06917.0743ecst.
[270] X. Guo, Z. Shao, Y. Xiao, Y. Zeng, S. Liu, X. Wang and B. Yi, "Improvement of the proton exchange membrane fuel cell (PEMFC) performance at low-humidity conditions by exposing anode in Ultraviolet light," Electrochemistry Communications, vol. 44, pp. 16-18, 2014/7// 2014, doi: 10.1016/j.elecom.2014.03.022.
[271] S. Hou, Y. Ye, S. Liao, J. Ren, H. Wang, P. Yang, K. Du J. Li and H. Peng, "Enhanced low-humidity performance in a proton exchange membrane fuel cell by developing a novel hydrophilic gas diffusion layer," International Journal of Hydrogen Energy, vol. 45, no. 1, pp. 937-944, 2020/1// 2020, doi: 10.1016/j.ijhydene.2019.10.160.
[272] X. Wang, J. Wang, S. Yang, J. Guan, Z. Zhang, and F. Wang, "Ultraviolet-Induced Bi-gradient Gas Diffusion Electrode for High-Performance Fuel Cells," Industrial and Engineering Chemistry Research, vol. 61, no. 10, pp. 3561-3569, 2022/3// 2022, doi: 10.1021/acs.iecr.1c04957.
[273] Y. Aoyama, Y. Tabe, R. Nozaki, K. Suzuki, T. Chikahisa, and T. Tanuma, "Analysis of Water Transport inside Hydrophilic Carbon Fiber Micro-Porous Layers with High-Performance Operation in PEFC," Journal of The

Electrochemical Society, vol. 165, no. 7, pp. F484-F491, 2018, doi: 10.1149/2.0801807jes.
[274] T. Kitahara, H. Nakajima, M. Inamoto, and M. Morishita, "Novel hydrophilic and hydrophobic double microporous layer coated gas diffusion layer to enhance performance of polymer electrolyte fuel cells under both low and high humidity," Journal of Power Sources, vol. 234, pp. 129-138, 2013/7// 2013, doi: 10.1016/J.JPOWSOUR.2013.01.150.
[275] T. Kitahara, H. Nakajima, and K. Mori, "Hydrophilic and hydrophobic double MPL-coated GDL to enhance PEFC performance under low and high humidity conditions," in ECS Transactions, 2011, vol. 41, 1 ed., pp. 593-601, doi: 10.1149/1.3635592.
[276] T. Kitahara, H. Nakajima, M. Inamoto, and K. Shinto, "Triple microporous layer coated gas diffusion layer for performance enhancement of polymer electrolyte fuel cells under both low and high humidity conditions," Journal of Power Sources, 2014, doi: 10.1016/j.jpowsour.2013.10.066.
[277] L. Speyer, S. Fontana, S. Cahen, and C. Hérold, "Simple production of high-quality graphene foams by pyrolysis of sodium ethoxide," Materials Chemistry and Physics, vol. 219, 2018, doi: 10.1016/j.matchemphys.2018.08.020.
[278] F. M. Smits, "Measurement of Sheet Resistivities with the Four-Point Probe," Bell System Technical Journal, vol. 37, no. 3, pp. 711-718, 1958, doi: 10.1002/j.1538-7305.1958.tb03883.x.
[279] G. Tsotridis, A. Pilenga, G. De Marco, T. Malkow, and C. European Commission. Joint Research, EU harmonised test protocols for PEMFC MEA testing in single cell configuration for automotive applications. Publications Office, 2015.
[280] B. C. H. Steele and A. Heinzel, "Materials for fuel-cell technologies," 2001. [Online]. Available: www.nature.com
[281] S. J. Lee, S. G. Kim, G. G. Park, and C. S. Kim, "Quantitative visualization of temporal water evolution in an operating polymer electrolyte fuel cell," International Journal of Hydrogen Energy, vol. 35, no. 19, pp. 10457-10463, 2010/10// 2010, doi: 10.1016/j.ijhydene.2010.07.173.
[282] P. Deevanhxay, T. Sasabe, S. Tsushima, and S. Hirai, "In situ diagnostic of liquid water distribution in cathode catalyst layer in an operating PEMFC by high-resolution soft X-ray radiography," Electrochemistry Communications, vol. 22, no. 1, pp. 33-36, 2012/8// 2012, doi: 10.1016/j.elecom.2012.05.028.
[283] V. Ramani, H. R. Kunz, and J. M. Fenton, "Investigation of Nafion®/HPA composite membranes for high temperature/low relative humidity PEMFC operation," Journal of Membrane Science, vol. 232, no. 1-2, pp. 31-44, 2004/3// 2004, doi: 10.1016/j.memsci.2003.11.016.
[284] Z. Qi and A. Kaufman, "Improvement of water management by a microporous sublayer for PEM fuel cells."
[285] P. Avouris and F. Xia, "Graphene applications in electronics and photonics," in MRS Bulletin vol. 37, ed, 2012, pp. 1225-1234.
[286] S. Pérez-Rodríguez, E. Pastor, and M. J. Lázaro, "Electrochemical behavior of the carbon black Vulcan XC-72R: Influence of the surface chemistry,"

International Journal of Hydrogen Energy, vol. 43, no. 16, pp. 7911-7922, 2018/4// 2018, doi: 10.1016/j.ijhydene.2018.03.040.
[287] C. Simon, D. Kartouzian, D. Müller, F. Wilhelm, and H. A. Gasteiger, "Impact of microporous layer pore properties on liquid water transport in PEM fuel cells: Carbon black type and perforation," Journal of the Electrochemical Society, vol. 164, no. 14, pp. F1697-F1711, 2017, doi: 10.1149/2.1321714jes.
[288] H. Markötter, J. Haußmann, R. Alink, C. Tötzke, T. Arlt, M. Klages, H. Riesemeier, J. Scholta, D. Gerteisen, J. Banhart and I. Manke, "Influence of cracks in the microporous layer on the water distribution in a PEM fuel cell investigated by synchrotron radiography," Electrochemistry Communications, vol. 34, pp. 22-24, 2013/9// 2013, doi: 10.1016/J.ELECOM.2013.04.006.
[289] J. H. Chun, D. H. Jo, S. G. Kim, S. H. Park, C. H. Lee, and S. H. Kim, "Improvement of the mechanical durability of micro porous layer in a proton exchange membrane fuel cell by elimination of surface cracks," Renewable Energy, vol. 48, pp. 35-41, 2012/12// 2012, doi: 10.1016/J.RENENE.2012.04.011.
[290] W. Kast and C. R. Hohenthanner, "Mass transfer within the gas-phase of porous media," International Journal of Heat and Mass Transfer, vol. 43, no. 5, pp. 807-823, 2000/3// 2000, doi: 10.1016/S0017-9310(99)00158-1.
[291] C. C. Fan and M. H. Chang, "Improving proton exchange membrane fuel cell performance with carbon nanotubes as the material of cathode microporous layer," International Journal of Energy Research, vol. 40, no. 2, pp. 181-188, 2016/2// 2016, doi: 10.1002/er.3445.
[292] M. V. Williams, H. R. Kunz, and J. M. Fenton, "Influence of Convection Through Gas-Diffusion Layers on Limiting Current in PEM FCs Using a Serpentine Flow Field," Journal of The Electrochemical Society, vol. 151, no. 10, pp. A1617-A1617, 2004, doi: 10.1149/1.1789791.
[293] X. Du, I. Skachko, A. Barker, and E. Y. Andrei, "Approaching ballistic transport in suspended graphene," Nature Nanotechnology, vol. 3, no. 8, pp. 491-495, 2008, doi: 10.1038/nnano.2008.199.
[294] S. Tang, G. Sun, J. Qi, S. Sun, J. Guo, Q. X and G. M. Haarberg, "Review of New Carbon Materials as Catalyst Supports in Direct Alcohol Fuel Cells," Chinese Journal of Catalysis, vol. 31, no. 1, pp. 12-17, 2010/1// 2010, doi: 10.1016/s1872-2067(09)60034-6.
[295] M. A. Hickner, N. P. Siegel, K. S. Chen, D. S. Hussey, D. L. Jacobson, and M. Arif, "In Situ High-Resolution Neutron Radiography of Cross-Sectional Liquid Water Profiles in Proton Exchange Membrane Fuel Cells," Journal of The Electrochemical Society, vol. 155, no. 4, pp. B427-B427, 2008, doi: 10.1149/1.2826287.
[296] M. K. Cho, H-Y. Park, S. Y. Lee, B-S. Lee, H J. Kim, D. Henkensmeier, S. J. Yoo, J.- Y. Kim, J. Han, H.S. Park, Y-E. Sung and J. Hyun Jang , "Effect of Catalyst Layer Ionomer Content on Performance of Intermediate Temperature Proton Exchange Membrane Fuel Cells (IT-PEMFCs) under Reduced Humidity Conditions," 2016, doi: 10.1016/j.electacta.2016.12.009.

[297] K. Kang and H. Ju, "Numerical modeling and analysis of micro-porous layer effects in polymer electrolyte fuel cells," Journal of Power Sources, vol. 194, no. 2, pp. 763-773, 2009/12// 2009, doi: 10.1016/j.jpowsour.2009.05.046.
[298] G. Chen, G. Zhang, L. Guo, and H. Liu, "Systematic study on the functions and mechanisms of micro porous layer on water transport in proton exchange membrane fuel cells," International Journal of Hydrogen Energy, vol. 41, no. 9, pp. 5063-5073, 2016/3// 2016, doi: 10.1016/j.ijhydene.2016.01.074.
[299] C. J. Tseng and S. K. Lo, "Effects of microstructure characteristics of gas diffusion layer and microporous layer on the performance of PEMFC," Energy Conversion and Management, vol. 51, no. 4, pp. 677-684, 2010/4// 2010, doi: 10.1016/j.enconman.2009.11.011.
[300] J. Wu, X. Z. Yuan, H. Wang, M. Blanco, J. J. Martin, and J. Zhang, "Diagnostic tools in PEM fuel cell research: Part I Electrochemical techniques," in International Journal of Hydrogen Energy vol. 33, ed: Pergamon, 2008, pp. 1735-1746.
[301] A. Z. Weber and J. Newman, "Effects of Microporous Layers in Polymer Electrolyte Fuel Cells," Journal of The Electrochemical Society, vol. 152, no. 4, pp. A677-A677, 2005, doi: 10.1149/1.1861194.
[302] D. Ye, E. Gauthier, J. B. Benziger, and M. Pan, "Bulk and contact resistances of gas diffusion layers in proton exchange membrane fuel cells," Journal of Power Sources, vol. 256, pp. 449-456, 2014/6// 2014, doi: 10.1016/j.jpowsour.2014.01.082.
[303] R. B. Ferreira, D. S. Falcão, V. B. Oliveira, and A. M. F. R. Pinto, "Experimental study on the membrane electrode assembly of a proton exchange membrane fuel cell: effects of microporous layer, membrane thickness and gas diffusion layer hydrophobic treatment," Electrochimica Acta, vol. 224, pp. 337-345, 2017/1// 2017, doi: 10.1016/j.electacta.2016.12.074.
[304] E. M. Can, A. Mufundirwa, P. Wang, S. Iwasaki, T. Kitahara, H. Nakajima, M. Nishihara, K. Sasaki and S.M. Lyth, "Superhydrophobic fluorinated carbon powders for improved water management in hydrogen fuel cells," Journal of Power Sources, vol. 548, pp. 232098-232098, 2022/11// 2022, doi: 10.1016/j.jpowsour.2022.232098.
[305] X. L. Wang, W. K. Wang, Z. G. Qu, G. F. Ren, and H. C. Wang, "Surface roughness dominated wettability of carbon fiber in gas diffusion layer materials revealed by molecular dynamics simulations," International Journal of Hydrogen Energy, 2021/6// 2021, doi: 10.1016/j.ijhydene.2021.05.121.
[306] L. Chen, R. Lin, X. Chen, Z. Hao, X. Diao, D. Froning and S. Tang, "Microporous Layers with Different Decorative Patterns for Polymer Electrolyte Membrane Fuel Cells," ACS Applied Materials and Interfaces, vol. 12, no. 21, pp. 24048-24058, 2020/5// 2020, doi: 10.1021/acsami.0c05416.
[307] D.-H. Lee, M. K. Kim, H. Guim, S. Yuk, J. Choi, S Choi, G.Doo, D.W. Lee, J. Noh and H-T. Kim, "Ditch-structured microporous layers fabricated by nanosecond-pulse laser ablation for enhancing water transport in polymer electrolyte membrane fuel cells,"Mater. Adv, vol. 1, pp. 254-254, 2020, doi: 10.1039/d0ma00150c.

[308] S. Kaushal, A. K. Sahu, M. Rani, and S. R. Dhakate, "Multiwall carbon nanotubes tailored porous carbon fiber paper-based gas diffusion layer performance in polymer electrolyte membrane fuel cell," Renewable Energy, vol. 142, pp. 604-611, 2019/11// 2019, doi: 10.1016/j.renene.2019.04.096.
[309] P. Satjaritanun, J. W. Weidner, S. Hirano, Z. Lu, Y. Khunatorn, S. Ogawa, S. E. Litster, A. D. Shum, I. V. Zenyuk and S. Shimpalee, "Micro-scale analysis of liquid water breakthrough inside gas diffusion layer for PEMFC using X-ray computed tomography and Lattice Boltzmann Method," Journal of the Electrochemical Society, vol. 164, no. 11, pp. E3359-E3371, 2017, doi: 10.1149/2.0391711jes.
[310] C. Lim and C. Y. Wang, "Effects of hydrophobic polymer content in GDL on power performance of a PEM fuel cell," Electrochimica Acta, vol. 49, no. 24, pp. 4149-4156, 2004/9// 2004, doi: 10.1016/j.electacta.2004.04.009.
[311] O. S. Ijaodola, Z. El- Hassan, E. Ogungbemi, F.N. Khatib, T. Wilberforce, J. Thompson and A.G. Olabi, "Energy efficiency improvements by investigating the water flooding management on proton exchange membrane fuel cell (PEMFC)," Energy, vol. 179, 2019, doi: 10.1016/j.energy.2019.04.074.
[312] M. Salahuddin, M. N. Uddin, G. Hwang, and R. Asmatulu, "Superhydrophobic PAN nanofibers for gas diffusion layers of proton exchange membrane fuel cells for cathodic water management," International Journal of Hydrogen Energy, vol. 43, no. 25, pp. 11530-11538, 2018/6// 2018, doi: 10.1016/j.ijhydene.2017.07.229.
[313] F. C. Lee, M. S Ismail, D. B. Ingham, K. J. Hughes, L. Ma, S. M. Lyth and M. Pourkashanian, "Alternative architectures and materials for PEMFC gas diffusion layers: A review and outlook," Renewable and Sustainable Energy Reviews, vol. 166, p. 112640, 2022/09/01/ 2022, doi: https://doi.org/10.1016/j.rser.2022.112640.
[314] C. M. Hwang, M. Ishida, H. Ito, T.Maeda, A.Nakano, A.Kato and T. Yoshida, "Effect of titanium powder loading in gas diffusion layer of a polymer electrolyte unitized reversible fuel cell," Journal of Power Sources, vol. 202, pp. 108-113, 2012/3// 2012, doi: 10.1016/j.jpowsour.2011.11.041.
[315] L. Chen, R. Lin, S. Tang, D. Zhong, and Z. Hao, "Structural design of gas diffusion layer for proton exchange membrane fuel cell at varying humidification," Journal of Power Sources, vol. 467, 2020/8// 2020, doi: 10.1016/j.jpowsour.2020.228355.
[316] S. M. Lyth, H. Shao, J. Liu, K. Sasaki, and E. Akiba, "Hydrogen adsorption on graphene foam synthesized by combustion of sodium ethoxide," International Journal of Hydrogen Energy, vol. 39, no. 1, 2014, doi: 10.1016/j.ijhydene.2013.10.044.
[317] A. Mufundirwa, G. F. Harrington, B. Smid, B. V. Cunning, K. Sasaki, and S. M. Lyth, "Durability of template-free Fe-N-C foams for electrochemical oxygen reduction in alkaline solution," Journal of Power Sources, vol. 375, pp. 244-254, 2018/1// 2018, doi: 10.1016/j.jpowsour.2017.07.025.
[318] M. I. M. Kusdhany, H.-w. Li, A. Mufundirwa, K. Sasaki, A. Hayashi, and S. M. Lyth, "Hydrogen Storage on Nanoporous Carbon Foam for Electrochemical

Applications," ECS Meeting Abstracts, vol. MA2020-02, no. 7, 2020, doi: 10.1149/ma2020-0271123mtgabs.
[319] L. Chen, R. Lin, X.Yu, T. Zheng, M. Dong, M. Lou, Y. Ma, and Z. Hao, "Microporous layer containing CeO2-doped 3D graphene foam for proton exchange membrane fuel cells at varying operating conditions," ACS Applied Materials and Interfaces, vol. 13, no. 17, pp. 20201-20212, 2021/5// 2021, doi: 10.1021/acsami.1c03699.
[320] F. C. Lee, M. S Ismail, D. B. Ingham, K. J. Hughes, L. Ma, S. M. Lyth and M. Pourkashanian, "An Assessment of Novel Graphene Foam and Graphene-Based Microporous Layers for Polymer Electrolyte Fuel Cells: Fabrication and Characterisation," ECS Meeting Abstracts, vol. MA2020-02, no. 33, pp. 2116-2116, 2020/11// 2020, doi: 10.1149/MA2020-02332116mtgabs.
[321] M. Carmo, A. R. dos Santos, J. G. R. Poco, and M. Linardi, "Physical and electrochemical evaluation of commercial carbon black as electrocatalysts supports for DMFC applications," Journal of Power Sources, vol. 173, no. 2 SPEC. ISS., pp. 860-866, 2007/11// 2007, doi: 10.1016/j.jpowsour.2007.08.032.
[322] A. Grondein and D. Bélanger, "Covalent grafting of aminated compounds on Vulcan XC72R by melamine in situ diazotization," Carbon, vol. 50, no. 12, pp. 4335-4342, 2012/10// 2012, doi: 10.1016/J.CARBON.2012.04.050.
[323] C. Muñoz-Ferreiro, C. López-Pernía, Á. Gallardo-López, and R. Poyato, "Unravelling the optimization of few-layer graphene crystallinity and electrical conductivity in ceramic composites by Raman spectroscopy," Journal of the European Ceramic Society, vol. 41, no. 16, pp. 290-298, 2021/12// 2021, doi: 10.1016/J.JEURCERAMSOC.2021.09.025.
[324] B. Galindo, S. G. Alcolea, J. Gómez, A. Navas, A. O. Murguialday, M. P. Fernandez and R. C. Puelles, "Effect of the number of layers of graphene on the electrical properties of TPU polymers," in IOP Conference Series: Materials Science and Engineering, 2014, vol. 64, 1 ed., doi: 10.1088/1757-899X/64/1/012008.
[325] X. Y. Fang, X. X. Yu, H. M. Zheng, H. B. Jin, L. Wang, and M. S. Cao, "Temperature- and thickness-dependent electrical conductivity of few-layer graphene and graphene nanosheets," Physics Letters A, vol. 379, no. 37, pp. 2245-2251, 2015/10// 2015, doi: 10.1016/J.PHYSLETA.2015.06.063.
[326] J. B. Donnet, Carbon black: science and technology, Second Edition (Fuel and Energy Abstracts). 1993.
[327] T. Jawhari, A. Roid, and J. Casado, "Raman spectroscopic characterization of some commercially available carbon black materials," Carbon, vol. 33, no. 11, 1995, doi: 10.1016/0008-6223(95)00117-V.
[328] J. Lahaye and F. Ehrburger-Dolle, "Mechanisms Of Carbon Black Formation. Correlation With The Morphology of Aggregates," in "Carbon," 1994, vol. 32.
[329] J. Lahaye and G. Prado, "Mechanism Of Nucleation And Growth Of Carbon Black," in American Chemical Society, Division of Petroleum Chemistry, Preprints vol. 20, ed, 1975.
[330] R. O. Loutfy, "Electrochemical characterization of carbon black," Carbon, vol. 24, no. 2, 1986, doi: 10.1016/0008-6223(86)90106-5.

[331] E. C. Orion, "What is Carbon Black?," Www.Orioncarbons.Com, 2014.
[332] X. L. Wang, H.M. Zhang, J.L. Zhang, H.F. Xu, Z.Q. Tian, J. Chen, H.X. Zhong, Y.M. Liang and B.L. Yi, "Micro-porous layer with composite carbon black for PEM fuel cells," Electrochimica Acta, vol. 51, no. 23, pp. 4909-4915, 2006/6// 2006, doi: 10.1016/j.electacta.2006.01.048.
[333] J. H. Chun, K. T. Park, D. H. Jo, J. Y. Lee, S. G. Kim, E. S. Lee, J-Y Jyoung, and S. H. Kim, "Determination of the pore size distribution of micro porous layer in PEMFC using pore forming agents under various drying conditions," International Journal of Hydrogen Energy, vol. 35, no. 20, pp. 11148-11153, 2010/10// 2010, doi: 10.1016/j.ijhydene.2010.07.056.
[334] Z. Chen, W. Pan, D. Yao, M. Gao, Y. Gao, X. Chen, J. Krzywanski and F. Wang, "Crack evolution during the film drying process of fuel cell microporous layer ink," Colloids and Surfaces A: Physicochemical and Engineering Aspects, vol. 650, pp. 129283-129283, 2022/10// 2022, doi: 10.1016/j.colsurfa.2022.129283.
[335] N. Hasegawa, A. Kamiya, T. Matsunaga, N. Kitano, and M. Harada, "Analysis of crack formation during fuel cell catalyst ink drying process. Reduction of catalyst layer cracking by addition of high boiling point solvent," Colloids and Surfaces A: Physicochemical and Engineering Aspects, vol. 628, 2021/11// 2021, doi: 10.1016/j.colsurfa.2021.127153.
[336] S. Takahashi, T. Mashio, N. Horibe, K. Akizuki, and A. Ohma, "Analysis of the Microstructure Formation Process and Its Influence on the Performance of Polymer Electrolyte Fuel-Cell Catalyst Layers," ChemElectroChem, vol. 2, no. 10, pp. 1560-1567, 2015/10// 2015, doi: 10.1002/celc.201500131.
[337] Z. Fishman and A. Bazylak, "Heterogeneous Through-Plane Porosity Distributions for Treated PEMFC GDLs. II. Effect of MPL Cracks," Journal of The Electrochemical Society, vol. 158, no. 8, pp. B846-B846, 2011, doi: 10.1149/1.3594636.
[338] J. Sim, M. Kang, and K. Min, "Effects of basic gas diffusion layer components on PEMFC performance with capillary pressure gradient," International Journal of Hydrogen Energy, vol. 46, no. 54, pp. 27731-27748, 2021/8// 2021, doi: 10.1016/j.ijhydene.2021.05.205.
[339] Y. R. J. Thomas, A. Benayad, M. Schroder, A. Morin, and J. Pauchet, "New Method for Super Hydrophobic Treatment of Gas Diffusion Layers for Proton Exchange Membrane Fuel Cells Using Electrochemical Reduction of Diazonium Salts," ACS Applied Materials and Interfaces, vol. 7, no. 27, pp. 15068-15077, 2015/7// 2015, doi: 10.1021/acsami.5b04428.
[340] P. G. Stampino, D. Molina, L. Omati, S. Turri, M. Levi, C. Cristiani and G. Dotelli, "Surface treatments with perfluoropolyether derivatives for the hydrophobization of gas diffusion layers for PEM fuel cells," Journal of Power Sources, vol. 196, no. 18, pp. 7645-7648, 2011/9// 2011, doi: 10.1016/j.jpowsour.2011.04.039.
[341] S. B. Park and Y. i. Park, "Fabrication of gas diffusion layer (GDL) containing microporous layer using flourinated ethylene prophylene (FEP) for proton exchange membrane fuel cell (PEMFC)," International Journal of Precision

Engineering and Manufacturing, vol. 13, no. 7, pp. 1145-1151, 2012, doi: 10.1007/s12541-012-0152-x.
[342] P. N. Nirmalraj, T. Lutz, S. Kumar, G. S. Duesberg, and J. J. Boland, "Nanoscale mapping of electrical resistivity and connectivity in graphene strips and networks," Nano Letters, vol. 11, no. 1, pp. 16-22, 2011/1// 2011, doi: 10.1021/nl101469d.
[343] K. S. Novoselov, A. K. Geim, S. V. Morozov, D. Jiang, M. I. Katsnelson, I. V. Grigorieva, S. V. Dubonos and A. A. Firsov , "Two-dimensional gas of massless Dirac fermions in graphene," Nature, vol. 438, no. 7065, pp. 197-200, 2005/11// 2005, doi: 10.1038/nature04233.
[344] N. Rouhi, Y. Y. Wang, and P. J. Burke, "Ultrahigh conductivity of large area suspended few layer graphene films," Applied Physics Letters, vol. 101, no. 26, 2012/12// 2012, doi: 10.1063/1.4772797.
[345] Y. W. Tan, Y. Zhang, H. L. Stormer, and P. Kim, "Temperature dependent electron transport in graphene," European Physical Journal: Special Topics, vol. 148, no. 1, pp. 15-18, 2007/9// 2007, doi: 10.1140/epjst/e2007-00221-9.
[346] K. I. Bolotin, K.J. Sikes, Z. Jiang, M. Klima, G. Fudenberg, J. Hone, P. Kim and H.L. Stormer, "Ultrahigh electron mobility in suspended graphene," Solid State Communications, vol. 146, no. 9-10, pp. 351-355, 2008/6// 2008, doi: 10.1016/J.SSC.2008.02.024.
[347] V. Gurau, M. J. Bluemle, E. S. De Castro, Y.-M. Tsou, J. A. Mann, and T. A. Zawodzinski, "Characterization of transport properties in gas diffusion layers for proton exchange membrane fuel cells: 1. Wettability (internal contact angle to water and surface energy of GDL fibers)," Journal of Power Sources, vol. 160, no. 2, pp. 1156-1162, 2006/10// 2006, doi: 10.1016/j.jpowsour.2006.03.016.
[348] J. P. Owejan, J. E. Owejan, W. Gu, T. A. Trabold, T. W. Tighe, and M. F. Mathias, "Water Transport Mechanisms in PEMFC Gas Diffusion Layers," Journal of The Electrochemical Society, vol. 157, no. 10, pp. B1456-B1456, 2010, doi: 10.1149/1.3468615.
[349] G. Lin, S. Liu, B. Yu, H. Wang, K. Yu, and Y. Hu, "Preparation of graded microporous layers for enhanced water management in fuel cells," Journal of Applied Polymer Science, vol. 137, no. 47, 2020/12// 2020, doi: 10.1002/app.49564.
[350] P. Shrestha, D. Ouellette, J. Lee, N. Ge, A. K. C. Wong, D. Muirhead, H. Liu, R.Banerjee and A. Bazylak, "Graded Microporous Layers for Enhanced Capillary-Driven Liquid Water Removal in Polymer Electrolyte Membrane Fuel Cells," Advanced Materials Interfaces, vol. 6, no. 21, 2019/11// 2019, doi: 10.1002/admi.201901157.
[351] W. Yoshimune, S. Kato, S. Yamaguchi, Y. Akimoto, A. Koiwai, and H. Nakamura, "Managing the Pore Morphologies of Microporous Layers for Polymer Electrolyte Fuel Cells with a Solvent-Free Coating Technique," ACS Sustainable Chemistry and Engineering, vol. 9, no. 23, pp. 7922-7929, 2021/6// 2021, doi: 10.1021/acssuschemeng.1c02105.
[352] A. K. C. Wong, R. Banerjee, and A. Bazylak, "Tuning MPL Intrusion to Increase Oxygen Transport in Dry and Partially Saturated Polymer Electrolyte

Membrane Fuel Cell Gas Diffusion Layers," Journal of The Electrochemical Society, vol. 166, no. 7, pp. F3009-F3019, 2019, doi: 10.1149/2.0021907jes.
[353] X. Shangguan, Y. Li, Y. Qin, S. Cao, J. Zhang, and Y. Yin, "Effect of the porosity distribution on the liquid water transport in the gas diffusion layer of PEMFC," Electrochimica Acta, vol. 371, pp. 137814-137814, 2021/3// 2021, doi: 10.1016/j.electacta.2021.137814.
[354] F. Chen, M. H. Chang, and P. T. Hsieh, "Two-phase transport in the cathode gas diffusion layer of PEM fuel cell with a gradient in porosity," International Journal of Hydrogen Energy, vol. 33, no. 10, pp. 2525-2529, 2008/5// 2008, doi: 10.1016/j.ijhydene.2008.02.077.
[355] J. H. Chun, K. T. Park, D. H. Jo, J. Y. Lee, S. G. Kim, S. H. Park, E. S. Lee, J-Y. Jyoung and S. H. Kim, "Development of a novelhydrophobic/hydrophilic double micro porous layer for use in a cathode gas diffusion layer in PEMFC," International Journal of Hydrogen Energy, vol. 36, no. 14, pp. 8422-8428, 2011/7// 2011, doi: 10.1016/j.ijhydene.2011.04.038.
[356] N. D. Neehall, M. S. Ismail, K. J. Hughes, and M. Pourkashanian, "Effect of composition and structure of gas diffusion layer and microporous layer on the through-plane gas permeability of PEFC porous media," International Journal of Energy Research, vol. 45, no. 15, pp. 20988-21005, 2021/12// 2021, doi: 10.1002/er.7158.
[357] C. S. Kong, D. Y. Kim, H. K. Lee, Y. G. Shul, and T. H. Lee, "Influence of pore-size distribution of diffusion layer on mass-transport problems of proton exchange membrane fuel cells," Journal of Power Sources, vol. 108, no. 1-2, pp. 185-191, 2002/6// 2002, doi: 10.1016/S0378-7753(02)00028-9.
[358] F. Jinuntuya, M. Whiteley, R. Chen, and A. Fly, "The effects of gas diffusion layers structure on water transportation using X-ray computed tomography based Lattice Boltzmann method," Journal of Power Sources, vol. 378, pp. 53-65, 2018/2// 2018, doi: 10.1016/j.jpowsour.2017.12.016.
[359] C.-H. Liu, T.-H. Ko, J.-W. Shen, S.-I. Chang, S.-I. Chang, and Y.-K. Liao, "Effect of hydrophobic gas diffusion layers on the performance of the polymer exchange membrane fuel cell," Journal of Power Sources, vol. 191, no. 2, pp. 489-494, 2009/6// 2009, doi: 10.1016/j.jpowsour.2009.02.017.
[360] A. Arvay, E. Yli-Rantala, C.-H. Liu, X.-H. Peng, P. Koski, L. Cindrella, P. Kauranen, P.M. Wilde and A.M. Kannan , "Characterization techniques for gas diffusion layers for proton exchange membrane fuel cells – A review," Journal of Power Sources, vol. 213, pp. 317-337, 2012/9// 2012, doi: 10.1016/j.jpowsour.2012.04.026.

Appendix 1: Doctoral Development and Modules Undertaken

Year 1

L34118	Energy Systems and Policy
H84PGC	Power Generation and Carbon Capture
H14RPS	Research and Professional Skills
H84CPE	Communication and Public Engagement
17MPP163	Industrial Case Studies
H141MP	Industrial Mini Project
H84RP3	Research Project Portfolio: Part 1
17BSPE01	Research Commercialisation

Year 2

H84FPT	Pilot Scale Facilities Training (PACT)
F84CSS	EngD Winter School and International visit
MAT405	Scientific writing
H84RP4	Research Portfolio 2
EAS6123	Japanese for non-specialists
CIC6001	Introduction to HPC Computing
MAT6005	X-Ray Experimental Techniques
CIC6005	Application Programming using FORTRAN

Year 3

CPE6331	Systems for Sustainability
MEC441	Sustainable Engineering Design

Appendix 2: Research Collaboration between Energy 2050 and I2CNER 2019

Research Collaboration between Energy 2050 and I^{2}CNER 2019

THE ROYAL SOCIETY

a

Table of Contents

Introduction

As part of the fuel cell research collaboration between the Energy 2050 group at the University of Sheffield and the I^{2}CNER group at Kyushu University, a PhD student from the University of Sheffield went on an exchange to Kyushu University. The research visit was funded by the bilateral Royal Society-JSPS International Exchange Grant (IEC\R3\170032). Previously, a PhD student and Professor Stephen Lyth from I^{2}CNER visited the University of Sheffield and in turn Kyushu University hosted post-doctoral and research staff from the Energy2050 group.

The trip duration was from 9th – 26th March 2019 and was based in the I^{2}CNER research facilities at Kyushu University Ito Campus in Fukuoka, Japan. The purpose of the PhD student visit was to exchange knowledge and facilitate collaboration between the two universities; in particular the research that Professor Lyth's group is undertaking on non-platinum catalysts for PEM fuel cells. The main accomplishments of the PhD student visit to Kyushu University were:

- The acquisition of knowledge on the fabrication of non-Pt catalyst for PEMFC
- The formation of carbon foam derived from Sodium Ethoxide.
- The production of free-form gas diffusion layers using carbon foam and PTFE.
- The coating of commercial carbon substrate gas diffusion layers with a micro-porous layer from carbon foam and PTFE.
- BET Analysis for surface area measurement and X-ray Absorption Spectrometry.

I^{2}CNER

The International Institute for Carbon-Neutral Energy Research, known as I^{2}CNER is a research institute based at Kyushu University. The objective of I^{2}CNER is to create a sustainable and environmentally friendly future by the reduction in CO_2 emissions and non-fossil based energy vectors. I^{2}CNER's work promotes the technological advancement of the hydrogen economy, and the capture and sequestration of CO_2. The covering the areas of hydrogen production and storage; hydrogen tolerant materials; fuel cells; "greening" chemical reactions and catalysts; CO_2 capture; as well as geological sequestration.

Research

Nitrogen-Doped Carbon Foam Derived from Sodium Ethoxide

Lyth's group at I^2CNER research institute have developed a carbon foam derived from Sodium Ethoxide which is subject to pyrolysis in a nitrogen atmosphere (Liu et al.,2016). The carbon foam possesses a macro-porous foam like structure, high porosity, and a very high surface area. This nitrogen-doped carbon foam was tested as a "metal-free" electro catalyst for PEM fuel cells; where the oxygen reduction reaction kinetics were good for non-metal catalysts, improved by the nitrogen doping, and good current density, attributed to high temperature pyrolysis.
Mufundirwa et al. (2017) investigated decorating the nitrogen-doped carbon foam with iron to improve catalytic activity.

Experimental Procedure

Pyrolysis: Pyrolysis of Sodium Ethoxide in nitrogen atmosphere converts the polymer into graphic carbon.
Vacuum Filtration: The purpose of vacuum filtration is to wash out the sodium products and impurities from the carbon foam. This leaves behind pores in the carbon foam that have the same size and shape as this original template. This increases the purity of the carbon foam and the available pores for the conductivity.
Heat Treatment: Heat treatment of the catalyst at 1400 ^oC graphitises the carbon foam improving the conductivity. It results in improved mass activity, increased onset potential and maximum current density. Graphitisation is important to enhance the electro-conductivity of the carbon foam catalyst.

Pyrolysis

25g of Sodium Ethoxide was measured and placed in a crucible. The lid was placed on top of the crucible leaving the contents partially exposed for airflow; the crucible was placed in the furnace and to be pyrolysed in an N_2 atmosphere. Temperature was increased by 5^oC/ minute until a temperature of 725^oC was reached. The temperature of 725^oC was then held for 120 minutes. The furnace was then returned to room temperature, 21^oC. The N_2 gas flow rate was 6L/ minute during pyrolysis. When the oven returned to 21^oC, the nitrogen flow to the furnace was turned off and the sample was removed from the oven whilst wearing gloves.

The sample was weighed at 17.694g. Indicating a mass loss of 7.306g.

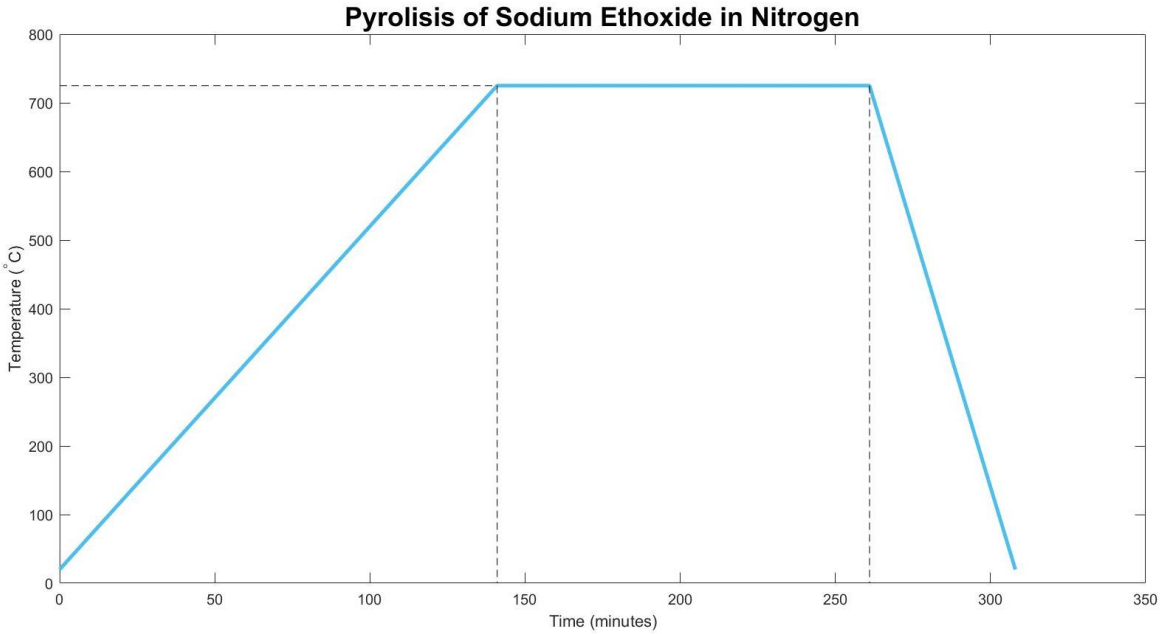

Figure 0-1: Temperature profile of sodium ethoxide in nitrogen

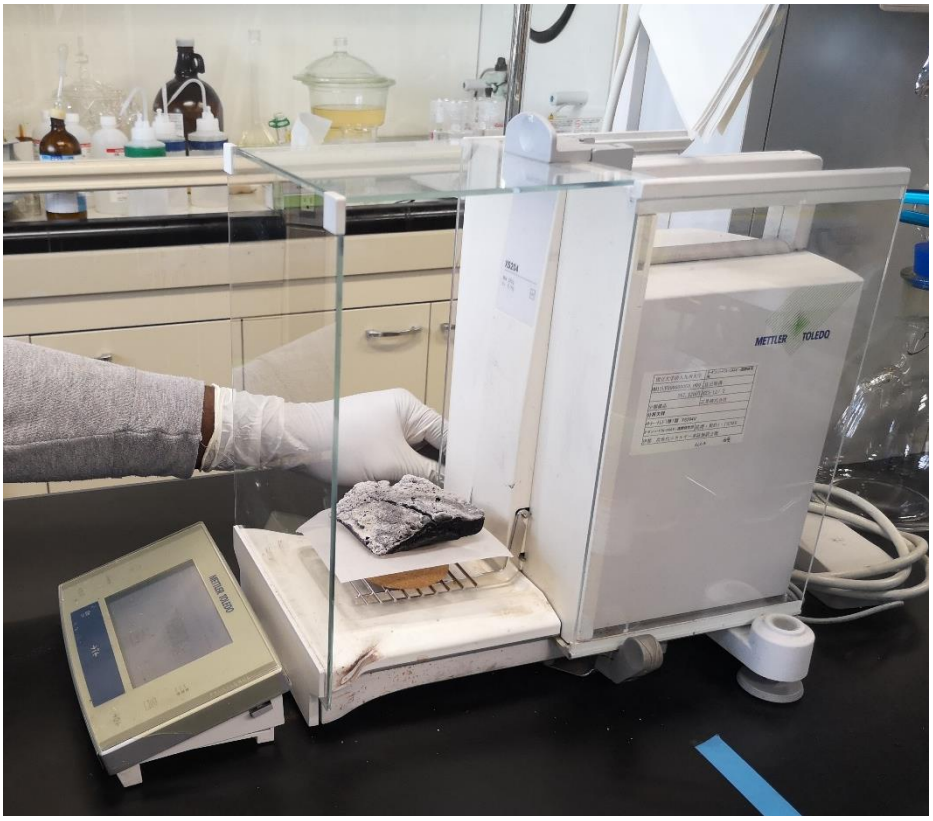

Figure 0-2: Weighing of carbon after pyrolysis of sodium ethoxide.

Vacuum Filtration

The sample was crushed in a pestle and mortar until it was a homogenous fine powder. Carbon powder was added to a 2 litre measuring jug. The residual carbon powder left in the crucible was rinsed out with distilled water and added to the measuring jug.

Figure 0-3: Graphitised carbon from sodium ethoxide pyrolysis

1600 ml of distilled water was added to the measuring jug; it was covered with cling film and magnetically stirred for 24 hours. A 2L capacity vacuum filter and pump were used for the vacuum filtration. A Nylon membrane filter of 0.2µm pore size was used. The vacuum filtration process was repeated with 5 litres of distilled water ensure that the carbon foam sample was thoroughly cleaned of impurities. Remaining on the membrane filter the sample was removed from vacuum filter assembly.
The filter with the sample was the placed in a petri dish and covered with a petri dish lid. It was then placed in an oven at 50 ºC and left for 20 hours. The dried sample was removed from the oven and weighed at 1.772g. The sample was then crushed into a homogenous powder and put into a plastic specimen bottle. The sample was labelled and stored in a vacuum box.

f

Figure 0-4: Vacuum filtration of carbon foam and water solution

Heat Treatment/ Graphitisation

Samples of the carbon foam were taken for heat treatment. These were weighed and placed.
into boat crucibles. The samples were weighed at 246.7 mg and 246.2 mg. The boat crucibles were then placed in a tube furnace and heated to 1400 ºC in nitrogen atmosphere, the temperature profile of the furnace was set using software. Temperature was increased by 5ºC/ minute until a temperature of 1400ºC was reached. The temperature of 1400ºC was then held for 120 minutes. The furnace was then returned to room temperature, 21ºC. The samples were removed from the furnace and weighed.

Sample	First	After 1400 Pyrolysis
1	236.7 mg	69.2 mg
2	246.2 mg	48.8mg

Sample 2 contained white ash after pyrolysis; this was removed before weighing.

Sample	First	After 1400 Pyrolysis
3	253.1 mg	118.8mg
4	254 mg	105.3 mg

Sample 4 contained white ash after pyrolysis; this was removed before weighing.

Free-form Gas Diffusion Layer

As a highly porous substance the heat treated nitrogen-doped carbon foam has potential as use as a free-standing gas diffusion layer as an alternative to conventional carbon substrate gas diffusion layers. The production of the nitrogen-doped carbon foam is cheaper than carbon substrate and has favourable electrochemical properties. As the carbon foam already has potential as a non-platinum catalyst, the potential for it being the only porous media in PEM fuel cells depends on its ability to act as a free standing gas diffusion layer.

Free-standing gas diffusion layers were produced from a filtered dispersion of heat treated carbon foam and PTFE and was heat treated to improve electro-chemical conductivity.

Experimental Procedure

Dispersion/ Vacuum Filtration: Carbon foam and PTFE are dispersed in EthOH solution to encourage binding between the two substances.

Heat Treatment: Carbon foam GDL is heat treated to increase the porosity and the conductivity of the GDL as well as melting the PTFE to bind with the carbon.

Dispersion/ Vacuum Filtration:

100mg of CF_{1400} was dispersed in 15ml ethanol and stirred. 400mg of PTFE in H_2O 60% wt. solution was then added to the solution. The CF_{1400} and PTFE solution was then sonicated in an ultrasonic processor for 1 hour to ensure even dispersion of CF_{1400} and PTFE in the solvent. The solution was vacuum filtered using a PTFE membrane filter of 0.2µm pore size. It was then left to dry for 1 hour.

Figure 0-5: Carbon foam GDL in the filter and (right) Omnipore PTFE membrane filter.

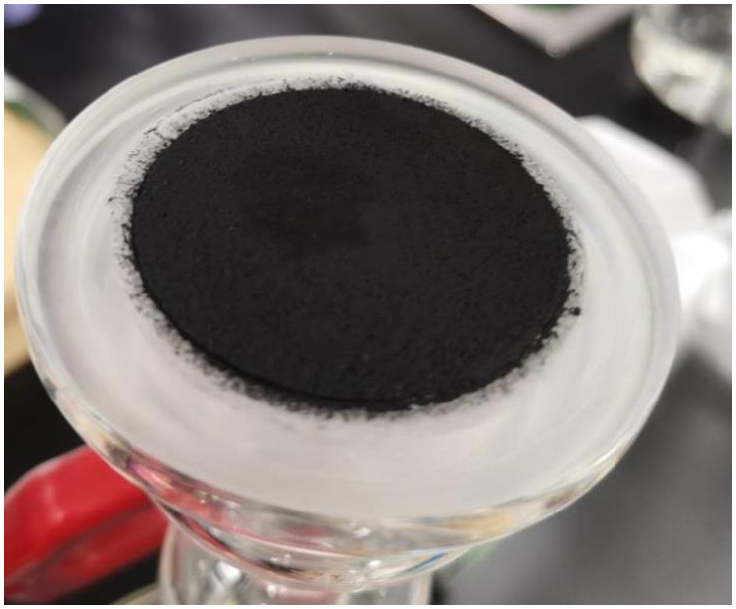

Figure 0-6: Carbon powder GDL before drying.

The CF_{1400} and PTFE solid was removed from the filter and placed between two sheets of aluminium foil. The carbon GDL was hot-pressed at 450 ^{o}C on a hot plate for one hour. This was allowed to cool and removed after one hour.

Figure 0-7: Carbon powder GDL after drying and heat treatment.

Microporous Layer Coating of Carbon Substrates

The nitrogen-doped carbon foam has been explored as an alternative to carbon black. Conventionally carbon black is used in the micro-porous layer coating for carbon substrate gas diffusion layers. The heat treated nitrogen-doped carbon foam was dispersed with PTFE in an ethanol solution and applied to commercial gas diffusion layers as a micro-porous layer.

Experimental Procedure

Dispersion: Carbon foam and PTFE are dispersed in EthOH solution to encourage binding between the two substances.

MPL Coating: The MPL layer was applied to the GDL with an atomiser to ensure an even coating of the carbon/PTFE solution.

Heat Treatment: The MPL sprayed GDL is heat treated to increase the porosity and the conductivity of the MPL layer. Over 350 heat-pressing melts the PTFE in the MPL to bind with the carbon substrate.

Dispersion

100mg of CF_{1400} was dispersed in 30ml ethanol and stirred. 100mg of PTFE in H_2O 60% wt. solution was then added to the solution. The CF_{1400} and PTFE solution was then sonicated in an ultrasonic processor for 1 hour to ensure even dispersion of CF_{1400} and PTFE in the solvent.

j

MPL Coating

A 50mm x 20mm sample of Sigracet SGL- 10BA carbon substrate was measured in the z-plane, this measurement was recorded. The CF_{1400} and PTFE solution was then applied to carbon substrate using a hand atomiser to ensure even coating. This was done on a hot plate at 375 ^{o}C. The coated substrate was allowed to cool and removed from the hot plate. It was then measured in the z-plane and the value was recorded.

Figure 0-9: Carbon substrate GDL on hot-plate for MPL coang

Heat Treatment

2cm x 2cm sample of the coated substrate was taken for heat treatment; this was done at 500 ^{o}C for 30 minutes.

Figure 0-10: Heat treated carbon substrate commercial GDLs after MPL coating and heat treatment. (Left) Toray 60 (right) Sigracet SGL 10BA.

k

Seminars

I^{2}CNER group hosts research seminars where members of the department and visiting researchers present their work. Two seminars were attended whilst visiting the I^{2}CNER institute.

15th March 2019

Progress in molecular X-ray absorption spectroscopy
Prof. Nobuhiro Kosugi, the director of KEK Institute of Materials Structure Science (IMSS)

18th March 2019

Humidity and e oxygen diffusion in La0.6Sr0.4Co0.2Fe0.8O3+δ
Dr. Vincent Thoreton, Post-doctoral Research Associate, Electrochemical Energy Conversion
Effect of Polymer Coating on Carbon Supports for Polymer Electrolyte Membrane Fuel Cells Electrocatalyst
Dr. Tsuyohiko Fujigaya, Professor, Electrochemical Energy Conversion

Conclusions and Personal Reflection

The collaboration between the University of Sheffield and Kyushu University gave me the opportunity to work with a different research group and take part in their work on PEM fuel cells. The work of Lyth's group at I^{2}CNER has been beneficial to my thesis on gas diffusion layers for PEM fuel cells, as it widened the scope of focus of my research to include carbon foam as an alternative material for gas diffusion layers. My intention is to test the gas diffusivity and contact angle as well image the carbon foam free-form gas diffusion layers in order to compute the transport properties. I am extremely grateful to have the opportunity to go to Japan and work with the I^{2}CNER research group.

References

Liu, J., Cunning, B., Daio, T., Mufundirwa, A., Sasaki, K. and Lyth, S. (2016). Nitrogen-Doped Carbon Foam as a Highly Durable Metal-Free Electrocatalyst for the Oxygen Reduction Reaction in Alkaline Solution. Electrochimica Acta, 220, pp.554-561.

Mufundirwa, A., Harrington, G., Smid, B., Cunning, B., Sasaki, K. and Lyth, S. (2018). Durability of template-free Fe-N-C foams for electrochemical oxygen reduction in alkaline solution. Journal of Power Sources, 375, pp.244-254.

Appendix 3: Research Collaboration between Energy 2050 and I2CNER 2020

Research Collaboration between University of Sheffield and Kyushu University 2020

m

Table of Contents

Introduction

The fuel cell research collaboration between the Energy 2050 group at the University Sheffield and the i^{2}CNER and Q-Pit groups at Kyushu University has been active since 2018, sharing knowledge and research techniques for the improvement of PEFC efficiency.

In 2019, two separate visits to Kyushu University were undertaken by University of Sheffield PhD students. During these visits they were able to conduct experiments using the specialised fuel cell equipment that is available at the University, to see the research being undertaken by Professor Lyth's group, and thus broaden their research horizons. Similarly, as a part of this collaboration post-doctoral and research staff from the Energy 2050 group visited Kyushu University during Energy Week, an annual international conference hosted by the University. In turn, Professor Stephen Lyth and a PhD student from Kyushu University were hosted at the University of Sheffield several times throughout the collaboration period.

From the 14th January to the 16th February 2020, a PhD student from the Energy 2050 group carried out a one-month placement at the i^{2}CNER and Q-Pit research facilities at Kyushu University Ito Campus in Fukuoka, Japan. The aim of this visit was to exchange knowledge and research findings between the Energy 2050 group and Professor Lyth's group at Kyushu University. Particularly the work that Professor Lyth's group is conducting on non-precious metal catalysts and fluorinated carbons, both of which are significantly linked to the research being conducted by Dr. Ismail's PhD students in the Energy 2050 group. The main accomplishments of the PhD student visit to Kyushu University were:

- Platinum catalyst fabrication and its application to the polymer electrolyte membrane.
- Fabrication of the fuel cell membrane electrode assembly through hot-pressing.
- In-situ power measurements; pre-test membrane tempering and polarisation curves.
- Production of hydrogen-doped graphene foam from pyrolysis in hydrogen atmosphere.
- Microporous layer coating of commercial gas diffusion layers with using a casting machine.

Figure 0-1: The International Institute for Carbon-Neutral Energy Research (i^{2}CNER, Kyushu University.

Research

Synthesis of Hydrogen-doped Carbon Foam

A novel carbon foam was developed by Prof. Lyth derived from the pyrolysis of Sodium Ethoxide in a nitrogen atmosphere (Liu et al., 2016). The carbon foam possesses a macro-porous foam like structure, high porosity, and a very high surface area, and thus is ideal for use as a catalyst support material and for hydrogen storage applications. The nitrogen-doped carbon foam was found to be a good non-metal electrocatalyst for PEFC; where the nitrogen doping improved the reaction kinetics, and high pyrolysis temperature improved the porosity of the foam-structure.

This novel carbon holds potential for use as an alternative to carbon black in the MPL. As the foam is highly macroporous which allows for improved reactant and water transport and has a high electrical conductivity. The foam-like structure can also have a better contact with the catalyst layer compared to conventional carbon black. The carbon foam is naturally hydrophobic, the hydrophobicity of which is improved from pyrolysis in a hydrogen atmosphere.

Experimental Procedure

Carbon foam was produced from 25g of Sodium Ethoxide pyrolised at 725ºC in a nitrogen atmosphere with a flow rate of 6 litres/minute.

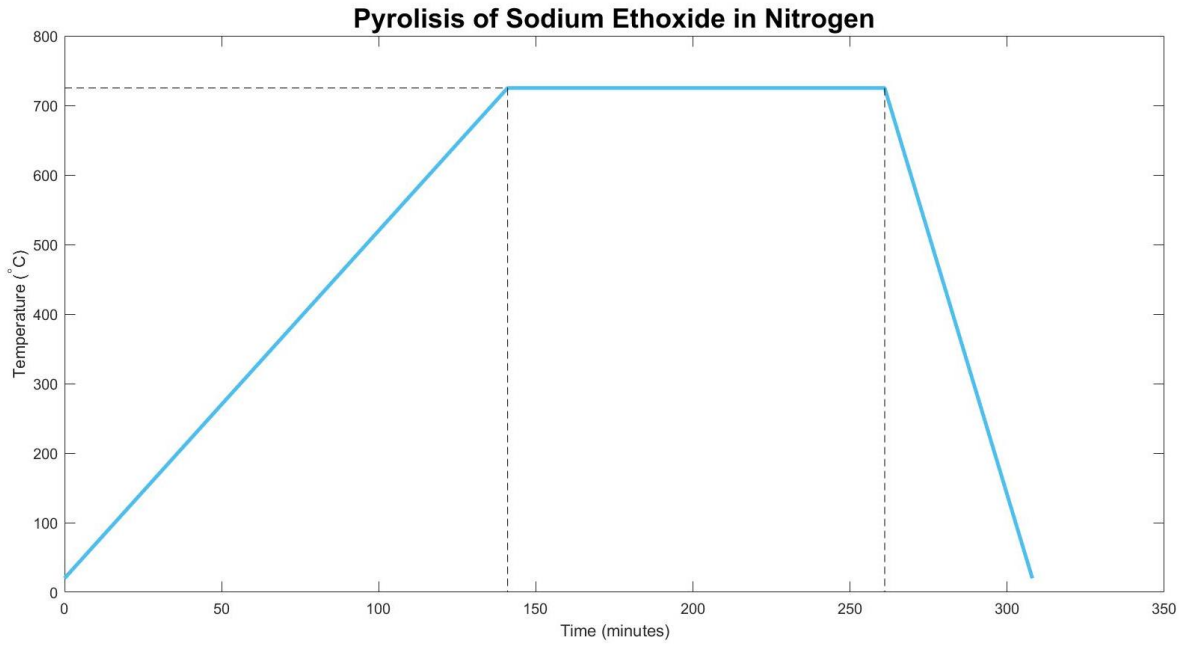

Figure 0-2: Temperature profile for initial pyrolysis of Sodium Ethoxide.

The sample was then washed with 5 litres of deionised water, filtered and dried in an oven at 50°C overnight. The dried sample was then crushed and weighed. The actual yield was 16.5g, indicating a mass loss of 8.5g.

8g of the sample was placed in a sample pot and labelled “Carbon 725”.

Figure 0-3: Operating the tube furnace used for 2nd pyrolysis.

8g of the sample was then used to produce “hydrogen-doped carbon foam”, where it underwent second pyrolysis in a 95:5 nitrogen: hydrogen atmosphere at 1250ºC and a total gas flow rate of 6 litres/minute. The pyrolised product was weighed and was then washed with 5 litres of deionised water and dried in an oven at 50°C overnight. The final product was weighed, then placed in a sample pot and labelled “5% hydrogen carbon”.

A small sample of the hydrogen-doped carbon was then placed in a petri-dish with deionised water and left covered for 72 hours. The carbon displayed hydrophobic/hydrophilic characteristics with the majority of the sample floating on the surface (hydrophobic) with a small amount falling to the bottom.

Figure 0-4: Hydrogen-doped carbon foam in deionised water to test its hydrophobicity.

Microporous Layer and Casting on to the GDL.

A microporous layer (MPL) is applied to the gas diffusion layer of PEFC to increase contact with the catalyst layer and to improve water management, by increasing capillary pressure and channelling water through the substrate to the flow fields. Previously research at the University of Sheffield had focused on spray coating technique to apply the MPL coating, at Kyushu University other methods such as blade coating and casting were used. The coating method has been shown to affect the ex-situ characteristics of the gas diffusion layer and overall cell performance.

Experimental Procedure

Following Simon et al. (2019) methodology, 1g Carbon black was dispersed in 5.3ml deionised water and magnetically stirred in a 100ml beaker at 750 rpm 10 minutes. 120 mg Methyl cellulose was then added as a thickener, with an additional 0.5ml of deionised water added and the stirrer was increased to 1000 rpm. When all of cellulose was completely dispersed in the solution then 27.5 mg Triton X 100 (surfactant) was added to the solution, which was stirred for a further 10 minutes before adding 0.276 ml PTFE dispersion (60 % wt.) The result was an extremely viscous, treacle-like solution.

Figure 0-5: The viscous MPL slurry used for casting and Dr. Blade coating of the GDL.

The solution was then applied to a Toray TGP H-060 gas diffusion layer using a casting machine, where the thickness of the MPL was set to 100µm. This can then be compared to gas diffusion layers with an MPL of the same thickness but applied by spraying. The casting-coated gas diffusion layer was characterised by an extremely homogenous surface with no visual evidence of surface cracking or patches of PTFE.

Figure 0-6: Toray TGP H-060 carbon cloth cast coated with an MPL.

The coated gas diffusion layer was then heat treated in an atmospheric oven in order to sinter the PTFE particles in the MPL and to decompose all additive components (Triton X-100, methyl cellulose). The temperature profile of the heat treatment process is show below.

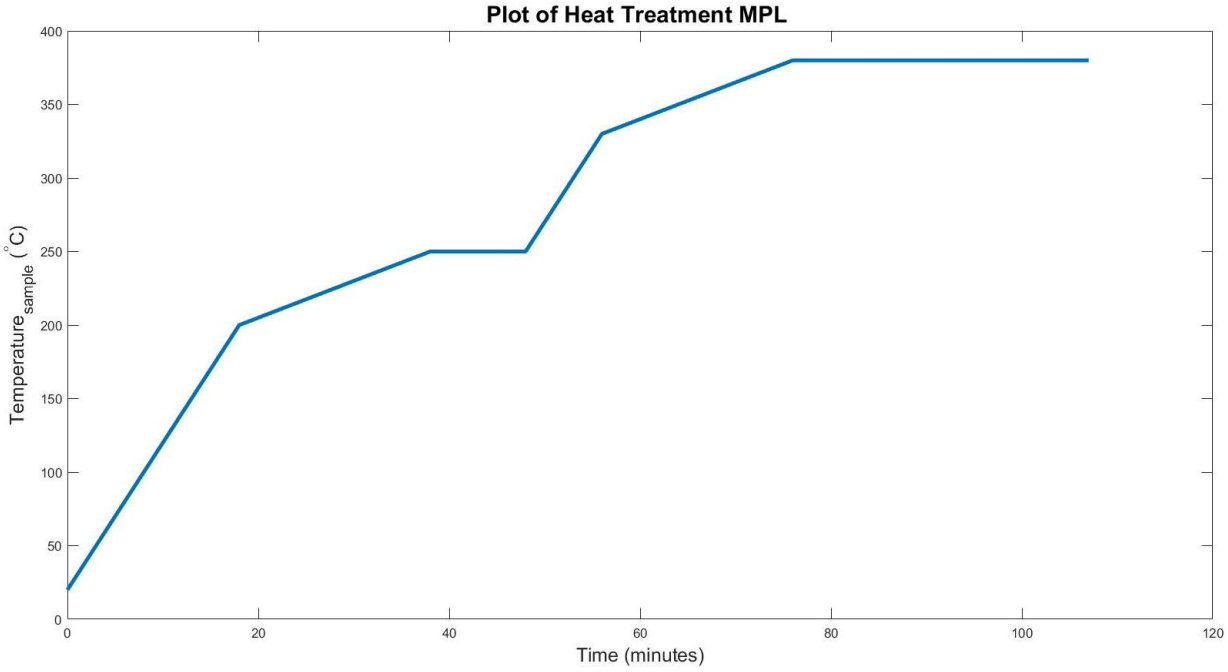

Figure 0-7: A plot of the heat treatment of the MPL-coated GDL from Simon et al., (2019).

t

Platinum Catalyst Fabrication and Application to the Nafion Membrane

Platinum-based catalysts are the most widely used catalysts in commercial Polymer Electrolyte Fuel Cells; this is due to their superior performance in improving the oxygen reduction reaction (ORR) kinetics. The oxygen reduction reaction is the main power-generating electro-chemical reaction of the PEFC, and thus the catalytic activity determines the efficiency of the fuel cell.

Experimental Procedure

For the catalyst ink preparation, 46.2% platinum carbon catalyst (Tanaka) was dispersed in a mixture of ethanol, of deionised water and Nafion (5% wt. solution), where the ratio was 19:6:0.1, as optimised for Pt-based electrocatalysts (Liu et al., 2014). The catalyst ink was then magnetically stirred for 30 minutes at 750 rpm, then sonicated with a probe sonicator for 10 minutes for homogeneity.

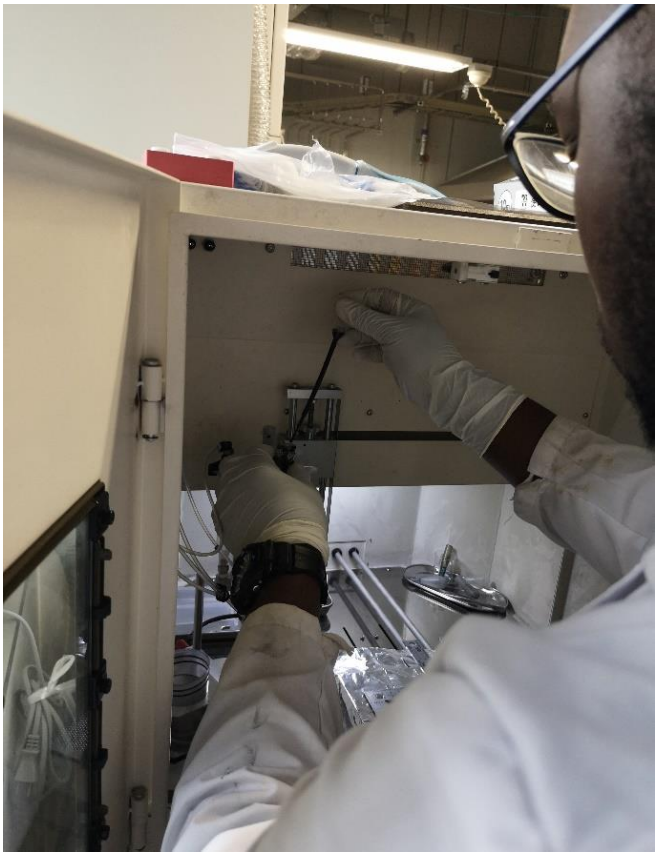

Figure 0-8: Platinum catalyst ink added to the spray coating machine.

The catalyst was applied directly to a 25 cm^2 Nafion membrane using a spray coating machine. As a cell with 1cm^2 flow channels and active area was used for in-situ testing, a mask was used to limit the catalyst deposition to a circular area of 0.79cm^2. The membrane was sprayed several times until Pt loading of 0.4 mg cm^{-2} was achieved, this is typical of PEFC. This process was then repeated for the other side to achieve a membrane with catalyst deposited on both the anodic and cathodic side.

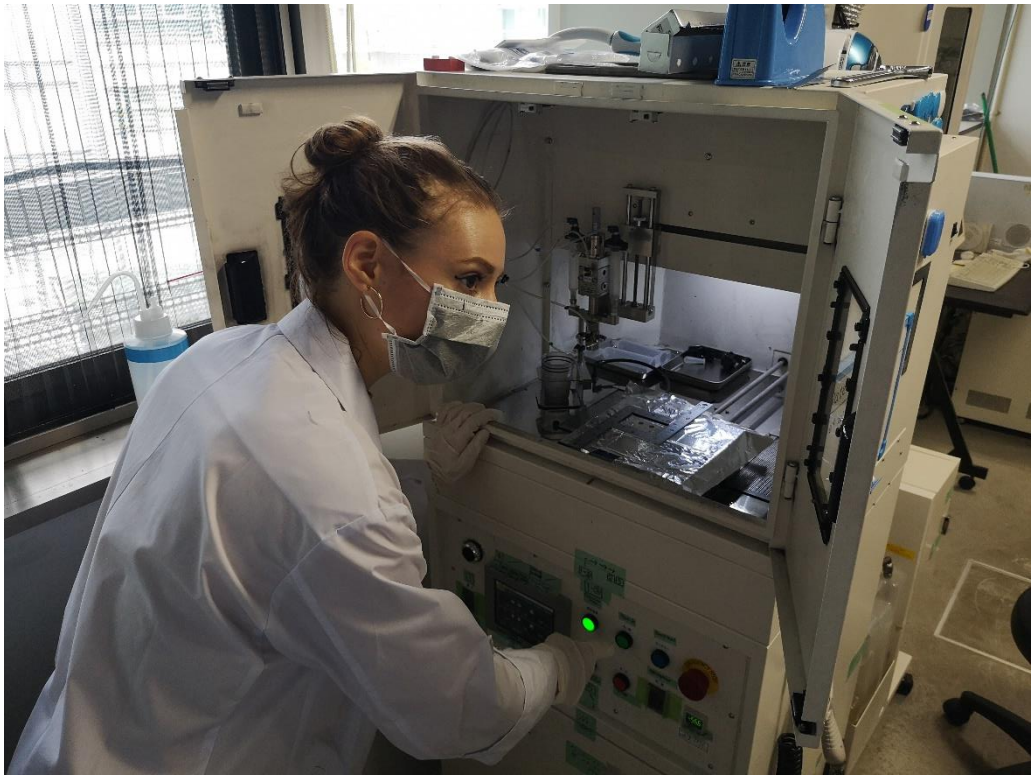

Figure 0-9: Using the spray machine cabinet, the user determines the number of sprays, spray strength, position using controls.

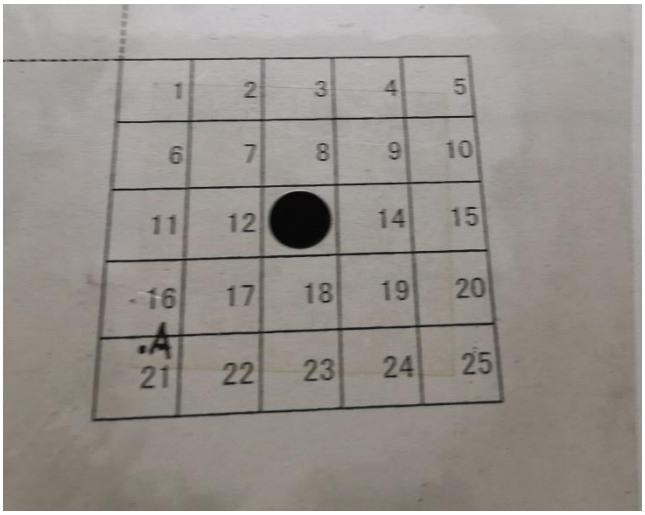

Figure 0-10: The coated membrane where the catalyst is at position 13 on the grid. The reverse "A." signifies that this is the cathode side.

The Pt/C coated membrane was then hot pressed at a force and temperature of 4 MPa and 130ºC respectively for 90 seconds to ensure that good contact between the catalyst and the Nafion membrane. After which the membrane was removed and labelled as "46.2% Pt/C 0.4 mg cm^{2}".

Figure 0-11: Hot press used to hot press the Pt catalyst onto the Nafion membrane.

This process was then adapted to reduce the production time for one coated membrane. Instead, Pt/C ink was applied to a PTFE sheet which was weighed and resprayed until 0.4 mg cm^{-2} of Pt was achieved. Disks of 1 cm in dimeter were then cut from the PTFE sheet and hot pressed on to the membrane, this allowed multiple membranes to be produced more efficiently.

Fuel Cell Assembly and Test Station Measurements

Power measurements of MEA for PEFC are fundamental for component testing as they provide an indication of how well the component affects fuel cell performance and efficiency. Fuel cell performance is given by the polarisation curve (also known as the IV curve), this shows DC potential delivered at the cell terminals as a function of the current density drawn from the external load.

Experimental Procedure

To conduct the MEA testing a fuel cell with an active area of $1cm^2$ fuel cell was used. An uncoated Toray TGP-H060 was used as the anodic GDL whereas an MPL-coated Toray TGP-H060 used as the cathodic GDL. The anodic GDL was initially placed onto the flow field plates, the catalyst coated membrane was then placed on top with the anodic side facing down.

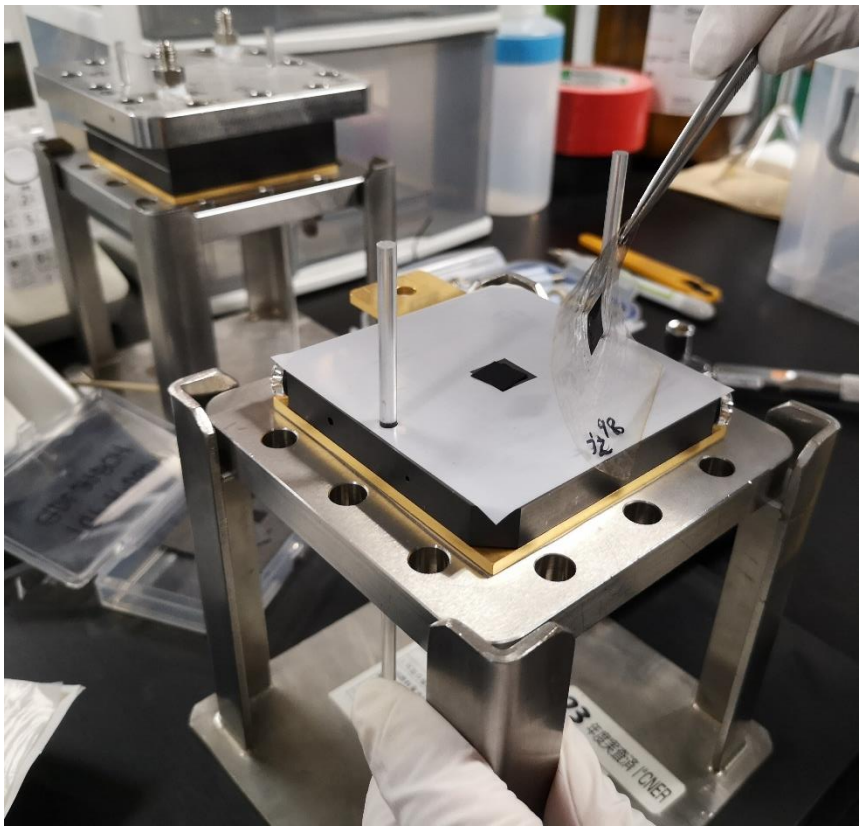

Figure 0-12:The catalyst coated membrane added to the fuel cell assembly.

The cathodic GDL was then placed on the catalyst coated membrane with the MPL in contact with the catalyst. Lastly, the cathodic current collector plate was bolted to the anodic current collector using a torque wrench to ensure optimal compression of the MEA components.

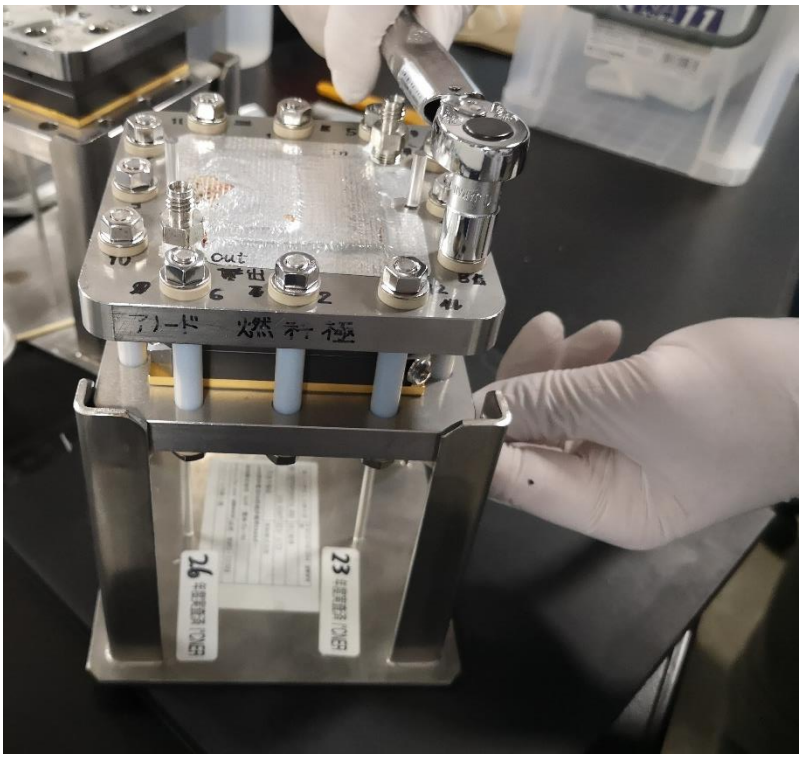

Figure 0-13: Tightening the bolts of the PEFC with a torque wrench to ensure optimal compression of MEA components. The numbers indicate the order in which the bolts need to be tightened.

Before power measurements can be taken it is important that the MEA is activated to provide enough hydration to the membrane, to allow optimal proton conductivity, and to activate the cathodic catalyst due to its slow reaction kinetics. In order to activate the MEA, the cell temperature was set to 70 °C and the humidification temperatures set to 60 °C on both sides for 1 hour before the polarisation curve was measured.

It is also critical when using hydrogen to test for hydrogen leakage using a portable sensor.

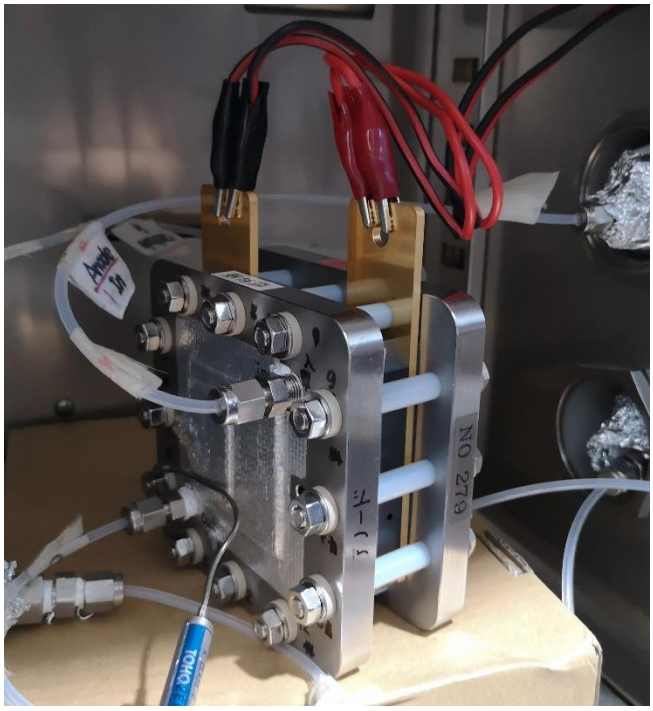

Figure 0-14: The Polymer Electrolyte Fuel cell connected in-situ. The anode inlet and outlets are clearly visible as well as the temperature sensor and busbar connectors.

Power measurements were taken using air as the cathode inlet, where the flow rates for both air and hydrogen were 0.1 litres/ minute. The operational temperature of the fuel cell was 80^{o}C with fully humidified gases.

The polarisation curves could not be included in this report as they are commercially sensitive.

Seminars

Energy Week 2020

27th – 31st January 2020

Energy Week is an annual international conference hosted by Kyushu University at the International Institute for Carbon-Neutral Energy Research (i2cner) and Kyushu University Platform for Inter-/Transdisciplinary Energy Research (Q-Pit). As an inter-disciplinary event focusing on "future energy", it features symposia, lectures and workshops centred on the transition towards a sustainable energy system. During the 5-day event, internationally recognised speakers, and prominent experts from the fields of academia, industry and government deliver presentations on solving the energy-trilemma, from sustainable energy conversion devices to internationally connected energy systems.

Energy Week 2020 featured academic speakers from Kyushu University's own research centres, Duke University, and the University of Hawaii University, as well as representatives from the Renewable Energy Institute, and the Asian Development Bank. A range of topics were addressed under the umbrella of sustainable energy futures, including the prominent issue of microplastic pollution and international grid connectivity.

Figure 0-15: Mika Ohbayashi, Director of Renewable Energy Institute.

aa

THE ROYAL SOCIETY

5th Kyushu-Sheffield Workshop
21st January 2020

Kyushu-Sheffield workshops are held when researchers from the two Universities come together to discuss their research. They are an excellent opportunity to demonstrate research progress, share findings and receive criticism and input on work undertaken.

The 5th Kyushu- Sheffield Workshop saw speakers from Professor Lyth and Professor Nishihara's lab groups, as well as an EngD student from the University of Sheffield.

Conclusions and Personal Reflection

The collaboration between the University of Sheffield and Kyushu University has been a fantastic opportunity to further my research skills and broaden my knowledge in the area of PEFC. Moreover, the work with Professor Lyth's group has enabled me to establish strong connections in this academic field and life-time friends and colleagues. We have already produced one paper together and are working on more to continue our mutual research goals and to maintain this collaboration Having undertaken this work in Kyushu University, I intend to continue in this course by using the same methodology for MPL coating of gas diffusion layers, researching alternatives to carbon black and PTFE. I am extremely grateful for the support of the Royal Society (RS): The bilateral Royal Society (RS) – Japan Society for the Promotion of Science (JSPS) research grant (IEC\R3\170032) for providing me with this unique opportunity.

Figure 0-16: The end of a busy day of lab work. (From left Prof. Stephen Lyth, Albert Mufundirwa, Florence Lee, Dr. Mohammed Ismail and Enes Can).

References

1. Liu, J., Cunning, B., Daio, T., Mufundirwa, A., Sasaki, K. and Lyth, S. (2016). Nitrogen-Doped Carbon Foam as a Highly Durable Metal-Free Electrocatalyst for the Oxygen Reduction Reaction in Alkaline Solution. Electrochimica Acta, 220, pp.554-561.
2. Simon et al. (2019). Interaction of Pore Size and Hydrophobicity/Hydrophilicity for Improved Oxygen and Water Transport through Microporous Layers. Journal of The Electrochemical Society, 166(13): F1022-F1035.